

Stabilization and structural study of new nanocomposite materials

Jessica Link

▶ **To cite this version:**

Jessica Link. Stabilization and structural study of new nanocomposite materials. Material chemistry. Université de Lyon, 2019. English. NNT : 2019LYSE1238 . tel-02447268

HAL Id: tel-02447268
https://theses.hal.science/tel-02447268

Submitted on 21 Jan 2020

HAL is a multi-disciplinary open access archive for the deposit and dissemination of scientific research documents, whether they are published or not. The documents may come from teaching and research institutions in France or abroad, or from public or private research centers.

L'archive ouverte pluridisciplinaire **HAL**, est destinée au dépôt et à la diffusion de documents scientifiques de niveau recherche, publiés ou non, émanant des établissements d'enseignement et de recherche français ou étrangers, des laboratoires publics ou privés.

N°d'ordre NNT :
2018LYSE1238

THESE de DOCTORAT DE L'UNIVERSITE DE LYON
opérée au sein de
l'Université Claude Bernard Lyon 1

Ecole Doctorale N° 34
Matériaux

Spécialité de doctorat : Science des Matériaux

Soutenue publiquement le 08/11/2019, par :
Jessica, Link

Stabilization and structural study of new nanocomposite materials

---

Devant le jury composé de :

Mme Hélène MONTES	Professeure	*Présidente du jury*
M. Frédéric PIGNON	Directeur de Recherche	*Rapporteur*
Mme. Laurence RAMOS	Directeur de Recherche	*Rapporteure*
Mme. Eliane ESPUCHE	Professeure	*Examinatrice*
M. Paul SOTTA	Directeur de Recherche	*Directeur de thèse*
M. Mathieu TAUBAN	Ingénieur de Recherche	*Encadrant industriel*

Remerciements

Toutes les bonnes choses ayant (enfin) une fin, il est maintenant grand temps de remercier toutes les personnes impliquées, qui m'ont aidée, soutenue et tant appris durant ces trois années (ou légèrement plus…) de thèse.

Je tiens à remercier tout d'abord Florence Clément et Didier Long, directrice et directeur adjoint du Laboratoire des Polymères et Matériaux Avancés (LPMA), de m'avoir permis de réaliser ma thèse dans votre laboratoire dans de si bonnes conditions mais aussi pour nos nombreux échanges concernant mon travail et mes projets futurs.

Mes plus profonds remerciements vont à mon directeur de thèse et mon encadrant industriel. Paul, je te remercie grandement pour ton soutien, ta pédagogie, la confiance que tu m'as accordée, tes conseils et surtout ta disponibilité. Merci aussi pour ces riches échanges, même si, je te l'accorde, les cinq minutes de discussion que je te vendais à chaque fois étaient très souvent dépassées. Mathieu, en plus de l'intérêt que tu as porté à mon travail, tu as sur essuyer mes quelques passages de doutes d'un revers de la main et m'as soutenu quel que soit le problème (la disparition d'une micropipette, un frigo ATEX pour 1mL de solution ou le manque d'un polymère plus difficile que prévu à identifier). Tu m'as aussi permis de discuter de mon travail et de rencontrer de nombreuses personnes chez Solvay donnant une dimension industrielle à cette thèse. Merci à tous les deux de m'avoir laissé autant d'autonomie pour mener à bien cette thèse mais aussi de m'avoir poussé à me dépasser. Je pense avoir appris tant sur le plan scientifique que sur le plan humain avec vous. Merci aussi à Olivier qui a suivi avec intérêt ce travail et pour ses conseils tout au long de cette thèse.

Je remercie Laurence Ramos et Frédéric Pignon d'avoir accepté d'être les rapporteurs de ce travail ; ainsi que Eliane Espuche et Hélène Montès pour l'intérêt porté à cette thèse.

J'ai eu l'opportunité de travailler avec Cédric Lorthioir, du Laboratoire de Chimie de la Matière Condensée de Paris. Je tiens à remercier Cédric pour son temps, la pédagogie dont il a fait preuve pour m'expliquer la RMN ainsi que pour son accueil très chaleureux.

J'adresse mes remerciements aux membres du LPMA et de PM2D pour cette ambiance de travail forte de convivialité, ce qui m'a offert un cadre de travail idéal. Entourée de vous tous j'ai beaucoup apprécié ces trois ans en majeure partie grâce à nos discussions plus ou moins scientifiques, parfois autour d'un café, quelques viennoiseries ou de galettes des rois des thésards. Un grand merci à Sylvie pour son aide tout au long de ces trois ans notamment pour la mise en place (parfois compliquée) des expériences au laboratoire et aussi pour sa gentillesse.

Merci aussi au laboratoire de microscopie, Pauline Grau, Baptiste Gros, Clémence Abadie et Magalie Fontana pour leur aide et leur temps ce qui m'a permis d'obtenir de superbes images illustrant ma thèse.

Lors de ces trois ans j'ai aussi eu la chance de découvrir différentes centres R&D de Solvay en France. Tout d'abord au centre de recherche d'Aubervilliers, avec Cédric Féral-Martins où j'ai appris la synthèse des solutions de silice nanométriques et Frédéric Colbeau-Justin qui s'est appliqué à m'expliquer la chimie de surface des nanoparticules et le procédé de transfert de phase. Enfin à Bordeaux au Laboratoire du Futur (LoF) où j'ai découvert un monde que je pensais effrayant, celui de

la rhéologie. Pour leur accueil, leur aide, leur disponibilité et leur savoir sur ce domaine je tiens à remercier Guillaume Ovarlez et Julien Laurens.

Je tiens également à remercier les membres de la GBU Solvay Silica pour leur intérêt pour mon projet de thèse et plus particulièrement merci à Jules Valente et Anne-Laure Pinault.

Merci aussi aux membres de la GBU Solvay Specialty Polymers qui ont suivi ce travail et donné de nombreux conseils. Je remercie fortement Riccardo Pieri pour son implication dans cette thèse, pour nos nombreux échanges et ses conseils.

Un grand merci aux « non-permanents » du LPMA (Nicolas, Julien, Stéphanie, Francesco, Eléonore, Ludovic, Rita, Thomas, Agathe V et Agathe C) pour ces nombreux bons moments : en pauses-café, lors des ateliers galettes des rois, avec la Twingo Mag(n)ico bus, lors des quelques séances de course à midi auxquelles j'ai participé, aux salons du vin, lorsque j'ai retrouvé mon bureau scotché ou en *afterworks.* Mingxing, ce fut un plaisir de travailler avec toi et de constater les excellents résultats que tu as obtenu. Anne-Charlotte, merci pour tes conseils et nos échanges sur le domaine des gels ou autres potins peu scientifiques un peu partout en France et en dehors : à très vite pour une soirée italo-belge arrosée de bière, frites, pâtes et de mozzarella (mission bouboules). Un énorme yallah à Aurélien - *Serge* pour, entre autres, ta bonne humeur, tes glaces, mon initiation à l'escalade et nos histoires abracadabrantes.

Enfin mes remerciements vont vers tous mes proches avec qui nous avons toujours su partager inquiétudes et joies ou d'incroyables moments et fou rires aux quatre coins du monde sans que la distance ne change rien. Gabriel, Loïs (j'attends vos retours respectifs en France avec impatience), Mélanie, Pauline, Thomas, Louise, Morgann, Julien, Jérémy, Elissa, Paul, et j'espère n'oublier personne ; merci pour ces soirées « open bulles » à pleurer de rire, ces « questions du jour » parfois horribles, ces brunchs et ces discussions sérieuses ou (très souvent) non. Merci à Adrienne, Véronique et Sarah qui malgré les kilomètres, variables selon les années, ont toujours été là; surtout autour d'un verre de vin, un cocktail et une planche de fromages ou un après-midi shopping.

A mes parents, mon frère, ma sœur, ma grand-mère, mon oncle, ma tante, mes cousins et ceux qui ne sont malheureusement plus là : un merci infini, tout ça c'est grâce à vous.

Outline

General introduction 1

General context 1

Overview of this work 2

Notations 5

Chapter 1: State of the art 7

1.1. Polymer physics 8

1.2. Fluorinated polymers: PVDF and VDF-based copolymers 13

1.3. Fillers 21

1.4. Polymer gels 29

1.5. Polymer nanocomposites 37

1.6. Context of the PhD work 46

Chapter 2: Materials and methods 49

2.1. Materials 50

2.2. Dynamical and structural characterization of gels 62

2.3. Characterization of polymer – silica hybrid membranes 78

Chapter 3: Thermoreversible gelation of P(VDF-co-HFP) in linear ketone solvents: dynamics and structure 81

3.1. First investigations: gelation kinetics and gel-melting temperatures 82

3.2. Polymer dynamics in the gel: ^{19}F NMR 87

3.3. Structural information 92

3.3.1. Thermal behavior of the gels: DSC 92

3.3.2. WAXS 95

3.3.3. SAXS 97

3.4. Influence of the HFP fraction of the copolymer and its microstructure on gelation 101

3.5. General discussion: gelation mechanism(s) involved in the thermoreversible gelation of P(VDF-co-HFP) copolymers in linear ketone solvents 104

3.6. Conclusions 109

Chapter 4: Influence of the presence of fillers on the thermoreversible gelation of P(VDF-co-HFP) in linear ketone solvents: MEK and 2-heptanone 111

4.1. An additional mechanism: polymer – silica interactions 112

4.2. Dispersion state of silica in the gel state: USAXS study 113

4.3. Gelation kinetics 125

4.4. Dynamics of P(VDF-co-HFP) – silica gels in MEK 127

4.5. General discussion: modification of the gelation mechanism with the incorporation of silica nanoparticles 130

4.6. Conclusions 133

Chapter 5: Non-linear rheology study of P(VDF-co-HFP) – 2-heptanone thermoreversible gels 135

5.1. Non-linear behavior of P(VDF-co-HFP) – 2-heptanone gels 137

5.2. Effect of the addition of silica nanoparticles on the nonlinear behavior of P(VDF-co-HFP) – 2-heptanone gels 147

5.3. General discussion: non-linear behavior of P(VDF-co-HFP) gels in 2-heptanone 152

5.4. Conclusions 156

Chapter 6: P(VDF-co-HFP) – silica hybrid membranes 159

6.1. Results 160

6.2. General discussion 167

6.3. Conclusions 175

General conclusion 177

References 181

Illustration table 191

General introduction

General context

In recent years, polymer materials with enhanced mechanical, thermal or electrical properties have attracted growing interest to replace metal and ceramic materials. They are now daily used in energy, transport, building and consumer goods for example. Among these classes of materials are polymer nanocomposites which consist in introducing small (submicrometric) solid filler particles into a polymer matrix. Nanocomposites combine the advantages of the inorganic fillers (rigidity, thermal stability …) and the organic polymer (flexibility, dielectric insulation, mechanical toughness…) (Zou, Wu et al. 2008) and often exhibit remarkable reinforcement properties. However, their properties strongly depend on many factors: structure, size, surface chemistry, distribution state of the fillers and interfacial interactions between the polymer and the fillers.

For industrial applications, nanocomposites are used for the development of functional or advanced materials for energy storage, harvesting and conversion. Indeed, due to the increasing demand in energy, the development of such materials is a key challenge. The materials must fulfill several conditions: a high dielectric constant, a strong breakdown strength, good mechanical properties and resistance to high temperatures. In this context fluorinated polymers are good candidates and have been studied extensively due to their versatility (thermoplastic, elastomers, plastomers that can be semicrystalline to amorphous) and their combination of properties. Among this class of polymers, poly(vinylidene fluoride) (PVDF) and VDF-based copolymers such as P(VDF-co-hexafluoropropylene) (P(VDF-co-HFP)) are emerging (co)polymers because of their high thermal, chemical and abrasion resistance, high dielectric constant and their piezoelectric and pyroelectric properties (Ameduri 2009). These polymers can be filled with silica nanoparticles to mechanically reinforce them but also to improve their electrical performances (Roy, Nelson et al. 2007).

Solvay is a chemical company producing specialty polymers such as PVDF and VDF-based copolymers for Li-ion batteries, fuel cells or films (e.g. in photovoltaic applications), as they constitute coatings or films very resistant to abrasion, moisture, etc. Solvay also produces dispersible precipitated silica for the tire, home-care or battery separator industry. The objective of this study is therefore to develop P(VDF-co-HFP)-based nanocomposites highly filled with silica nanoparticles. Major attention has to be paid to the control of the dispersion state of the nanoparticles within the polymer matrix as it directly impacts the characteristic properties of the polymer nanocomposite.

This study was the initiation of the development of polymer materials processed by solvent route in LPMA. Previous PhD theses carried out in LPMA were related to the development of polymer blends (Argoud 2011, Epinat 2014) or reinforced rubbers (Vieyres 2013) by melt mixing (in internal mixers or extruders). The underlying purpose of this work is to see whether the solvent route allows better control of the dispersion states of fillers in polymer matrices compared with melt mixing, the latter being only possible for elastomers. Understanding how the filler surface chemistry and distribution state, as well as the process (nature of the solvent, concentration of filler, solvent casting step) affect the mechanical and electrical properties of the films was also a key objective of the work

Overview of this work

The main objective of this study has been to develop highly filled P(VDF-co-HFP) – silica nanocomposites by solvent route. These materials are prepared by casting and drying P(VDF-co-HFP) – silica solutions in an adequate solvent. The structure and properties of these materials are related to the processing of the materials and their composition. In this manuscript, we report the preparation methods and properties of P(VDF-co-HFP) films prepared from a polymer – silica solution in linear ketone solvent, namely methyl ethyl ketone (MEK) and 2-heptanone.

However, prior to the development of the nanocomposites, we found that PVDF and VDF-based copolymers (filled or not with nanoparticles) form thermoreversible gels in these solvents, the morphologies of which strongly depend on the exact nature of the solvent, the polymer chain structure and molecular weight. It is generally agreed that thermoreversible gelation is the result of the formation of a three-dimensional network in which the junction points consist in physical bonds: hydrogen bonds, crystalline zones or liquid-liquid phase separation. Several studies on the gelation of PVDF were published in the literature in the past forty years in solvents very different from those we use in this work, where no consensus on the gelation mechanisms were found (Mal and Nandi 1998).

It is therefore important to understand the mechanisms responsible for the gelation of this copolymer and the influence of the presence of fillers prior to characterizing the properties of the final dry nanocomposites. The strategy that we have adopted consists in changing different variables: nature of the solvent, copolymer fraction, temperature, amount of filler and filler surface chemistry. Several characterization methods were used to investigate the phenomenology of thermoreversible gelation.

The first chapter presents a literature review on the different notions involved in this PhD. Some basis on polymer physics and the influence of the nature of the solvent and concentration of copolymer on the conformation of polymer chains, characteristics of PVDF and VDF-based copolymer and fillers, are first introduced. Then, a literature overview on the gelation of polymers and more particularly PVDF is presented. Finally, the preparation methods, structural, electrical and mechanical characterizations of polymer – silica nanocomposites are presented.

The various materials (copolymer, solvents, silica sources and silica coating agents) that have been used to manufacture P(VDF-co-HFP) – silica – solvent gels and P(VDF-co-HFP) – silica hybrid films are introduced in Chapter 2. The experimental conditions used to prepare these materials and the characterization methods are presented in a second part of this chapter.

The first part of the work was guided by two questions: **What are the mechanisms responsible for the gelation of P(VDF-co-HFP) in linear ketone solvents? What is the influence of experimental factors: fraction of copolymer, temperature, solvent polarity and presence of nanoparticles on the dynamics and structure of the gels?** Chapters 3, 4 and 5 address these questions

In Chapter 3, the gelation of P(VDF-co-HFP) is first investigated in MEK by combining different experimental approaches and the hypotheses on the gelation mechanisms were extended to a longer ketone solvent, here 2-heptanone. The influence of the crystallinity and organization of the copolymer on the gelation was also studied. In Chapter 4, the influence of silica nanoparticles on gelation mechanisms is investigated. The distribution state of silica nanoparticles in physical polymer – silica gels was investigated. Studies on the dynamics of these systems were conducted by the same techniques as for unfilled gels. An overview of the nonlinear rheological behavior of P(VDF-co-HFP)

physical gels in 2-heptanone is given in chapter 5. The effects of the concentration of copolymer, and of the presence of silica nanoparticles are discussed.

Finally, the structure – properties relationship of P(VDF-co-HFP) – silica hybrid films are presented in Chapter 6. A possible relationship between the distribution state of silica nanoparticles in the gel and in the films is suggested. Also the influence of the process, types of silica nanoparticles and their concentration on the structure and properties of the materials will be presented.

Notations

PVDF	Poly(vinylidene fluoride)
P(VDF-co-HFP)	Poly(vinlylidene-co-hexafluoropropene)
VDF	Vinylidene fluoride
HFP	Hexafluoropropene
MEK	Methyl Ethyl Ketone
2MeTHF	2-methyl tetrahydrofurane
EtOH	Ethanol
CTAB	Cetyl TrimethylAmmonium Bromide
VTMS	VinylTrimethoxySilane
H_2SO_4	Sulfuric acid
IR	Infra-Red
TGA	Thermogravimetric Analysis
TEM	Transmission Electron Microscopy
SEM	Scanning Electron Microscopy
USAXS	Ultra Small Angle X-ray Scattering
SAXS	Small Angle X-ray Scattering
WAXS	Wide Angle X-ray Scattering
DSC	Differential Scanning Calorimetry
NMR	Nuclear Magnetic Resonance
MSE	Magic Sandwich Echo
CMPG	Carll-Purcell-Meiboom-Gill
DQ	Double-Quantum
SAOS	Small Angle Oscillatory Shear
LAOS	Large Angle Oscillatory Shear
M_n	Number average molecular weight

M_w	Weight average molecular weight
χ	Flory interaction parameter
T_g	Glass transition temperature
$X_{polymer}$	Weight fraction of polymer
ϕ	Volume fraction
d	Density
V_M	Molar volume
δ	Hansen solubility parameter
t_{gel}	Gelation time
t^{-1}	Gelation rate
γ	Strain
$\dot{\gamma}$	Strain rate
ω	Angular frequency
σ	Stress
G^*	Dynamic modulus
G'	Storage modulus
G''	Loss modulus
ε_0	Vacuum permittivity
ε_r'	Dielectric permittivity
ε_r''	Dielectric loss
E_b	Breakdown strength

Chapter 1: State of the art

This chapter begins with the general literature on polymer physics, fluorinated polymers and fillers. It then presents an overview on the research in the fields of polymer gels and nanocomposites. From this state of the art the context of the PhD thesis is developed.

1.1. Polymer physics 8

1.1.1. Basics on polymer physics 8

1.1.2. Polymers in solution 9

1.2. Fluorinated polymers: PVDF and VDF-based copolymers 13

1.2.1. Synthesis 13

1.2.2. Solubility in organic solvents 15

1.2.3. Properties 17

1.2.4. Applications 20

1.3. Fillers 21

1.3.1. General introduction on fillers 21

1.3.2. Silica particles and nanoparticles 22

1.3.3. The surface chemistry of silica 23

1.3.4. Surface-modification of silica 25

1.3.5. Characterization of surface-modified silica nanoparticles 27

1.4. Polymer gels 29

1.4.1. Physical and chemical gels 30

1.4.2. Gelation theories 31

1.4.3. Gelation mechanisms 32

1.4.4. Gel characterizations 34

1.5. Polymer nanocomposites 37

1.5.1. Fillers dispersion state in polymer matrices 37

1.5.2. Formulation of polymer nanocomposites 38

1.5.3. Characterization methods of nanocomposites 40

1.6. Context of the research 46

1. State of the art

This chapter presents a literature review on the important notions studied during the PhD thesis. After a short introduction on the physico-chemistry of polymers and more particularly the evolution of the conformation of polymer chains with the nature of the solvent and the concentration of polymer, basic properties of PVDF and VDF-copolymers and silica nanoparticles will be presented. PVDF and its copolymer form gels in various organic solvents. However, even if gels were widely studied for different polymer – solvent systems by numerous characterization methods, we show in this part that there is no consensus on the gelation mechanisms, which strongly depend on the polymer – solvent interactions. Finally, a short literature review on the preparation methods (melt and solution blending) and characterizations of polymer nanocomposites is exposed.

1.1. Polymer physics

1.1.1. Basics on polymer physics

A polymer is a macromolecule formed by the covalent linking of a very large number of repeating units, the degree of polymerization, which are derived from one or more monomers (ie base molecule). The polymerization process allows to link monomers into a chain and it usually occurs in presence of a catalyst. To date, different types of polymerization processes are used:

i. Polycondensation: this is a step polymerization that does not require monomer activation but requires heating and a catalyst. Monomers (di or pluri-functional) will react together and a molecule (water, thiol, ammonium) will be released. Polyamides (Nylon 6,6, Nylon 6, Kevlar), polyesters and polyurethanes are produced by this method
ii. Radical initiated polymerization: chain polymerization that involves radical active center. It breaks down into initiation, propagation, termination and chain transfer principal steps. Main industrial polymers are obtained by radical initiated polymerization such as polyethylene, polystyrene and PVDF
iii. Ionic polymerization: The process is identical to radical polymerization except that the active center is a charged species (anions or cations)
iv. Transition metals polymerization: This process requires using organometallic complexes of transition metals such as titanium or zirconium under Ziegler-Natta catalyst. Most common polymers developed by this method are: polyethylene, polypropylene and polystyrene

Polymers can also be classified as a function of their composition. When the polymer chains contain only one type of monomers they are called *homopolymers* and they can arrange in linear, branched or stared chains. Macromolecules which contain at least two different monomers are called *copolymers*, which can be defined as alternating, statistical block or graft, depending on the sequence in which their monomers are bonded together, as shown in Figure 1.

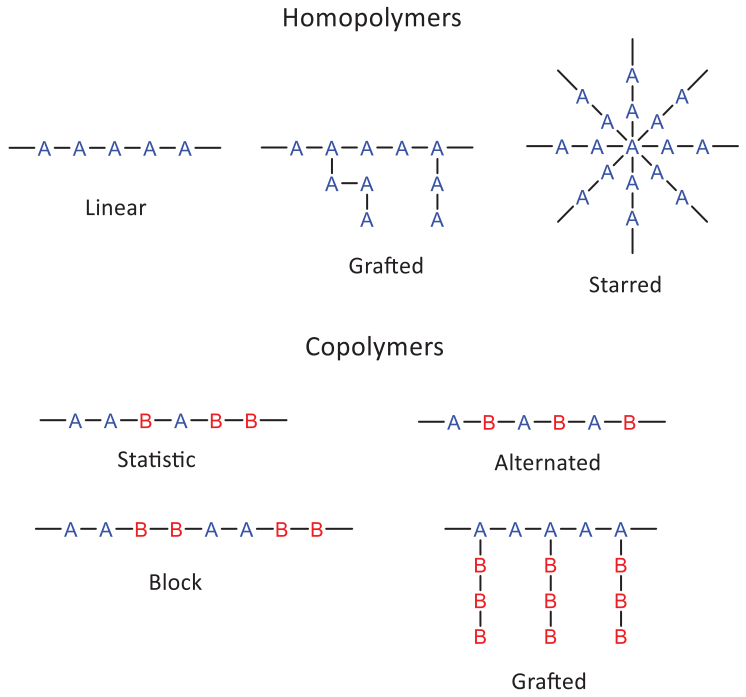


Figure 1 Schematic structures of homopolymers and copolymers

The molar masses of the polymers (number-average molar mass M_n and weight-average molar mass M_w) can be determined by different characterization methods (e.g. tonometry, osmometry, light scattering or size exclusion chromatography). It is then possible to calculate the polydispersity index $I_p = \frac{M_w}{M_n}$ which will reflect the distribution of the polymer sizes. Thermal information on the polymer (melting temperature, glass transition temperature and decomposition temperature) are obtained by Differential Scanning Calorimetry (DSC).

1.1.2. Polymers in solution

Influence of the solvent on polymer conformation

In polymer solutions, the solute molecules are much larger than solvent molecules. The conformation of a polymer chain in a solvent depends on the balance of the interactions between monomers, between solvent molecules and between a monomer and a solvent molecule. The solubility of a polymer within a solvent is described by three limit cases: good solvent, theta solvent and poor solvent.

In the case of a good solvent, interactions between the polymer and the solvent are favored and solvent-polymer contacts are maximized: polymer chains will expand and swell in the solvent. On the contrary, in a bad solvent, the contacts between monomers and solvent molecules are unfavorable. The polymer chains will contract to minimize the interactions with the solvent. Finally, in between these two cases, an ideal case is reached: the polymer chains adopt unperturbed dimensions and behave like an ideal polymer. Here the volume of the macromolecule in solution will remain unchanged compared to its volume at the dry state: we are working with a θ solvent. These three situations (behavior of polymer chains in solution) are schematized in Figure 2.

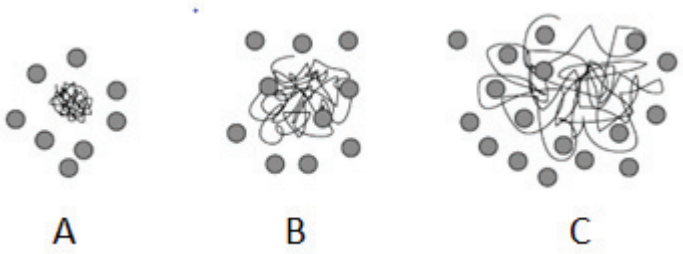


Figure 2 Polymer behavior in solvent in the case of a (A) bad, (B) θ (theta) and (C) good solvent

The Flory-Huggins theory predicts the behavior of solvent-polymer solutions and the solubility of polymers (Flory 1953). The Flory-Huggins free energy of mixing F per unit volume for polymer chains of N monomers (more precisely statistical segments), as a function of the polymer volume fraction φ, is given by:

$$\frac{a^3 F}{k_B T} = \frac{\varphi}{N}\ln\varphi + (1-\varphi)\ln(1-\varphi) + \chi\varphi(1-\varphi) \quad (1)$$

Where a^3 is the volume of a monomer (or solvent molecule, supposed to be the same) and χ is the Flory-Huggins interaction parameter which takes into account the balance of the interactions between monomers, between solvent molecules and between a monomer and a solvent molecule

For small polymer volume fraction $\varphi \ll 1$ the free energy can be approximated by

$$\frac{a^3 F}{k_B T} = f(\varphi) = \frac{\varphi}{N}\ln\varphi + \frac{\varphi^2}{2}(1-2\chi) + \frac{\varphi^3}{6} \quad (2)$$

The quantity $f(\varphi)$ is the free energy per monomer expressed in units of $k_B T$. The stability of the solution is determined by the variations of $f(\varphi)$ as a function of φ, and more precisely by the sign of the coefficient of φ^2, i.e. the second virial coefficient given by the quantity $(1-2\chi)$:

- for $1-2\chi > 0$, that is $\chi < 0.5$ the solvent is a **good solvent** of the polymer. There is a total miscibility of the polymer at any concentration of polymer. A special case is when $\chi = 0$ (so-called athermal solvent case), which corresponds to the best possible solvent.

- for $1-2\chi < 0$, that is $\chi > 0.5$ $f(\varphi)$ has two minima, and the solution will demix in two phases corresponding to the minima of $f(\varphi)$. The second virial coefficient is negative and the solvent is a **poor solvent** of the polymer.

- for $1-2\chi = 0$, that is $\chi = 0.5$ the second virial coefficient is equal to zero. Here the solution is ideal and the solvent is a **θ solvent** of the polymer. As χ depends on temperature, the temperature at which $\chi = 0.5$ is called the θ-temperature. More precisely, it depends on the length of the chain $T_\theta \approx \theta\left(1 \mp \frac{1}{\sqrt{N}}\right)$. Special care should be taken on temperature control when performing experiments in the θ conditions.

Behavior of a polymer in a good solvent: influence of the concentration

The section above presents the effect of the solvent/polymer interactions on the conformation of polymer chains. However, it supposed that the segment density is uniform in the system which is not correct in reality, specifically in dilute solution. De Gennes has revisited the theory of Flory by noting the importance of the concentration c^* at which chains start to fill the whole volume of the solution (DeGennes 1979). Depending on the polymer concentration *c* (expressed here in g/cm^3), a distinction is made between dilute solutions where the chains are separated ($c < c^*$), and semi-dilute or concentrated solutions when chains overlap ($c > c^*$). At the overlap concentration ($c = c^*$) the chains begin to be densely packed. These various regimes are illustrated in Figure 3 for a good solvent of the polymer.

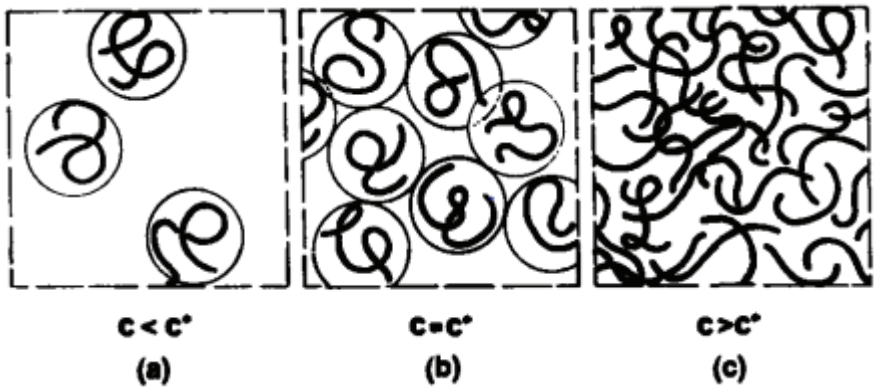


Figure 3 Polymer solutions at various concentrations in a good solvent (a) dilute solution ($c < c^*$), (b) semi-dilute where polymer starts to overlap ($c = c^*$) and (c) semi-dilute with overlapped polymer chains ($c > c^*$). (DeGennes 1979)

In a dilute solution ($c < c^*$) polymer chains are separated from each other and occupy spherical regions with a diameter equal to R_F (radius of an isolated chain). This case corresponds to the condition

$$\frac{4\pi}{3} R_F^3 \frac{c}{M_p} < 1 \tag{3}$$

Where $M_p = m_0 N$ is the mass of a polymer chain (m_0 is the mass of one monomer). The polymer chains start to overlap ($c = c^*$) when

$$c^* = \frac{M_p}{\frac{4}{3}\pi R_F^3} \tag{4}$$

Which shows that $c^* \propto N/R_F^3$. In a good solvent $R_F \sim N^{\upsilon}\ with\ \upsilon = \frac{3}{5}$ and as a consequence $c^* \propto N^{-4/5}$. It appears that the overlap concentration strongly depends on the molar mass of the polymer: when the molar mass increases the overlap concentration decreases and can become very low.

In dilute solutions polymer chains are described by the radius of an isolated chain R_F. However, at concentrations larger than c^* it is necessary to introduce a shorter characteristic length: the correlation length ξ which corresponds to the average distance between polymer chains as shown in Figure 4.

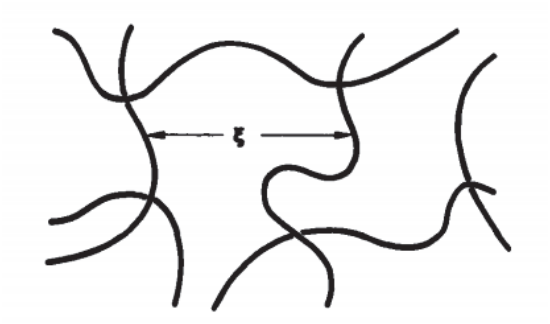


Figure 4 Correlation length between polymer chains in semi-dilute solution (*c*>*c) (DeGennes 1979)**

This length only depends on the polymer concentration and does not depend anymore on the polymerization degree N, according to the relation:

$$\xi \propto R_F \left(\frac{c}{c^*}\right)^{-3/4} \propto c^{-3/4} \tag{5}$$

In the semi-dilute regime, above the correlation length the long-distance interactions are inexistent. De Gennes expresses this by saying that a polymer chains can be split in N/g units called blobs. These units have a length ξ and contain *g* segments. Blobs will not interact with other chains while inside a blob there are excluded volume interactions and the size of the blob is given by the expression $\xi \propto g^{3/5}$.

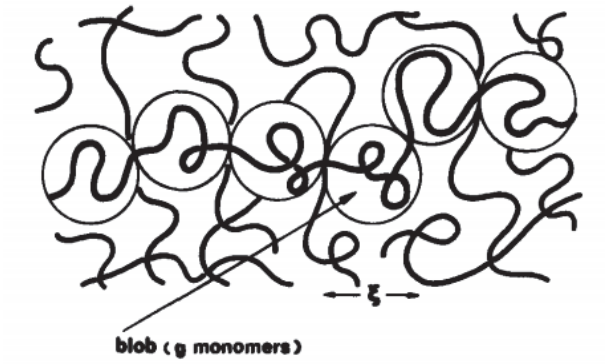


Figure 5 Schematic representation of blobs in a semi-dilute solution of polymer (DeGennes 1979)

The end-to-end size of a polymer chains containing N/g blobs of size can be written as:

$$\langle r^2 \rangle \propto \frac{N}{g}\xi^2 \propto N\xi^{1/3} \propto Nc^{-1/4} \tag{6}$$

Finally, in a concentrated solution when c is much larger than the concentration $c^{¥}$ the behavior of the polymer chains is similar to the behavior of the pure polymer: the dimensions are independent of the concentration.

1.2. Fluorinated polymers: PVDF and VDF-based copolymers

1.2.1. Synthesis

The first aqueous polymerization of vinylidene fluoride (VDF, see Figure 6) was reported in 1948 (T.A. Ford 1948). VDF was polymerized using a peroxide initiator in water at temperature between 50 – 150 °C and a pressure of 30MPa. No surfactants or suspending agents were used in this polymerization process. Since, a large number of methods have been developed to synthesize PVDF, including emulsion, suspension and solution polymerization (Ebnesajjad 2013).

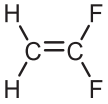


Figure 6 Vinylidene fluoride structure

In 1960, a manufacturing process was developed and PVDF (see Figure 7) was first introduced to the market.

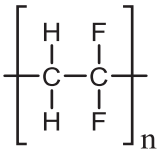


Figure 7 Polyvinylidene fluoride structure

Usually PVDF is produced by radical initiated polymerization of VDF, through aqueous emulsion or suspension processes. In these cases pressures of 10 - 300 atm, temperatures of 10 - 130°C and a fluorinated surfactant are required (Ameduri 2009). Indeed, only these processes are commercially practiced because water provides a sufficient heat sink for the large heat release associated with VDF polymerization (J.E. Dohany 1989). The suspension polymerization process leads to polymers with fewer structural defects ("head-to-head" or reverse monomer additions) in the molecular chains, i.e. polymers which are more crystalline. Thus the melting temperature and crystallinity ratio are higher than those of the homopolymers with the same average molecular weights obtained by emulsion polymerization.

The polymerization procedures, temperature, pressure, recipe ingredients, monomer feeding strategy and post-polymerization processing are variables that influence the characteristics and quality of the obtained polymer.

Emulsion polymerization

In the emulsion process of vinylidene fluoride, a water-soluble perfluorinated-emulsifying agent (a surfactant) is used to avoid radical scavenging reactions during polymerization and produce a stable latex with the desired solid content. The most suitable surfactant for this polymerization is a fluorine-containing acid salt of a fluoroalkanoic: perfluoroalkylcarboxylate salts are cited in many VDF polymerization process patents (Dohany , McCarthy, Williams et al. 1998). Chain transfer agents, buffers, or both, may also be used. Chain transfer agents will regulate the molecular weight of the polymer, and buffers will regulate the pH of the aqueous polymerization media. Water-soluble or monomer-soluble initiators for the emulsion process are used as a source of free radicals to initiate

the reaction. They can be: persulfate salts, organic peroxides such as disuccinic acid peroxide, β-hydroxyalkylperoxide, alkylperoxybutyric acid or di-tert-butyk peroxide (Ameduri 2009). A redox system or a combination of fluoroaliphatic sulfonate and bromate salts can also be used as a source of free radicals to initiate VDF polymerization. Usually the polymer particles are solid and partially crystalline with diameters ranging from 100 to 250 nm depending on the surfactant concentration. Particles are formed in the early stage by a homogeneous nucleation mechanism since VDF is in the vapor state. After filtration, rinsing and drying, a fine powder is recovered.

Suspension polymerization

The processes described for the emulsion polymerization are similar to those used for suspension polymerization. This method requires a dispersing medium (water + suspending agent). A large variety of suspending agents exists and they are used to reduce coalescence and agglomeration of polymer particles during polymerization (J.E. Dohany 1989). These colloidal dispersants are generally water-soluble polymers such as cellulose derivatives or poly(vinyl alcohol). In addition, organosoluble initiators such as diisopropylperoxydicarbonate, tert-butylperoxypivalate or di-tert-butyl peroxide are used depending upon the polymerization temperature. The choice of the nature and concentration of the initiator is fundamental to obtain a correct reaction kinetic and a good quality of the final product. In some cases, chain transfer agents are added to control the molecular weight of the polymer and can be diethylcarbonate or ethylacetate. The product is a slurry of suspended particles, usually spheres of 15 to 120 µm. The PVDF powder can then be recovered by filtering or separating the particles from water, through rinsing and drying.

Secondary polymerization methods

In addition, still other polymerization processes, such as solution or supercritical CO_2 polymerization, have been investigated to produce PVDF.

In the case of solution polymerization, VDF can be polymerized in fluorinated or chlorofluorinated solvents. Organic peroxides (e.g. bis(perfluoropropionyl) peroxide or bis-4-tert-butylperoxycyclohexyldicarbonate) or radiation are used as initiators. In the case of organic initiators, radicals are produced by a hemolytic scission of the oxygen – oxygen bond. Polymerization takes place in a homogeneous phase, and the resulting PVDF is insoluble in the solvent, making the polymer easily separable from the solvent. In the case of solution polymerization, conversion rates of PVDF and molar weights are lower than those obtained during emulsion or suspension polymerizations.

The polymerization technology based on supercritical CO_2 has been first reported by DeSimone (Ahmed, DeSimone et al. 2007). This method offers an advantage in the polymer isolation step where a clean dry polymer is produced by a simple depressurization. The residual monomer(s) and CO_2 are then recycled back to the reactor. However, the adequate CO_2 density requires a pressure higher than in a conventional emulsion polymerization. The obtained PVDF is not soluble in CO_2 and will precipitate during the polymerization.

Copolymerization of VDF: synthesis of P(VDF-co-HFP)

Poly(vinylidene fluoride-co-hexafluoropropylene) (P(VDF-co-HFP), see Figure 8) was first developed in 1957 by DuPont company, under the Viton trade name (Améduri, Boutevin et al. 2001).

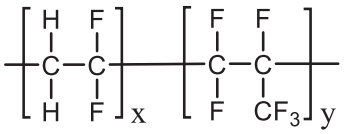


Figure 8 Poly(vinylidene fluoride-co-hexafluoropropylene) structure

The polymer is produced by radical copolymerization of VDF and hexafluoropropylene (HFP) at temperatures up to 100°C. The same processes than for the polymerization of PVDF can be used for the production of P(VDF-co-HFP): emulsion, suspension, solution (Gelin and Ameduri 2005) or supercritical CO_2 (Costa, Storti et al. 2010) as shown in Figure 9.

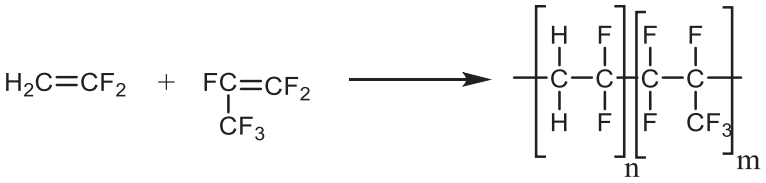


Figure 9 Radical copolymerization scheme

The emulsion copolymerization of VDF and HFP and its kinetics was investigating by the group of Apostolo (Apostolo, Arcella et al. 1999). In this case the experimental conditions are a temperature between 40 and 90°C and a pressure from 1 to 4 MPa. In such conditions the two monomers are in gas phase. No emulsifier was needed, ammonium persulfate (APS) was used as free-radical initiator and ethyl acetate was used as chain transfer agent.

Depending on the fraction of HFP within the polymer, different kinds of products were obtained. To date, thermoplastic P(VDF-co-HFP) copolymers are currently produced by Solvay (under the name Solef) or Arkema (under the name Kynar) while elastomeric P(VDF-co-HFP) are produced by Solvay, DuPont, Daikin…

1.2.2. Solubility in organic solvents

To develop materials by a solvent route it is highly important to understand the solubility behavior of PVDF in solvents.

Bottino et al. (Bottino, Capannelli et al. 1988) have studied the solubility of PVDF in about 50 solvents having known solubility parameters. From these experiments the solubility envelope of the polymer in the Hansen three-dimensional space and the values of the solubility parameters have been evaluated. Liquids were first classified in four categories depending on their ability to dissolve PVDF:

i. Solvents: clear polymer – solvent solutions are obtained after cooling at 20°C
ii. Good swelling agent: the polymer strongly swells and partially dissolves at high temperature but precipitates as temperature decreases
iii. Bad swelling agent: the polymer undergoes only little swelling even at high temperature
iv. Non solvent: the polymer undergoes no apparent physical change and/or precipitate

Good solvents of PVDF are: N,N-dimethylacetamide (DMA), N,N-dimethylformamide (DMF), dimethylsulfoxide (DMSO), hexamethylphosphoramide (HMPA), N-methyl-2-pyrrolidone (NMP), tetramethylurea (TMU), triethylphosphate (TEP) and trimethylphosphate (TMP) even though it is

generally necessary to increase the polymer – liquid solution temperature (to 60°C) of all solutions to enable the dissolution of the polymer. Moreover, the kinetic of dissolution of the polymer strongly depends on the nature of the liquid. PVDF is a semi-crystalline polymer and, to be dissolved, it requires disrupting crystalline regions. At ambient temperature the interaction energy between the polymer and the liquid are not strong enough compared to the interaction energy of polymer chains. As a consequence, the polymer will not be dissolved and will only swell due to the penetration of the liquid in the amorphous phase. As temperature increases, the polymer dissolves due to the reduction of the interchain interactions and the penetrarion of the liquid in the crystalline regions.

In addition, among the forty-six studied liquids, thirteen were found to be good swelling agents: in these liquids, under heating, the polymer strongly swells and partly dissolves but when the temperature decreases the polymer will precipitate. Among these good swelling agents we can find ketone solvents like methyl ethyl ketone (MEK) and γ-butyrolactone, that are widely used to solubilize PVDF and VDF-based copolymers, as well as tetrahydrofuran (THF).

After this extensive study of the solubility of PVDF in different liquids, it was found that semicrystalline PVDF and VDF-based copolymers converted to thermoreversible gels (Okabe, Wada et al. 2003) in ketones and lactones. In this context the Flory-Huggins interaction parameter between PVDF or P(VDF-co-HFP) and a large range of organic solvents was investigated. Among these solvents we can find alkane, alkene, ketone, lactone and nitrogen-containing solvents. The Flory-Huggins interaction parameter was determined by inverse gas chromatography (IGC) measurements and then this parameter was correlated with the thermoreversible gelation of solutions of PVDF and its copolymer. Figure 10 shows the relation between the Flory-Huggins interaction parameter (χ_{12}) and temperature (T) for different P(VDF-co-HFP) solutions in different solvents.

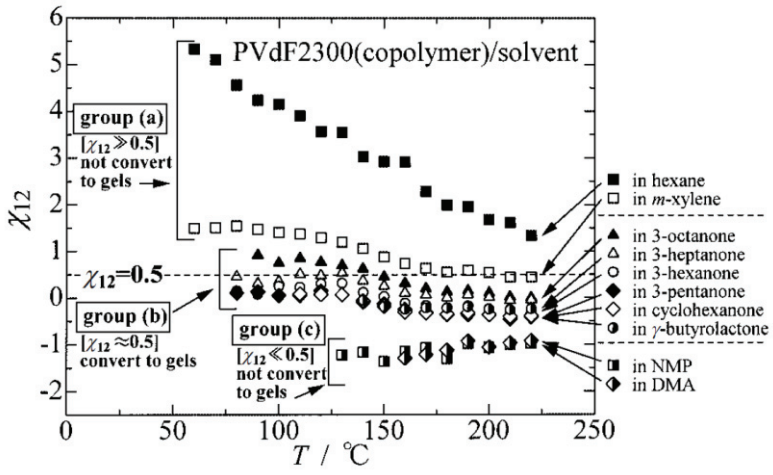


Figure 10 Relation between the Flory-Huggins interaction parameter and temperature for P(VDF-co-HFP) solutions in ten solvents (Okabe, Wada et al. 2003)

It can be seen that for all the solvents, the parameter χ_{12} decreases by increasing the temperature meaning that at lower temperatures all the solvents behave as poor solvents for P(VDF-co-HFP). Moreover, depending on the value of the Flory-Huggins interaction parameter at room temperature it was possible to distinguish three groups of solvents:

i. Group a: alkane and alkene solvents (here hexane and m-xylene) with $\chi_{12} \gg 0.5$. These solvents are considered to be poor solvents of the polymer and will lead to a liquid/solid phase separation and precipitation of crystallites with cooling.
ii. Group b: ketone and lactone solvents with $\chi_{12} \approx 0.5$. In this group of solvent P(VDF-co-HFP) (and PVDF) solutions will convert to thermoreversible gels at room temperatures. By going back to the study of Bottino et al. it appears that these solvents are in reality good swelling agents of the polymer. Moreover we can see that by increasing the number of carbons of the carbon backbone chains, the χ_{12} parameter increases and becomes closer or superior to 0.5 meaning that the solvents become poorer solvents of the PVDF.
iii. Group c: polar solvents (here NMP and DMA) with $\chi_{12} \ll 0.5$. P(VDF-co-HFP) and PVDF solutions in polar solvent will not convert to gels when cooling back to room temperature. No phase separation will occur: these solvents, in relation with the study of Bottino et al., are effectively good solvents of the polymer.

1.2.3. Properties

Properties of PVDF and VDF-based copolymers

In comparison to other perfluorinated polymers (like PTFE), PVDF is mechanically stronger, more resistant to abrasion and this polymer shows an excellent resistance to both creep under long-term stress and fatigue during cyclic loading (Bretz, Hertzberg et al. 1981, Castagnet, Gacougnolle et al. 2000). PVDF also presents an excellent thermal stability, resistance to UV light and high energy radiation and is inert to various solvents like oils and acids and shows low permeabilities to gases and liquids. Moreover PVDF is not hygroscopic and adsorbs less than 0.05 wt% of water at room temperature (J.E. Dohany 1989).

The properties of PVDF strongly depend on the chemical composition, molecular weights and molecular architecture (Carraher 1984). These characteristics are dictated by the polymerization method, namely the reactants and the thermal and mechanical history during the polymerization. For example, the choice of initiator and chain-transfer agent will determine the chemistry of the end groups that will affect the thermal stability.

PVDF is a very attractive polymer due to its piezoelectric, pyroelectric and ferroelectric properties. However it is important to highlight that these properties of PVDF and its copolymers are highly dependent on the crystalline content and crystalline structure of the polymer (El Mohajir and Heymans 2001). Long sequences of VDF units are involved in the polymer chain and several conformations of the polymer exist. Usually as produced PVDF is 35-70% crystalline depending on the polymerization method and the finishing conditions (Ameduri 2009). This semi-crystalline polymer has a complex structure and can exist in five crystalline polymorphs α, β, γ, δ and ε (Lovinger 1982). Figure 11 represents the most frequently observed crystalline conformations of PVDF: α, β and γ (Martins, Lopes et al. 2014). The polymorphism is related to the fact that the Van der Waals radius of the fluorine atom (1.35 Å) is larger to the radius of the hydrogen atom (1.20 Å).

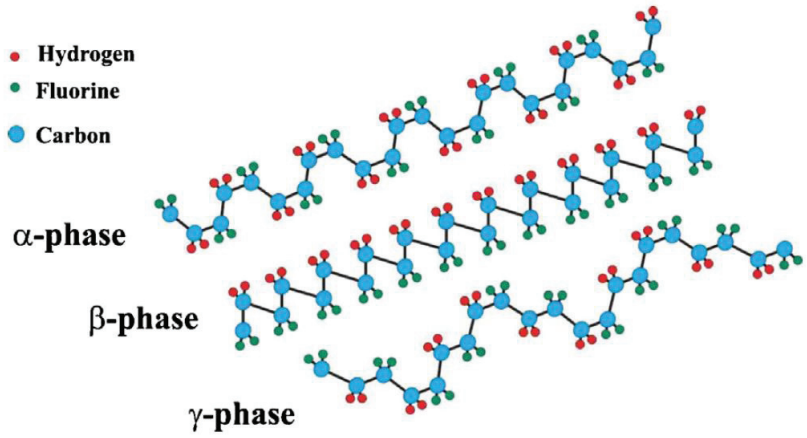


Figure 11 Main polymorphs of PVDF

The most common crystalline phase (Bachmann and Lando 1981) of PVDF is the α phase (or Form II) which has a density of 1.92 g.cm^{-3}. In the α phase, polymer chains are in trans-gauche-trans-gauche (TGTG') nonpolar conformation: hydrogen and fluorine atoms alternate in a regular way on both sides of the chain. This phase is the most kinetically favorable polymorph and its conformation (a combination of a helical and planar zigzag conformation) minimizes the steric influence between fluorine atoms along the chain. The β phase (Form I) is the most thermodynamically stable form (density of 1.97 g.cm^{-3}). This phase of the PVDF has all trans (TTT) planar zigzag conformation (Nasef, Saidi et al. 2002, Salimi and Yousefi 2003): fluorine atoms are located on one side of the carbon backbone chain and hydrogen atoms on the other side of the chain. This crystalline phase of the polymer is less favored but is obtained by mechanical deformation of PVDF or thermal treatment: straining, stretching or quenching the PVDF. The orientation of the $-CH_2CF_2-$ units along the polymer chain, with all the fluorine atoms on the same side of the chain, is at the origin of the very interesting piezoelectric, pyroelectric and ferroelectric behavior of the β polymorph of PVDF, as fluorine atoms are strongly electonegative (Kepler and Anderson 1978). Finally, the γ phase consists essentially of a distortion of the α phase. The γ phase (Form III) shows an intermediate polar conformation (T_3GT_3G'). This polymorph, with a density of 1.93 g.cm^{-3}, is usually obtained for ultra-high molecular weight PVDF or when the polymer is moderately stressed or annealed under high temperature (Weinhold, Litt et al. 1982). The two other crystalline forms are not typical structures that exist in commonly produced polymer. These crystalline phase structures have been widely characterized especially with the influence of the molecular weight and chain end groups on crystal forms of PVDF polymers (Hasegawa, Takahashi et al. 1972, Kobayashi, Tashiro et al. 1975). In addition, PVDF has a density of 1.68 g.cm^{-3} in the amorphous state. Moreover, the melt density of PVDF homopolymers is approximately 1.45-1.48 g.cm^{-3} at 230°C under a pressure of 1 bar. PVDF also presents four relaxation temperatures at 100°C (α'), 50°C (α"), -38°C (β) and -70°C (γ).

The main interesting properties of PVDF strongly depend on the crystalline structure of the polymer. A superior dielectric permittivity was highlighted for the β form and is due to the orientation of dipoles in the crystalline phase. The more polar β phase attracts technological interest because it accounts for the pyroelectric and piezoelectric properties. Indeed, the origin of the piezoelectricity in PVDF is usually explained in terms of a "dipole model". Because of the difference between the electronegativity of fluorine atoms with hydrogen and carbon atoms, VDF monomer units show a

strong electrical dipole moment (5-8 x 10^{-30} C.m). By packing the VDF units in different conformations, the final morphology shows an overall dipolar contribution per unit cell. The β phase is the phase with the highest dipolar moment per unit cell (8 x 10^{-30} C.m). The crystalline phase of the PVDF is composed of two major contributions: α (antiparallel packing of dipoles) and β (parallel alignment of dipoles). When an electrical field is applied dipoles will rotate around the axis that will lead to chain alignment. As a consequence, a net polarization will occur and will be responsible for the piezoelectric effect in PVDF.

Different characteristics of the PVDF were assessed: a dielectric constant between 8.15 – 10.46, a dissipation factor between 0.005 – 0.026 at 25°C and 1 kHz and a Curie temperature in the range of 195 – 197 °C. The glass transition (T_g) of the amorphous PVDF regions is in the range of -40°c to -30°C while the melting temperature of the crystalline regions is in the range of 155°C to 192°C, depending on the sample (molecular weight, defects of chaining) and the testing method.

Properties of P(VDF-co-HFP)

However, three major disadvantages are highlighted for PVDF: the high melting temperatures which generate energetic costs for processing the polymer, the poor solubility in common organic solvents and the difficult curing of these materials. In this context VDF-based copolymers have drawn more interest. Using P(VDF-co-HFP) copolymer allows in a first step to work with polymers with a better thermal stability, resistance to chemicals and a lower swelling to oils and hydrocarbons compared to PVDF and other PVDF copolymers such as polyvinylidene –co- tetrafluoroethylene (P(VDF-co-TFE)) (Dixon, Rexford et al. 1957). By varying the content of hexafluoropropylene it is possible to tune the properties of the copolymer and it will lead to various kinds of products. Moreover, incorporating HFP groups enhances the fluorine content, which results in even higher hydrophobicity of P(VDF-co-HFP).

The influence of the HFP concentration in the final copolymer on different properties of the polymer has been widely studied:

i. Influence of the VDF/HFP ratio and fluorine content on the structure and end use properties
ii. Influence of the VDF (or HFP) content on the crystallinity of copolymers (Moggi, Bonardelli et al. 1982)
iii. Influence of the composition on the glass transition temperatures (T_g) (Bonardelli, Moggi et al. 1986)
iv. Influence of the composition on the crosslinking mechanism

Previous works on P(VDF-co-HFP) demonstrated that crystallinity and order decrease as the HFP concentration increases. Figure 12 shows that at less than 19 mol% of HFP, the copolymer will still be semi-crystalline and will have a thermoplastic behavior (Lo 1965), while pure elastomeric behavior can be found for a higher HFP content (Moggi, Bonardelli et al. 1982, Logothetis 1989). A concentration of 20-21 mol% of HFP represents in reality the best compromise between the requirements of a low T_g and a fully amorphous polymer (Ajroldi, Pianca et al. 1989).

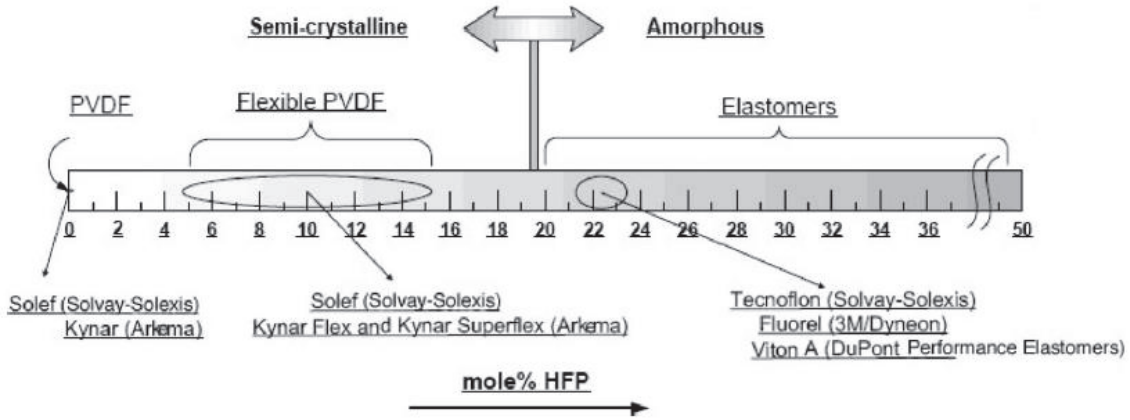


Figure 12 Variation of the properties (thermoplastic or elastomer) of P(VDF-co-HFP) according to the HFP content

The polymorphisms of PVDF is not significantly affected in the presence of a small amount of HFP. Indeed, the correlation of the copolymer microstructure with the glass transition, melting temperature and crystallinitie of P(VDF-co-HFP) was investigated by Moggi's group (Moggi, Bonardelli et al. 1982). It was also found that the concentration of HFP will impact the melting temperature of the thermoplastic copolymer: by increasing the concentration of HFP the melting point of the copolymer decreases (Tarascon, Gozdz et al. 1996).

P(VDF-co-HFP) has gained much interest due to its excellent properties such as high conductivity and high dielectric constant (ε≈8.4). However, the dielectric properties are lower than those of polyvinylidene fluoride –co- trifluoroethylene (P(VDF-co-TrFE)) copolymers.

1.2.4. Applications

PVDF homopolymers and copolymers have a wide range of applications: high-purity semiconductors, wire and cable products, coatings and paints, food and pharmarceutical industries, water treatment membranes, component of electrolytes and Li-ion batteries or binder for electrode materials (Ebnesajjad 2013). Indeed since 1996 an increasing interest was developed in the use of PVDF in the battery industry as binders for cathodes and anodes in Li-ion batteries and as battery separators in Li-ion polymer batteries (J.E. Dohany 1989). It is known that PVDF polymers and copolymers can bring specific electrical properties and find energy applications in electronics and electronical devices as insulation, sensors, energy harvesting devices and actuators (Xia and Zhang 2018).

In this part we will study in more details the energy applications of P(VDF-co-HFP) because Chapter 6 is focussed on the processing and characterization of films obtained by solvent route for energy storage applications. One advantage of P(VDF-co-HFP) is that it can be tuned from semicrystalline to amorphous according to the HFP content. The energy related applications of P(VDF-co-HFP) extend to (i) polymer electrolyte membranes for fuel cell (PEMFC) like in the work of Niepceron et al. (F. Niepceron 2008) where nanosilica was embedded inside (i) rechargeable lithium-ion batteries (Tarascon, Gozdz et al. 1996, Sanchez, Alloin et al. 2005) as a host for liquid electrolyte (ii) dye-sensitized solar cells (DSSC) in a microporous state with incorporation of nanoparticles like silica (Wang, Zakeeruddin et al. 2004), TiO_2, etc. (Zhang, Han et al. 2008) Recently, thin films of PVDF-HFP have also been extensively studied for their high breakdown strength, which is an important factor in determining energy density and shows potential for applications like capacitors.

Zhou X. and al. (Zhou, Zhao et al. 2009) obtained ultrahigh energy density (>25 J/cm3) by improving the PVDF-HFP film quality. Chu B. and al. (Chu, Zhou et al. 2006) have shown the possibility to reach a high electric energy density and fast discharge speed. At the same time, R. Dong and al. assessed this capability by simulations (Dong, Ranjan et al. 2016).

1.3. Fillers

1.3.1. General introduction on fillers

Fillers are solid particles which can change the physical and chemical properties of materials by surface interaction and by their own physical characteristics (Wypych 2016). Fillers were first added to materials to reduce the cost of the materials. However, in addition to cost reduction, fillers also modify the materials density, their surface, thermal, electrical, mechanical, optical properties, durability, permeability properties… In this context fillers are now widely used because they can be modified and tailored to any application and they can modify or improve practically all properties of the material. Depending on the nature and properties of the fillers, they are used in different applications like plastics, construction, energy-storage, paints and coatings.

Among these materials nanoparticles have gained more and more attention over time. Nanoparticles are particles or aggregates with a size between 1 and 100 nanometers which are made of carbon, metal oxides or organic matter (Hasan 2015). Nanoparticles are characterized by the surface layer (which can be functionalized by small molecules, metal ions, surfactants or polymers), and the core (the central portion of the nanoparticle) (Shin, Cho et al. 2016). Nanoparticles are synthesized by various methods which are divided in two classes (i) bottom-up (sedimentation and reduction techniques) and (i) top-down (decomposition of a larger molecule into smaller units) (Wang and Xia 2004). Nanoparticles may be classified according to their morphology, shape, size and chemical properties, to date there are well-known classes (Cho, Holback et al. 2013),(Khan, Saeed et al. 2017):

i. Carbon-based: fullerenes and carbon nanotubes (the two major classes of carbon-based nanoparticles) have electrical conductivity, high strength, structure, versatility and electron affinity. They are often used as fillers in nanocomposite materials.
ii. Metal: they are made of metals precursors (Cu, Ag, Au…) and possess unique optoelectrical properties.
iii. Ceramics: inorganic nonmetallic compounds
iv. Semiconductors: they possess properties between metals and nonmetals and show wide bandgaps
v. Polymers: organic based nanoparticles that are mostly nanospheres and nanocapsules.
vi. Lipid-based

Compared to the similar particles at higher scales, nanoparticles exhibit enhanced and unique physicochemical properties. Indeed, nanoparticles show an extremely large specific surface area, leading to an increased reactivity or stability in a chemical process, enhanced mechanical strength, etc (Anu Mary and Saravanakumar 2017). Their unique properties have led to their use in various applications: cosmetics and sunscreens, electronics (Teng, Jeng et al. 2008, Lu, Xu et al. 2010), catalysis, medicine, food, construction (Nazari and Riahi 2011), tyres or energy.

In this context silica (Zou, Wu et al. 2008), carbon black (Zhang, Wang et al. 2000) and clay (Jeevanandam, Barhoum et al. 2018) are widely used as nanoparticles fillers in industrial applications.

1.3.2. Silica particles and nanoparticles

Silica (or silicon dioxide) can be crystalline or amorphous. Even though silica is commonly found in natural products (quartz, plants…), amorphous silica is synthetized to be commercially used (Iler 1979). Commercial sources of silica nanoparticles exist as powder or colloid and different fabrication processes are used (Leyden 1996). Nanosilica powder is produced by the fuming method or the precipitation method in industry while colloidal silica solutions are produced by sol-gel or microemulsion methods (Darbandi, Thomann et al. 2007).

Various processes are used to produce **colloidal silica** and lead to colloidal dispersions of micro- or nano- particles of silica. In 1968, Stöber, Fink and Bohn (Stöber, Fink et al. 1968) developed a process now widely used and named as the Stöber process to synthesize colloidal silica by a sol-gel method. This process consists on a hydrolysis-condensation reaction of tetraalkoxysilanes (usually tetraethoxysilane, TEOS) in an alcoholic medium (ethanol or water-ethanol mixture) with an ammonium catalyst. The overall reaction is expressed as follows:

$Si(OC_2H_5)_4 + 2H_20 \rightarrow SiO_2 + 4C_2H_5OH$ (Ibrahim, Zikry et al. 2010)

This reaction appears to be a simple, effective and reproducible way to produce monodisperse and stable particles with diameters ranging from tens of nanometers to about 2 microns. On the other hand the group of Osseo-Asare (Osseo-Asare and Arriagada 1990) later used an inverse microemulsion method to prepare monodisperse silica nanoparticles.

Colloidal silica solutions are stable: solid particles will not sediment or agglomerate within a wide range of conditions. Indeed, these solutions are stabilized against interparticle siloxane bonding by (a) ionic charge on particles where particles will be separated by charge repulsion or (b) steric repulsion induced by functionalizing silanol groups. Stabilization of silica nanoparticles by ionic charges can be explained by the DLVO theory on spherical particles (Verwey 1947, Derjaguin and Landau 1993). It describes the stability of colloidal suspensions in terms of interaction energy between the particles which depends on the distance between particles. Silica particles in suspension are stabilized due to the superposition of Van der Waals forces upon repulsion forces which occur when particles approach each another. The development of surface charge on the particle is accompanied by the formation of a countercharge which results in an electrochemical double layer which is essential in the stabilization of colloids in suspension (Wypych 2016). As a consequence the stability of silica solution strongly depends on different factors: pH (see Figure 13), particle size and concentration, electrolytes and solvents and finally temperature.

Steric stabilization of particles solutions was introduced by Smitham, Evans and Napper (Smitham, Evans et al. 1975), and Bagchi (Bagchi 1974): they have shown that aqueous silica solutions were stabilized by adsorbing nonionic surfactants on the surface of silica particles. Steric stabilization consists in grafting molecules/ligands to the surface of the colloidal particles to form a protective layer and prevent agglomeration of the particles. This method is usually used to prevent agglomeration and obtain good filler dispersion when particles are transferred from their original polar solvent (often water or ethanol) to other solvents (by solvent exchange or distillation). Indeed, changing the solvent may strongly destabilize the particles and promote agglomeration.

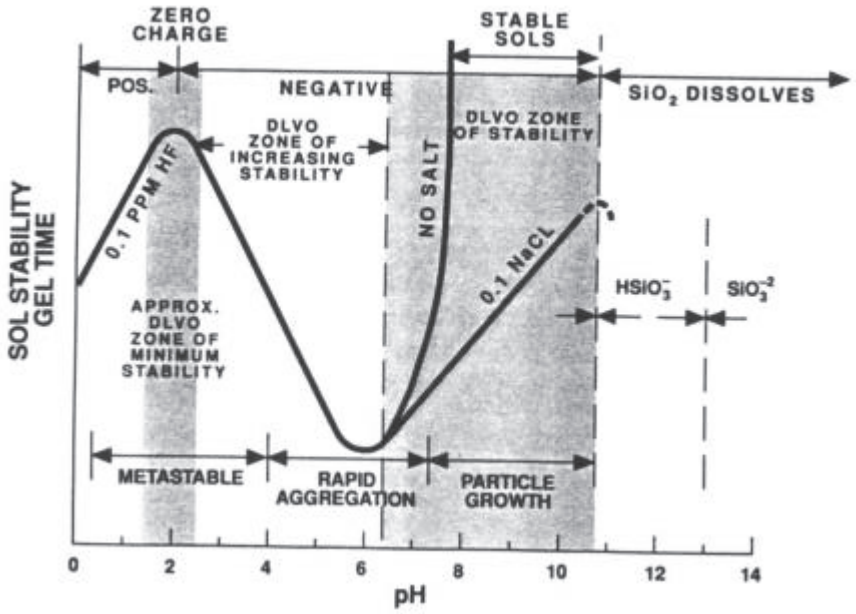


Figure 13 Effect of pH in the colloidal silica - water system

Alternatively, silica powders are commercially obtained by fuming or precipitation methods. **Fumed silica** is obtained by a high-temperature vapor process (Vassiliou, Papageorgiou et al. 2007). During the reaction $SiCl_4$ is hydrolyzed in a flame of oxygen-hydrogen:

$$SiCl_4 + 2H_2 + O_2 \rightarrow SiO_2 + 4HCl$$

P**recipitated silica** consists on aggregates of particles of colloidal size and is usually prepared from the reaction of an acid (sulfuric or hydrochloric) on a sodium silicate solution by fixing the pH to 7 (H.S. Katz 1987). The sodium silicate is neutralized by the acid and leads to the formation of silanol groups (hydrolysis) which combine to form Si-O-Si siloxane bonds (condensation) according to the reaction (Iler 1979):

$$SiO_4^{4-} + 4H^+ \rightarrow Si(OH)_4 \text{ (hydrolysis)}$$

$$-SiOH + HOSi- \rightarrow -SiOSi- + H_2O \text{ (condensation)}$$

The formation of strong siloxane chemical bonds between the particles induces the formation of aggregates which cannot be destructured by grinding or by dispersion. Hydrogen or Van der Waals bonds will then arrange aggregates into agglomerates, which can be broken e.g. during melt mixing in a higher viscous polymer.

1.3.3. The surface chemistry of silica

Free silica surface is mainly constituted of two types of chemical groups (see Figure 14): (i) siloxane bridges (Si-O-Si) with oxygen atoms on the surface. These groups are poorly reactive and have a hydrophobic behavior and (ii) silanol groups (Si-OH) that can lead to interactions and/or chemical reactions (like grafting) between silica nanoparticles and reagents.

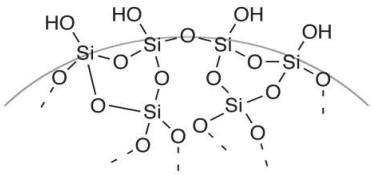


Figure 14 The surface of silica

Hydroxyl groups are randomly located on the surface of silica. It is then possible to classified surface silanols into three groups with different reactivities (Iler 1979, Morrow and McFarlan 1990, Zhuravlev 2000, Christy 2014), which are represented in Figure 15:

a) Isolated silanols: silicon atom forms three covalent bonds with core oxygen atoms and one covalent bond with the surface hydroxyl
b) Vicinal or bridged silanols: hydroxyl groups are close to each other and can interact through hydrogen bonds
c) Geminal silanols: two hydroxyl groups are bonded to the same silicon atom. These hydroxyl groups are too close to each other to interact via hydrogen bonds.

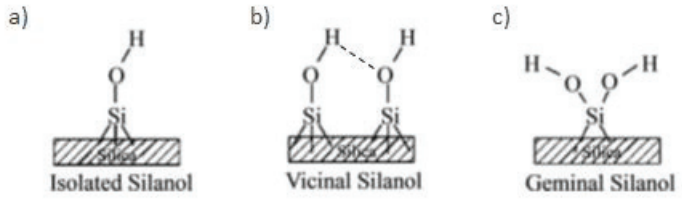


Figure 15 Surface silanol groups of silica

^{29}Si NMR and infrared spectroscopy (IR) can be used to characterize surface silanols. Vicinal silanols can easily be followed by IR while the other silanols are difficult to discriminate by IR (Takei, Kato et al. 1999). ^{29}Si NMR can be used to distinguish them, as each type of silanol will has a different chemical shift (Maekawa, Maekawa et al. 1991). Chemical shifts in ^{29}Si NMR (Leonardelli, Facchini et al. 1992) and characteristic IR peaks for all the different silanols are summed up in Table 1.

Table 1 Characteristic data in ^{29}Si NMR and IR

	isolated	vicinal	geminal
IR	3747 cm^{-1}	3650 cm^{-1}	3736-3742 cm^{-1}
^{29}Si NMR	Q^3 -100ppm	Q^3 -100ppm	Q^2 -90ppm

The density of silanols at the surface of the silica (i.e. the number of hydroxyl groups per unit of surface area) was found to be independent on the type of silica (E.F. Vansant 1995). Various experimental methods can be used to determine the fraction of silanols: proton NMR, infrared or Raman spectroscopy, dosage by compounds using boron trichloride or diazomethane (Mueller, Kammler et al. 2003) or TGA (Ek, Root et al. 2001). It is then possible to calculate theoretically the concentration of surface hydroxyl groups by several ways. Based on geometry of the particles and the density of the amorphous silica, Iler determined that there should be 7.8 silicon atoms and 7.8 SiOH groups per per nm^{-2} (Iler 1979). According to several studies it can be supposed that the number

of silanol on the precipitated silica surface is usually between 7 and 10 $SiOH/nm^{-2}$ (H.S. Katz 1987, Tuel, Hommel et al. 1990).

Moreover, it is important to highlight that at ambient temperature the silica surface is covered by water molecules adsorbed by hydrogen bonding. These bounded water molecules form layers at the surface of the silica. The amount of water varied according to the type of silica, humidity of the atmosphere and the surface modification of silica. Tripp and Hair (Tripp and Hair 1992) measured the amount of adsorbed water on silica surface and found that it would be around 2.5 to 4 water molecules/nm^2. To completely eliminate this layer of water, it is necessary to dry the silica at a temperature close to 190-200°C (Zhuravlev 2000): it will expose the surface hydroxyl groups. At higher temperatures (around 450°C) surface silanols will condense and form siloxane bonds. This will lead to the release of water molecules: this phenomenon is named deshydroxylation (E.F. Vansant 1995). However, to eliminate completely all silanols (isolated, vicinal and germinal) it is necessary to heat up to 1200°C.

As a consequence, the size, surface area, and surface chemistry of the nanoparticles will have a strong impact on the interactions between the particles or between the particles and the solvent and/or the polymer.

1.3.4. Surface-modification of silica

In reality the differences in the surface properties between the polymer and the silica particles often cause a phase separation phenomenon: indeed, silica nanoparticles are hydrophilic while polymers of interest are often hydrophobic (e.g. PVDF). As a consequence the interfacial interaction between the fillers and the polymer is a decisive factor: it is necessary to increase the compatibility between these two ingredients in order to have homogeneous properties of the final material (Schadler, Kumar et al. 2011). For similar reasons the solubility and dispersion of silica particles in organic solvents (alcohols, amides, ketones…) is also limited which restricts the use of these fillers is various applications. To enhance the interactions between silica particles and the solvent or the polymer and reach a good dispersion state as well as enhanced properties (Leyden 1996), the surface modification of the silica nanoparticles is required. This surface modification method can be performed on precipitated, fumed or colloidal silica (Iler 1979) and will modify their physical and chemical properties. The modification of silica nanoparticles can be carried out by different ways (Rong, Zhang et al. 2006):

i. Physical interaction: surfactants or macromolecules will adsorb onto the surface of silica nanoparticles via secondary forces (Van der Waals, hydrogen and electrostatic forces). In the case of a surfactant, adsorption on silica is driven by electrostatic interactions (a bond is formed between the silanol and the surfactant), up to the isoelectric point of the interface (Tyrode, Rutland et al. 2008). This method will allow reducing the interaction between silica particles and it will therefore prevent the agglomeration and promote the silica – polymer interactions. As a consequence, these particles can be easily incorporated into a polymer matrix. An usual surfactant is Cetyl TrimethylAmmonium Bromide (CTAB) which has been used to hydrophobize the surface of the silica (Liu, Tourbin et al. 2013) and improve the chemical interactions between silica nanoparticles and a polymer (Wu and Chu 2005). Polymers can also be adsorbed onto silica nanoparticles to promote their hydrophobicity (Reculusa, Poncet-Legrand et al. 2002, Reculusa, Poncet-Legrand et al. 2005, Yang, Dai et al. 2006).

ii. Chemical interaction: by creating a covalent bond between the modifiers and the silica nanoparticles, stronger interactions are obtained (Price, Clark et al. 2000). Typical modifiers are polymers or coupling agents (usually silanes).

Regarding the chemical modifications of silica surface by polymers, two main approaches exist: "grafting-to" and "grafting-from". As a consequence the interaction between particles will be reduced: a stable dispersion of silica is obtained and agglomeration of the nanoparticles will be prevented as shown in Figure 16. In the "grafting-to" method, end-functionalized polymers are first synthesized and then react with the surface of the silica and form a covalent bond (Ranjan and Brittain 2007). This is the simplest method to graft a polymer at the surface of the silica. However due to the steric hindrance at the silica surface it is difficult to attach additional chains and a relatively low graft density is usually obtained (Mora-Barrantes, Valentín et al. 2012).

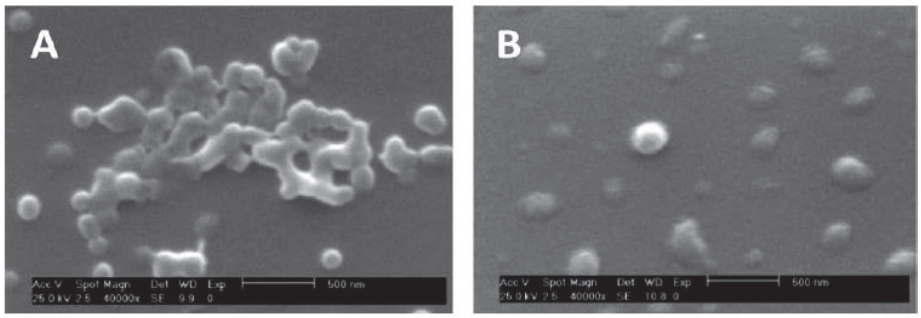


Figure 16 SEM micrographs of (A) unmodified fumed silica (b) polymer-grafted silica particles (Mora-Barrantes, Valentín et al. 2012)

On the contrary, in the "grafting-from" technique (also called surface-initiated polymerization), an initiator is grafted to the surface and it is followed by in situ polymerization of the monomer leading to the formation of "polymer brushes" or "hairy nanoparticles" (Zou, Wu et al. 2008). A large variety of mechanisms have been employed to synthesize these grafted nanoparticles: conventional radical (Shirai and Tsubokawa 1997), controlled radical (von Werne and Patten 1999), anionic (Zhou, Wang et al. 2002), cationic (Spange 2000) and ring opening polymerizations (Carrot, Rutot-Houzé et al. 2002).

The "grafting-from" approach may lead to a dense layer of polymer covering the nanoparticles while "grafting-to" methods provide a lower graft density.

In addition, a popular method to modify the surface of silica is the reaction of silanol groups with silane coupling agents in a suitable solvent (both for the silica nanoparticles and the coupling agents). The general structure of the organosilane is $R_nSiX_{(4-n)}$ where X represents a hydrolysable group (chloro, ethoxy or methoxy groups) and R an organofunctional non-hydrolysable end group (Mittal 2009). The R group can have a variety of functionalities and interact with the reacting medium. The X group will react with the hydroxyl groups on the silica surface and the R chain can react with a polymer in a second step: hydrophobic silica will be obtained. One of the most used organosilane is the bis[3-(triethoxysilyl)propyl] tetrasulfide (TESPT) (Dohi and Horiuchi 2007) but other silane coupling agents are commonly used such as the [3-(methacryloxy)propyl]trimethoxysilane (MPS).

Chemical and physical modifications of silica nanoparticles improve the reinforcing efficiency of silica and therefore final polymer – silica materials will show enhanced properties. However, it is

important to better understand the grafting mechanism of the silane at the surface of the silica. Silane grafting will be influenced by different parameters: silane nature, concentration, addition method as well as experimental conditions (pH, temperature, presence of water…) (Goerl, Hunsche et al. 1997). One of the crucial points is the presence of water at the surface of the silica particles or within the solvent. The presence of water will hydrolyze the functionalized groups of the silane molecules. As a consequence hydrolyzed silanes will condense with the silica surface groups and form siloxane bonds Si-O-Si (see Figure 17) (Arkles 1977, Azzopardi and Arribart 1994).

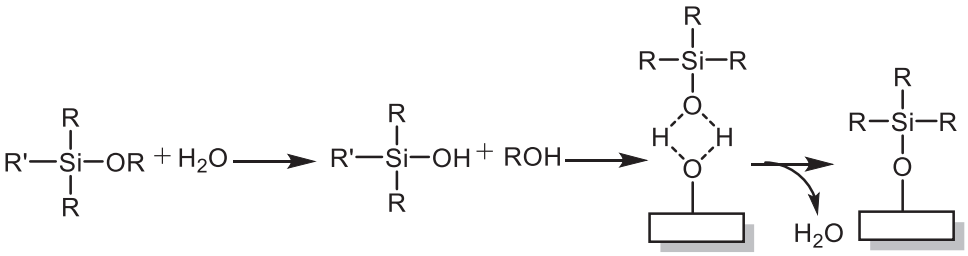


Figure 17 Grafting mechanism of a (monoalkoxy)silane on silica surface

However, this mechanism is an ideal mechanism. In reality complex reactions can occur. In the case of multifunctional silanes, groups which did not react will be hydroxylated from the water present in the reaction bath and will lead to further condensation steps. Moreover, this mechanism is based on the presence of water coming from the solvent or the silica surface. In the case of anhydrous solvent with dehydrated silica, the hydrolysis of the silane will not happen. In this case the reaction must occur between the surface and the reactive groups of the organosilane. Figure 18 describes the mechanism in the gas phase: the silane will exclusively react on siloxane bridges. In a first step, siloxane bridges are opened according to a concerted nucleophilic attack (between an oxygen atom of the siloxane bridge and an oxygen atom of the silane). Then a condensation of a second alkoxy on a close silanol occurs. It can be considered that the same mechanism is responsible of the grafting of silane on silica surface in an apolar and anhydrous medium (Bluemel 1995, Sutra, Fajula et al. 1999).

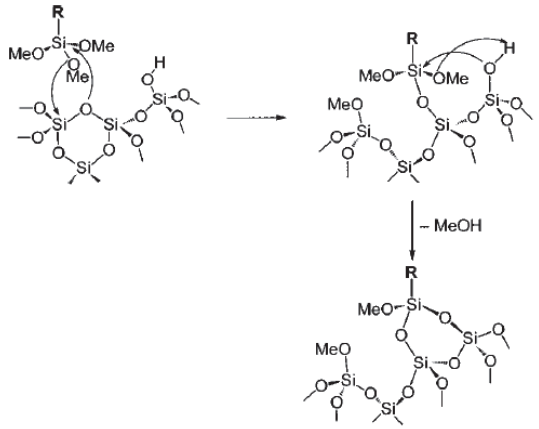


Figure 18 Silylation mechanism in the gas phase (Brunel, Cauvel et al. 2000)

1.3.5. Characterization of surface-modified silica nanoparticles

Different techniques can be used to characterize the surface of modified silica nanoparticles:

i. **^{29}Si solid-state NMR** has been widely used (Park and Cho 2003, Ramier, Chazeau et al. 2005, Valentin, Lopez-Manchado et al. 2006) for the analysis of the surface structure of silica. It allows the determination of the chemical species bounded to the silica (Albert, Evers et al. 1985, Mijatovic, Binder et al. 2000). Indeed, solid-state NMR allows distinguishing the different silanol groups and the siloxane bonds at the surface of the silica. As shown on Figure 19 the ^{29}Si CP-MAS NMR spectrum of untreated silica provides information on the type of silanol groups present on the surface of the silica and their proportions. The same measurements are then performed on surface-modified silica and the spectra are compared to the unmodified silica. Here we can see that there is a decrease of the resonances at -91ppm and -101ppm while there is an increase of the resonance at -109ppm. New resonances appear for the surface-modified silica. It is then possible to quantify the fraction of silanols which react with silane agents from the differences between the intensities of the peaks.

ii. **Infrared spectroscopy** is the second most used technique and is used to probe the existence of silane – silica grafting and is sometimes used to quantify the grafting ratio. Different methods are used: Raman spectroscopy, FT-IR (Vilmin, Bottero et al. 2014) or ATR. Indeed the intensity of the characteristic band of free silanols will decrease as well as the intensity of bounded silanol while the intensity of silane increases (Pathmamanoharan, Wijkens et al. 1996, Zhao and Lu 1998, Fadeev and Kazakevich 2002). For example Li et al. (Li, Xu et al. 2012) studied the functionalization of silica nanoparticles by click chemistry and ATRP (atom transfer radical polymerization) especially by FT-IR. The existence of siloxane groups is proved by the existence of adsorption peaks at 1113 cm^{-1} for both silica nanoparticles. When the surface of the nanoparticles is modified new adsorption peaks appear.

iii. **Thermogravimetric analysis (TGA)** will give an approximate fraction of silane at the silica's surface. Knowing the degradation temperatures of silanes it is indeed possible to extract from the TGA curves the fraction of grafted silane. This technique is widely used as a first investigation method (Chen, Zhou et al. 2005, Li, Xu et al. 2012).

In addition to these common methods, several complementary techniques can also be used to characterize the surface of surface-modified nanoparticles: X-ray photoelectron spectroscopy (XPS) or transmission electron microscopy (TEM) to study the morphology and size of grafted silica nanoparticles (Li, Xu et al. 2012, Pauly, Genix et al. 2015), atomic force microscopy (AFM) to study the organization of the functional groups at the surface of the silica (Berger, van der Werf et al. 1995, Baumgärtel, von Borczyskowski et al. 2013), zeta potential (Bagwe, Hilliard et al. 2006) or contact angle measurements (Belyakova and Varvarin 1999).

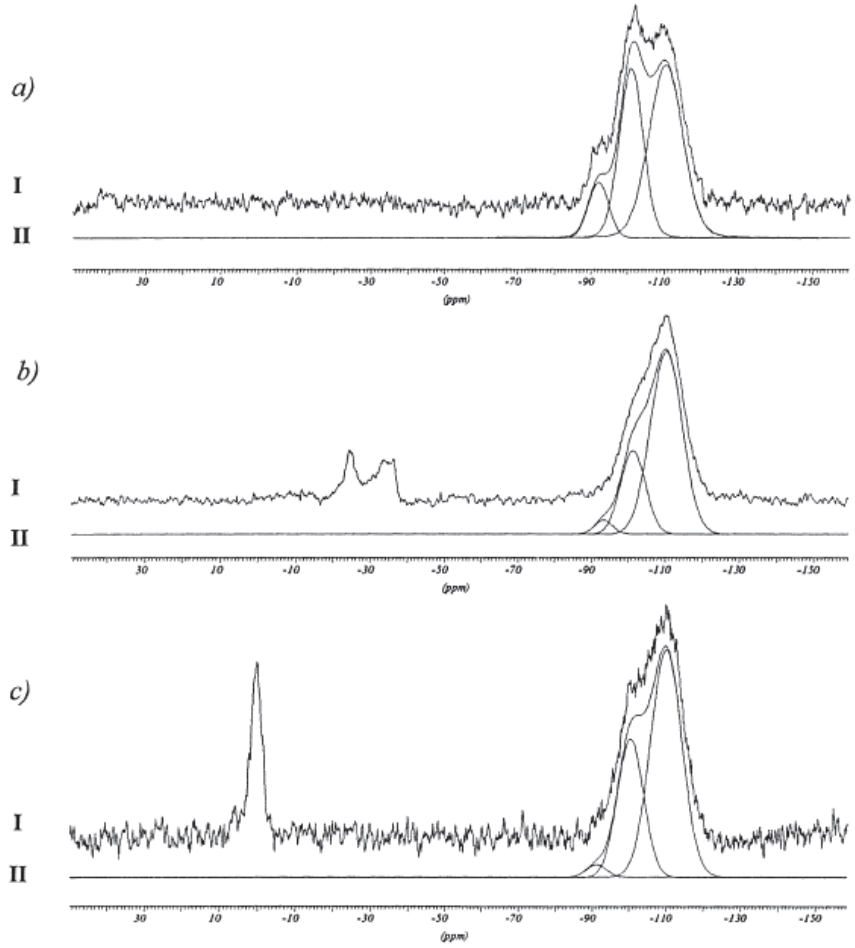


Figure 19 ^{29}Si CP-MAS NMR spectra of (a) unmodified silica (b) silica modified with dichloromethylvynilsilane (c) silica modified with chloromethylvynilsilane (Mijatovic, Binder et al. 2000)

1.4. Polymer gels

Numerous materials and especially polymer solutions in a solvent show a transition from liquid state to a soft solid state due to the formation of crosslinks between polymer chains: a tridimensional network is therefore formed. This phenomenon is called gelation.

Gels can be classified according different factors:

i. According to the source: natural or synthetic gels
ii. According to the solvent: hydrogels or organogels
iii. According to the type of crosslinks: chemical (permanent) or physical (thermoreversible) gels

Different types of gelation can occur depending on the interactions between polymer chains. Gels can be physical when gelation occurs by physical interactions (hydrogen bonding, Van der Waals interactions, chains overlap, hydrophobic or ionic interactions…) or chemical when the connection between polymers is permanent (covalent bonds through chemical crosslinks).

This phenomenon was described by critical percolation theory as early as 1970 and then numerous models have been developed to describe the kinetics of aggregation and gelation.

1.4.1. Physical and chemical gels

Physical gels

Physical gels are observed in natural materials (gelatin, proteins or polysaccharides) or in synthetic polymers such as polyesters, polyurethanes for example. In this case crosslinking is not due to a chemical reaction and the association between chains in physical gels is not permanent (Osada, Ping Gong et al. 2004). The density and strength of the crosslinks depend on the mechanical and thermodynamical state of the gel. Association between polymer chains can lead to strong or weak physical gels depending on the nature of the physical bonds:

i. Associative interactions: coulomb, dipole/dipole, Van der Waals interactions or hydrogen bonds
ii. Phase transition interactions: colloidal interactions, crystalline or glassy zones.

For strong physical gels the interactions between polymer chains are strong and gels may be considered to be permanent under proper experimental conditions (temperature, pH, presence of salts…). These types of gels are often thermoreversible. Schematics of thermoreversible gels are shown in Figure 20 (Nijenhuis 1997). Depending on the system (polymer, solvent…) the gelation comes from: (A) micellar crystallites, (B) helix formation, (C, D and E) phase separation, (F) complex formation or (G) interactions between mesogenic groups in the main chain and/or side chain (in liquid crystalline polymers). The strong physical gels are comparable to chemical gels.

Weak physical gels are formed by temporary association between chains leading to reversible links. These temporary bonds have finite lifetimes, breaking and forming continuously. Here the interactions can be hydrogen bonds, block copolymer micelles above the glass transition or ionic associations. Weak physical gels are not truly solids but in a certain time scale they can be considered as solid materials. These interactions can be easily broken by stirring, spraying or brushing.

It appears that the microscopic organization of physical gels is complex and strongly depends on the interactions between polymer chains, which in turn strongly depend on experimental conditions (and more specifically on temperature) (An, Solis et al. 2010).

Chemical gels

In contrast, chemical gels are formed by covalent bonds between polymer chains. This will lead to strong and permanent interactions (and therefore strong and permanent materials) which will not depend on the experimental conditions. There are three main processes to form a chemical gel: addition polymerization, condensation and vulcanization.

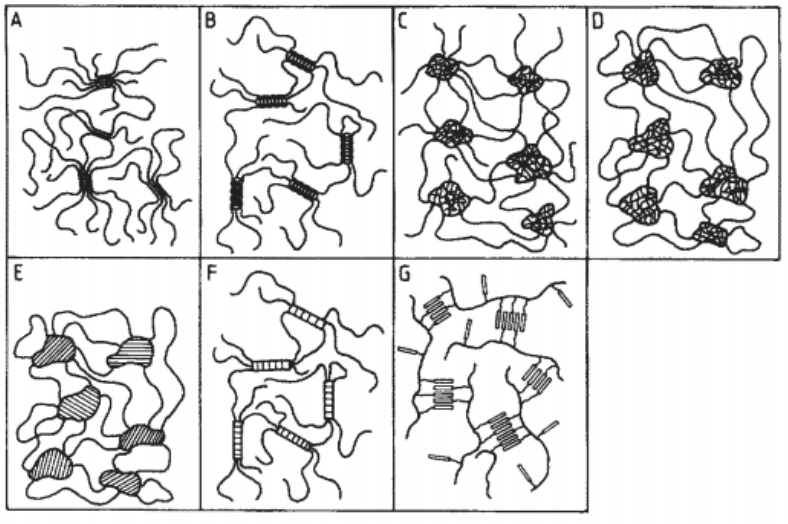


Figure 20 Schematic view of different kinds of thermoreversible gels (A) PVC/plasticizer (B) aqueous gelatin (C) attactic PS in CS2 (D) triblock copolymer SBS in tetradecane (E) PO-EO-PO triblock copolymer in water (F) s-PMMA and i-PMMA in toluene (G) dissolved SCLCP (Nijenhuis 1997)

A first approach to synthesize chemical gels is addition polymerization (Walling 1945). A typical example is the transfer of free radical from one vinyl to another: linear chains will be generated. In some case some monomers with two double bonds (divinyl derivatives: CH_2=CH-R_2-CH=CH_2) will react twice with free radicals: as a consequence, R_2 will become a cross-linking bridge in the structure. Condensation of polyfunctional units is a second method to prepare chemical gels. The idea is to start from a melt or a solution of monomers which will react with each other (Osada, Ping Gong et al. 2004). For example, chemical gels can be prepared from the condensation reaction of a difunctional acid with a trifunctional alcohol. When the three functions of the trialcohol react, the trialcohol becomes a branch point and lead to randomly branched polyesters (and a network) (Flory 1953, Osada and Gong 1999).. Finally, vulcanization corresponds to the bonding of long chains by sulfur. This approach is close to the condensation process.

When immersed in a solvent, chemical gels swell to various degrees depending on the compatibility with the solvent and the crosslink density but they do not dissolve, due to the covalent bonding between polymer chains.

1.4.2. Gelation theories

The sol-gel transition has been described by different types of models (Martin and Adolf 2003).

As in the Flory-Stockmayer theory, gelation can be described as a connectivity transition. It can be described as a percolation model at the crosslinks (Tokita 1989, M. Rubinstein 2003). Initially, monomers are uniformly dispersed and when the chemical reaction between monomers occurs, it can be modelled by randomly connecting monomers on neighboring sites by bonds. A parameter *p* called extent of reaction is then used to describe the fraction of bonds formed during the reaction. This parameter varies from zero to one: p=1 when the reaction is complete and all the bonds are formed (the entire polymer forms a network). Below the gel point the system is a solution of branched macromolecular chains while, above the gel point, the system is a gel that percolates through the whole volume (Figure 21). At the gel point (percolation point) defined as p_c, an infinite

cluster appears. At this point the structure of the material is very different from the structure of the final gel, with only a small fraction of the polymer belonging to the percolating cluster (far above p_c).

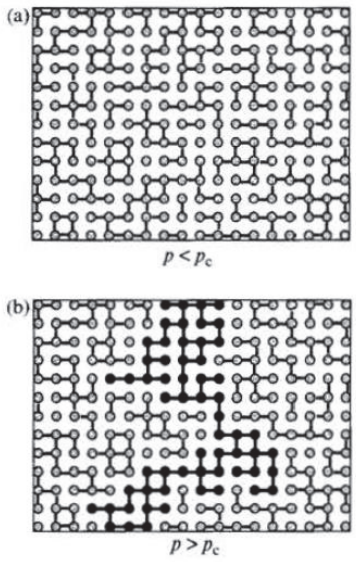


Figure 21 Bond percolation responsible of gelation. Infinite chain is dark (M. Rubinstein 2003)

At any moment *p*, it is possible to define a dimensionless number density of molecules *n* having N monomers: *n*(*p*, *N*). The fraction of sol is defined as the fraction of monomers that did not react or belong to a finite size cluster:

$$P_{sol}(p) = \sum_{N=1}^{\infty} Nn(p,N)$$

As a consequence the gel fraction $P_{gel}(p) = 1 - P_{sol}(p)$ is defined as the fraction of monomers which belong to the gel, i.e to the infinite cluster. Below the gel point, the gel fraction is equal to zero and the sol fraction is unity. Conversely above the gel point the gel fraction increases while the sol fraction decreases.

1.4.3. Gelation mechanisms

It is generally agreed that gelation is the result of network formation. Physical gels can be compared to chemically cross-linked systems, except that the junction points of the network are not chemical bonds (Komatsu, Inoue et al. 1986, Kawanishi, Komatsu et al. 1987). The gelation process has been widely investigated on PVC, polyvinyl alcohol or acrylonitrile-vinyl acetate gels. However, the nature of the junction points in the network has often been a subject of controversy. Indeed, the nature and structure of these physical junction points are so complex that they need to be further clarified.

Paul (Paul 1967) suggested that gelation is due to a phase separation into polymer rich and polymer poor regions. A classic model considers that gelation occurs due to hydrogen-bonding association of polymer chains (Eldridge and Ferry 1954). Finally, a predominant point of view is to consider that the junction points are small polymer crystallites interconnected by long chains. This last hypothesis was supported by thermodynamics of gel melting and crystallographic studies on the crystallites. As the crystalline regions are supposed to be small and constituted from only a small fraction on the total

polymer, it seems difficult to clearly identify the rigid zones as crystallites (Paul 1967). Crystallization and phase-separation appear to be the most recognized gelation mechanisms in polymer solutions and will be briefly described in this section.

Crystallization

Crystallization corresponds to a process through which the molecular chains undergo partial alignment. The gelation by crystallization mechanism has been widely reported in the literature (Tazaki, Wada et al. 1998) and may occur with highly crystallizable polymers (polyethylene). This mechanism depends on the experimental conditions. For example, in the case of PVDF gels, the solvent nature influences the morphology of the polymer network. PVDF – acetophenone gels will have a spheroidal morphology while PVDF – glyceryl tributyrate gels have fibrillar morphology (Mal and Nandi 1998). Moreover by changing the solvent, different conformations of the crystallites can be obtained: α-type crystals are obtained in PVDF – cyclohexanone gels and γ-type crystals in PVDF - γ-butyrolactone gels. Temperature also influences the morphology of the gels. Polyethylene (PE) gels in xylene have different morphologies depending on temperature and stirring (Berghmans 1988). Cooling PE – xylene solutions give paste-like dispersions of single crystals, while transparent and elastic gels are obtained on stirring the solutions at higher temperatures.

Phase separation

In addition to gelation through the formation of crystallites or hydrogen-bonding interactions, a third mechanism associated to liquid – liquid phase separation (or spinodal decomposition) was introduced by Labudzinka et al. (Łabudzińska and Ziabicki 1971) and Paul (Paul 1967). They suggested that gelation is induced by separation of the system into polymer-rich and polymer-poor phases.

Gels do not have a definite supramolecular structure and their structure depends on the gelation process. Studies on polyacrylonitrile (PAN), polyvinylalcohol (PVA) and gelatin solutions show that the mechanism of gelation through molecular aggregation or crystallization is not consistent in some cases. X-ray diffraction on PAN, PVA and gelatin solutions and gels show that gelation occurs without change in light or X-ray scattering: thus, this gelation does not come from crystallization of hydrogen-bonds. Due to the optical heterogeneities of these samples, it was suggested that gelation could also occur via liquid-liquid phase separation. A molecular mechanism was therefore proposed, as illustrated in Figure 22. The polymer solution (a) is thermodynamically unstable at the gelation temperature; as a consequence, compact aggregates are formed (b) and then connect to form a heterogeneous gel system (c).

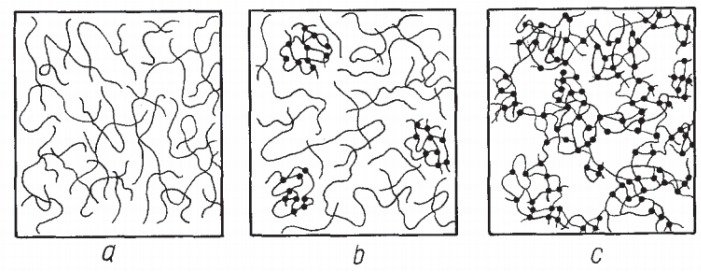


Figure 22 Molecular mechanism of gelation accompanied by phase separation (a) interpenetrating coils in supercooled solution (b) formation of compact molecular aggregates (c) connection of aggregates and formation of a heterogeneous network (Łabudzińska and Ziabicki 1971)

Gelation of polymer solutions involves a connectivity phase transition which causes the viscosity to diverge at the gel point. Since binary phase separation is driven by a diffusive process it is very likely that the onset of gelation would drastically slow down the kinetics of the phase separation process.

Phase separation and crystallization

Liquid-liquid phase separation can sometimes occurs in addition to the liquid-solid transition (crystallization), and the gelation mechanism becomes more complex. This mechanism was investigated on PVDF gels in γ-butyrolactone by (Cho, Song et al. 1993). They proved that, in this solvent, gelation is a two-step process: liquid-liquid phase separation followed by crystallization, though liquid-liquid phase separation alone may be responsible for gelation. Indeed, by performing DSC, SEM and X-ray diffraction measurements on (dried) gels, they show that depending on the polymer concentration, different crystalline forms exist in the gel: form I for high concentrations of PVDF and forms I and II for low concentrations of polymer. They indicate that the gelation mechanism at high polymer concentration is due to the formation of crystalline zones. Conversely, at low concentrations, the solutions turn to gels in two steps with, first, liquid-liquid phase separation, followed by crystallization. Gelation may thus be caused only by the formation of polymer-rich zones and the overlapping of polymer chains in this phase, and crystallization may not be not necessary to form a gel in that case.

In conclusion gelation of semi-crystalline polymers is complex. The nature of the gel depends on the chain structure and molecular weight of the polymer, and also on the nature of the solvent.

1.4.4. Gel characterization: determination of the gel point

Several methods have been used in the literature to characterize gels and more particularly to determine the gel point:

i. **Tube-tilting test and falling ball method**: these two techniques are the easiest way to determine the gel points or gel melting temperatures. In the tube-tilting test, the polymer solution (or gel) is observed while rotating the tube during a certain period of time. The gel point of the solution is defined as the time where the system stops to flow. However, for high-concentration solutions it is difficult to discriminate infinite to high viscosity. The falling ball method is used to determine the melting temperature of gels. A ball with a small diameter is placed on the surface of the gel and when the temperature increases and reaches the melting point, the ball will move through the polymer solution. However, this method is not adapted to fragile gels.

ii. **Rheological measurements:** The accepted definition of a gel is usually based on a rheological approach: a network which possesses an elastic modulus at zero frequency (oscillatory measurements) or at infinite time (relaxation experiments). Mortimer and al. determined the gel point (during a crosslinking reaction) as the crossover of the shear storage (G') and loss (G'') moduli in small-angle oscillatory shear measurements (Figure 23). A second condition to define the gel state is the independence of the tanδ with the frequency (Winter and Chambon 1986)

These three methods are widely used to characterize the gelation time of polymer solutions. In addition, numerous structural, thermal, mechanical analyses were performed on gels. Various characterization approaches will be presented here for PVDF organogels in various solvents.

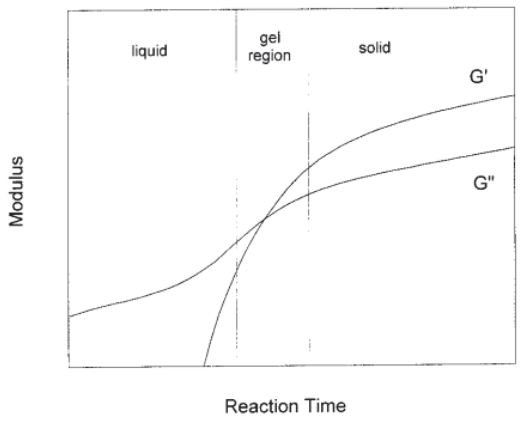


Figure 23 Schematic representation of the storage and loss moduli during gelation (formed by a crosslinking reaction) (Mortimer, Ryan et al. 2001)

X-ray techniques (SAXS, WAXS) can be used to characterize crystalline structures at different scales. WAXS experiments were performed to identify the crystalline phases of PVDF dried gels in glyceryl tributyrate (Mal and Nandi 1998), ethylene carbonate (Dasgupta, Manna et al. 2008), acetophenone (Mal, Maiti et al. 1995) or propylene carbonate (Kim, Baek et al. 2004). Depending on the solvent and the polymer concentration, different crystal structures are present in the gel especially α, β or γ phases of PVDF. The dependence on the concentration was studied by (Cho, Song et al. 1993) on PVDF gels in γ-butyrolactone. At low concentrations gels crystallize in a two-step process and crystals of α and β phases are formed. This two-step process is caused by liquid-liquid phase separation, followed by crystallization. Conversely, at high polymer concentrations, gels are formed by crystallization alone in a one-step process which leads to β-type crystallites.

Infrared spectroscopy can be used to follow the gelation process: it can provide an insight into the assembly of molecular scale building blocks and allow the determination of non-covalent interactions. UV and fluorescence spectroscopies are also widely used. Dasgupta (Dasgupta, Manna et al. 2008) studied the structure of PVDF- ethylene carbonate gels by FTIR. They reported the formation of PVDF gels with crystallites of the β-form, which could lead to interesting materials with piezoelectric properties (see page 17).

Microscopy techniques (SEM, TEM, and AFM) were performed on the same materials to identify the morphology of the gels. Mal et al. (Mal and Nandi 1998) studied the influence of various solvents on the structure of PVDF gels. As shown in Figure 24, the morphologies of the gels strongly depend on the nature of the solvent (and therefore the solvent – polymer interaction): in acetophenone, the gel presents a spheroidal morphology while in glyrecyl tributyrate it is fibrillary and in ethyl benzoate it gel combines both the spheroidal and fibrillar morphologies.

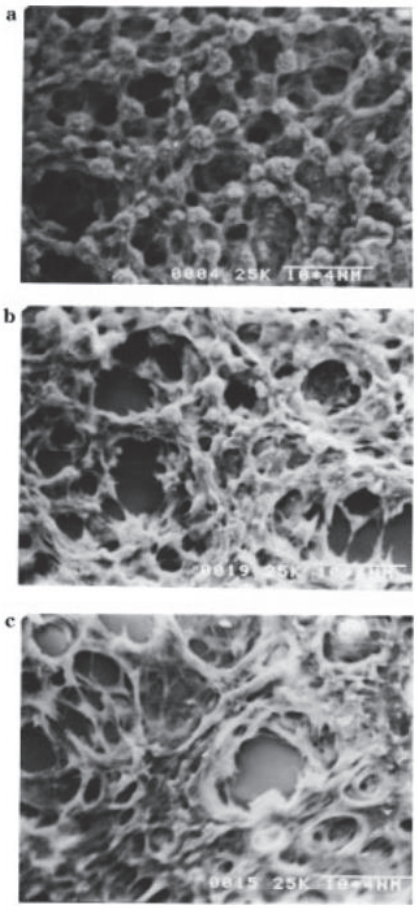


Figure 24 SEM micrographs of 7wt% PVDF gels in (a) acetophenone (b) ethyl benzoate and (c) glyceryl tributyrate (Mal and Nandi 1998)

Rheology was performed on PVDF – ethylene carbonate gels to study the influence of temperature on the liquid – gel transition of the material (Dasgupta, Manna et al. 2008). They first performed frequency sweep measurements at different temperatures and they show that at low temperatures the system behaves as a gel: the storage and loss moduli are independent of frequency and the storage modulus is higher than the loss modulus. As temperature increases the system behaves like a sol at every frequency. Linear rheology measurements also allow determining the melting temperature of the gels: at the melting temperature the storage and loss moduli become equal. In addition to the information on gelation kinetics, rheology also provides structural information on the polymer network. Indeed, according to classical theories of gel elasticity, the crosslink density ν (number of crosslinks per unit volume) can be estimated from the plateau modulus G_N^0 with the equation:

$$G_N^0 = k_B T \nu \tag{7}$$

As a consequence, it is possible to determine the crosslink density and also the lifetime of our network. Additional information on gels could be obtained by nonlinear rheology measurements. These experiments should provide information on the strength of the gel network. To our knowledge, no non-linear rheology studies have yet been performed on PVDF organogels.

Thermal analysis (DSC) is also used to obtain structural information and determine gel melting temperatures. In studied systems (for example gelation of PVDF in propylene carbonate (Kim, Baek et

al. 2004)) DSC thermograms showed a endothermic peak which may suggest the existence of crystallites in the materials: these crystalline regions might then be bridged by portions of chains in solution to form a three-dimensional network characteristic of the gel state.

Finally, NMR spectroscopy is a powerful technique for studying polymer gels and will give information on the structural properties of the components, the presence of aggregates and the regions participating in the interactions.

1.5. Polymer nanocomposites

Polymer composites have been widely studied over the past decades due to their interesting properties and various applications: elastomers for damping, electrical insulators, thermal conductors, packaging, bio-medical… Indeed, such materials will combine the properties of both the polymer (e.g. flexibility, dielectric, ductility and processability) and the inorganic fillers (e.g. rigidity, abrasion resistance, stiffness, thermal and electrical thermal stability). In this context polymer nanocomposites (or organic-inorganic hybrids) were developed: it consists on organic/inorganic materials where the inorganic phases become nanosized (below 100nm). By decreasing the size of the inorganic particles, properties of the final materials will be enhanced because the small size of the fillers leads to a dramatic increase of the interfacial area (in comparison with composite materials). Common nanoparticles used in nanocomposites are nanotubes, layered silicates, metals, metal oxides, semi-conductors (see page 21).

However, the dispersion of the filler nanoparticles is the major issue in order to have optimized properties of the materials. The dispersion of the nanoparticles are controlled by filler-filler and filler-polymer interactions (Tessema, Zhao et al. 2017).

1.5.1. Fillers dispersion state in polymer matrices

It is first necessary to distinguish the dispersion and distribution states of the nanoparticles, as schematized in Figure 25 Difference between distribution and dispersion: (a) good distribution and poor dispersion (b) poor distribution and dispersion (c) poor distribution and good dispersion (d) good dispersion and distribution (Schadler 2004). The dispersion is related to the level of aggregation of nanoparticles within the materials while the distribution describes the homogeneity throughout the sample. Both strongly depend on the amount and surface chemistry of the nanoparticles.

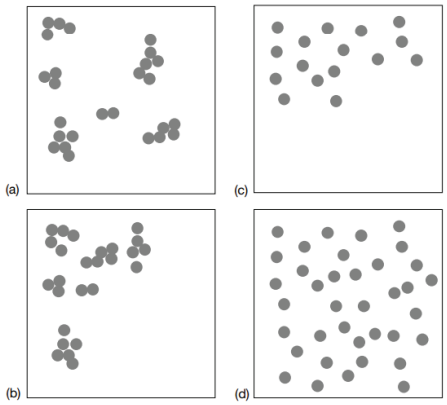


Figure 25 Difference between distribution and dispersion: (a) good distribution and poor dispersion (b) poor distribution and dispersion (c) poor distribution and good dispersion (d) good dispersion and distribution (Schadler 2004)

The dispersion state of nanoparticles results from the balance between particle-particle, polymer-polymer and particle-polymer interactions. When nanoparticles are added to the polymer matrix, clustering (via the formation of aggregates/agglomerates) of the particles can occur and deteriorate the properties of the materials (Zare 2016). Clustering of the nanoparticles has been attributed to particle-particle interactions via Van der Waals forces (or chemical covalent bonds) (Tessema, Zhao et al. 2017) when particles are at short distances. This aggregation/agglomeration phenomenon can be prevented by electrostatic repulsions or steric repulsions between particles for example by modifying the surface of the nanoparticles or by using optimal parameters during the production process. The surface modification of nanoparticles (especially on silica nanoparticles) was detailed in the previous section page 25.

1.5.2. Formulation of polymer nanocomposites

Nanocomposite materials can be produced by several routes (Hajji, David et al. 1999): the nanoparticles, the polymer or both can be synthesized *in situ* or used in the final state. Three general methods are used to prepare polymer/nanoparticles nanocomposites: blending (melt and solution), sol-gel processes or *in situ* polymerization. In this part only melt and solution blending will be described as they represent the traditional and simplest methods for processing nanocomposites.

Melt blending

Melt blending is the simplest way to prepare nanocomposites and is commonly used in the industry. Nanocomposites are produced by the addition of fillers (and other reactants) into polymer melts under mechanical action and high temperature (above the glass transition temperature of the polymer). The viscosity of the polymer – nanoparticles melts can impact this processing method: the addition of nanoparticles can rapidly and strongly increases the viscosity of the melt making the process not possible anymore (Schadler 2004). Moreover due to the tendency of nanoparticles to agglomerate this method leads to random particle dispersion in the polymer matrix (Caseri 2007). Final materials are then formed of clusters of nanoparticles which badly impacts their properties. Several methods were developed to break these clusters:

i. **Surface-modification of nanoparticles** prior to mixing, without introducing chemical bonds between the nanoparticles and the polymer (He, Allard et al. 1999)
ii. **Crosslinking** between silica nanoparticles and polymer (Bikiaris, Karavelidis et al. 2006) or between polymer chains
iii. **Process modification:** High shear stress (Bikiaris, Papageorgiou et al. 2006), addition of other ingredients (Jana and Jain 2001, Kim, Ahn et al. 2003)

Finally melt blending process can degrade the polymer matrix because of the shear heating, especially for long-time and high-temperature experiments. Addition of nanoparticles into polymer melts may enhance or inhibit this degradation phenomenon. By measuring the torque as a function of time and temperature it is possible to assess the influence of nanoparticles on the degradation of the polymer: if degradation, for example chain scission, occurs, the torque will drop.

Solution blending

A way to prevent polymer degradation and particle agglomeration is to mix nanoparticles into a polymer solution. Solution blending, based on the mixing of nanoparticles and polymer into a solvent, is a common method to prepare nanocomposites. Here surface modification of nanoparticles can be

performed without drying and therefore it will minimize the agglomeration of nanoparticles. Polymer nanocomposites can then be obtained by casting the solution followed by evaporation of the volatile solvent (at room temperature or under heating). However, as presented in the previous section page 37, polymer/nanoparticle interactions impact the dispersion and distribution of nanoparticles in the liquid medium. This widely used method is not limited to a solution, it can include a latex or a suspension (Zou, Wu et al. 2008). Different experimental factors, such as the nanoparticle size and concentration, the pH, the solvent or the drying step, may impact the structure and properties of the final materials.

Albayrak Ari et al. (Albayrak Ari and Aydin 2008) developed nanocomposites of poly(vinyl chloride) (PVDF) and calcium carbonate ($CaCO_3$) nanoparticles by solution blending. They studied the influence of the nanoparticles size on the microstructure and mechanical properties of the final nanocomposites. Solutions of PVC-$CaCO_3$ (with different sizes of nanoparticles and concentrations of particles) in tetrahydrofuran (THF) were prepared and cast onto glass plates. Final films were obtained by evaporation of THF at ambient conditions. Figure 26 shows the microscope images of PVC – $CaCO_3$ nanocomposites with different sizes and contents of nanoparticles. They show that nanoparticles have a strong tendency to agglomerate. Especially by decreasing the size of the nanoparticles the density of agglomerates increases. Same result is observed with the increase of filler concentration. The formation of agglomerates in the dry material is mainly due to the agglomeration of the nanosized fillers during the processing.

The group of van Zyl (van Zyl, García et al. 2002) show the influence of the pH of the polymer – filler solution on the dispersion of the final material. They optimized the processing conditions, considering that the properties are related to the distribution of inorganic filler in the polymer matrix and as a consequence this dispersion has to be as homogeneous as possible. To do so they chose an appropriate solvent both for the polymer and the filler and control the pH of the solution. Nylon 6 – silica solutions in formic acid were formed and the pH was controlled around 2 to keep good silica dispersion in the solution. The pH was maintained to 2 by the addition of HCl to reach a pH below the isolectric point of silica (pH 2-3). This solvent was chosen not only to dissolve the polymer but also to keep the charge on the silica surface which will prohibit the charge aggregation and as a consequence the formation of a gel. After a casting onto glass plates and elimination of the solvent the films were analyzed with TEM: silica nanoparticles were well-dispersed and not aggregated.

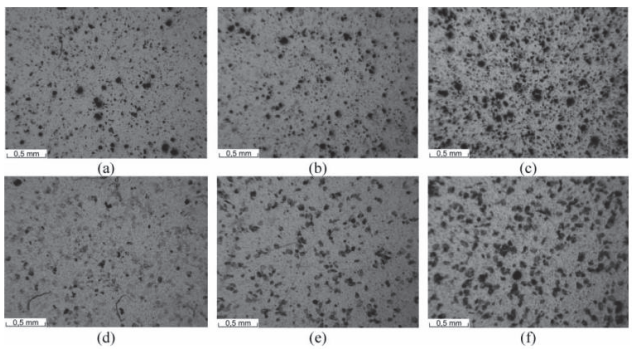


Figure 26 Microscope images of PVC - CaCO3 films with (a,b,c) 40nm and (d,e,f) 220nm CaCO3 particles. Particle contents are (a,d) 3phr (b,e) 5phr (c,f) 10phr (Albayrak Ari and Aydin 2008)

Similar works were performed on Polystyrene – silica nanocomposites in various solvents like methyl ethyl ketone (MEK), THF or dimethylacetamide where different dispersion states were obtained according to the solvent nature and the kinetics of evaporation. The influence of the solvent on the final dispersion state of silica nanoparticles in poly(2-vinylpyridine) (P2VP) – silica nanocomposites was investigated by Jouault et al. (Jouault, Zhao et al. 2014). Two theta/good solvents of the polymer and the nanoparticles, MEK and pyridine, were chosen and the dispersion state of nanoparticles in solution was compared to the dispersion in dried nanocomposites. They show that in solution in MEK, P2VP adsorbs on the silica surface and forms a bound layer leading to a good dispersion of silica in the solution and therefore in the dried material (see Figure 27). Conversely P2VP does not adsorb in silica surface in pyridine solvent and silica aggregates in the solution. As a consequence, nanocomposites prepared from pyridine solution present large aggregates of silica nanoparticles. This means that the dispersion of nanoparticles in the solution have a strong impact on the dispersion of silica in the dry nanocomposite: the solvent plays a critical role and the properties of the materials can be determined from the solvent considered for the processing of the material.

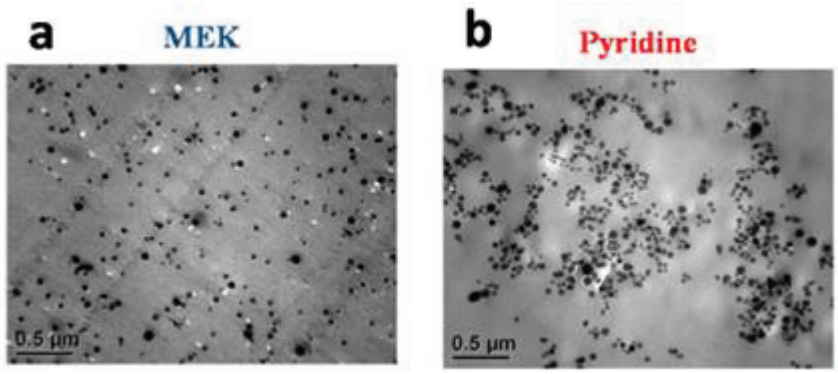


Figure 27 TEM of 10 wt% silica - P2VP nanocomposites using (a) MEK (b) Pyridine as solvent (Jouault, Zhao et al. 2014)

The solvent evaporation during the drying step also influences the silica dispersion is the final material. X-ray scattering and neutron scattering experiments were performed on different systems to understand the evolution of the nanoparticles dispersion in the polymer matrix at different drying steps: polyvinyl alcohol (PVA) – silica (Kim, Hyun et al. 2016), polystyrene – silica (Sen, Xie et al. 2007), poly(methyl methacrylate) (PMMA) – silica (Jouault, Dalmas et al. 2012). They all show that the processing affects the final dispersion state and in more detail the nature of the particle – polymer interactions: the kinetics of solvent evaporation strongly affects the interactions at the particle – polymer interfaces. When the solvent evaporates the solution becomes more and more viscous and "freezes" in a specific aggregation state depending on the kinetic of evaporation. It seems that a fast evaporation of the solvent allows reaching a well dispersed state which may be due to the formation of a bound polymer layer at the surface of the nanoparticles that keeps the silica in a well dispersed state.

1.5.3. Characterization methods of nanocomposites

The properties of the nanocomposites strongly depend on the structure of the materials (e.g. composition of the material, size of the nanoparticles, and distribution of the fillers in the polymer matrix) and also on the dynamics of the fillers and the polymer chains which strongly affect the mechanical, thermal and other properties of the materials. Some examples of different

characterization techniques to assess the structure, thermal, mechanical and electrical properties of the materials are presented in this part.

Structure and morphology

Microscopy is commonly used to study the microstructure of nanocomposites. Transmission electron microscopy (TEM), scanning electron microscopy (SEM) and atomic force microscopy (AFM) are three powerful methods to evaluate the structure of the nanocomposite as shown on Figure 28.

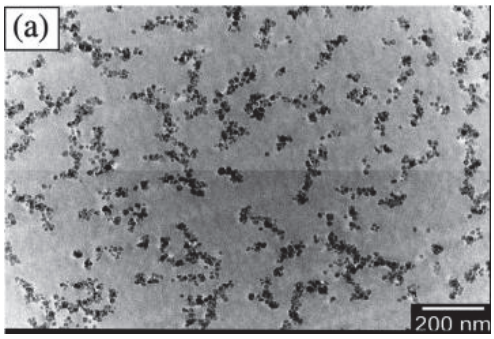


Figure 28 TEM image of a polystyrene - silica nanocomposite (Jouault, Vallat et al. 2009)

AFM provides characterization of the structure and morphology of the sample surface and give information on the material properties from nanometric to the millimetric scale (Mittal 2012). It can be combined to TEM (or SEM) experiments. For example dispersion of carbon nanotubes at different fractions in natural rubber was studied by TEM (Figure 29) and AFM showing a relatively homogeneous dispersion of fillers related to the preparation process.

Microscopy techniques are time-intensive and give local information on the sample. As a consequence, microscopy is often used in combination with X-ray scattering/diffraction or neutron scattering methods.

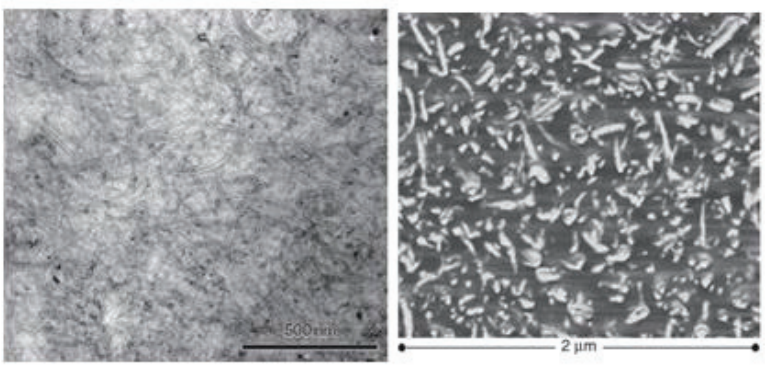


Figure 29 (left) TEM and (right) AFM images of natural rubber filled with 60phr carbon nanotubes (Mittal 2012)

WAXD can be first performed on nanocomposites to investigate the changes in the crystallinity degree of the final materials (Zou, Wu et al. 2008). It is usually observed that adding silica nanoparticles decreases the crystallinity degree of the polymer even at low content of filler (van Zyl, García et al. 2002). The material structure at larger scale can be studied by SAXS: the shape and size of the inhomogeneities of the sample can be obtained. Jouault et al. (Jouault, Vallat et al. 2009, Jouault, Dalmas et al. 2012) investigated the dispersion of silica nanoparticles in polystyrene or

PMMA nanocomposites by SAXS, SANS and TEM and they studied the influence of the polymer and the type of silica on the aggregation of the nanoparticles (Figure 30). The combination of these techniques is widely used on different systems, such as: (i) thermoplastic – silica nanocomposites (Becker, Kutsch et al. 1998) to characterize the morphology of thermoplastic nanocomposites (ii) latex – silica nanocomposites (Banc, Genix et al. 2014) to investigate the influence of the molecular weight of the polymer on the aggregation of silica nanoparticles (ii) polypropylene – clay nanocomposites (Maiti, Nam et al. 2002) to study the effect of crystallization and temperature on the structure and morphology of nanocomposites

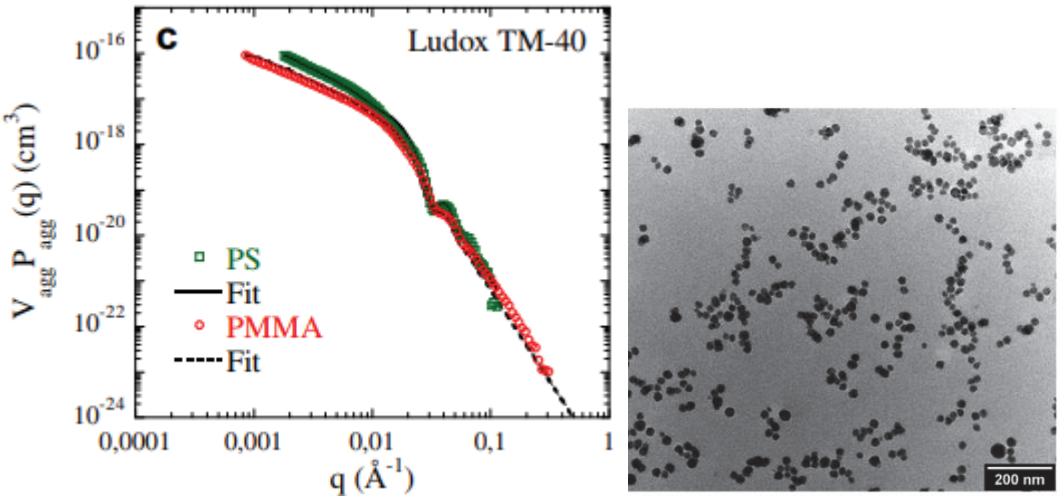


Figure 30 (left) SAXS measurements for nanocomposites filled with 5%v/v of Ludox TM-40 ion PS or PMMA (right) TEM image for 5% v/v Ludox TM-40/PMMA nanocomposite (Jouault, Dalmas et al. 2012)

The last scattering method is neutron scattering because of its extended q-range which gives access to length scales between angstroms and several thousands of angstroms. It probes the structural and molecular interactions between the polymer matrix and the nanoparticles, and the conformation of polymer chains. Latex – silica films were analyzed by means of SANS experiments (Oberdisse and Demé 2002). They studied the structure of the nanocomposites and the influence of the pH value, the presence of salt, the fraction of silica and the silica/latex ratio on the dispersion of silica nanoparticles within the materials. From the position of the structure factor peak of the scattering curves, it is possible to estimate the aggregation number. They pointed out that the pH, quantity of salt and silica volume fraction have a direct influence on the final structure of the film.

Finally, spectroscopy techniques (^{1}H NMR, positron annihilation lifetime spectroscopy, infrared…) are other approaches to characterize the structure and morphology of polymer nanocomposites. They will not be detailed in this section.

Thermal characterizations

A polymer nanocomposite with bad thermal performances would not be suitable for high-temperature processing and applications. Thermal performances of nanocomposites are investigated to analyze the effect of the fillers on the microstructure of the material and to assess the possibility of using such materials for different applications which requires temperature expositions. Thermal properties are studied by thermogravimetric analysis (TGA) and differential scanning calorimetry (DSC).

It is generally observed that the addition of fillers in a polymer matrix enhances the thermal behavior of the pure polymer (or filler). However, additives (silanes for example) used to improve the distribution state of the fillers can affect the thermal properties. For example, Zheng et al. (Zheng, Yao et al. 2006) studied the thermal properties of silica graft poly(propylene) (PP) nanocomposites in order to estimate the thermal degradation kinetics of the material. They investigated the influence of the silica content in the nanocomposite compared to the pure polymer (Figure 31-a) and then the influence of the heating rate (Figure 31-b) on the onset temperature of degradation. These measurements prove the improvement of the thermal stability of the polymer with the addition of nanoparticles. Moreover, by increasing the heating rate, the thermal decomposition temperature increases due to the shorter time required for a sample to reach a given temperature at a faster heating rate.

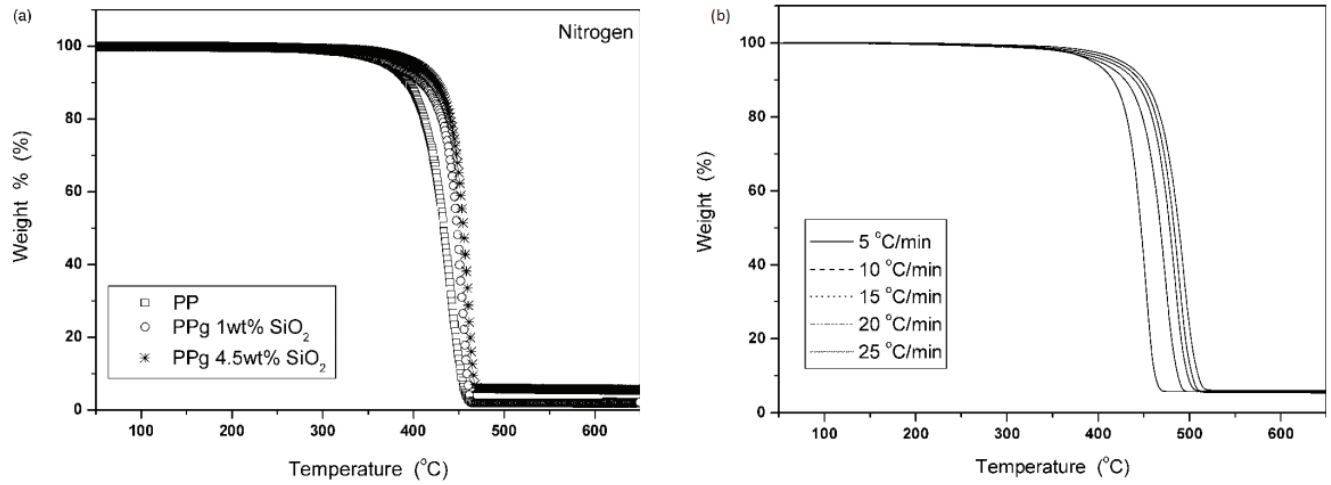


Figure 31 TGA thermogram of (a) pure PP and silica-PP nanocomposites with different content of silica (b) silica-PP nanocomposites at different heating rates in nitrogen (Zheng, Yao et al. 2006)

Similar improvement of the thermal degradation temperatures was observed with different systems and fillers for example montmorillonite and carbon nanotubes in PMMA (Blumstein 1965), PDMS (Burnside and Giannelis 1995) and polyamide (Ide and Hasegawa 1974).

DSC experiments must be performed on nanocomposites to study the effect of fillers addition on thermal phenomena such as melting, crystallization and glass transition (T_g). The variation of T_g of the polymer matrix when fillers are added to the material has been studied for different filler – polymer systems. Depending on the system there are contradictory results on the effect of fillers on the glass transition of nanocomposites: it can decrease (Ash, Schadler et al. 2002) or increase (Pham, Mitchell et al. 2003). Modulated DSC measurements were performed on nanocomposites with different types, concentrations, sizes and dispersion states of fillers to analyze the effect on the T_g.

Mechanical characterization

The mechanical behavior of the nanocomposites strongly depends on the polymer-nanoparticles interactions and the dispersion state of the nanoparticles. The addition of inorganic fillers to a polymer matrix generally enhances the mechanical properties. However, it is important to increase the strength/stiffness without decreasing the toughness of the nanocomposites.

Tensile tests were performed on various nanoparticles – polymer nanocomposites (Rong, Zhang et al. 2000, Bikiaris, Papageorgiou et al. 2006). The influence of the silica content on the mechanical properties of silica – polyamide nanocomposites (prepared by sol-gel method) was studied by Sarwar et al. (Sarwar, Zulfiqar et al. 2008). The addition of silica nanoparticles increases the values of the yield stress up to a certain concentration of silica (10wt% here). Above this concentration the value decreases and at even higher concentration the sample breaks near the yield point, i.e. becomes fragile. The modulus was calculated from the initial slope of the stress-strain curves and the same trend was observed: the modulus increases up to 10w% of silica and decreases at higher silica content. The elongation at break decreases as the silica content increases. Different properties were obtained for silica – polyimide by a sol-gel method using a coupling agent (Shang, Zhu et al. 2002). In this case the Young's modulus of the nanocomposite increases linearly with the concentration of silica as shown in Figure 32 - a. As shown in Figure 32 –b,c both tensile strength and elongation at break increases as the silica content increases up to 20wt% with modified silica and 10wt% for neat silica. At concentrations higher than 20wt% of silica the tensile strength and elongation at break decrease. Moreover, the moduli and tensile strengths are higher in nanocomposites with coupling agents, certainly because of an improved interaction between the polymer and the silica nanoparticles. Conversely the elongation at break dramatically decreases with the addition of coupling agent, which may be due to the increase of the crosslinking density.

The fracture toughness is an important mechanical properties of a material. It corresponds to the resistance to crack propagation. The fracture toughness is generally enhanced by the addition of silica nanoparticles up to a certain concentration of silica (Lach, Kim et al. 2006, Dorigato, Sebastiani et al. 2012)

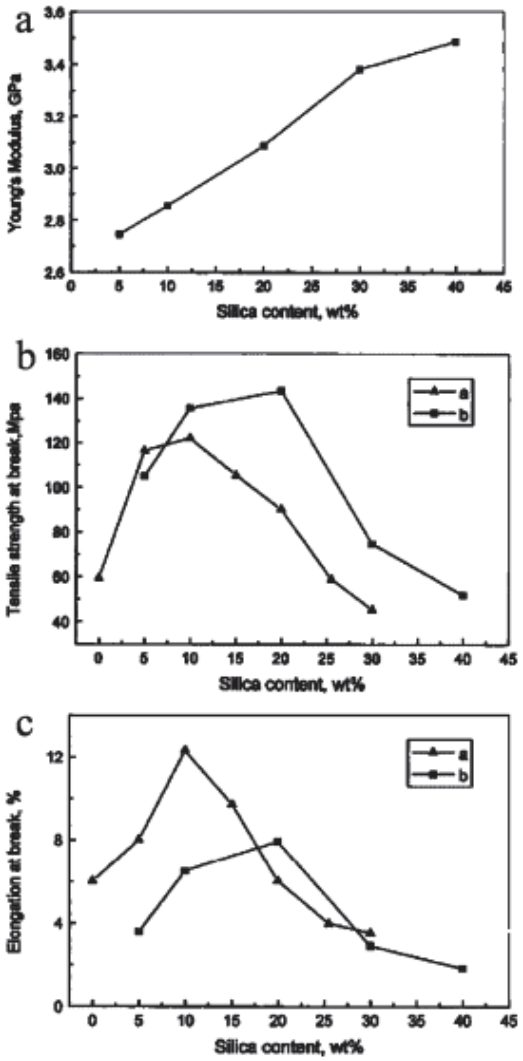


Figure 32 (a) Correlation between Young's modulus and silica content (b) effect of the coupling agent on the tensile strength at break (▲without coupling agent ■with coupling agent) (c) effect of coupling agent on elongation at break (▲without coupling agent ■with coupling agent) on polyimide - silica nanocomposites (Shang, Zhu et al. 2002)

Electrical properties

As for all the properties of nanocomposites, electrical performances of materials strongly depend on the crystallinity of the sample, dispersion state of fillers and polymer –silica interactions. For example polyethylene (XLPE) – silica nanocomposites and microcomposites were formulated with different types of silica (without or with different surface modifications) by Roy et al. (Roy, Nelson et al. 2007). Figure 33-a show that the addition of nanometric fillers strongly increases the breakdown strength of the materials and this increase depends on the surface modification of the silica nanoparticles. Moreover dielectric spectroscopy showed an increase of the dielectric permittivity (Figure 33-b) in microcomposites, which suggests the existence of interfacial polarization. On the contrary, the addition of nanometric silica particles leads to lower values than the pure polymer. These differences are attributed to the strong difference in interfacial area between microcomposites and nanocomposites. From the loss tangent measurements, it appears that the addition of nanoparticles reduces the chain movement of the polymer through physical bonding or confinement. In both experiments, the surface modification of silica nanoparticles strongly modifies the properties of the material.

It is also possible to investigate the conductivity of nanomaterials. Depending on the type of polymer, the silica distribution state and silica – polymer interactions, the conductivity of the nanocomposite can increase or decrease. However, generally, the conductivity of the nanocomposites decreases with the addition of silica nanoparticles (Han and Armes 2003). Indeed, the addition of silica nanoparticles and the immobilization of the polymer on nanoparticles hinders the transport of carriers in the polymer matrix. To increase the conductivity of the nanocomposite, silica must be completely coated by a conductive polymer.

It is also possible to investigate the conductivity of nanomaterials. Depending on the type of polymer, the silica distribution and silica – polymer interactions, the conductivity of the nanocomposite can increase or decrease. However, generally the conductivity of the nanocomposites decreases with the addition of silica nanoparticles (Han and Armes 2003). Indeed, the addition of silica nanoparticles hinders the transport of carriers in the polymer matrix and the immobilization of the polymer on nanoparticles decreases the charge carrier mobility. correlation length of the polymer. To increase the conductivity of the nanocomposites by the addition of silica nanoparticles, silica must be completely coated by a conductive polymer. However, in case of precipitated silica, the presence of residual water and silanol groups at the surface often has the effect of increasing the conductivity.

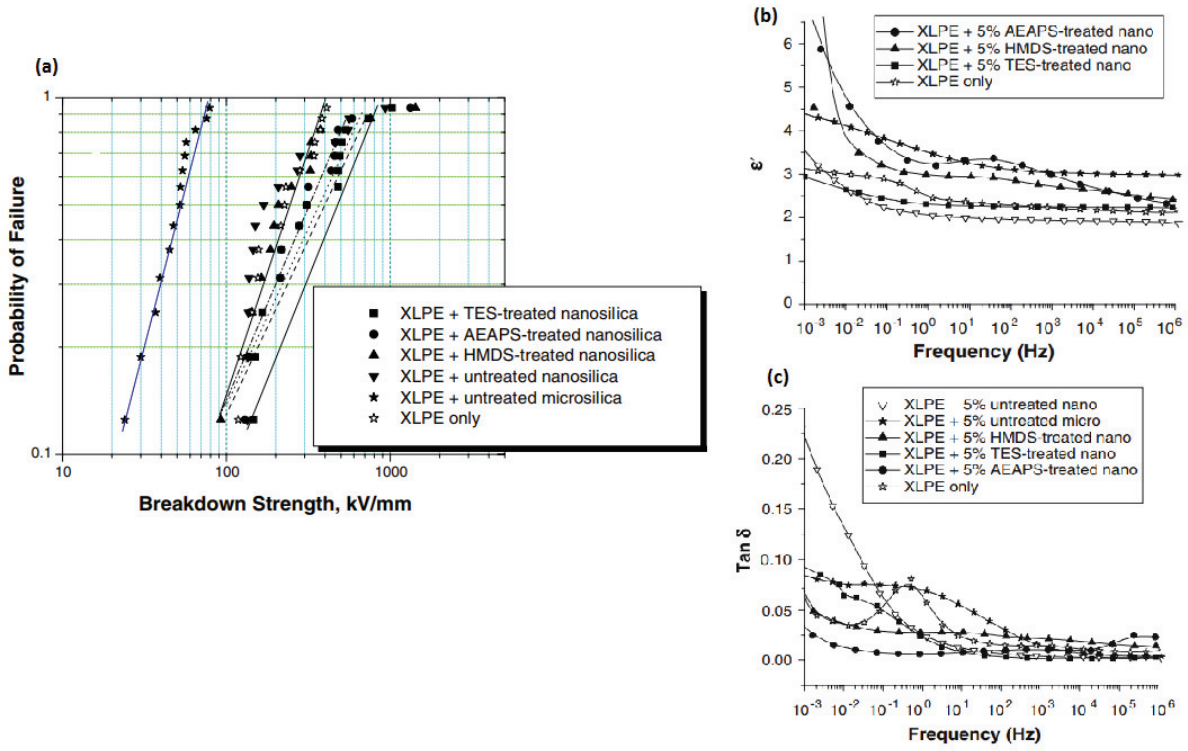


Figure 33 (a) Weibull plot of the breakdown probability of PE - silica composites and nanocomposites (b) dielectric permittivity of XLPE composites (c) loss tangent of XLPE composites (Roy, Nelson et al. 2007)

1.6. Context of the PhD work

The purpose of this chapter was to present a summarized review of different subjects involved in this PhD.

The initial objective of this PhD consists in the processing of P(VDF-co-HFP) films filled with silica nanoparticles by solvent route. Great attention must be paid to the control of the dispersion state of silica in the nanocomposites and the characterization of their (electrical and mechanical) properties.

However, the addition of nanoparticles to a polymer solution impacts the rheological properties and thus, the processing through a casting or printing with sol gel method may not be possible anymore. This is typically the case of the semi-crystalline P(VDF-co-HFP) copolymer (filled or no with nanoparticles) which forms thermoreversible gels in certain solvents, the morphologies of which strongly depends on the nature of the solvent.

It appears highly important to understand the gelation kinetic and gel structure of the materials prior to working on the properties of the final nanocomposites. To do so the purpose of this work is to develop a model system to study the phenomenology of VDF-copolymer thermoreversible gelation in ketone solvents in order to use it as an advantage for the processing on materials.

As detailed in this chapter, different studies were performed on the gelation of PVDF in different solvents leading to the conclusion that the morphology of the gels strongly depends on the nature of the solvent: phase separation and/or crystallization can cause gelation of the polymer. It appears that the gelation of a semi-crystalline polymer is a complex phenomenon and that the morphology of the gels depends on the polymer chain structure and molecular weight as well as on the nature of the solvent, and more precisely on polymer – solvent interactions. However, the investigations on the dynamics and structure of these gels reported in literature were mostly performed in the dried state, considering that the morphology of the dried material is representative of the structure of the gel in the presence of solvent. Moreover, to our knowledge no studies on the gelation of P(VDF-co-HFP) in linear ketone solvents (and more precisely in MEK and 2-heptanone) have been reported in the literature.

In this context one of the objective of this work is to understand the gelation kinetic, mechanism(s?) and gel structure of P(VDF-co-HFP) gels in linear ketone solvents (MEK and 2-heptanone) and to understand the influence of the presence of silica nanoparticles on the gelation. This work allowed in a last step, the development for hybrid P(VDF-co-HFP) – silica membranes by solvent casting method.

Gelation kinetic was investigated by tube-tilting test and linear rheology. A combination of ^{19}F NMR, DSC, SAXS, WAXS and nonlinear rheology was performed to probe the gelation mechanism and structure of these systems. First experiments were performed on P(VDF-co-HFP) materials in MEK at the liquid and gel states. In a second step of the PhD, the hypotheses on the gelation mechanism of P(VDF-co-HFP) were extended to another ketone solvent which is 2-heptanone. Same experiments were performed on these materials. Silica nanoparticles were then added to the materials and same experiments were carried out to study the influence of silica in the gelation. In the last part of our work, the structural characterization of nanocomposites was performed by SEM and USAXS experiments while mechanical and electrical performances were characterized.

The experimental part of the manuscript is divided in five chapters.

1. Presentation of the studied silica solutions, polymer and solvents as well as the formulations of the studied gels and nanocomposites. Descriptions of the experimental methods which allow the determination of structure and dynamic of the gels as well as the structural,

electrical and mechanical characterizations of the hybrids films are also presented in this chapter.

2. Study of the gelation of P(VDF-co-HFP) in linear ketone solvents: first investigations were performed on gels in MEK and the hypotheses on the gelation mechanism was extended to another ketone solvent which is 2-heptanone. A part of this chapter is dedicated to the study of the crystallinity degree and structure of the copolymer on the gelation.
3. The influence of the presence of silica nanoparticles on the gelation kinetics and gel structure was studied in the third chapter.
4. Nonlinear rheology measurements on P(VDF-co-HFP) gels show very interesting behavior which is strongly impacted by the presence of silica nanoparticles
5. Structure – properties relationship of P(VDF-co-HFP) – silica hybrid nanocomposites will be presented in the last chapter. Influence of the types of silica nanoparticles and their concentrations on the structure of the material and their mechanical properties will be presented.

Chapter 2: Materials and methods

This chapter presents first the materials used in this study: grades of VDF-copolymer, solvents (2MeTHF, acetone, MEK and 2-heptanone), different sources of silica nanoparticles and silica coating agents. The techniques used in this PhD to develop silica solutions in organic solvents and prepare PVDF – silica gels and hybrid membranes are detailed. In a second part the different characterization methods on gels and nanocomposites are presented.

2.1. Materials 50

2.1.1. P(VDF-co-HFP) polymers 50

2.1.2. Solvents 51

2.1.3. Silica solutions 52

2.1.4. Phase transfer of aqueous silica solution in organic solvents 54

2.1.5. Silane grafting of silica nanoparticles in organic solvents 60

2.1.6. Solvent-exchange method to prepare silica solutions in 2-heptanone: from Nissan Chemical solutions in MEK 60

2.1.7. Formulation of P(VDF-co-HFP) organogels filled with silica 61

2.1.8. Processing of P(VDF-co-HFP) – silica nanocomposites films 61

2.2. Dynamical and structural characterization of gels 62

2.2.1. Gelation kinetic: tube-tilting 62

2.2.2. Rheology 63

2.2.3. ^{19}F NMR 67

2.2.4. DSC 73

2.2.5. X-ray scattering 74

2.3. Characterization of polymer – silica hybrid membranes 78

2.3.1. Structural characterizations 78

2.3.2. Mechanical characterizations: tensile strength tests 80

2. Materials and methods

In this PhD the gelation of P(VDF-co-HFP) was first studied in 2-methyltetrahydrofuran (2MeTHF)/acetone mixtures filled or not with silica nanoparticles. In this system 2MeTHF was used as a solvent of the silica nanoparticles and acetone as a solvent of the copolymer. In order to work with one solvent and to generalize the study of the gelation mechanisms of P(VDF-co-HFP) in one single class of solvents, the gels then were prepared in linear ketone solvents (methyl ethyl ketone and 2-heptanone). Silica nanoparticles came from two sources: aqueous silica solution in organic solvent obtained by a phase transfer method developed during the PhD and silica solution in MEK provided by Nissan Chemical Industry. The influence of the crystallinity of the polymer and its chemical microstructure on the gelation kinetics and dynamics were also investigated. As a last step of the PhD, P(VDF-co-HFP) – silica hybrid membranes were developed by solvent casting method.

In this chapter the components (polymers, solvents, silica sources, and silica modifiers), the formulation and processing methods to prepare the gels and hybrid membranes (nanocomposites) are described. In addition, the characterization techniques used during the PhD to investigate the structure and properties of the materials will be presented. Dynamics and structure of P(VDF-co-HFP) gels filled or not with silica in MEK and 2-heptanone were investigated using tube-tilting, ^{19}F NMR, X-ray scattering, DSC and rheology techniques. Structure and properties of P(VDF-co-HFP) – silica hybrid membranes were studied by combining structural (SEM and USAXS), and mechanical (tensile tests) characterizations.

2.1. Materials

2.1.1. P(VDF-co-HFP) polymers

The P(VDF-co-HFP) copolymer considered in this work (see Figure 34) is provided by SOLVAY under the trade name Solef® 21510. This copolymer is available as a white powder and is semi-crystalline.

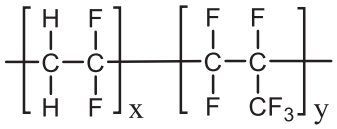


Figure 34 Poly(vinylidene fluoride-co-hexafluoropropylene) structure

The molar fraction *y* of HFP monomer within the copolymer is not known precisely but is smaller than 20wt%. The main properties of the copolymer are reported in Table 2.

Three additional P(VDF-co-HFP) copolymers were provided by Solvay and used to study the influence of crystallinity and microstructure on gelation:

i. P(VDF-co-HFP) 1 contains the same fraction of HFP than Solef® 21510 but has a different microstructure: compared to the Solef® 21510 which is statistical, the comonomer is not homogeneously distributed in the chain but HFP-rich zones exist
ii. P(VDF-co-HFP) 2 has the same polymeric chain structure but has a lower HFP fraction compared to Solef® 21510: the crystalline fraction is higher
iii. Amorphous P(VDF-co-HFP) called Tecnoflon® N535 has a HFP content larger than 20% mol.

Table 2 Chemical, physical, mechanical, thermal and electrical properties of P(VDF-co-HFP) Solef® 21510

Number average molecular weight ($M_n.10^{-3}$)	150-160 $kg.mol^{-1}$
Mass average molecular weight ($M_w.10^{-3}$)	290-300 $kg.mol^{-1}$
Density (23°C)	1.75 to 1.80
Water absorption (24hr, 23°C)	< 0.040%
Tensile Modulus (23°C)	360 to 480 MPa
Glass transition temperature	-40°C
Melting temperature	130 to 136 °C
Heat of fusion	23 J/g
Surface resistivity	> $1.0x10^{14}$ ohms
Volume resistivity	> $1.0x10^{14}$ ohms.cm

2.1.2. Solvents

P(VDF-co-HFP) – silica gels were first prepared in 2MeTHF/acetone mixtures: 2MeTHF (Figure 35-a) was used as an organic solvent wherein silica was transferred and acetone (Figure 35-b) as a solvent of the polymer. We then identified a common solvent which can be used both in the silica phase transfer and as a good solvent of P(VDF-co-HFP): MEK (Figure 35-c) and 2-heptanone (Figure 35-d). All the solvents were provided by Sigma Aldrich, France. They are reagent grade and were used as received without further purification.

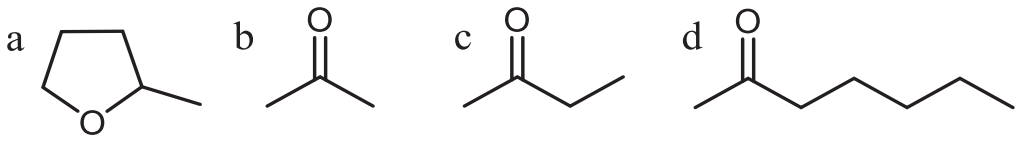


Figure 35 Chemical structure of (a) 2MeTHF (b) acetone (c) MEK (d) 2-heptanone

The properties of these solvents are presented in Table 3.

Table 3 Physico-chemical properties of the studied solvents

	2MeTHF	Acetone	MEK	2-heptanone
Molar mass ($g.mol^{-1}$)	86.13	58.08	72.11	114.19
Density (at 23°C, $g.mL^{-1}$)	0.854	0.785	0.805	0.820
Melting point (°C)	-136	-94.7	-86	-35
Boiling point (°C)	80.2	56.05	79.64	150
Solubility in water	14g / 100mL	Miscible	27.5g / 100mL	4.21g / 1L

2.1.3. Silica solutions

Two sources of silica nanoparticles were used: (i) an aqueous precipitated silica solution was synthesized by a sowing process (Research and Innovation Center, Aubervilliers) and (ii) a silica solution in MEK provided by Nissan Chemical Industry.

Synthesis of monodisperse silica solution: sowing process

In order to elaborate model P(VDF-co-HFP) – silica nanoparticle systems, monodisperse, spherical silica nanoparticles with a **50nm diameter** were synthesized by sowing process. It is an alternative method for the synthesis of well calibrated silica solutions. It consists in the growth of an already existing silica solution to the desired size by adding a precursor. This process corresponds to a modified Stöber process with:

i. Sodium silicate used as a precursor instead of TEOS
ii. Synthesis in aqueous rather than alcoholic medium
iii. Growth from a commercial silica solution

During this synthesis a commercial silica sol Klebosol 30R25 (30wt% of silica with a diameter of 25nm) is used in order to obtain spherical particles of 50nm. To increase the size of the particles the precursor used is an alkaline sodium silicate. The commercial silica solution is diluted in water to reach a silica concentration of 2.3wt%. Sodium silicate is added to the reactor with a flow rate of 3.6g/min. The addition of silicate increases the pH of the solution. To maintain its value at 8.5 a solution of sulfuric acid is added during the reaction. The temperature is controlled at 85°C during the reaction.

The addition of sodium silicate increases the size of the particles and the excess of salt in the reaction medium during the synthesis is eliminated by ultrafiltration. Test samples of the solutions are taken off at each reaction – ultrafiltration step and are analyzed by Dynamic Light Scattering measurements to measure the size of the nanoparticles. The reaction + ultrafiltration steps are stopped when silica nanoparticles have the desired sized (50nm). At the end an aqueous solution of **monodisperse, spherical silica nanoparticles with a 50nm diameter** are obtained (see Figure 36). The concentration

of silica in the solution is **4.6wt%** and it has a **pH of 9**: surface silanols are deprotonated (see Figure 13).

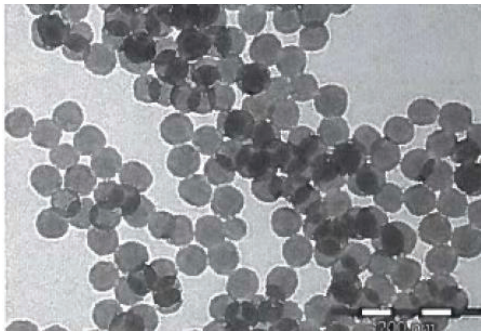


Figure 36 Aqueous silica solution produced by sowing process

Silica solutions in MEK from Nissan Chemical

Silica solutions in MEK are commercially produced by Nissan Chemical Industry with particles in the range of 10 to 100nm. A standard grade of silica nanoparticles in MEK, denoted MEK-ST-L, with a diameter similar **(40-50nm)** to that of the aqueous silica solution at higher concentration of nanoparticles **(30wt%)** was kindly provided by Nissan (see Table 4).

Table 4 Silica solutions in MEK from Nissan Chemical

Grade	**MEK-ST-L**
SiO_2 (wt%)	30
Particle size (nm) [BET]	40-50

It has to be noted that the size distribution of silica in this solution is more polydisperse than the synthetized aqueous silica solution as illustrated in Figure 37.

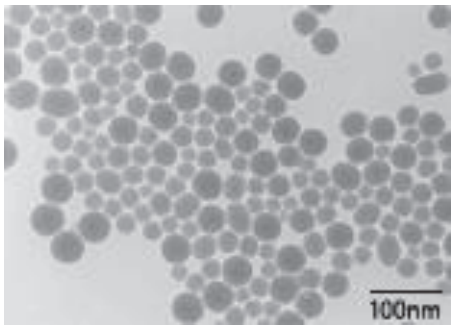


Figure 37 Representation of an example of L-type Nissan silica in organic solution to show qualitatively the size distribution (http://www.nissanchem-usa.com/products/organosilicasol)

The surface chemistry of Nissan silica is not known in details. Chen et al. (Chen, Justice et al. 2008) used various experimental techniques to investigate the surface of the silica: TGA, FTIR and solid state ^{29}Si and ^{13}C NMR. It was found that the surface organic layer represents approximately 3wt% of the dried silica. The surface functionalization contains **trimethylsilyl groups** (-$SiCH_3$), **short chain alkoxysilanes** (Si-OCH_3 or Si-CH_2-CH_3) and a small amount of **hydroxyl groups** (-OH) and was used to

partially hydrophobize the silica surface: due to the remaining hydroxyl groups the silica surface is still a little hydrophilic. However, the fraction of each modifier groups was not measured quantitatively.

2.1.4. Phase transfer of aqueous silica solution in organic solvents

PVDF-HFP is a fluorinated polymer and is thus hydrophobic and silica is a hydrophilic material. Silica must thus be transferred into an organic solvent.

To do so, a transfer agent was used to hydrophobize the silica surface: cetyl trimethylammonium bromide (CTAB, structure shows in Figure 38) which is composed of a cationic polar head and a hydrophobic carbon tail. Adsorption of the surfactant on silica is driven by electrostatic interactions between the cationic polar head group of the surfactant ($N^+(CH_3)$) and siloxane groups (SiO^-) on the nanosilica surface, up to the isoelectric point of the interface (Tyrode, Rutland et al. 2008). Indeed, silica is in an alkaline aqueous solution (pH 9.04 at 21.0°C). As a consequence, surface silanols are deprotonated and negatively charged. As CTAB is positively charged, an electrostatic bond is formed between the silanol and the CTAB.

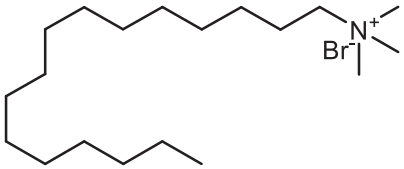


Figure 38 Structure of CTAB surfactant

In our case the concentration of CTAB is lower than its cmc (to prevent micellization) and silica nanoparticles will be covered by a monolayer of CTAB, with polar heads on the silica and hydrophobic tails toward the solvent (Liu, Tourbin et al. 2013). Adsorption of CTAB on the nanoparticle surface increases their hydrophobicity, which provides a driving force for the migration of the nanoparticles to the hydrophobic solvent (Ravera, Santini et al. 2006).

To stabilize the organic solution a silane must then be grafted on silica nanoparticles. All silanols on the surface should not be covered by CTAB molecules. The minimum amount of CTAB required for phase transfer to occur was optimized (at Functional Inorganic Materials Laboratory, Aubervilliers). It was found that covering 18.4mol% of the surface silanols with CTAB is sufficient for the phase transfer.

To calculate the quantity of CTAB adsorbed on silica, we assume that silica nanoparticles are spherical with a diameter of 50nm and that there are 6 Si-OH per nm^2 (Iler 1979) and that each Si-OH interacts with only one CTAB molecule. The calculation of the quantity of CTAB necessary to cover silica nanoparticles is detailed below.

The surface of one silica nanoparticle is $4\pi r^2 = 4\pi\left(\frac{50}{2}\right)^2 = 7854$ nm^2, which corresponds to about 47×10^3 SiOH, considered to be potential grafting sites.

The mass of a silica sphere is $\rho\frac{4}{3}\pi r^3 = 2.2 \times \frac{4\pi}{3}\left(\frac{50\times10^{-7}}{2}\right)^2 = 1.44 \times 10^{-16}$ g. The number of silanols per gram is thus (N_A is the Avogadro number)

$$n_{OH} = \frac{1}{N_A} \times \frac{47124}{1.44 \times 10^{-16}} = 5.43 \times 10^{-4}\ mol_{OH}/g_{SiO2}$$

The mass of CTAB per gram of silica to introduce to saturate x% of the silica monolayer with CTAB is thus:

$$m_{CTAB} = n_{OH} x M_{CTAB}$$

where M_{CTAB} = 349 g/mol is the molar mass of CTAB

Phase transfer in 2MeTHF

The transfer of silica in organic solvent was first developed in 2MeTHF. This process is performed in several steps shown in Figure 39. CTAB is first dissolved in ethanol (EtOH), then the aqueous silica solution is added and a CTAB-treated silica solution in water is formed. 2MeTHF (with a volume equal to the volume of water) is added in a second step and CTAB-treated silica nanoparticles migrate to the organic solvent. In this process the ethanol plays an important role and its quantity was optimized: water-CTAB-2MeTHF forms an emulsion which is difficult to break, the addition of ethanol helps breaking the emulsion and forming a biphasic system.

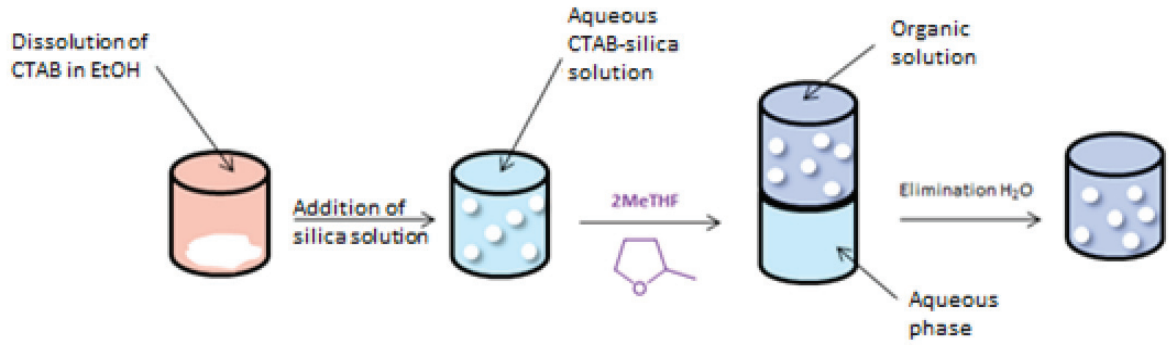


Figure 39 Phase transfer in 2MeTHF

After the phase transfer step a stable silica organic solution is obtained. It would be interesting to characterize the silica surface to quantify the adsorbed surfactant and verify that 18.4% of silanols are covered by CTAB. This characterization was not performed in this work.

However, 2MeTHF is not a good solvent of P(VDF-co-HFP). To develop materials (gels or nanocomposites) the polymer must be added in the form of a solution in another solvent (acetone) which complexifies the obtained systems, as the ratio 2MeTHF/acetone may vary (Ma, Zhang et al. 2008). As a consequence, to develop gels and nanocomposites we had to identify a single common solvent. **This leads to a generic approach of the phase transfer which can be used in various solvents**

The new solvent should match the conditions below:

i. Be immiscible with water to perform the phase transfer
ii. Have a boiling point above 60°C to perform the silane grafting (details in the next paragraph)
iii. Be a good enough solvent for the PVDF-HFP (good solubility and a Flory-Huggins parameter between 0 and 0,5)

iv. Have a low toxicity and be non-Carcinogenic, Mutagenic of toxic for Reproduction (CMR)

The solubility of P(VDF-co-HFP) in ketone solvents was discussed in the first chapter. Ketones are composed of a carbon-oxygen double bond and a carbon backbone. By increasing the number of carbons of the carbon chain the hydrophobicity of the solvent increases. However, at the same time the Flory-Huggins interaction parameter with P(VDF-co-HFP) increases and becomes closer to 0,5: the solvent quality for the polymer decreases. A compromise has to be found between the hydrophobicity of the solvent and its quality for PVDF-HFP. **Linear ketone solvents and more particularly MEK and 2-heptanone** (see structures in Figure 35) are usually used for dissolving PVDF-HFP and seem to be a good compromise for developing our materials. Indeed, at room temperature their Flory-Huggins parameters are between 0 and 0.5 (they are good solvents of the polymer), moreover their solubilities in water are relatively low.

Phase transfer in linear ketone solvents: MEK and 2-heptanone

The phase transfer process in 2MeTHF was adapted and optimized in other solvents, and more particularly MEK. Indeed, while ethanol plays a crucial role in the phase transfer in 2MeTHF, it acts as a co-solvent in MEK and promotes miscibility of MEK and water, leading to the precipitation of silica. To avoid this problem, ethanol was removed from the process. The water-CTAB-MEK emulsion breaks spontaneously after 24 hours (see Figure 40).

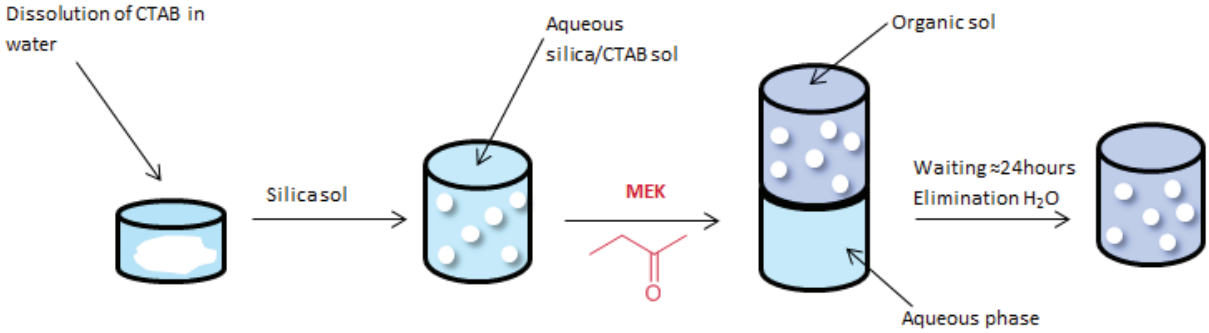


Figure 40 Phase transfer process in MEK

CTAB is dissolved in a small amount of water. The silica solution is then added to the CTAB/water mixture. In the third step the organic solvent is added and a neat phase separation occurs after 24hours. A stable silica solution in MEK is recovered.

Characterization of the phase transfer by solvent NMR relaxometry

Proton NMR solvent relaxation measurements rely on the fact that protons belonging to mobile (liquid-like behavior) and immobile (solid-like) molecules have very different relaxation times. The proton spin-spin relaxation time (T_2) is proportional to the inverse of the correlation time (τ_c), which describes the lifetime of a dynamic process (e.g. rotation of the molecule) (Nelson, Jack et al. 2002). Free solvent molecules are highly mobile and thus possess T_2 spin relaxation times of order of several seconds while solvent molecules bound to an interface have strongly constrained molecular motions and relax with a relaxation time typically lower than 1ms. It is therefore possible to distinguish a pure solvent (without silica) to a silica solution (aqueous or organic). In a silica solution, solvent molecules are either diffusing freely within the liquid phase (long $T_2^{(free)}$ relaxation time) or constrained near

the interface (small fraction ϕ, short $T_2^{(bond)}$ relaxation time). If solvent molecules exchange very fast between these two populations, then a single average T_2 relaxation time is measured, given by:

$$\frac{1}{T_2(\phi)} = \frac{\phi}{T_2^{(bond)}} + \frac{1-\phi}{T_2^{(free)}} \quad (8)$$

As $T_2^{(bond)}$ is extremely short compared to $T_2^{(free)}$ the measurement of $T_2(\phi)$ is very sensitive to the presence of even a small quantity of interfaces in the system. Figure 41 shows the decay curves of water and aqueous silica solution containing 4.6wt% of silica nanoparticles and it is obvious that the presence of silica leads to a strong decrease of the relaxation time T_2. T_2 drops from 3.43 s in pure water down to 1.1 s in the silica solution.

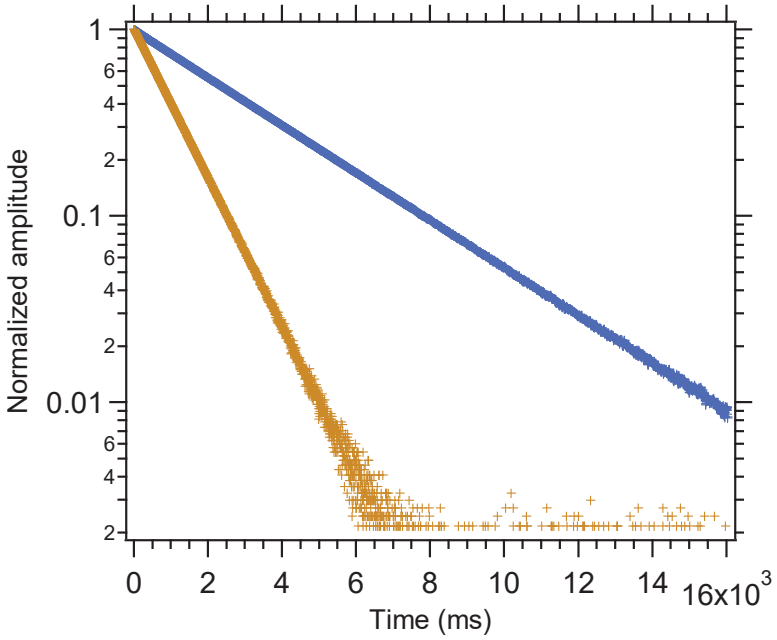


Figure 41 Solvent relaxation curves of water (top curve, blue ■) and aqueous silica solution containing 4.6wt% of silica (bottom curve, brown +)

We performed ^{1}H relaxometry NMR measurements on the aqueous and organic phases recovered after the phase transfer process to verify that all the silica particles were transferred in the organic solvent (MEK here). Due to its partial solubility in water, the silica solution in MEK contains approximately 15wt% water and the aqueous phase contains 25wt% of MEK (Siegelman and Sorum 1960) as shown in Figure 42. For further comparison, the same ^{1}H NMR experiments were carried out on reference MEK-rich (85wt% MEK + 15wt% water) and water-rich solvent mixtures (75wt% water + 25wt% MEK) without silica nanoparticles.

All measurements were conducted on a Bruker Minispec *mq*20 at 20MHz proton resonance frequency. The standard Carr-Purcell-Meiboom-Gill (CPMG) sequence was used with a τ spacing of 2ms. 4000 data points were collected and 8 scans were collected for each acquisition. The decay curves were normalized to the amplitude M_0 of the transverse magnetization following a single 90° pulse. T_2 relaxation times were determined from the single-exponential normalized relaxation curves.

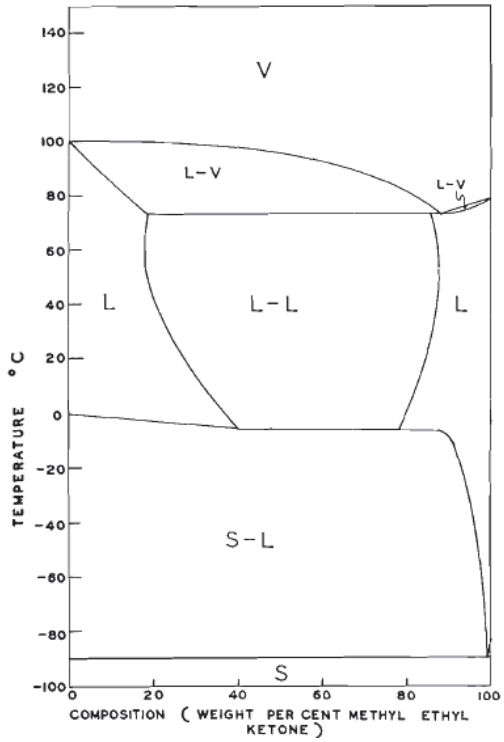


Figure 42 MEK – water phase diagram (Siegelman and Sorum 1960)

After the phase transfer process, the aqueous and organic (MEK-rich) phases were taken and measured separately. Figure 43 shows the relaxation curves of the organic (in MEK) and aqueous phases recovered after the phase transfer process. Different relaxation times are determined and can be attributed to the presence of silica nanoparticles only in the organic phase that shows a lower T_2.

To be more precise the relaxation curve of the aqueous phase after phase transfer was compared to the curve of the water-rich solvent mixture (75wt% water + 25wt% MEK) and results are shown in Figure 44 –a. It is clear that the signals are very similar and almost identical relaxation times were determined: $T_{2,\ \text{water-rich solution}}$=3894,1s and $T_{2,\ \text{aqueous phase}}$=4031,6s. This indicates that no silica nanoparticle remain in the aqueous phase as the relaxation times are equal. The presence of residual silica nanoparticles would decrease the relaxation time as it was shown in Figure 41. Relaxation curves of the MEK-rich phase (85wt% MEK + 15wt% water) and silica organic solution in MEK are presented in Figure 44 –b. In this case the relaxation time is strongly affected, which is due to the presence of silica nanoparticles. The presence of silica in the organic phase after phase transfer is also confirmed by the presence of a small (a few %) contribution in the signal which relaxes very fast. This may correspond to the protons in CTAB molecules which are stuck on the silica surface. A contribution may also come from water molecules trapped on the silica surface.

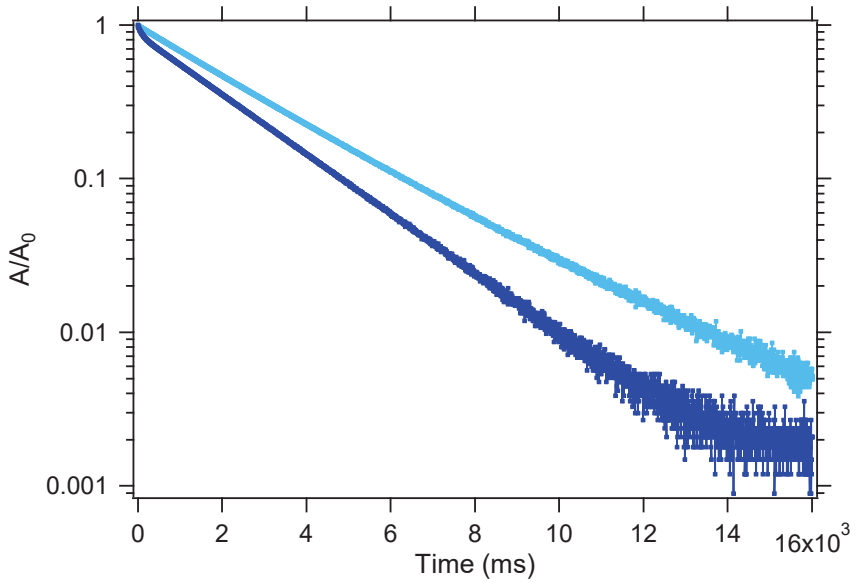


Figure 43 Solvent relaxation curves of aqueous (light blue ■) and organic (blue ■) phases recovered after the phase transfer process

From this result it is possible to note that there is no significant amount of silica nanoparticles in the aqueous phase recovered during the phase transfer process, its relaxation times being similar to those of an aqueous solution without silica. Therefore, it is possible to conclude that, with this method, **all the silica nanoparticles have been transferred into MEK.**

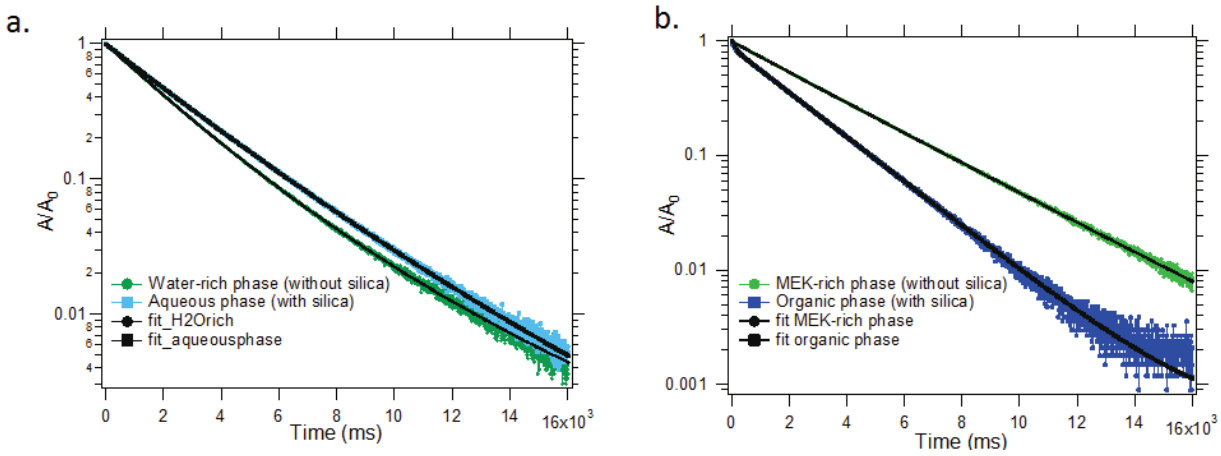


Figure 44 ^{1}H NMR on (a) (experimental: green ●, fit : black ●)water-rich phase (without silica) and (experimental: blue ■, fit : black ■)aqueous phase of the phase transfer process; (b) (experimental: green ●, fit : black ●)MEK-rich phase (without silica) and (experimental: blue ■, fit : black ■)organic phase of the phase transfer process

A **generic approach of the transfer of silica nanoparticles from water to organic solvents** was developed. By adapting the processes detailed in this section to the desired solvent (changing the surfactant, covering rate of silica with surfactant, additives to break the emulsion…), it would be possible to **obtain silica solutions in various organic solvents**. However, the precise conditions must be adapted in each case. Due to the different polarity of 2-heptanone in comparison with MEK, CTAB is not miscible in 2-heptanone and as a consequence the transfer of silica nanoparticles was not adapted in 2-heptanone with this process. A solvent exchange method from Nissan Chemical silica solution in MEK was developed and will be detailed in a further Section.

2.1.5. Silane grafting of silica nanoparticles in organic solvents

Previous works (in RIC Aubervilliers) on silica nanoparticles dispersed in a VDF terpolymer have shown that grafting a silane on silica nanoparticles in organic solution stabilizes the silica solution but also improves the dispersion state in PVDF-based silica nanocomposites by improving the polymer – silica interactions.

Different silanes were grafted on silica surface and their influence on the stability and homogeneity of the silica organic solution has been studied. All the silanes studied in this work are summed up in Figure 45. Silanes are grafted to the silica – CTAB organic solution under refluxing at 60°C overnight. In three cases, silica particles precipitate: triethoxy(ethyl)silane, diethoxydimethylsilane and ethoxytrimethylsilane. Conversely, after one day, the particles remain in solution in the grafted silica sol with Vinyltrimethoxysilane (VTMS) and triethoxymethylsilane. For now, we did not yet relate the structure of the grafted silane and the stability of the organic solution. It would be an interesting point to study in the future.

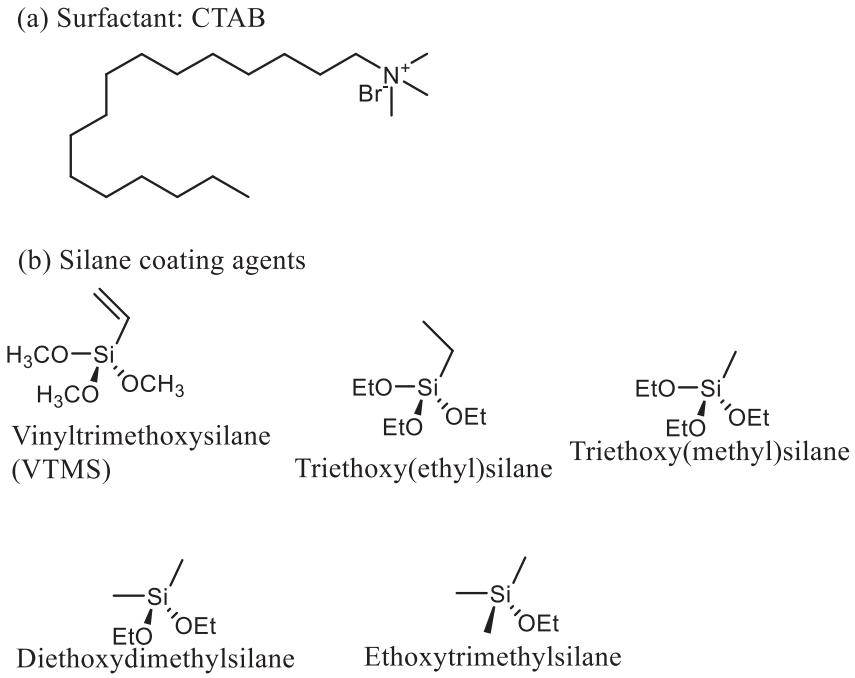


Figure 45 Surface silica modifiers

Only VTMS will be used in what follows, in particular because of its carbon – carbon double bond which may potentially be used to create a covalent silica–polymer bond after further functionalization steps. This point will not be discussed here and we will only focus on CTAB and VTMS treated silica solutions in MEK, which will be dispersed in P(VDF-co-HFP). No covalent bonds will exist between the silica and the polymer, but physical interactions can occur (hydrophobic interactions, H-bondings…)

2.1.6. Solvent-exchange method to prepare silica solutions in 2-heptanone: from Nissan Chemical solutions in MEK

2-heptanone was used to generalize the study of gelation mechanisms of P(VDF-co-HFP) in linear ketone solvents and also because of its low volatility, which makes characterization easier in

comparison with MEK. Rather than adapting the phase transfer process in this solvent, we developed a solvent exchange method from the Nissan Chemical silica solution in MEK (MEK-ST-L).

2-Heptanone is added into the MEK-ST-L silica solution. The mass of 2-Heptanone added is equal to the mass of MEK in the silica solution. Then MEK is evaporated from this mixture of solvents by means of vacuum rotary evaporation. This process is illustrated in Figure 46. A stable silica solution in 2-heptanone is recovered and is diluted to the desired concentration (4.6wt.%) by adding again 2-Heptanone.

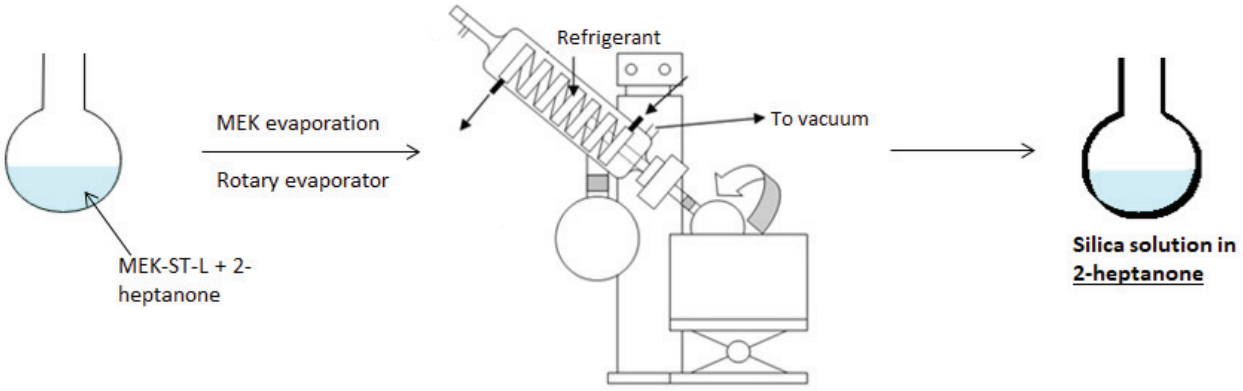


Figure 46 Preparation of silica solution in 2-heptanone by solvent exchange

It has to be highlighted that a small fraction of MEK may still remain in the solution of silica in 2-heptanone.

P(VDF-co-HFP) – silica model systems were developed in MEK and 2-heptanone. Stable silica solutions in organic solvents were first prepared as detailed previously. Gels were then formulated by adding the copolymer into the silica solution. Then hybrid membranes were obtained by means of solvent casting. These different steps will be detailed in the following sections.

2.1.7. Formulation of P(VDF-co-HFP) organogels filled with silica

Silica (in MEK and 2-heptanone) in P(VDF-co-HFP) materials are prepared by dissolving an appropriate amount of P(VDF-co-HFP) in the silica solution to reach the desired concentration of silica in the gel and in the final film. The mixture is stirred with a magnetic bar at 500rpm under reflux at 60°C for silica solutions in MEK and 80°C for silica solutions in 2-heptanone for at least 2.5 hours.

P(VDF-co-HFP) – silica solutions are then cooled to room temperature (or other desired temperatures) in sealed vials and the solutions turn to a gel with different gelation times depending on the polymer and silica concentrations, temperatures and solvent.

P(VDF-co-HFP) gels in MEK and 2-heptanone were also prepared by dissolving an appropriate amount of the polymer in the desired solvent under reflux at 60°C and stirring with a magnetic bar at 500 rpm for 2 h in order to obtain homogeneous solutions. The solutions are cooled to different temperatures in sealed vials.

2.1.8. Processing of P(VDF-co-HFP) – silica nanocomposites films

P(VDF-co-HFP)-nanosilica-solvent systems form a gel within some minutes to some hours. In this situation, the gels are reheated at 60°C (for gels in MEK) or 80°C (for gels in 2-heptanone) in order to

obtain viscous solutions which is required for solvent casting. The solutions are then cooled down to room temperature or lower temperature (for solutions in 2-heptanone, the solution gelifies again before reaching RT: solvent casting in 2-heptanone was carried out at a temperature a little higher than RT around 40°C).

Once the solution is ready, the film can be casted by doctor blade (Elcometer). The solution is poured uniformly in the front of a knife on a glass substrate. The mechanical arms of the doctor blade are then activated and spread the solution on the substrate. This process is described in Figure 47.

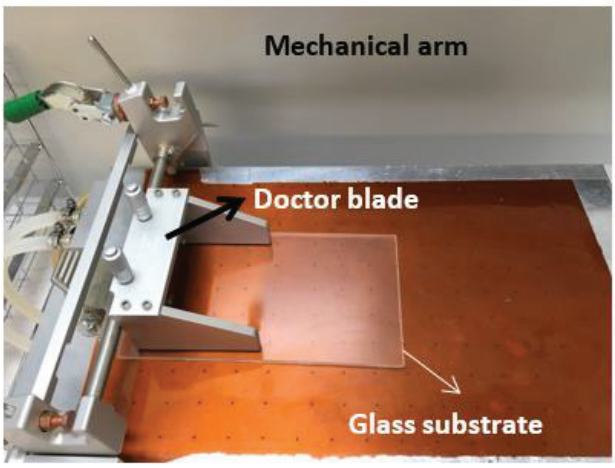


Figure 47 Formation of P(VDF-co-HFP) - silica films by solvent casting

The initial thickness set on the knife is 500µm leading to dry materials with a final thickness between 30 to 60 µm depending on the composition of the solutions. After solvent casting, the films are firstly dried in the fume hood at room temperature for some hours. In a last step the films are dried in vacuum oven at: 60°C for 2 hours for films made from P(VDF-co-HFP) – silica solutions in MEK and 80°C for 2 hours for films made from P(VDF-co-HFP) – silica solutions in 2-heptanone. TGA measurements were carried out on films to verify that no trace of solvents is found in the films.

2.2. Dynamical and structural characterization of gels

A combination of characterization methods has been used to investigate the gelation kinetics, mechanisms and gel structure of our materials: tube tilting, linear and non-linear rheology, ^{19}F NMR, DSC and X-ray scattering. Rheology measurements were performed at the Laboratory of the Future (LoF, Bordeaux, France), ^{19}F NMR was carried out at the "Institut de Chimie des Matériaux Paris Est" (ICMPE, Thiais, France), WAXS measurements were performed at the Henri Longchambon Diffractometry Center (University of Lyon, France), SAXS measurements were performed at SWAXS laboratory (IRAMIS, Saclay, France) and ESRF (ID02 beamline, Grenoble, France).

In this section, the concepts and protocols of these different measurements are reported.

2.2.1. Gelation kinetic: tube-tilting

The kinetic study of the gelation process was carried out using a tube tilting method in 24 mm diameter vials at different temperatures between -40°C to 60°C. The gelation time t_{gel} is considered to be the time at which no macroscopic flow of the sample is observed when the tube is tilted. This

characterizes the time at which the solution becomes a soft elastic solid or at least a Bingham fluid (see Figure 48) with a yield stress $\sigma > \rho g h \approx 400\ Pa$ (see Figure 48).

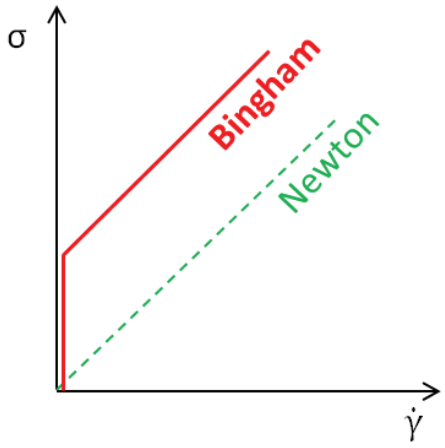


Figure 48 Schematization of Newton and Bingham fluids

Depending on the sample concentration and temperature, the range of durations investigated stands between about 2 min and about 1 month.

2.2.2. Rheology

Principles of rheology applied to gels

During a rheological measurement a sample is sheared between two flat surfaces. Oscillatory (or dynamic) rheology consists in imposing a sinusoidal strain with an angular frequency ω at low amplitude γ_0: $\gamma(t) = \gamma_0 \sin \omega t$. In the linear regime, the response of the material is a sinusoidal function with the same pulsation but with a phase shift δ:

$$\sigma(t) = G'\gamma(t) + \frac{G''}{\omega}\dot{\gamma}(t) \tag{9}$$

$$\sigma(t) = \sigma_0 \sin(\omega t + \delta) \tag{10}$$

Which may be written equivalently

$$\sigma(t) = G'\gamma_0 \sin \omega t + \frac{G''}{\omega}\gamma_0 \omega \cos \omega t \tag{11}$$

$$\sigma(t) = G'\gamma(t) + \frac{G''}{\omega}\dot{\gamma}(t) \tag{12}$$

G' is the storage modulus and corresponds to the elastic response of the material while G'' is the loss modulus and corresponds to the viscous (dissipative) response of the material.

The complex modulus G* is defined as:

$$G^*(\omega) = G'(\omega) + iG''(\omega) \tag{13}$$

It is then possible to plot the stress as a function of the strain or the strain rate (Lissajous plots). The stress-strain curves of viscoelastic materials in the linear regime would be ellipses with major and minor axes which depend on the contributions of viscous and elastic response (see Figure 49). If the material is purely viscous the (stress, strain) Lissajous plot will be an horizontal ellipse and when the stress is plotted as a function of the strain rate, the Lissajous plot will be a straight line with a slope equal to $\frac{G''}{\omega} = \eta$ the viscosity of the material.

In the case of an elastic material, the stress is expressed as $\sigma(t) = G'\gamma(t)$ leading to a straight line in the Lissajous plot.

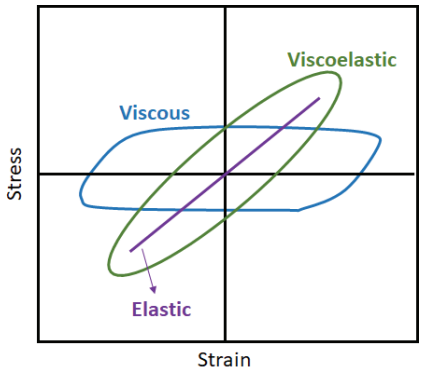


Figure 49 Stress - strain curves (Lissajous plot) for viscous, elastic and viscoelastic materials

Linear rheology measurements were performed to determine the evolution of both storage and loss moduli as a function of time and frequency. These measurements were performed on P(VDF-co-HFP) gels in 2-heptanone to follow the gelation kinetics and characterize the gel state.

The gelation time may be conventionally defined as the crossover point between the storage modulus G' and loss modulus G''. Indeed, the response in the liquid state is viscous, and G' < G'', while in the gel state G'>G''. Another criterion was introduced by Winter and Chambon (Chambon, Petrovic et al. 1986) to determine the gel point. When the gel state is reached, $\tan\delta = \frac{G''(\omega)}{G'(\omega)}$ should be independent of the frequency.

The above considerations can be extended to the nonlinear regime, in so-called large amplitude oscillatory shear (LAOS) measurements.

In the linear viscoelastic regime (small strain amplitude), both viscoelastic moduli are independent of strain amplitude (see Figure 50) and the stress is sinusoidal. When the strain amplitude increases, the storage and loss moduli are functions of the strain amplitude and the stress can be expressed as $\sigma(t) = G'(\gamma)\gamma(t) + G''(\gamma)\dot{\gamma}(t)$. An example observed for P(VDF-co-HFP) gels in 2-heptanone is shown in Figure 51. With the increase of the strain amplitude, the moduli become dependent on the strain.

In the nonlinear regime, the stress may also become non-sinusoïdal. It follows that stress-strain Lissajous curves may be stretched and deformed ellipses. The deformation of theses ellipses can be described in terms of the softening and/or hardening of the material at large strains.

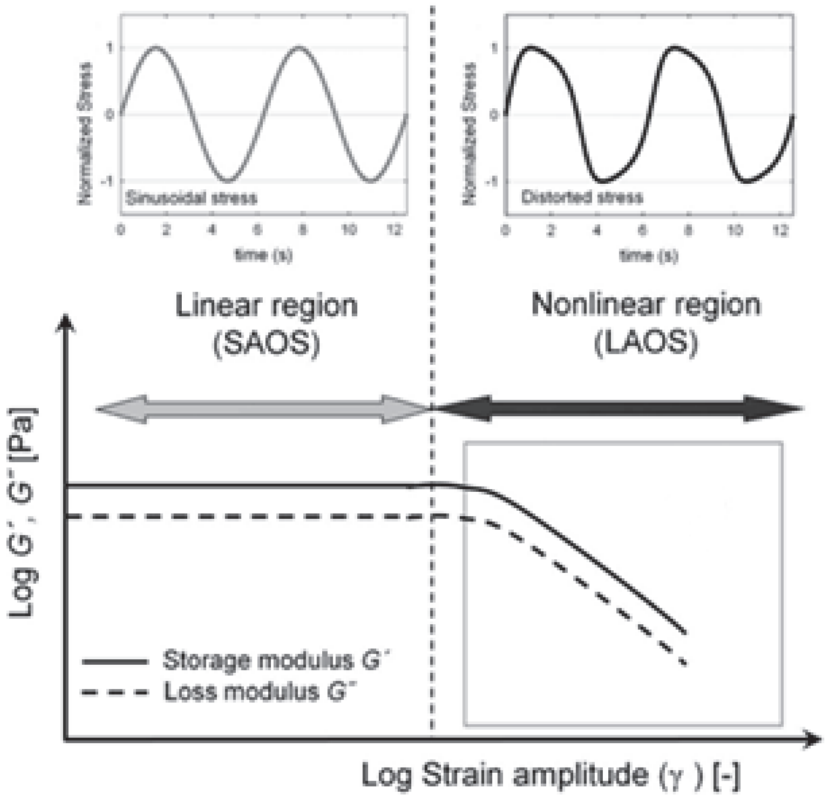


Figure 50 Illustration of the strain sweep test (LAOS) at fixed frequency (Hyun, Wilhelm et al. 2011)

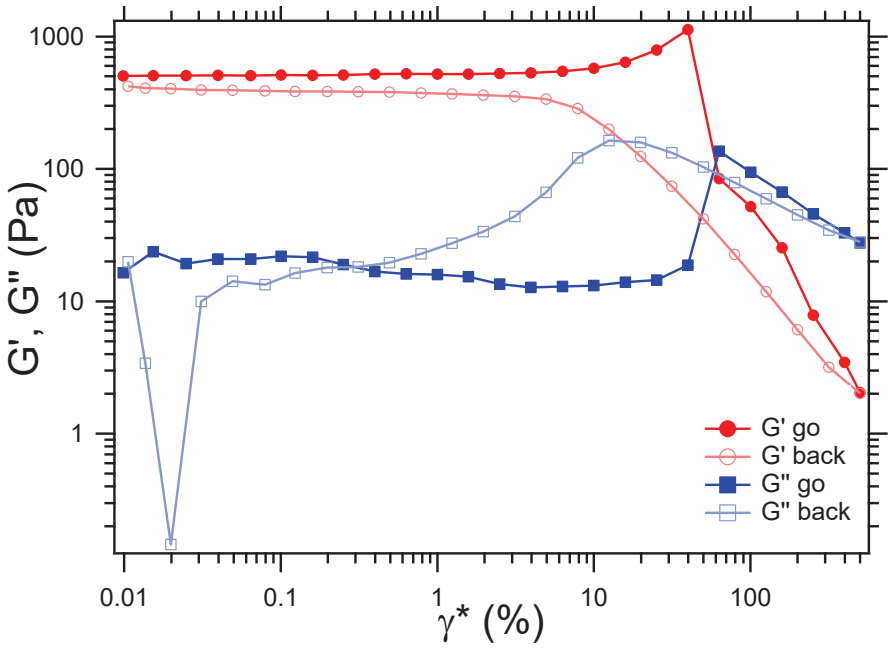


Figure 51 Strain sweep test at fixed frequency for a 8wt% P(VDF-co-HFP) gel in 2-heptanone

Experimental protocol

Rheological measurements of gels were performed on a Kinexus rheometer (Anton Paar) with a cone-plate geometry (CP4/40: 4°angle and diameter of 40mm) and an enclosure to prevent the evaporation of the solvent (see Figure 52).

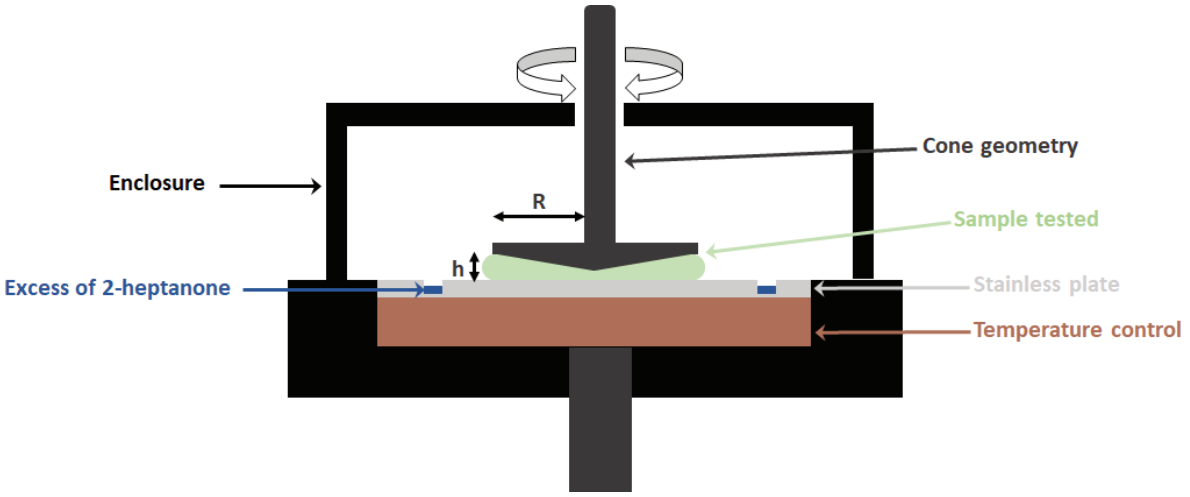


Figure 52 Schematic view of the rheometer equipped with a cone-plan geometry, excess of solvent and an enclosure to prevent the evaporation of 2-heptanone

Large Amplitude Oscillatory Shear (LAOS) measurements were performed to study the behavior of gels under large strains.

Both linear and non-linear rheology measurements were carried out on P(VDF-co-HFP) gels filled or not with silica. Due to the high volatility of MEK, even with an enclosure, only P(VDF-co-HFP) gels in 2-heptanone were measured.

The sample is introduced in the liquid state on the pre-heated lower plate at 75°C and cooled down to the desired temperature at a heating rate of about 60°C/min.

Linear rheology

"Oscillation single frequency" measurements were performed to determine the gelation time and gel melting temperatures of our materials. Temperature was in the range 25°C – 75°C. The frequency was fixed at 1Hz with the target shear strain at 0.1%. Storage and loss moduli as a function of time and temperature are extracted from this experiment.

Oscillatory frequency sweeps on gels were conducted over the frequency range of 0.1Hz to 10Hz at 25°C and 75°C. The shear strain during the experiment is fixed at 0.1%. This sequence assesses the gel state of our materials.

Non-linear rheology: LAOS

Oscillatory strain sweeps were performed to determine the linear viscoelastic region of the gel and the behavior of the gel under large oscillatory shear. These experiments were conducted at 25°C at 1Hz over a strain range of 0.01% to 500%. Storage and loss moduli are measured as a function of the shear strain and raw data (angular displacement θ and torque T) are saved in order to determine the strain and stress as a function of time and to plot the Lissajous curves of the material. The stress σ and strain γ are defined as:

$$\sigma = \frac{3T}{2\pi R^3} \tag{14}$$

$$\gamma = \frac{R\theta}{h} \quad (15)$$

where R is the radius of the plate and h the gap between the cone and the plate.

2.2.3. ^{19}F NMR

Principle of NMR

NMR was used to investigate the dynamics of P(VDF-co-HFP) chain segments at different concentrations in MEK. In NMR, the so-called transverse magnetic signal, excited after a single pulse, relaxes to zero under the effect of various interactions imposed on spins. The corresponding NMR transverse relaxation time (also called spin-spin relaxation time, as it depends mostly on dipolar interactions between spins), denoted T_2, depends on molecular motions, because dipolar interactions depend on molecular orientation, and therefore are modulated by molecular reorientation motions. Therefore, measuring NMR relaxation times (so-called time-domain NMR) gives dynamic information on a system.

PVDF polymer is predominantly fluorinated while the solvent is hydrogenated. Therefore, fluorine NMR (^{19}F NMR) allows observing selectively the contribution from the polymer in solution or in the gel state in MEK. Flurorine has a ½ spin as in that respect is similar to protons (^{1}H). The same concepts as in proton NMR may thus be applied. There is however a difference which makes ^{19}F NMR a little bit more complex, which is that ^{19}F NMR has very large chemical shifts and chemical shift anisotropies.

Within this context ^{19}F NMR was used here for two distinct purposes: first, to study dynamical heterogeneities (discriminate rigid and mobile fractions of polymers) and secondly, to study the structure of the network in polymer gel systems.

The basic principle of relaxation NMR is that fluorine atoms (same as for protons and any nucleus observed in NMR in general) belonging to mobile (liquid-like behavior) and immobile (solid-like) molecules have very different relaxation processes with vastly different time scales. Mobile entities (molecules or monomers) have a long transverse relaxation time T_2, inversely proportional to the correlation time τ_c of molecular motions. The T_2 relaxation time can vary over orders of magnitude depending on the system, between typically a few tens of ms up to a few seconds. Conversely, molecules or monomers immobilized or with strongly constrained motions have a very fast NMR transverse relaxation, typically of the order 20 to 40 microseconds. There are thus several orders of magnitude difference in the NMR relaxation rates depending on the mobility.

The second objective was to characterize the mobile fraction in terms of structure of the network forming the gels. Proton and deuterium NMR have been widely used to characterize elastomer networks. The basic principle here is that, while chain segments have fast molecular motions (like in the molten state), crosslinks introduce local constraints which induce local anisotropy of chain segment reorientation motions. As spin interactions are sensitive to molecular orientation, this local anisotropy (even though it may be very small) induces a specific contribution to NMR relaxation. This contribution can be discriminated and quantified using appropriate NMR methods. Specifically, double-quantum (DQ) NMR measurements have been shown to be well suited for that (Saalwächter 2007).

Therefore, two types of experiments were performed on the materials: transverse relaxation and double-quantum (DQ) NMR measurements. These methods, reported in this manuscript, are described schematically in this part.

Transverse relaxation NMR

Transverse relaxation (time-domain) NMR allows to distinguish different populations within a heterogeneous or composite polymer system, as schematized in Figure 53:

- A rigid fraction of polymer can be discriminated from a mobile fraction (crosslinks and crosslinked chains). This is based on the fact that rigid and mobile fractions have very different types of NMR relaxation behavior, with very different time scales.
- In the mobile part of a gel, the chains belonging to the network can be discriminated from dangling chains and polymer chains in solution. This is based on the fact that chains attached to the network have a local preferred orientation, which gives a distinct contribution to the NMR relaxation. This contribution can be discriminated and measured by appropriate methods.

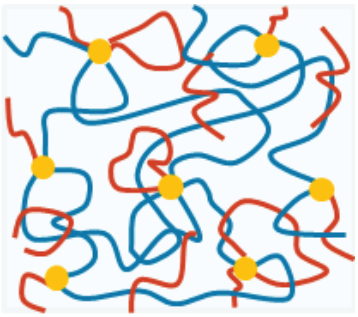


Figure 53 Schematic representation of a polymer network

The time scales of transverse relaxation are very different for a mobile polymer (far above T_g or in solution) and a polymer in the solid state or in which motions are strongly constrained. For a polymer in solution, it can range typically from 100 milliseconds up to 1 seconds. For a solid polymer it is of the order 20 to 40 ms. Thus in a heterogeneous system the signal is composite with two very distinct contributions as schematized in Figure 54.

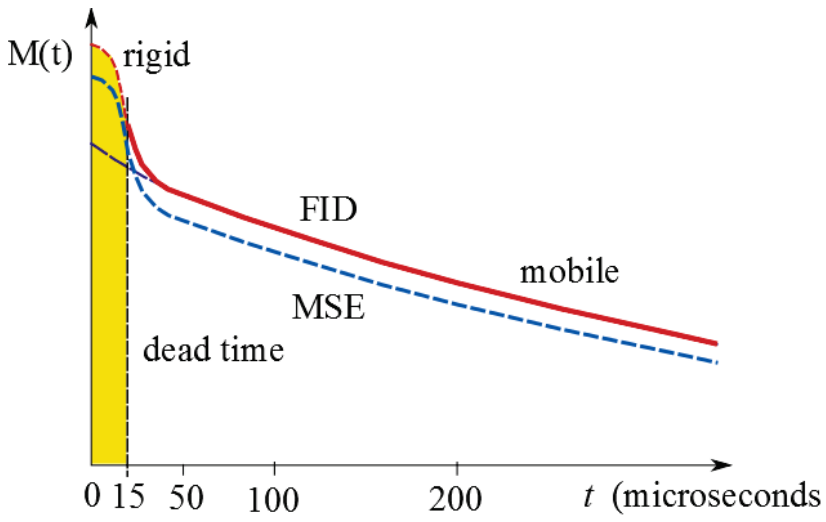


Figure 54 Schematics of the transverse relaxation signal of a gel with a rigid fraction of polymer. The signal (FID, red curve) cannot be observed in the dead time, before about 15 ms. The MSE allows observing the signal from t = 0 (blue curve), at the expense of a small decrease of the overall intensity, which can then be renormalized (dashed red curve).

Detection of rigid zones: Solid-echo pulse sequence – "Magic Sandwich Echo" (MSE)

One very important problem is that the signal cannot be observed immediately after a single excitation pulse (the so-called Free-Induction decay or FID in the NMR language) (time 0 in Figure 55), this is the so-called dead-time of the NMR spectrometer, as schematized in Figure 54.

It follows that a very fast relaxing signal cannot be observed directly using the FID. The method used to circumvent this problem is the so-called solid-echo or the more sophisticated version 'Magic Sandwich Echo' (MSE) sequence, as schematized in Figure 54

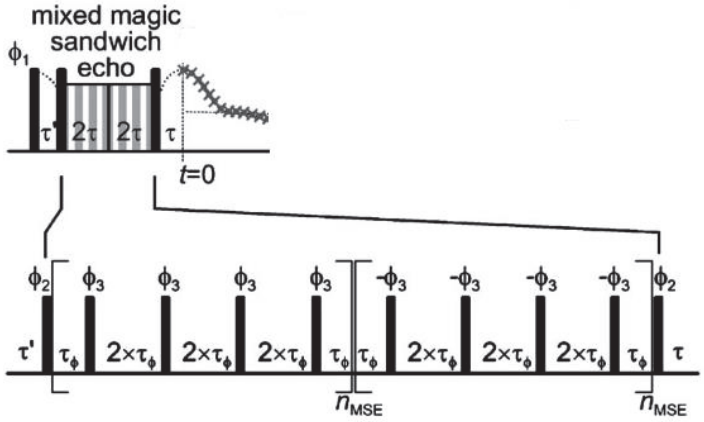


Figure 55 MSE sequence (Maus, Hertlein et al. 2006)

The way in which the MSE sequence operates on the spin system will not be explained in details here. The principle is that it creates a spin-echo, which is a time at which all spin interactions contributing to relaxation practically cancel (in the NMR language, they are 'refocused'). The signal thus has a maximum (because relaxation effects are cancelled) and this maximum can therefore be used as time 0, as indicated in Figure 54.

In this way the signal, including a very short solid signal, can be effectively observed from the beginning. The MSE intensity is a little smaller than the 'true' intensity (compare the blue and red

curves in Figure 54). To minimize this decrease, the 'phase switching time' τ_ϕ in the sequence should be taken as short as possible.

Transverse relaxation in the mobile part, CPMG pulse sequence

In practice the relaxation time of the mobile fraction cannot be measured directly because the observed relaxation is dominated by inhomogeneities of the static magnetic field. A classical spin echo technique must be used. The principle is the following one. A single 90° pulse applied at time t = 0 gives the observed relaxation signal

$$M(t) = M_0 \exp\left(-\frac{t}{T_2}\right)\langle \exp(-i\delta\omega_0 t)\rangle \tag{16}$$

In which, in addition to the T2 relaxation term (which is intrinsic to the studied sample and reflects the molecular mobility), there is a contribution to relaxation from magnetic field inhomogeneities. This contribution may be written as due to a distribution of small shifts $\delta\omega_0$ of the Larmor frequency, depending on the local value of the magnetic field. At a time t, a 180° pulse is applied. Its effect is to revert the phase factor due to field inhomogeneities $-i\delta\omega_0\tau \rightarrow +i\delta\omega_0\tau$ (see Figure 56). The signal then continues to relax as before starting from t = τ, which gives:

$$\begin{aligned} M(t) = M_0 \exp\left(-\frac{t}{T_2}\right)\langle \exp(i\delta\omega_0\tau)\exp\big(-i\delta\omega_0(t-\tau)\big)\rangle = \\ = M_0 \exp\left(-\frac{t}{T_2}\right)\langle \exp(-i\delta\omega_0(t-2\tau))\rangle \end{aligned} \tag{17}$$

So that at time $t = 2\tau$ (the top of the spin echo) the effect of magnetic field inhomogeneities cancels out.

$$M(t = 2\tau) = M_0 \exp\left(-\frac{t}{T_2}\right) \tag{18}$$

A train of successive 180° pulses separated by 2τ can be then applied and the 'true relaxation curve $\exp\left(-\frac{t}{T_2}\right)$ is obtained by recording the amplitude of all successive spin echoes. This is the so-called Carr-Purcell-Meiboom-Gill (CPMG) sequence. In practice, one every two echo maxima is recorded, as schematized in Figure 56.

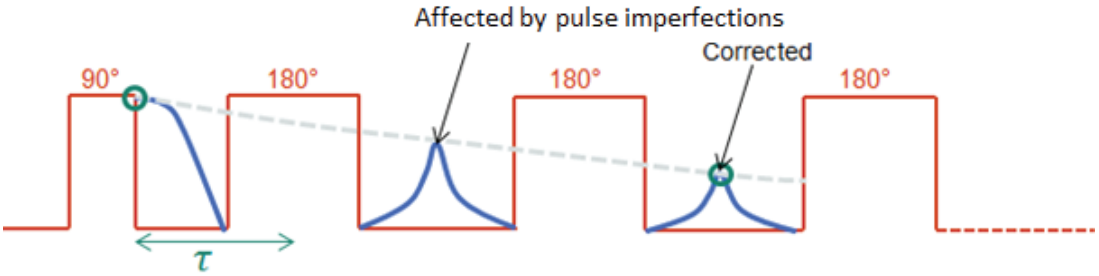


Figure 56 CPMG sequence

Study of the gel network structure: Double-quantum NMR

In elastomer networks and gels, the presence of chemical or physical crosslink points introduces restrictions on the motion of network chain segments (Sotta, Fülber et al. 1996). Since the dipolar spin-spin interaction between protons depends on orientation, this results in a non-zero average of the proton-proton interactions, resulting in a so-called 'residual interaction' D_{res}. The presence of this residual interaction induces an additional factor in the transverse relaxation signal, which may be schematically written as:

$$M(t) = M_0 \exp\left(-\frac{t}{T_2}\right) \langle \cos(D_{res} t) \rangle \quad (19)$$

Where brackets denote an average over all network chains. The parameter D_{res} is proportional to the crosslink density ν as shown in equation below:

$$D_{res} \sim \langle \frac{3\cos^2\theta - 1}{2} \rangle \sim \left(\frac{R^2}{N^2 b^2}\right) \sim \frac{1}{N} \sim \nu \quad (20)$$

θ is the angle between the proton-proton vector and the magnetic field of the NMR. The brackets denote a time average over typically a millisecond range. There are several methods to separate and possibly quantify each factor in equation 19.

DQ spectroscopy is one of the most versatile techniques to investigate the structure and dynamics of polymer networks.

These sequences provide information on dynamics and structural properties of the materials such as:

- Dynamic heterogeneity: present of rigid zones and mobile polymer (mesh size, dangling, end chains, polymer chains in solution…)
- Lifetime of junctions

In a more precise way, two sequences are used: Baum-Pines (also referred as "long-time") and 5-pulses ("short-time") sequences. Long time DQ sequence gives information on the local orientation of the polymer network and more precisely on the existence of "cross-linked chains" (elastically active chains). This sequence will be used to probe the existence of a polymer network in the gel. In addition, short time DQ NMR will also be used to investigate the existence of rigid zones in the gel state.

^{19}F double-quantum (DQ) NMR were carried out on P(VDF-co-HFP) – MEK solutions and gels, using the five-pulse sequence and Baum-Pines sequence.

Baum-Pines sequence

The sequence developed by Baum and Pines (Baum and Pines 1986) was later improved by Saalwächter (Saalwächter 2007). DQ coherences are first excited by an excitation block composed of 12 pulses. To observe the excited DQ coherences, a second block called reconversion block is added and is also composed of 12 pulses. The DQ coherences are then converted in a signal with the same amplitude. This sequence is represented in Figure 57.

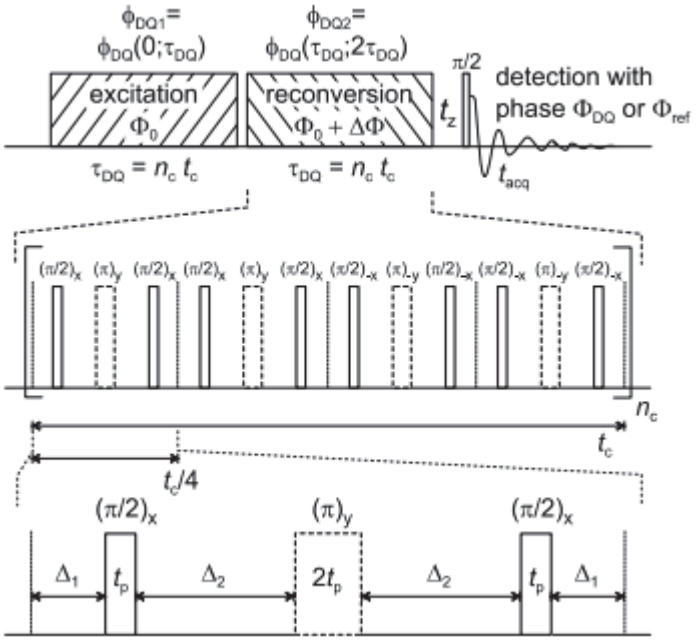


Figure 57 Schematic representation of the DQ experiments and schematic representation of the reconversion block (Saalwächter 2007)

The number of excitation and reconversion block (n_c) is then varied and as a consequence, the evolution of the amplitude of the signal as a function of the excitation time $\tau_{DQ} = n_c t_c$ (with t_c the cycle time and n_c the cycle number) gives the DQ coherences curve: $S_{DQ}(\tau_{DQ})$. The acquisition of the reference intensity $S_{Ref}(\tau_{DQ})$ is possible for DQ coherence selection using a 4-step phase cycle (n_c=4 here). Working with a normalized signal $I_{DQ}(\tau_{DQ})$ would be interesting; indeed, the effects of the dynamics at the origin of the transverse relaxation presents in the DQ coherence signal would be deleted. To do so the DQ coherence signal $S_{DQ}(\tau_{DQ})$ is normalized by the sum $S_{DQ}(\tau_{DQ})+ S_{Ref}(\tau_{DQ})$. This sequence will be applied on P(VDF-co-HFP) gels and solutions in MEK and the influence of the presence of silica nanoparticles will also be investigated by this method.

5-pulses sequence

Due to the relatively long duration of the excitation blocks in the Baum-Pines sequence (improved by Saalwächter), low time values cannot be reached. Indeed, the lowest time value obtained with this sequence is τ_{DQ}=100µs.

In order to obtain the DQ coherence signal at shorter time scales, a new sequence has been introduced called 5-pulses sequence (Munowitz 1987, Lorthioir, Khalil et al. 2012). It offers the possibility to probe the short-time range of the DQ excitation process, below 100-200 µs typically. In this case both the excitation and reconversion blocks will be narrower. Only 5 pulses of 90° (and two pulses at 180°) composed this sequence as shown in the following Figure 58. The two first pulses of 90° will excite the DQ coherences and the two following will allow the reconversion of these coherences.

However, it has to be highlighted that this DQ excitation sequence is far less efficient to refocus multi-spin dipolar interactions compared to the one proposed by Baum and Pines, later improved by Saalwächter.

In the case of hydrogenated polymers, the presence of crystallites within hydrogels may be investigated using ^{1}H magic-sandwich echo experiments. In this approach, the protons from the crystalline regions display a much faster transverse relaxation, over 50 µs typically, than the other mobile units of the polymer chains and the solvent molecules. Such a contrast in the relaxation behavior allows these rigid zones to be detected and quantified. For a fluorinated (co)polymer such as P(VDF-co-HFP), the large chemical shift difference between the different fluorines (more than 110 ppm) significantly influences the shape of the transverse relaxation signal, even below 200 µs. Therefore, both the detection and the quantification of the rigid fluorines based on magic-sandwich echo experiments were not straightforward in the present case and another NMR approach was used. ^{19}F double-quantum (DQ) NMR measurements were thus performed since DQ coherences may be excited only for the fluorines displaying a non-zero ^{19}F dipolar coupling. In particular, in these experiments, all the species displaying isotropic reorientational motions over the tens of microseconds time scale are filtered out.

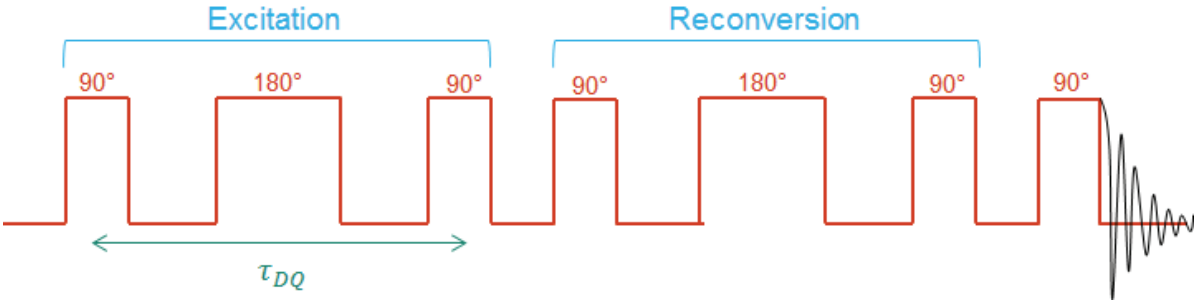


Figure 58 5-pulses sequence

Along this line, the amplitude of the ^{19}F DQ coherences was monitored as a function of the excitation time, τ_{DQ}, in the range 2 – 200 µs, for P(VDF-co-HFP) – MEK systems.

Experimental protocol

Time domain 19F NMR measurements were carried out at the Institut de Chimie et des Matériaux de Paris Est (ICMPE, Thiais, France) on a 400 MHz Bruker Avance III NMR spectrometer and a 4 mm MAS triple-resonance 1H/19F/X probe. Gels were inserted into 4 mm ZrO2 CRAMPS rotors with a Boron Nitride cap. All measurements were performed under static conditions. Polyethylene spacers were used to center the sample within the coil. The 90° (19F) pulse length was 5.7ms and the recycle delay, adjusted according to the longest T1(19F) value, was set to 3 s.

2.2.4. DSC

Principle of DSC

Differential Scanning Calorimetry (DSC) is a thermoanalytical method used to measure crystallization and melting temperatures and glass transition temperature in polymer materials. A temperature ramp is applied on two pans, one containing the material and an empty one which is the reference. The difference in the amount of heat required to increasing the temperature of the sample and reference is measured as a function of temperature. This difference is called heat flow and depending on how the heat flow varies with the temperature (endo- or exothermic) gives different information on the materials.

The crystallinity index (X_c) is determined using the following equation:

$$X_c = \frac{\Delta H_m}{\Delta H_m^0} \quad (21)$$

where ΔH_m is the heat of fusion (melting enthalpy) of the material measured during the experiment and ΔH_m^0 the enthalpy of melting for a 100% crystalline material. The value ΔH_m^0=104.7 J.g^{-1} was reported in the literature for PVDF (Rosenberg, Siegmann et al. 1991).

Experimental protocol

DSC measurements were performed on gels to identify melting temperatures in gels and investigate the crystalline structure of the materials. DSC data were acquired on a TA Instruments Q2000 calorimeter at a heating rate of 1°C/min. Hermetic pans were filled with 5-15 mg of gel samples at 20°C and let equilibrating for 20 min. Only the first heating scan between 20 and 60°C for gels in MEK and between 20 and 100°C for gels in 2-heptanone was considered throughout this work.

2.2.5.X-ray scattering

Principle of X-ray scattering

X-ray scattering is used to study the structural properties of solids, liquids or gels at various scales. This phenomenon is due to the existence of electron density heterogeneities in a material.

During the experiment, X-rays generated by an X-ray source are sent through a sample and collected on a 2D detector (see Figure 59). The scattered intensity is analyzed as a function of the scattering angle 2θ or equivalently the scattering vector defined as:

$$q = \left|\overrightarrow{k_s} - \vec{k}_0\right| = \frac{4\pi \sin\theta}{\lambda} \quad (22)$$

where $\overrightarrow{k_s}$ is the scattered wave vector, $\vec{k}_0$ the incident wave vector, 2θ the scattering angle and λ the X-ray wavelength. At high distances between the sample and the detector, very small scattering angles are reached.

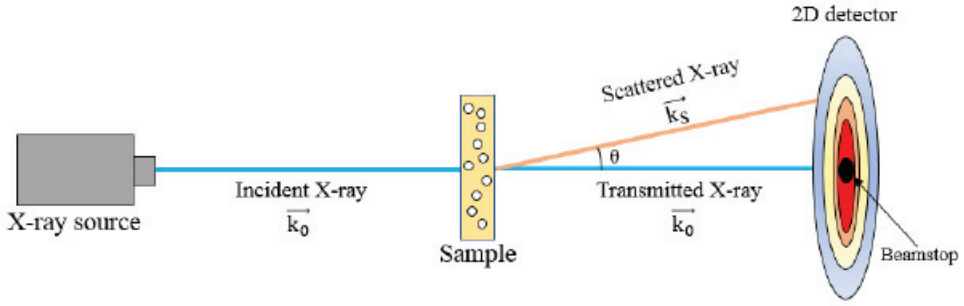


Figure 59 Schematic representation of SAXS measurement

Depending on the scattering angle, different characteristics of the material can be obtained:

i. At wide angles (WAXS), small distances from 0.1 to a few nm are probed and this measurement gives information at the scale of the crystalline unit cell. It allows the measurements of crystalline parameters, crystallinity ratio and sometimes the crystallite size.

ii. At small or ultra-small angles (SAXS, USAXS), larger distances up to a few hundreds of nm are probed and it is possible to characterize heterogeneities at large scales, such as the dispersion state of nanoparticles in a matrix.

Principles of (U)SAXS and WAXS measurements will be detailed in this section.

(Ultra) Small-angle X-ray scattering

For a collection of particles dispersed in a matrix, the scattered intensity is expressed as a function of the scattering vector q as:

$$I(q) = I_0 T h \beta^2 \Delta\rho^2 N V^2 S(q) F^2(q) \tag{23}$$

where I_0 is the incident intensity, T the transmission of the sample, h the thickness of the sample, β^2 the scattering cross-section of an electron ($\beta^2 = 7.8\times10^{-26}$ cm²), $\Delta\rho^2$ the contrast, N the number of particles per unit volume and V the volume of one particle. The contrast corresponds to the square of the difference between the electron density ρ of the particles and the electron density ρ_0 of the medium where the particles are dispersed. F(q) is the form factor of a particle (normalized to one at small q values) and S(q) the structure factor, related to the arrangement of particles in space. Note that for polydisperse particles, the separation in two distinct factors $S(q)F^2(q)$ is only an approximation

Usually the scattered intensity is normalized by the incident intensity, transmission and thickness of the sample to give the so-called scattering cross-section per unit volume:

$$I_{norm}(q) = \beta^2 \Delta\rho^2 N V^2 S(q) F^2(q) \tag{24}$$

$I_{norm}(q)$ is a cross-section per unit volume of sample, expressed as an inverse length (usually cm^{-1} or mm^{-1}).

For diluted, non-interacting spherical silica particles randomly dispersed in organic solvents or in a polymer matrix, the structure factor S(q) equals one and the scattered intensity can be written as:

$$I(q) = \beta^2 \Delta\rho^2 \int_{R_{min}}^{R_{max}} \left(\frac{4\pi}{3} R^3\right)^2 P(R) \left[F_{sphere}(q,R)\right]^2 dR \tag{25}$$

where

$$F_{sphere}(R) = 3\frac{\sin(qR) - qR\cos(qR)}{(qR)^3} \tag{26}$$

is the form factor of a sphere with a radius R and P(R) represents the size distribution of particles: $P(R)dR$ corresponds to the number of particles (per unit volume) with radius between R and R+dR. A log-normal distribution is often used to describe precipitated silica spheres:

$$P(R) = \frac{P_0}{Rw\sqrt{2\pi}} exp\left(-\frac{(\ln R - \mu)^2}{2w^2}\right) \tag{27}$$

The parameter μ is the log of the radius at the maximum of $P(R)$ and w is the width of the distribution. The total number of particles (per unit volume) is:

$$P_0 = \int_{R_{min}}^{R_{max}} P(R)dR = \int_{R_{min}}^{R_{max}} \frac{P_0}{Rw\sqrt{2\pi}} exp\left(-\frac{(\ln R - \mu)^2}{2w^2}\right) dR \quad (28)$$

The volume fraction Φ of particles is expressed as:

$$\Phi = \int_{R_{min}}^{R_{max}} \left(\frac{4\pi}{3}R^3\right) P(R)dR = \frac{4\pi}{3} P_0 e^{3\mu+9w^2/2} \quad (29)$$

And the average radius

$$R_{av} = \frac{\int R\, P(R)dR}{\int P(R)dR} = \mathrm{e}^{\mu+w^2/2} \quad (30)$$

Dilute silica solutions in MEK and 2-heptanone can be described in this way and information on their size distribution will be obtained.

The dispersion states of spherical silica solutions dispersed in organic solvents or in P(VDF-co-HFP) (in the gel or liquid state) were studied with USAXS measurements, as well as P(VDF-co-HFP) – silica films.

SAXS experiments were performed on P(VDF-co-HFP) gels and solutions in MEK and 2-heptanone to investigate the evolution of the scattered intensity with the sol – gel transition and with the fraction of polymer in the gel state.

The q range in this technique was between 0.03 and 0.3 $Å^{-1}$ and it gives us information on the volume fraction of object present in the gels (from the intercept) and information on the anisotropy and polydispersity of the object from the shape of the intensity curves.

Wide-angle X-ray scattering

Wide-angle X-ray scattering (WAXS) experiments were used to identify the presence of a crystalline fraction in P(VDF-co-HFP) gels in MEK and 2-heptanone. During the experiment, the X-Ray beam is sent to the sample at a given incident angle, it then penetrates in the sample and it is reflected. The reflected beam is recorded on a detector. Diffraction of X-rays on crystal planes are schematized on Figure 60.

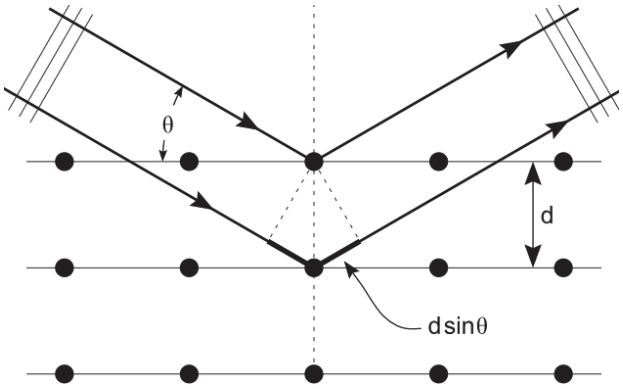


Figure 60 X-rays diffraction on crystal planes

The Bragg's law of diffraction allows identifying the presence of crystallites in a material and determining the parameters of the crystalline mesh: there will be reflection of X-rays on crystal planes only when

i. The scattering vector is perpendicular to the crystal planes
ii. $q = n\frac{2\pi}{d}$ or $\sin\theta = n\frac{\lambda}{2d}$

where n is an integer, λ the wavelength of the incident wave, d the spacing between the planes in the atomic lattice and θ (half the scattering angle) the angle between the incident ray and the scattering planes.

During the WAXS experiment, the presence of a crystalline fraction gives Bragg diffraction peaks, obtained as a function of the scattering angle or the scattering vector $\vec{q}$. From the position of the diffraction peaks, the crystalline structure can be identified.

Experimental protocols

Small-angle X-ray scattering

SAXS measurements were performed at the SWAXS laboratory (IRAMIS, Saclay, France) equipped with a 2D detector. The acquisition time is 15 min. The q range investigated extends from 10^{-2} to 5 $Å^{-1}$. Samples were placed in a cell located in between two thin Kapton windows. The sample thickness was kept to about 1 mm.

Ultra-Small-angle X-ray scattering

USAXS measurements were performed on the High brilliance Beamline (ID02 at the European Synchrotron Radiation Facility (ESRF, Grenoble, France). The wave length was fixed at 0,995 Å. A region of 100μm was scanned by the X-ray beam. The acquisition time was around 1 second. For each sample, three sample-to-detector distances were tested. In a first time, a distance d=31m allows a scattering range between 0.002 to 0.2 nm^{-1}. The second distance d=8m leads to a scattering range between 0.02 to 2 nm^{-1}. Finally scattering in the range of 0.09 to 9 nm^{-1} were obtained with a sample-to-detector d=1m. Curves were superimposed and combined as shown in Figure 61. Measurements were carried out on P(VDF-co-HFP) – silica gels and solutions in MEK and 2-heptanone. Polymer solutions were placed in glass capillaries with a thickness of 1.5 mm. Gels were placed in a cell located in between two thin Mica windows with a thickness of 1mm.

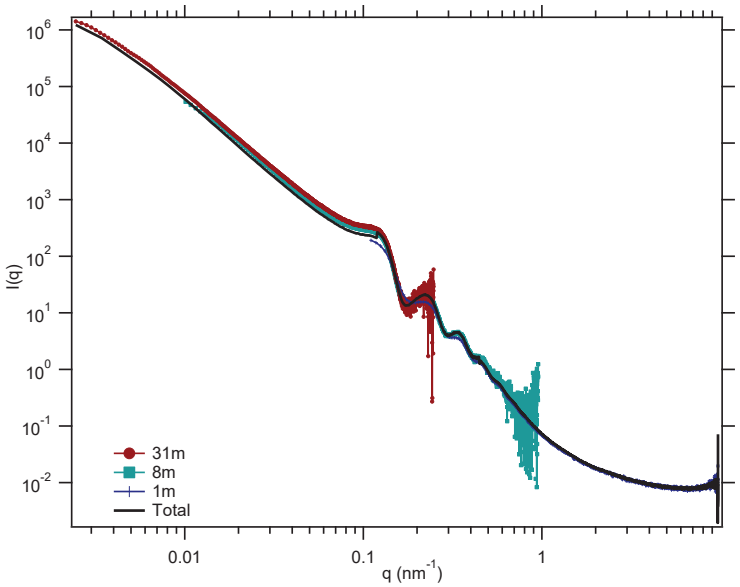


Figure 61 USAXS measurements at (●) 31m (■) 8m (+) 1m and (-) the total signal for a P(VDF-co-HFP) – silica gel in MEK (11wt%)

Wide-angle X-ray scattering

WAXS measurements were carried out at the Henri Longchambon Diffractometry Center (University of Lyon, France) on a D8 Bruker θ-2θ diffractometer using the Cu Kα line (wavelength λ = 0.154 nm). The gel sample was inserted into a glass capillary. A P(VDF-co-HFP) film sample, obtained by solvent casting a P(VDF-co-HFP)-MEK solution, was also investigated for comparison. The scattering intensities were measured using an angular range (2θ) from 10° to 45°, a resolution of 0.02° and a measurement time of 75 min.

2.3. Characterization of polymer – silica hybrid membranes

2.3.1. Structural characterizations

Electron microscopy

Principle of electron microscopy

Microscopy on materials is often used to study materials at the scale down to the nanometer and it is possible to visualize the surface and core morphologies. Among different methods, Scanning Electron Microscopy (SEM) can produce high resolution images of the surface of a sample using the principle of electron – matter interactions and it describes the reliefs on the surface of a material. The formation of an image is based on the detection of secondary emerging electrons from the surface under the impact of the primary electron beam that sweeps the observed surface. From this method it is possible to have topological or chemical information of the surface of the sample by different electron – matter interactions (back-scattered electrons, emission of photons, X…).

Secondary electrons:

As a result of the collision between the primary electrons and the atoms of the sample, a primary electron transfers a part of its energy to a secondary electron; the atom is ionized leading to an ejection of the secondary electron with a weak energy around 50 eV (see Figure 62). This is the

inelastic interaction or diffusion process. The detection of these electrons provides information on the topography of the sample to a depth of 10 nm (superficial layers close to the surface). The analysis of these electrons allows obtaining a characteristic image of the surface. It represents a good way to observe the contours and morphology of the sample.

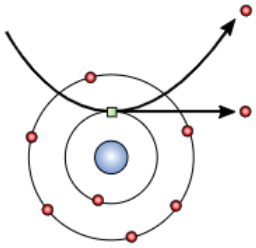


Figure 62 Emission of a secondary electron

Back-scattered electrons:

These electrons result from the interaction of the electrons of the primary beam with atomic nuclei of the sample which have reacted in a quasi-elastic way with the atoms of the sample. The electrons are reemitted in a direction close to the original direction with a small loss of energy (see Figure 63). Due to the high energy of back-scattered electrons (30 keV), they are emitted at a greater depth in the sample. These electrons are sensitive to the atomic number of atoms (heavy atoms will emit more electrons than light atoms: phase contrast). The image obtained is therefore function of the chemical composition of the sample.

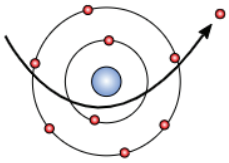


Figure 63 Emission of a back-scattered electron

Experimental protocol

Scanning electron microscopy was used for observing the dispersion of silica nanoparticles in the films. A surface observation of the film was realized by Scanning Electron Microscopy (SEM) ultra 55 Zeiss in topographic and chemical modes.

USAXS

Experimental protocol

The dispersion states of silica nanoparticles in the P(VDF-co-HFP) nanocomposite films were analyzed by USAXS measurements. USAXS were performed on beamline ID02 at ESRF (Grenoble, France). The acquisition time was around 1 second. For each sample, three distances were tested: 31m (q range 0.002 – 0.2 nm^{-1}), 8m (q range 0.02 – 2 nm^{-1}) and 1 m (0.09 – 9 nm^{-1}) with the same experimental protocol described in page 77 (Experimental protocols). Films of thickness around 50µm were analyzed.

2.3.2. Mechanical characterizations: tensile strength tests

In order to characterize the Young's modulus, yield stress and the elongation at break of P(VDF-co-HFP) – silica nanocomposites, tensile strength tests were carried out. Specimens were prepared from films made by solvent casting as described page 61.

Tensile tests were done with a Z020 ZWICK with stain observed by cameras of IMETRUM. The specimens for tensile test were obtained by a cutter under pressure. The shape and size of the specimen is described in Figure 64.

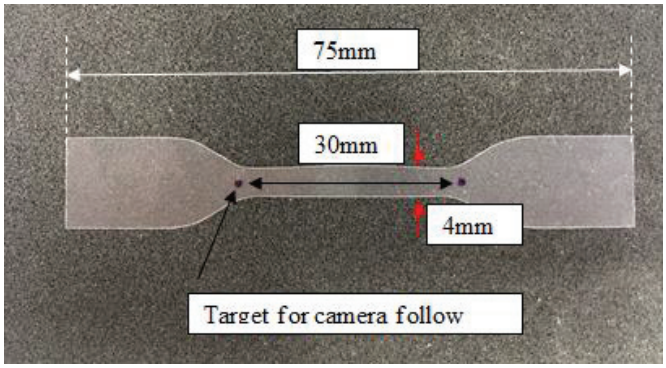


Figure 64 Specimen for tensile test

A pre-stress of less than 0.1N is applied to the film installed in the machine just before the tensile test. Tensile tests were done at a controlled crosshead speed 1 mmm/min up to 0,5% of deformation as a first part to determine the Young's modulus *E*, and then at 5 mm/min up to the failure of the specimen. For each film with a certain concentration of silica, 3 to 5 tests were carried out in order to validate the reproducibility and calculate an average of the Young's Modulus and Yield strength values.

Stress – strain curves are obtained from the experiments: the Young's modulus is defined as the slope of the stress – strain curve in the elastic domain (0,05% < strain < 0,25%) and the yield stress is defined as the observed maximum stress.

Chapter 3: Thermoreversible gelation of P(VDF-co-HFP) in linear ketone solvents: dynamics and structure

P(VDF-co-HFP) forms thermoreversible gels in ketone solvents. This chapter describes the combination of different original methods on the gel state to investigate the mechanisms involved in the gelation of the polymer. Influence of the number of carbon on the backbone chain of the solvent and the nature (crystallinity, organization) of the polymer on the gelation mechanism was studied.

3.1. First investigations: gelation kinetics and gel-melting temperatures 82

3.1.1. Tube-tilting method 82

3.1.2. Linear rheology 84

3.2. Polymer dynamics in the gel: ^{19}F NMR 87

3.2.1. Rigid domains 87

3.2.2. Network structure 89

3.3. Structural information 92

3.3.1. Thermal behavior of the gels: DSC 92

3.3.2. WAXS 95

3.3.3. SAXS 97

3.4. Influence of the HFP fraction of the copolymer and its microstructure on gelation 101

3.5. General discussion: gelation mechanism(s) involved in the thermoreversible gelation of P(VDF-co-HFP) copolymers in linear ketone solvents 104

3.6. Conclusions 109

3. Thermoreversible gelation of P(VDF-co-HFP) in linear ketone solvents: dynamics and structure

It has been found that semi-crystalline PVDF and VDF-based copolymers form thermoreversible gels in certain solvents, the morphologies of which strongly depend on the chemical nature of the solvent. As explained in the first chapter, it is generally agreed that thermoreversible gelation is the results of the formation of a three-dimensional network in which the junction points consist in physical bonds. Depending on the studied system, these physical bonds may result from hydrogen bonds, crystalline zones or liquid-liquid phase separation.

As reviewed in Chapter 1, for PVDF in γ-butyrolactone, liquid-liquid phase separation has been considered as the cause of the gelation. Investigations of PVDF gels in other solvents (aromatic diesters, acetophenone, ethyl benzoate, glyceryl tributyrate) have shown that crystallization may be responsible for the PVDF gelation. These studies have also highlighted that the morphology of the PVDF gels strongly depends on the nature of the solvent and the concentration of polymer.

The gelation of semi-crystalline polymers is a complex phenomenon and the nature of the gel depends on the polymer chain structure and molecular weight as well as on the nature of the solvent, or more precisely on polymer – solvent interactions. However, the structure, morphology and thermal behavior of these gels have mostly been studied in literature in the dried state rather than in the gel state, considering that the morphology of the dried material is representative of the initial structure of the gel in the presence of solvent.

In this chapter, the study of the thermoreversible gelation of P(VDF-co-HFP) copolymer in MEK and 2-heptanone is reported. The kinetics of gelation is investigated, while a combination of ^{19}F NMR, DSC, SAXS and WAXS experiments performed on the gels in the presence of solvent were used to probe the gelation mechanism and the structure of these systems. The preparation and measuring procedures were described in Chapter 2.

3.1. First investigations: gelation kinetics and gel-melting temperatures

As a first approach to investigate the gelation mechanisms, the gelation time t_{gel} was estimated using the tube-tilting method and linear rheology. The gelation time was determined as a function of the concentration of polymer and the temperature for both solvents (MEK and 2-heptanone).

3.1.1. Tube-tilting method

The gelation time t_{gel} is considered to be the time at which no macroscopic flow of the sample is observed when the tube is tilted (Ohkura, Kanaya et al. 1992). The gelation rate is defined as $1/t_{gel}$, the inverse of the gelation time. The gelation rate is a function of both concentration and temperature.

Figure 65 shows the evolution of the gelation rate t^{-1} of P(VDF-co-HFP) – MEK solutions as a function of concentration at various temperatures. Below a critical concentration, which amounts to 11wt% of P(VDF-co-HFP) at 20°C, it is considered that gelation does not occur over one month (and gelation time is then considered to be “infinite”). Gelation rate measurements for concentrations below this value are not reported in the figure.

It is clear that the gelation rate strongly depends on both gelation temperature and copolymer concentration. At a given temperature the gelation rate increases drastically as the concentration of P(VDF-co-HFP) increases. Also, at a given concentration, the gelation rate increases drastically as temperature decreases.

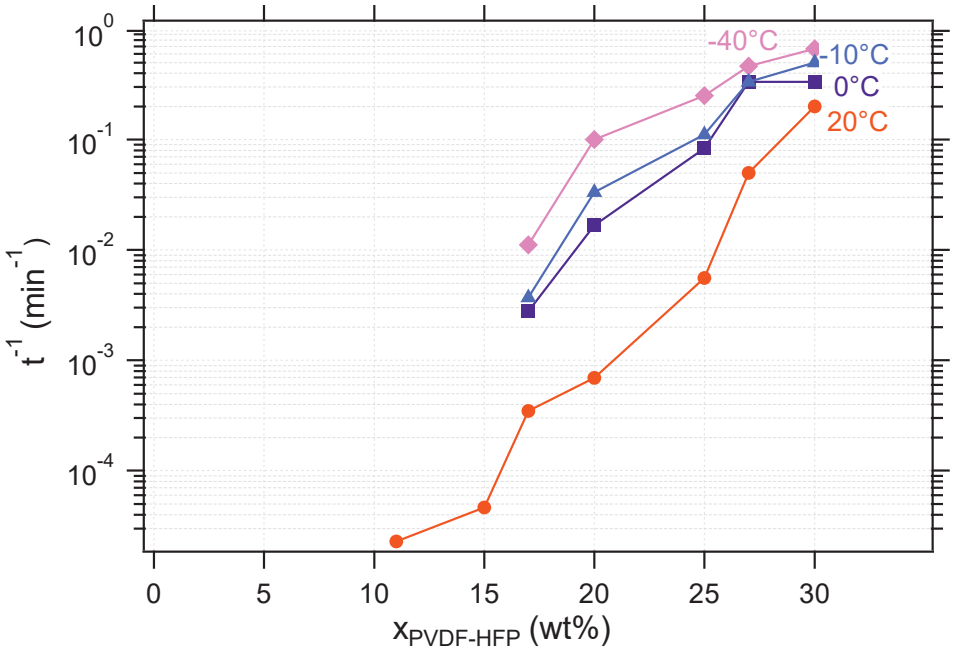


Figure 65 Gelation rate t^{-1} versus concentration for P(VDF-co-HFP) in solution in MEK measurement for temperatures ranging between -40°C and 20°C

The same experiments were performed on P(VDF-co-HFP) – 2-heptanone solutions and the evolution of the gelation rate as a function of the concentration of copolymer is plotted in Figure 66. Qualitatively, similar results are observed with a critical gelation concentration of 5wt % of P(VDF-co-HFP) at 20°C. Below this concentration, the gelation does not occur over two days at 20°C and are not reported in the graph. In comparison with the kinetic of gelation in MEK, it can be noticed that 2-heptanone strongly increases the gelation kinetics of the polymer. For example, at 20wt% of P(VDF-co-HFP) the gelation in MEK takes 1 day while in 2-heptanone it only takes 4.5 minutes. Due to the faster gelation kinetic in this solvent and thanks to the higher boiling point, a larger range of temperature (from -10°C to 60°C) was studied.

From this simple test it is clear that the nature of the solvent influences the gelation kinetic of the material possibly due to different interaction parameter between the polymer and the solvent. However, this method is qualitative and a more quantitative way to measure properly the gelation kinetics should be useful for better understanding.

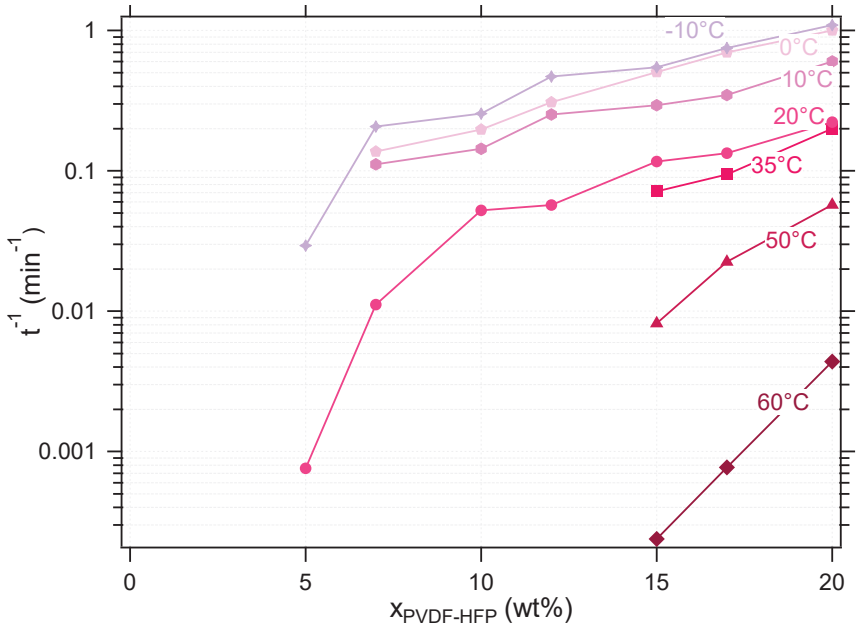


Figure 66 Gelation rate t^{-1} versus concentration for P(VDF-co-HFP) in solution in 2-heptanone measurement for temperatures ranging between -40°C and 20°C

3.1.2. Linear rheology

The linear viscoelastic behavior of both physical and chemical gels has been widely studied in the literature. Winter and Chambon (Winter and Chambon 1986) proposed that at the gel point (point where the material starts to form a gel), the storage and loss moduli follow a simple power law:

$$G'(\omega) \propto G''(\omega) \propto \omega^n \quad (31)$$

Where *n* may vary between 0 and 1 depending on the degree of connectivity in the system. In a gel with high density of contacts the exponent n is small. This equation reflects a power law distribution of relaxation times. At the gel point, the loss tangent is independent of the frequency. The gel state is therefore as $G'(\omega) > G''(\omega)$, $G' \sim \omega^0$ while the sol state is described as $G''(\omega) > G'(\omega)$, $G' \sim \omega^2$, $G'' \sim \omega$ at the lower frequency region (0.1-1Hz).

The linear viscoelastic behavior of P(VDF-co-HFP) gels in 2-heptanone only was investigated as a function of time to determine the gel point and thus the gelation kinetic of the system as a function of the fraction of polymer (reproducible experiments could not be performed in MEK because of its high volatility). In this work, the gel point was determined as the crossover between the storage modulus G' and loss modulus G''. In a second step frequency sweep measurements were performed at the end of the time sweep to study the evolution of both moduli with the frequency.

Figure 67 shows an example of the evolution of the linear storage G' and loss G'' moduli as a function of time during the gelation of a P(VDF-co-HFP) solution in 2-heptanone with 10wt% of copolymer (at 25°C, 1Hz and 0.1% shear strain). At short times, the loss modulus is higher than the elastic modulus while the opposite behavior is observed at long times. This is characteristic of the evolution of a viscoelastic material from a liquid state to a soft solid state. The experiments were conducted for concentrations of polymer between 6wt% and 10wt%. Beyond this concentration the gelation time is too fast to be determined with rheology measurements.

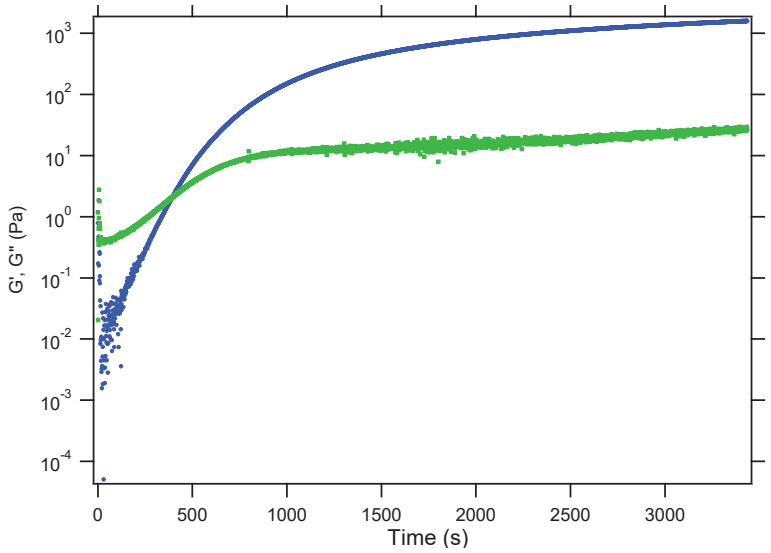


Figure 67 Evolution of G' (blue ●) and G'' (green ■) during the gelation of a P(VDF-co-HFP) solution in 2-heptanone with 10wt% of copolymer, at 25°C, a frequency of 1Hz and a shear strain of 0.1%

In Figure 68 are shown the storage and loss moduli of the system measured at time *t* = 3400 s at two different temperatures: 25°C and 100°C for the applied frequency range 0.1 – 10 Hz. It is apparent from the figure that at 25°C the storage modulus is independent of the frequency and its values are higher than those of the loss modulus, which is characteristic of the gel state. At 100°C the loss modulus values are higher than, but close to those of the storage modulus, with similar slopes as a function of the frequency. Note that values below about 5×10^{-2} Pa are not reliable as they are below the sensitivity of the rheometer. This indicates that at 100°C this material is close to, but above the gel point.

It was then possible to plot the gelation rate as a function of the concentration of P(VDF-co-HFP) as for the tube-tilting method for fractions of copolymer between 6wt% and 10wt% at 25°C (see Figure 69). The same conclusions than those obtained with the tube-tilting method can be formulated: the gelation rate strongly depends on the concentration of polymer and it increases drastically with the fraction of P(VDF-co-HFP). In the same way the temperature also modifies the gelation kinetic: at fixed copolymer concentration, the increase of temperature leads to slower gelation kinetics.

Temperature ramp experiments were also carried out to determine the gel melting temperature $T_{melting}^{gel}$ of the gels. It is clear from this measurement (an example is shown in Figure 70 for a 10wt% P(VDF-co-HFP) – 2-heptanone gel) that at low temperatures the system behaves like a (thermoreversible) gel when G'>G'', up to 64.5°C. At this temperature the gel melts and G' and G'' become equal. Beyond this concentration the material is in the liquid state. The influence of the concentration of polymer on the gel melting temperature was then studied and this characteristic temperature increases with the fraction of polymer up to 73°C (see Figure 71).

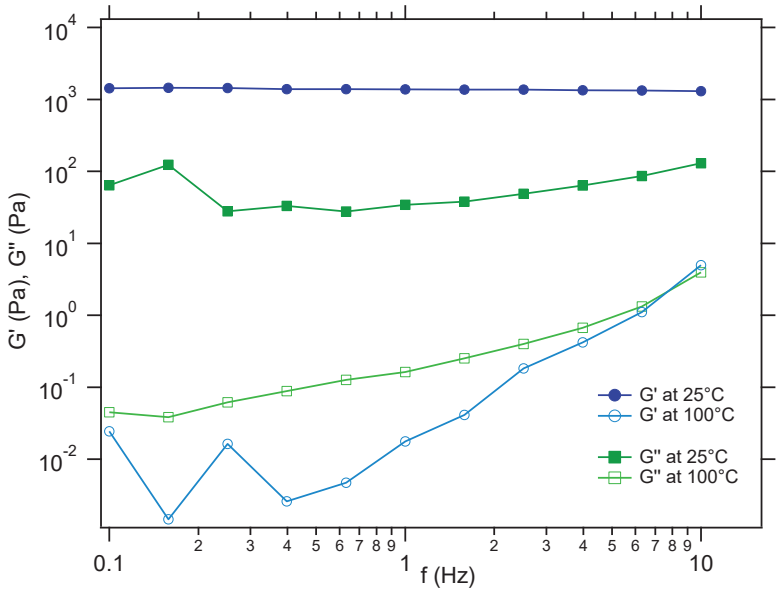


Figure 68 Plot of G' (●) and G'' (■) against frequency for P(VDF-co-HFP) - 2-heptanone ($X_{P(VDF\text{-}co\text{-}HFP)}$=10wt%) gel at indicated temperatures

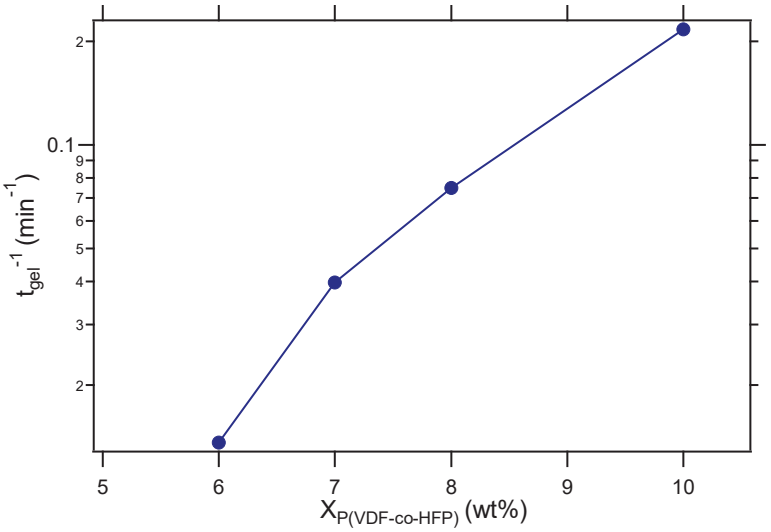


Figure 69 Gelation rate t^{-1} versus concentration for P(VDF-co-HFP) in solution in 2-heptanone measurements by linear rheology, at 25°C, a frequency of 1Hz and a shear strain of 0.1%

Tube-tilting and rheology methods are useful tools to first investigate the gelation mechanism of P(VDF-co-HFP) in MEK and 2-heptanone through the characterization of the gelation kinetic. Tube-tilting is a qualitative method while rheology is a more quantitative method to determine the kinetics of gelation of our materials, but it was only possible for the study of gels in 2-heptanone. They proved the influence of the concentration of copolymer and temperatures and above all the strong impact of the solvent nature (and more particularly the number of carbon of the backbone chain) on gelation kinetic. The last factor is certainly due to different polymer – solvent interactions (see Flory-Huggins parameter of PVDF in Chapter 1) and it may result different gel structures, corresponding to different types of three-dimensional network: a liquid-liquid phase separation leading to a percolating polymer-rich network and/or a network with junction points composed of crystalline zones. Thus, structural studies are necessary to elucidate the nature of effective junction points and the structure of the P(VDF-co-HFP) gels in MEK and 2-heptanone.

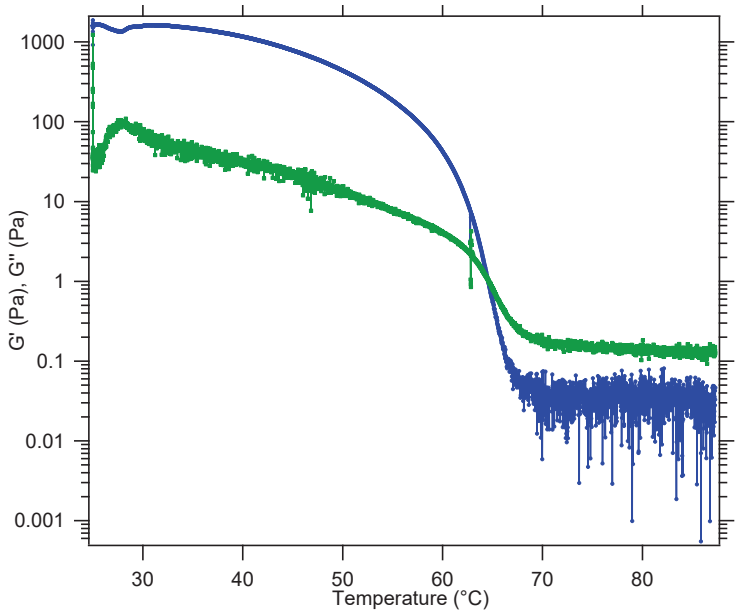


Figure 70 Plot of storage modulus (blue ●) and loss modulus (green ■) with temperature (measured at 1Hz and 0.1% shear strain) for a P(VDF-co-HFP) gel in 2-heptanone with 10wt% of copolymer

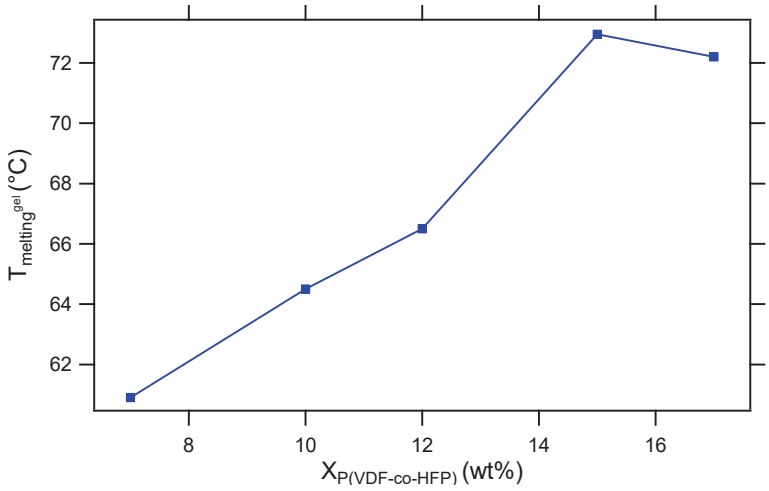


Figure 71 Evolution of the gel melting temperature $T_{melting}^{gel}$ with P(VDF-co-HFP) concentration for gels in 2-heptanone (measured at 1Hz and 0.1% shear strain)

3.2. Polymer dynamics in the gel: ^{19}F NMR

3.2.1. Rigid domains

NMR was used to investigate the segmental dynamics of P(VDF-co-HFP) chains in MEK solutions and gels at different concentrations. This copolymer is predominantly fluorinated while the solvent is hydrogenated. Therefore, fluorine NMR (^{19}F NMR) allowed to observe selectively the contribution from the polymer in solution or in the gel state. Note that, due to the large range of chemical shifts (more than 110 ppm) of fluorine (as compared e.g. to protons) which may potentially lead to irradiation bias, all reported time-domain NMR signal intensities were collected by Fourier transforming the observable decay after the considered pulse sequence and integrating the most

intense peak, corresponding to the fluorine atoms in the –CF2- groups, which was set at the center of the spectra.

Transverse relaxation measurements using standard Hahn echo and CPMG sequences were first performed. Transverse relaxation curves obtained in a P(VDF-co-HFP) solution and in gels in MEK at different weight fractions of polymer ($X_{P(VDF\text{-}co\text{-}HFP)}$) are shown in Figure 72. The relaxation becomes faster as the polymer concentration in the solution or gel increases, indicating that the dynamics of the polymer is more and more affected. The overall dynamics remain in the fast motion regime, as the overall average relaxation times remain long, in the few 10th of ms range. The dynamics seem to become more and more heterogeneous, as the relaxation curves deviate more and more from simple exponential shape. However, in gel systems, a small fraction of the signal with a significantly shorter relaxation time can be observed at short time. This fraction corresponds to a small fraction of the overall polymer. It would correspond to a small fraction of the polymer having a significantly slower and/or restricted dynamics. This fraction is not present in the signal from the liquid system at lower concentration.

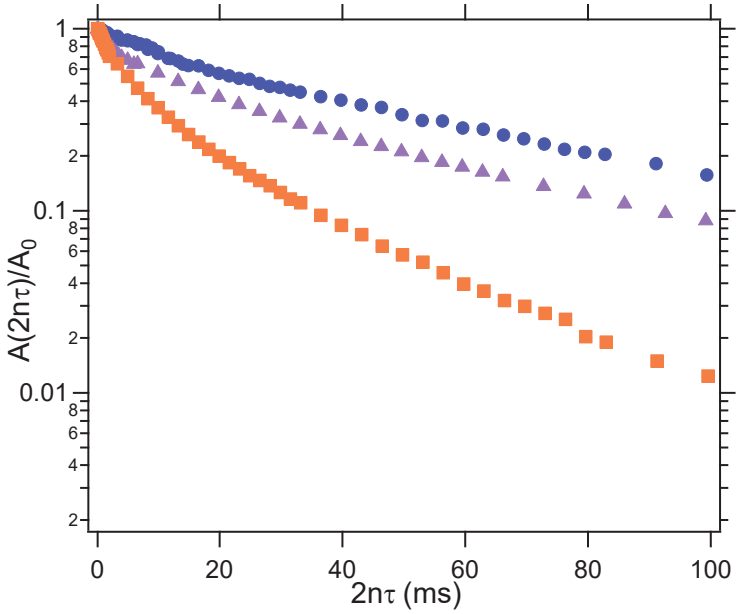


Figure 72 Transverse ^{19}F NMR relaxation obtained with Hahn echo and CPMG sequences for a liquid solution of P(VDF-co-HFP) in MEK with $X_{P(VDF\text{-}co\text{-}HFP)}$=6wt% (blue ●) and for P(VDF-co-HFP) - MEK gels: violet ▲: $X_{P(VDF\text{-}co\text{-}HFP)}$=20wt%; orange ■: $X_{P(VDF\text{-}co\text{-}HFP)}$=30wt%

It is however difficult to assess the existence of rigid zones from this measurement only. Another NMR approach was then used: ^{19}F double-quantum (DQ) NMR measurements were performed on polymer – solvent solutions and gels, using first the five-pulse sequence for DQ coherence selection and observation (Munowitz 1987, Lorthioir, Khalil et al. 2012). This sequence is far less efficient to refocus multi-spin dipolar interactions compared to the one proposed by Baum and Pines (Baum and Pines 1986), later improved by Saalwächter (Saalwächter 2017). However, it offers the possibility to probe the short-time range of the DQ excitation process, below 100-200µs typically.

The amplitude of the ^{19}F DQ coherences was monitored as a function of the excitation time t_{DQ}, in the range 2-200µs, for P(VDF-co-HFP) – MEK systems in the liquid or gel states, as reported in the Figure 73. In the case of the gels obtained with 20wt% and 30wt% of P(VDF-co-HFP), a non-zero signal is

clearly detected, which proves that a fraction of the polymer chain segments is frozen or has strongly restricted motions over the tens of microseconds motional time scale. Moreover, the ^{19}F DQ build-up curve displays a maximum for t_{DQ}=12µs. The static value of the apparent $^{19}F - {}^{19}F$ dipolar coupling D_{stat}, was recently calculated for Nafion and a value of 16.06 kHz was obtained for the vicinal fluorines of the backbone CF_2 groups (Yan, Brouwer et al. 2016). Interestingly, the value $(2\pi \times D_{stat})^{-1} \approx 10\mu s$ is very close to the t_{DQ} at the maximum of the ^{19}F DQ build-up curve shown in Figure 73. Therefore, these DQ NMR experiments indicate that for the gels of P(VDF-co-HFP) in MEK, a fraction of the copolymer is found to be immobile over the tens of microseconds time scale. However further experiments (DSC and WAXS) need to be performed to characterize the nature of these immobilized zones. A control experiment was carried out on a liquid solution with 6wt% of P(VDF-co-HFP) in MEK (below the critical gelation point). As shown in Figure 73, whatever the t_{DQ} value below 200µs, no excitation of the ^{19}F DQ coherences was observed at this concentration, meaning that no rigid fraction of the polymer is present in a material at the liquid state.

In Figure 73, the amplitude of the raw ^{19}F DQ signal was normalized by the initial value of the ^{19}F transverse relaxation signal. However, the fraction of strongly dipolar coupled fluorine or, in other words, the rigid fraction of P(VDF-co-HFP) units involved in the gels, cannot be rigorously quantified from the ^{19}F DQ signal intensity, for several reasons. First, the five-pulse sequence has an efficiency to generate DG coherence signal which is not 100%. Second, for each value of the t_{DQ} time, the detection process is affected by the dead time of the spectrometer, which means that the signal at very short time is not detected quantitatively. For these reasons, the amplitude of the signal shown in Figure 73 cannot be related quantitatively to a rigid fraction in the material. The overall DQ conversion efficiency generally observed for rigid organic compounds typically ranges between 20 and 30%.

The measured amplitudes at the maximum of the build-up curves shown in Figure 73 are of order of 1.5 ± 0.3 %. Therefore, one may thus consider that roughly 5 to 7% of the copolymer units are involved in rigid zones. We don't have enough data points to assess the evolution with the copolymer concentration. In any case ^{19}F NMR clearly confirms that a small fraction of P(VDF-co-HFP) forms rigid zones only in systems which have undergone gelation.

3.2.2. Network structure

The relaxation behavior observed at long time (in the tens of ms range) is related to the mobile copolymer fraction. The gel structure should induce anisotropic reorientational motions for the copolymer chain portions exhibiting topological constraints (effective crosslinks, trapped entanglements) at both extremities. As these chain portions are surrounded by MEK, they display a high level of segmental mobility around the local axis defined by the topological constraints. As a result, the $^{19}F - {}^{19}F$ dipolar couplings related to these elastically active chains portions are strongly reduced compared to their static value (observed in rigid zones), but they are not fully averaged to zero. It follows that the growth of the corresponding ^{19}F DQ coherences is expected to occur over a much longer time scale than for rigid zones. The contribution from these coherences to the build-up curve may already be observed above 60µs in Figure 73.

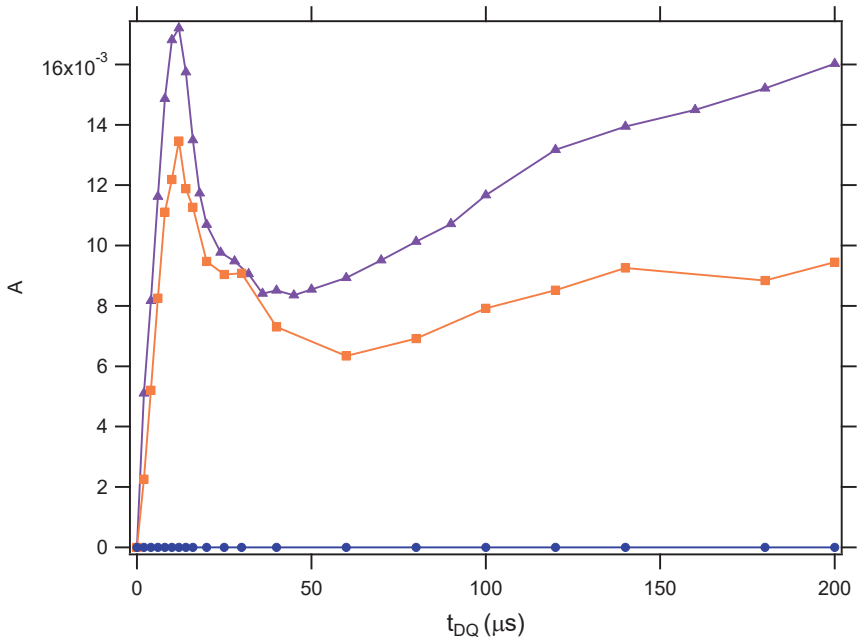


Figure 73 ^{19}F DQ build-up curve obtained after a 5-pulse Baum and Pines sequence as a function of the DQ excitation/reconversion time in the sequence: for gels of P(VDF-co-HFP) in MEK with $X_{P(VDF\text{-}co\text{-}HFP)}$=30wt% (orange ■) and $X_{P(VDF\text{-}co\text{-}HFP)}$=20wt% (purple ▲) and for a solution with $X_{P(VDF\text{-}co\text{-}HFP)}$=6wt% (blue ●). The amplitude of the signal was normalized by the initial transverse relaxation amplitude

However, for this longer time scale, the DQ excitation scheme proposed by Baum and Pines (Baum and Pines 1986), further improved by Saalwächter (Saalwächter 2017) was preferred as it is more efficient. An example of the build-up curve for a gel with 30wt% of P(VDF-co-HFP) is shown in Figure 74. It is clear that a non-zero signal exists, with a maximum at about 1ms. The presence of this signal demonstrates the existence of a polymer network. The same experiments were carried out on P(VDF-co-HFP) – MEK solutions and gels at different concentrations and the corresponding build-up curves are reported in Figure 75. For 6wt% of P(VDF-co-HFP), in which no rigid zones are formed, no signal is detected in the same conditions. Conversely, as for the gel with 30wt% of copolymer, in the gel with 20wt% of copolymer, a non-zero ^{19}F DQ signal is detected. This assesses the presence of elastically active chains in the gel state only, with a fraction that increases with the copolymer concentration.

While the whole copolymer contributes to the reference signal (black curve in Figure 74), the DQ signal (orange curve) comes from elastically active (i.e. effectively crosslinked) chains only, excluding so-called 'network defects' such as dangling or unattached chains. In principle, by comparing the intensities of both signals, it may thus be possible to estimate the fraction of elastically active chains in the gel network. By plotting the ratio of the DQ build-up signal over the reference signal it was possible to roughly estimate the fraction of elastically active chains of P(VDF-co-HFP) units involved in the gels (and more specifically the polymer network). The resulting curve was fitted with an exponential function (see Figure 76) and it the fraction of crosslinked chains is of order of 12% for the gel formed with 20wt% of copolymer and 19% for the gel formed with 30% of copolymer. The fraction of elastically active chains appears to increase with the concentration of copolymer, contrary to the rigid polymer fraction.

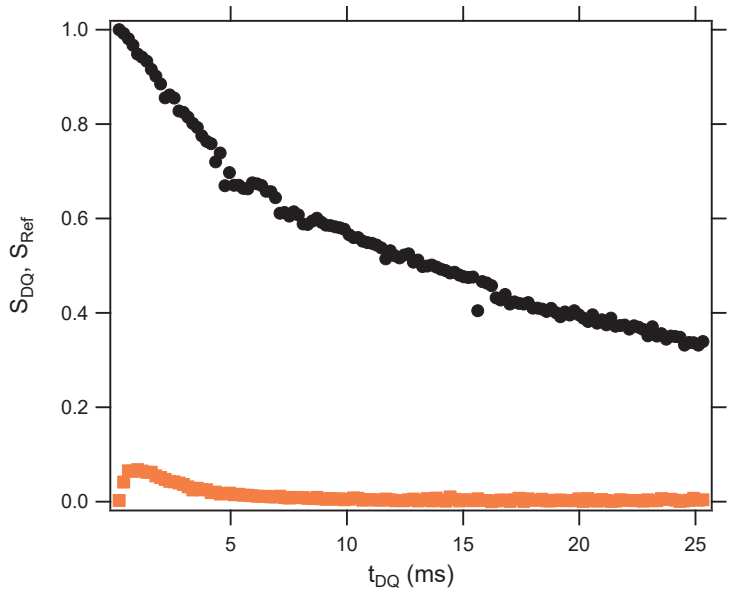


Figure 74 ^{19}F DQ build-up curve obtained after a Baum and Pines sequence (improved by Saalwächter) as a function of the DQ excitation/reconversion time in the sequence for a gel of P(VDF-co-HFP) in MEK with $X_{P(VDF\text{-}co\text{-}HFP)}$=30wt% (orange ■) the reference signal (black ●). The amplitude of the signal was normalized by the maximum value of the reference signal

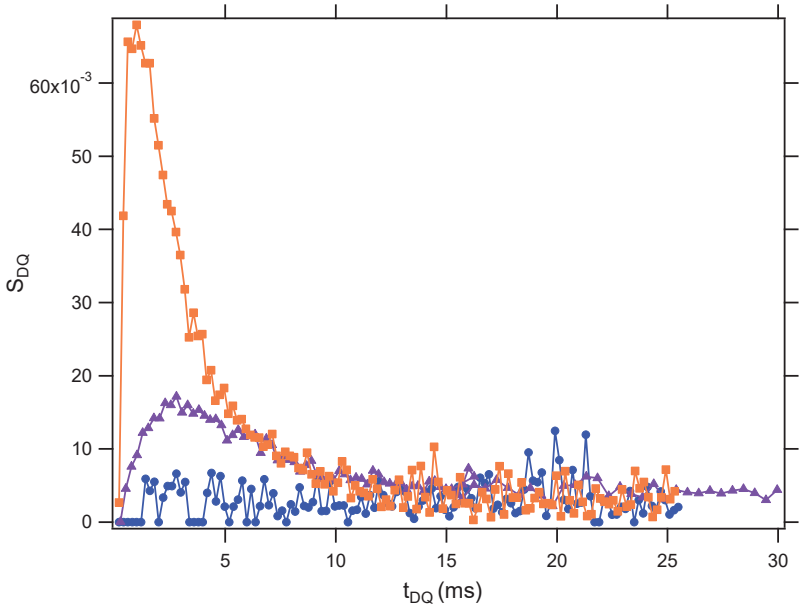


Figure 75 ^{19}F DQ build-up curves obtained after a Baum and Pines sequence (improved by Saalwächter) as a function of the DQ excitation/reconversion time in the sequence for gels of P(VDF-co-HFP) in MEK with $X_{P(VDF\text{-}co\text{-}HFP)}$=20wt% (purple ▲), $X_{P(VDF\text{-}co\text{-}HFP)}$=30wt% (orange ■) and for a solution with $X_{P(VDF\text{-}co\text{-}HFP)}$=6wt% (blue ●). The amplitude of the signal was normalized by the maximum value of the reference signal.

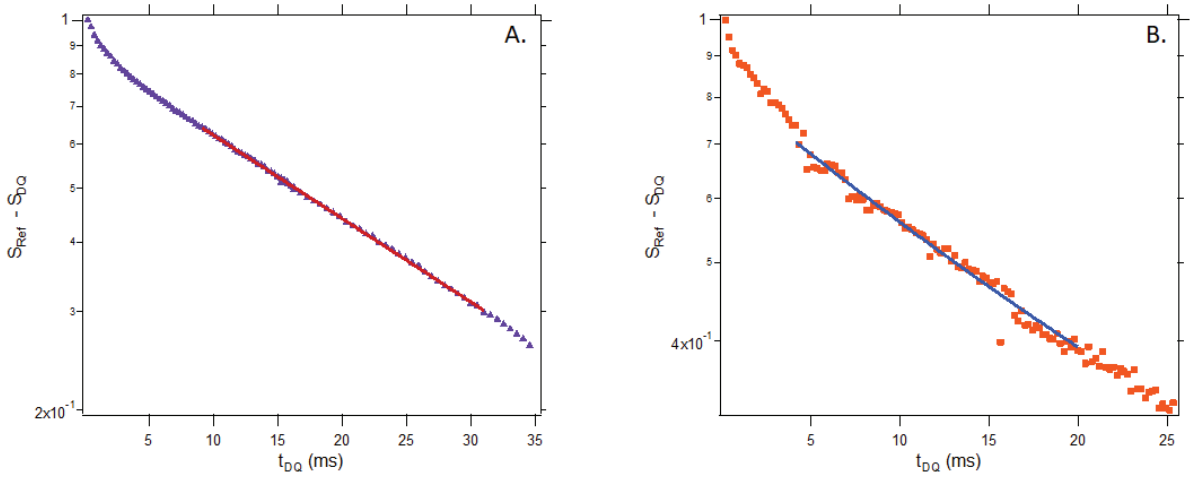


Figure 76 Plots S_{Ref}-S_{DQ} as a function of the DQ excitation/reconversion time in the sequence for gels of P(VDF-co-HFP) in MEK with (a) $X_{P(VDF\text{-}co\text{-}HFP)}$=20wt% (purple ▲, fitting curve in red) and (b) $X_{P(VDF\text{-}co\text{-}HFP)}$=30t% (orange ■, fitting curve in blue)

3.3. Structural information

3.3.1. Thermal behavior of the gels: DSC

P(VDF-co-HFP) – MEK or P(VDF-co-HFP) – 2-heptanone solutions are converted to gels on cooling and turn back to fluid solutions on heating. The sol-gel transition is thus thermoreversible. As seen above, the gelation behavior of this copolymer is highly dependent on both polymer concentration and temperature. DSC experiments were performed to further investigate structural and/or thermodynamic changes occurring at the sol-gel transition. From a macroscopic point of view, once formed, all gels transform into a fluid in a similar range of temperature, between 40 and 45°C for gels in MEK and around 65°C for gels in 2-heptanone, and no systematic dependence on the concentration was detected.

DSC thermograms during the first heating scan are shown in Figure 77 for gels in MEK with various copolymer concentrations. A weak endothermic peak systematically appears at a temperature T_m in between 40 and 50°C. This range of temperature matches with the sol-gel transition of the P(VDF-co-HFP) – MEK systems. This endothermic peak is not due to solvent evaporation, as the boiling temperature of the solvent is close to 80°C and DSC measurements were performed using hermetic pans. The melting temperature $T_{melting}{}^{gel}$ varies from 41°C to 44°C and does not follow a systematic variation with the gel concentration. In contrast, the melting enthalpy increases as the concentration of the copolymer in the gel increases. The DSC results suggest that crystallites are present in the gels. Therefore, the gelation of P(VDF-co-HFP) in MEK is certainly due to the formation of crystalline zones of the copolymer in the gels. These crystalline regions might then be bridged by portions of chains in solution to form a three-dimensional network characteristic of the gel state.

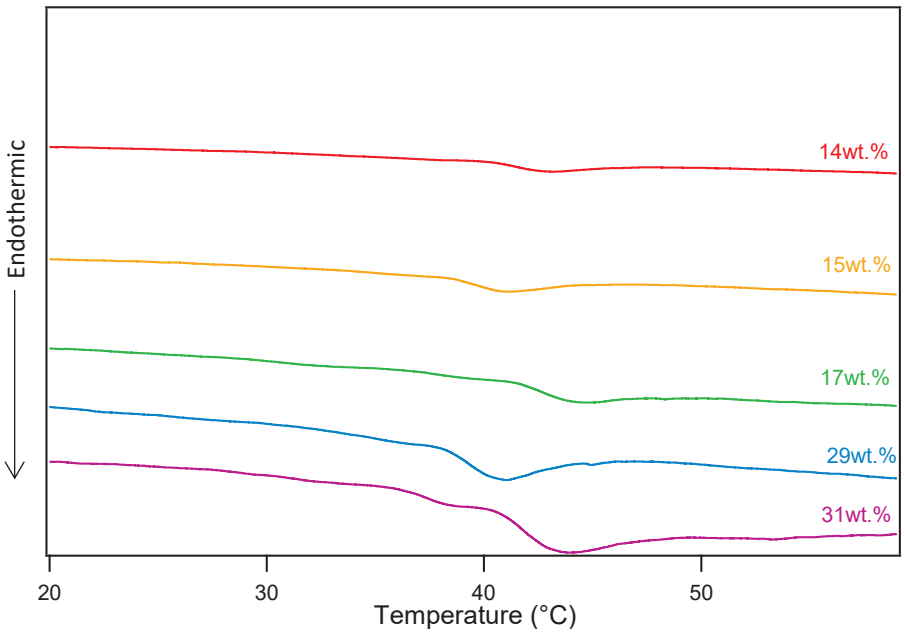


Figure 77 DSC thermograms of P(VDF-co-HFP) - MEK gels with various P(VDF-co-HFP) concentrations. Heating ramp was fixed at 1°C/min and only the first cycle of the DSC measurement was considered.

The percentage of crystalline zones in the different gels may be determined from DSC measurements using the following equation:

$$X_c = \frac{\Delta H_m}{\Delta H_m^0} \times 100\ (\%) \qquad (32)$$

where ΔH_m is the heat of fusion measured in the P(VDF-co-HFP) gels, normalized to take into account the mass of the copolymer in the gel. ΔH_m^0 stands for the enthalpy of melting for a 100% crystalline material. The value ΔH_m^0=104.7 J.g^{-1}, reported for PVDF, was considered here (Rosenberg, Siegmann et al. 1991). Using this approach, the mass fractions of crystalline zones referred to the total mass of P(VDF-co-HFP) – MEK gels was found to range between 0.3 to 0.7%, depending on the copolymer concentration. Referred to the amount of P(VDF-co-HFP) copolymer, it would correspond to a crystallized fraction of order 2.5%.

However, at high concentration of copolymer in MEK it can be seen in the thermograms that more than a simple endothermic fusion exists: see the thermogram of P(VDF-co-HFP) gel with 31wt% of copolymer. It is even more obvious in the thermograms of P(VDF-co-HFP) gels in 2-heptanone as shown in Figure 78. Indeed, an endothermic peak can also be detected at temperatures around 35°C which do not vary with the copolymer concentration. This endothermic peak does not correspond to the evaporation of the solvent, as the boiling temperature of the solvent is close to 150°C and DSC measurements were performed using hermetic pans and is not due to the melting of the gel, as the melting temperature $T_{melting}^{gel}$ was determined by rheology measurements to be around 65°C depending on the copolymer concentration. These results suggest that in the case of P(VDF-co-HFP) gels in 2-heptanone, crystallites are present in the gel and, as for gels in MEK, gelation is certainly due to the formation of crystallites zones of the copolymer in the gel. Therefore, the endothermic peak should correspond to the melting temperature of the crystallites which differs from the melting temperature of the gel. As a consequence, an additional mechanism should be considered in the case

of P(VDF-co-HFP) gels in MEK at high concentration and in P(VDF-co-HFP) gels in 2-heptanone: maybe phase separation of the gel in polymer-rich and solvent-rich regions. Within the polymer-rich region the polymer chains should arrange into a three-dimensional network where crystalline zones act as crosslinks. During the experiments a second endothermic peak at temperatures around 75°C were determined and appears to correspond to the gel-melting temperature.

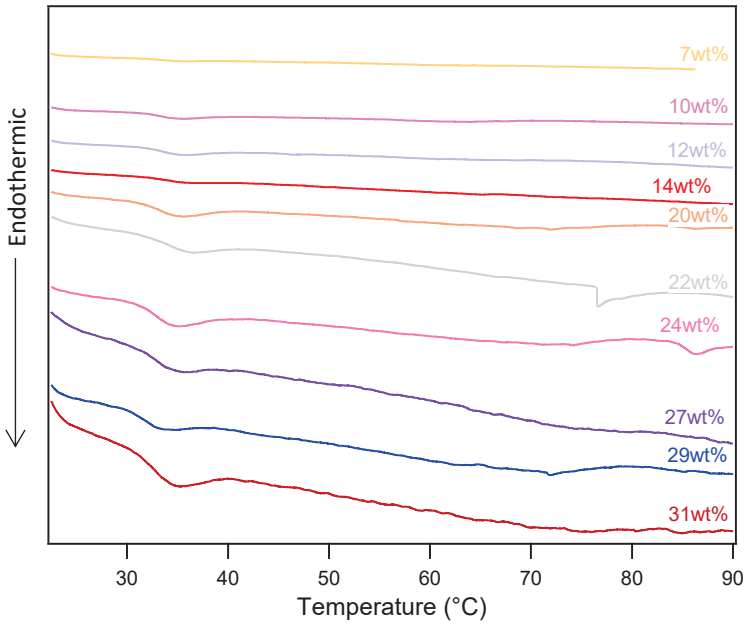


Figure 78 DSC thermograms of P(VDF-co-HFP) – 2-heptanone gels with various P(VDF-co-HFP) concentrations. Heating ramp was fixed at 1°C/min and only the first cycle of the DSC measurement was considered.

The fractions of crystalline zones in the gels in 2-heptanone was determined from the DSC thermograms. The mass fraction of crystalline zones referred to the total mass of P(VDF-co-HFP) – 2-heptanone gels was found to range between 0.3 to 1.4% and increases with the concentration of copolymer. Referred to the amount of P(VDF-co-HFP) copolymer, it would correspond to a crystallized fraction of copolymer of order 4.6%. In comparison with gel in MEK, there is a two-fold increase of the fraction of crystallites which can be explained by the difference of affinity between the copolymer and the solvent (χ parameter).

In a last step, the influence of the heating ramp on the crystalline fractions was studied. A heating ramp of 10°C/min was applied on P(VDF-co-HFP) gels in 2-heptanone and DSC thermograms are displayed in Figure 79. An endothermic peak was also detected at 39°C, which is a temperature close to the endothermic peak determined during the measurement at 1°C/min. Similar fraction of crystalline zones was determined: between 0.4 to 1.4% referred to the total mass of the gel and around 4.7%. The tendency of the thermograms does not change with the heating rate. However, the melting temperatures of the gels are more easily determined in this case: a clear endothermic peak is detected at temperature T_m in between 56 and 80°C. This range of temperature matches with the sol-gel transition of the P(VDF-co-HFP) – 2-heptanone systems and varies with the concentration of copolymer. The melting temperatures of the gels and their evolution with the polymer concentration determined by DSC are also concordant with those determined by rheology.

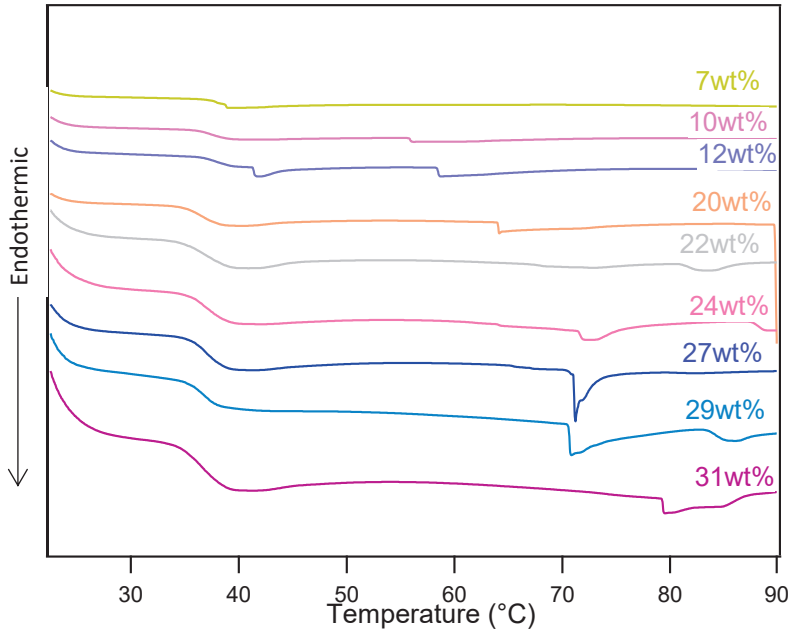


Figure 79 DSC thermograms of P(VDF-co-HFP) – 2-heptanone gels with various P(VDF-co-HFP) concentrations. Heating ramp was fixed at 10°C/min and only the first cycle of the DSC measurement was considered.

DSC measurements on P(VDF-co-HFP) gels in MEK and 2-heptanone indicated that a small fraction of crystalline zones, which may act as effective junction points, are present in the gels. In the case of gels in MEK, the crystalline zones melt in a similar temperature range as the one characterizing the gel-sol transition. However, at high concentration of copolymer in MEK and in gels in 2-heptanone the melting of the crystallite differs from the gel-sol transition, assuming that an additional phenomenon may occur in this case.

3.3.2. WAXS

To further validate the results obtained with ^{19}F NMR and DSC measurements, WAXS experiments were performed, on copolymer – MEK or 2-heptanone gels.

The WAXS pattern of a P(VDF-co-HFP) – MEK gel with a copolymer concentration of 20wt% is shown in Figure 80. For the sake of comparison, the diffractogram measured on bulk P(VDF-co-HFP) was also included. For this latter WAXS pattern, the main diffraction peaks observed at $2\theta = 18.07°$ (corresponding to 100/020 families of planes), 20.10° (110 planes), 26.86° (021 planes) and 39.06° (131 planes) are similar to the ones detected for the α phase (Form II) of neat PVDF (V. Tomer 2011). Interestingly, the WAXS pattern for the P(VDF-co-HFP) gel in MEK shows tiny but significant peaks at 2θ positions corresponding exactly to the main peaks observed on neat P(VDF-co-HFP). Besides, though tiny, these Bragg peaks are not detected on the WAXS measurements determined on a sample in the liquid state (data not shown). This result confirms the presence of crystalline zones in the gels. The gelation of the P(VDF-co-HFP) copolymer in MEK results from the formation of PVDF crystalline zones, which do not exist in the liquid state. Analyzing WAXS data quantitatively involves some difficulties. First, the (potentially) reduced size of the crystalline regions should induce a significant broadening of the corresponding peaks, making them again more difficult to be observed. Second, there is a large contribution from the solvent and/or amorphous part of the sample. Therefore, the intensities of the crystalline peaks relative to the amorphous background cannot be

safely used to quantify the degree of crystallinity or to estimate the apparent crystallite size for this gel.

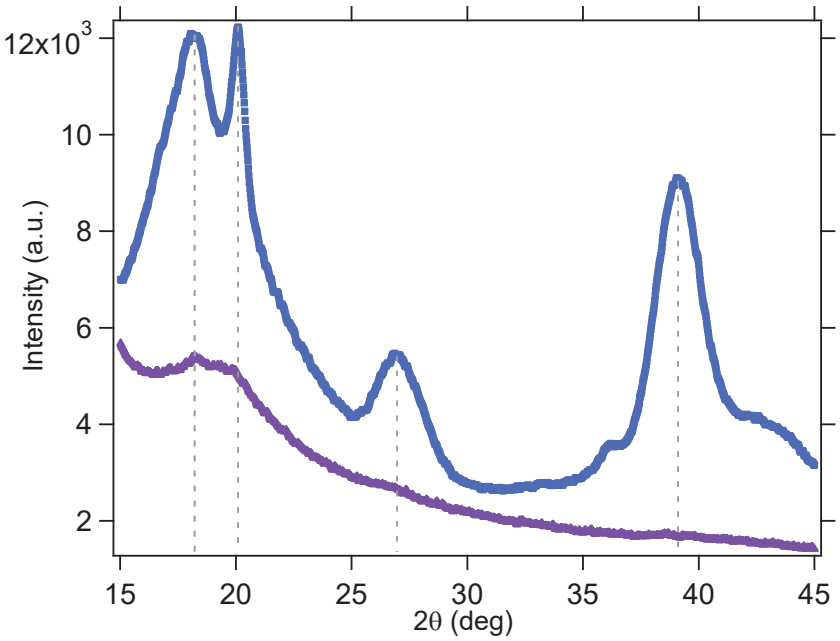


Figure 80 WAXS pattern of a P(VDF-co-HFP) – MEK gel with a composition $X_{P(VDF\text{-}co\text{-}HFP)}$=20wt% (▲, bottom curve) and a neat P(VDF-co-HFP) film (■, top curve), used as reference. Measurement time was fixed at 75 minutes.

Influence of the solvent nature on the gel's structure was investigated with WAXS measurements on P(VDF-co-HFP) gels in 2-heptanone. WAXS patterns of P(VDF-co-HFP) – 2-heptanone gels with different concentrations of copolymer are displayed in Figure 81. In both case, the main diffraction peaks observed at $2\theta = 18.27°$ (corresponding to 100/020 families of planes), 20.03° (110 planes), 26.12° (021 planes) and 39.06° (131 planes) are similar to the ones detected for the α phase (Form II) of neat PVDF. It confirms the DSC results proving that crystalline zones exist in the gel state are composed of VDF and HFP units. Experiments were performed at two different concentrations (12wt% and 20wt% of P(VDF-co-HFP)) to study the evolution of the crystalline peaks and fractions with the concentration. As for P(VDF-co-HFP) gels in MEK, due to the large contribution of the solvent and the amorphous part of the copolymer, it is impossible to determine the degree of crystallinity within the gels. Moreover, it is difficult to show an evolution of the crystalline fractions with the concentration of copolymer. Additional experiments (^{19}F NMR or DSC) are necessary to quantify this fraction.

DSC experiments were confirmed by WAXS measurements on P(VDF-co-HFP) – MEK and 2-heptanone gel. WAXS pattern on gels confirm in both case the presence of crystallites which do not exist in the liquid state. As a consequence, the gelation of P(VDF-co-HFP) in MEK and 2-heptanone may be attributed to the formation of PVDF crystallites which act as crosslinks between polymer chains.

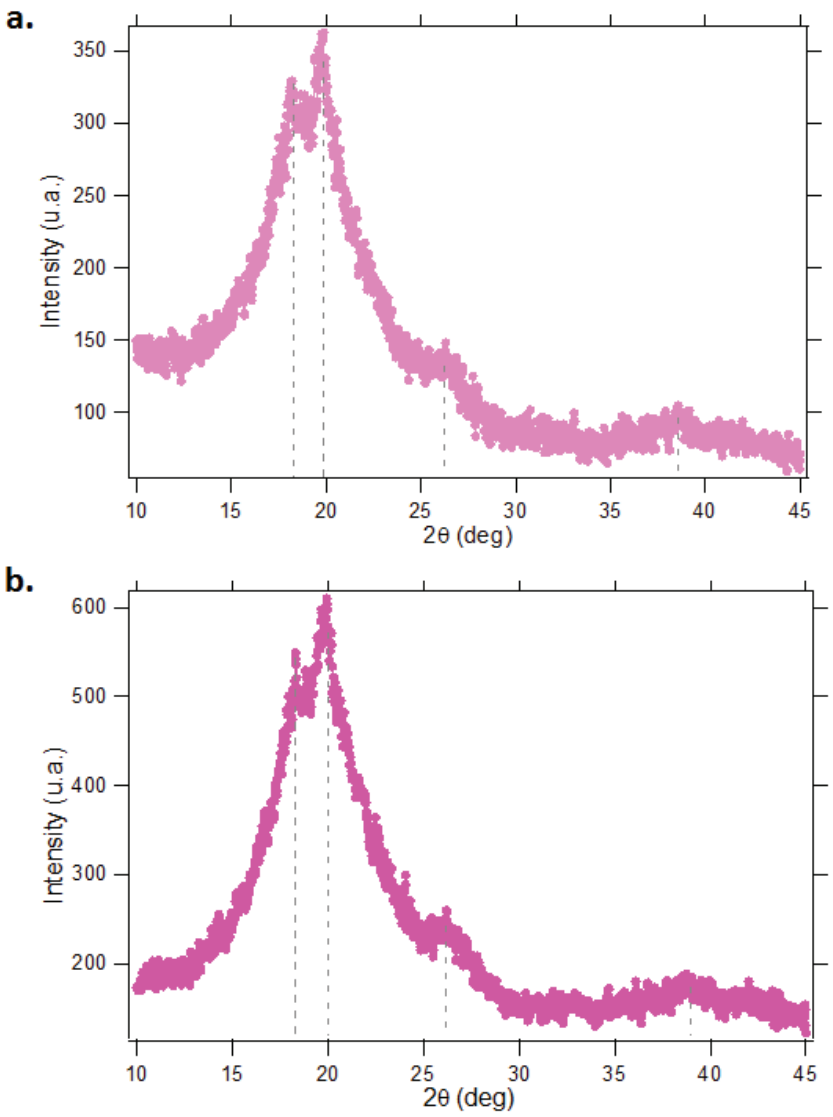


Figure 81 WAXS pattern of P(VDF-co-HFP) – 2-heptanone gels with a composition (a) $X_{P(VDF\text{-}co\text{-}HFP)}$=12wt% (light pink ●, 6minutes measurement time) and (b) $X_{P(VDF\text{-}co\text{-}HFP)}$=20wt% (pink ▲, 30minutes measurement time).

3.3.3. SAXS

As the electron densities of the fluorinated copolymer and the solvent are significantly different (electron density difference of about 2.3 x 10^{20} electrons/mm^3 between P(VDF-co-HFP) and MEK), Small Angle X-ray Scattering (SAXS) should be an appropriate technique to obtain pieces of information on the structure of the system, and specifically in the gel state, in the same way as when neutron scattering is used with deuterated polymers in solution.

The scattered intensities measured for P(VDF-co-HFP) – MEK mixtures at different concentrations are shown in Figure 82. In liquid solution below the sol-gel transition (4wt% and 13wt% of P(VDF-co-HFP)) the scattering is typical of a single-phase polymer-solvent mixture. The scattering intensity starts increasing at very small angle in the system with 15wt% of P(VDF-co-HFP), which is very close to the gel point. This indicates the presence of weak, large scale heterogeneities in the system. Above the sol-gel transition (gel corresponding to 20wt% and 26wt% of P(VDF-co-HFP) in Figure 82), the scattering patterns change and qualitatively new features appear. Above a critical q_c value of about

0.1 $Å^{-1}$ typically, the shape of the scattering does not change significantly, while below this value a large additional scattering appears. The scattering intensity at low q values increases as the polymer concentration is raised up while keeping essentially the same shape. This scattering shape is typical of polymer-polymer or polymer-solvent phase separated systems It has been observed in neutron scattering experiments on phase separating polymer blends (Lefebvre, Lee et al. 1999, Lefebvre, Lee et al. 2002, Balsara, Rappl et al. 2004).

More precisely, the fact that the scattering appears below a well-defined value q_c indicates that phase separation occurs in the nucleation regime rather than in the spinodal regime. In the nucleation regime, there is a critical size r_c below which a nucleated droplet of the phase will vanish, while above r_c it will grow. Thus all droplets which grow as the system phase separate are larger than r_c, and this gives a scattering only at q values smaller than $q_c = 2\pi/r_c$. As phase separation proceeds, the scattering may be described by the Debye-Bueche equation:

$$I(q) \approx \beta^2 \Delta\rho^2 \varphi(1-\varphi) \frac{\xi^3}{(1+q^2\xi^2)^2} \tag{33}$$

Where $\beta^2\Delta\rho^2$ is the contrast factor (see Chapter 2), φ the volume fraction occupied by one of the phases (e.g. the polymer-rich phase) and ξ the characteristic size (correlation length) of the domains of the phases. This describes domains of the coexisting phases (one rich in polymer and one rich in solvent) with sharp interfaces. Examples of fits are shown in Figure 82. The obtained ξ values are of the order 3.6 nm.

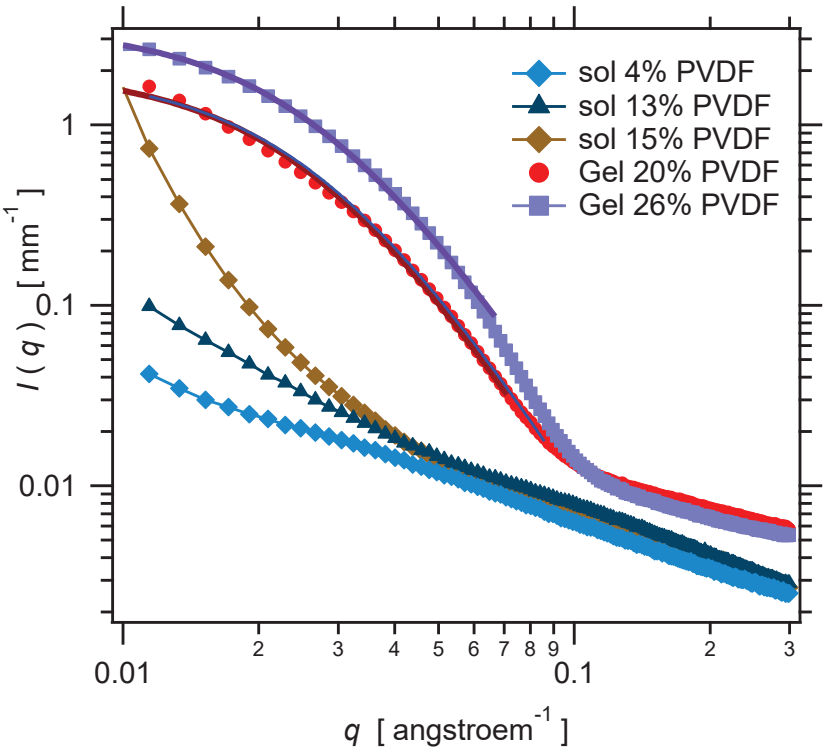


Figure 82 Normalized SAXS profile for P(VDF-co-HFP) - MEK systems of different composition (light blue ◆) $X_{P(VDF\text{-}co\text{-}HFP)}$=4wt%, (blue ▲) $X_{P(VDF\text{-}co\text{-}HFP)}$=13wt%, (brown ◆) $X_{P(VDF\text{-}co\text{-}HFP)}$=15wt%, (red ●) $X_{P(VDF\text{-}co\text{-}HFP)}$=20wt%, (violet ■) $X_{P(VDF\text{-}co\text{-}HFP)}$=26wt%. The systems with $X_{P(VDF\text{-}co\text{-}HFP)}$=20wt% and 26wt% were in the gel state. Fits of the curves of the gels with Equation 36 are shown.

The scattered intensities measured for P(VDF-co-HFP) – 2-heptanone mixtures at different concentrations are shown in Figure 83. Results are qualitatively similar to those in MEK. In liquid solution below the sol-gel transition (2wt% of copolymer) the scattering curve has the same trend as gels (from 3wt% of P(VDF-co-HFP)). Large additional scattering is present at low *q* values (below 0.1 $Å^{-1}$) and the intensity increases with the concentration of copolymer. Heterogeneities (with a characteristic size between 6 and 60 nm) would also exist in the liquid state certainly because 2-heptanone is a poorer solvent of the P(VDF-co-HFP) compared with MEK. The intensities at small q (measured at 0.01 $Å^{-1}$) are plotted in Figure 83 (b) as a function of $\varphi(1-\varphi)$. A linear relationship is observed, in accordance to Equation 36.

By taking an electron density difference $\Delta\rho = 2 \times 10^{20}$ mm^{-3} and ξ = 5.5 nm, a value 50 mm^{-1}, equal to the slope of the line in Figure 83-b is obtained.

Altogether, both the shape of the measured scattering curves and the absolute intensities are roughly coherent with Equation 36.

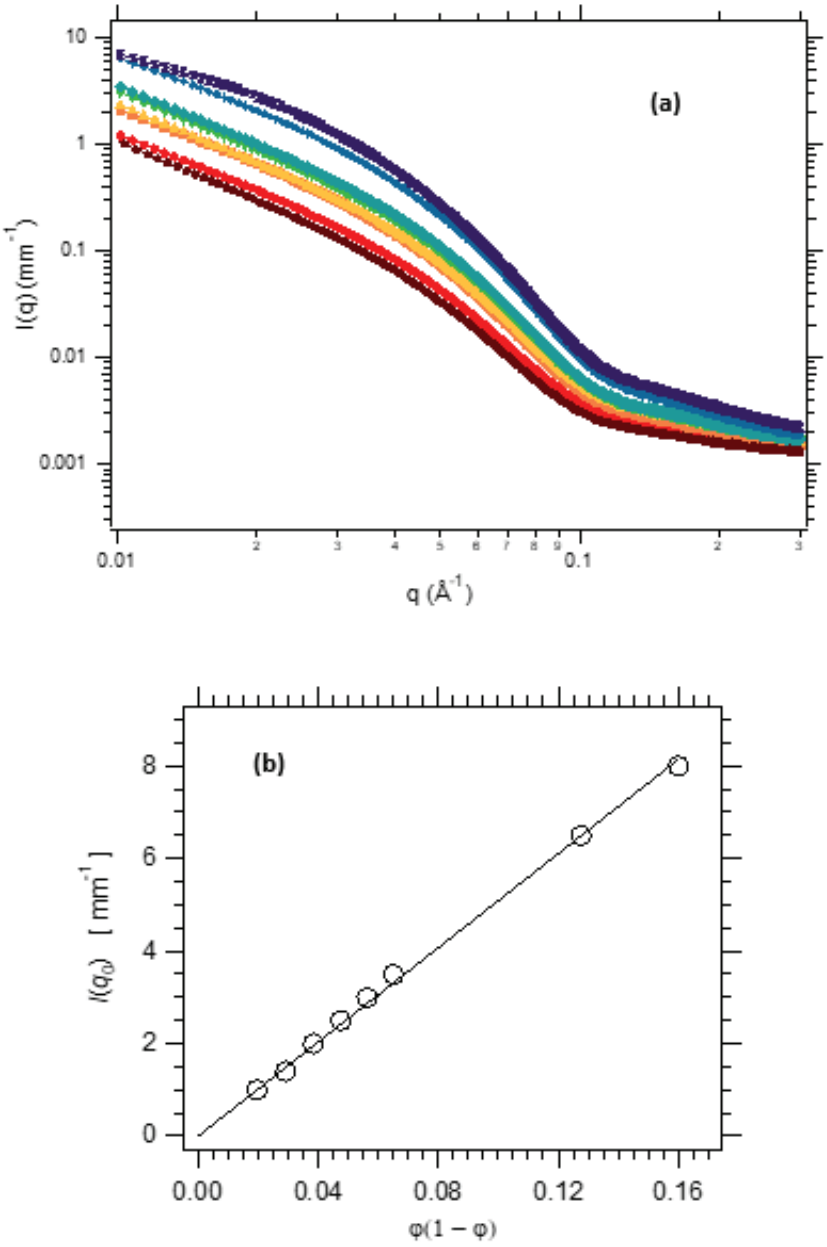


Figure 83 (a): Normalized SAXS profile for P(VDF-co-HFP) – 2-heptanone systems of different composition (brown ⬟) $X_{P(VDF\text{-}co\text{-}HFP)}$=2wt%, (red ●)$X_{P(VDF\text{-}co\text{-}HFP)}$=3wt%, (orange ■) $X_{P(VDF\text{-}co\text{-}HFP)}$=4wt%, (yellow ▲)$X_{P(VDF\text{-}co\text{-}HFP)}$=5wt%, (green ▼)$X_{P(VDF\text{-}co\text{-}HFP)}$=6wt%, (blue ◆)$X_{P(VDF\text{-}co\text{-}HFP)}$=7wt%, (dark blue ✦) $X_{P(VDF\text{-}co\text{-}HFP)}$=15wt%, (black ⧗) $X_{P(VDF\text{-}co\text{-}HFP)}$=20wt%. Only the system with $X_{P(VDF\text{-}co\text{-}HFP)}$=2wt% is at the liquid state. (b): the intensities of the curves shown in (a) measured at q = 0.01 Å^{-1} as a function of φ(1 − φ).

Due to the low volatility of 2-heptanone, it was possible to follow the evolution of the structure of the solution during gelation using SAXS experiments. An example is shown in Figure 84 for a solution of P(VDF-co-HFP) in 2-heptanone with a composition $X_{P(VDF\text{-}co\text{-}HF°}$=7wt%. Samples were introduced in cells in the liquid state at temperature 60°C and then rapidly cooled down to 20°C and the evolution of the scattering signal was recorded every five minutes (which corresponds to the acquisition time). As shown previously, in the liquid state heterogeneities already exist within the material. A low *q* the scattering intensity increases during the gelation phenomenon while scattering patterns roughly keep the same shape. It is then possible to estimate the gelation time as the time when no further

evolution of the scattering signal is detected. At this composition, the gelation time was found to be around 1,5 hours, which is in good agreement for the gelation time measured with the tube-tilting method. However, in comparison with the SAXS profile of a P(VDF-co-HFP) – 2-heptanone gel with the same composition studied previously, the scattering intensity at low *q* is still lower in the freshly prepared gel, meaning that the gels certainly evolve before reaching a final state, i.e. a final composition of heterogeneities.

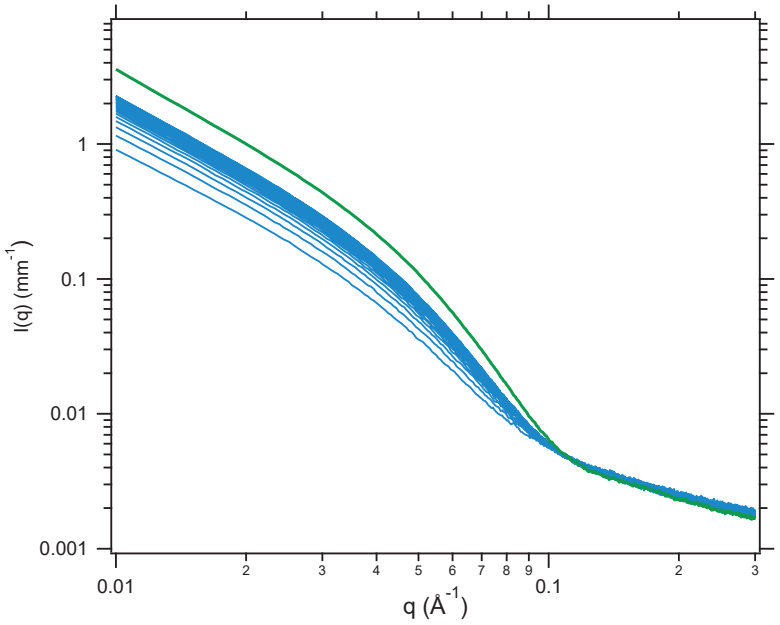


Figure 84 Evolution of the scattering intensity during gelation: SAXS measurements on a P(VDF-co-HFP) solution in 2-heptanone with $X_{P(VDF\text{-}co\text{-}HFP)}$=7wt% (blue curve) and comparison with a gel with the same composition previously prepared (green curve). Curves are recorded every 5 min.

3.4. Influence of the HFP fraction of the copolymer and its microstructure on gelation

It was found that the formation of rigid crystalline zones which act as crosslinks between polymer chains might be responsible for the thermoreversible gelation of P(VDF-co-HFP) in MEK or 2-heptanone. Thus gelation might be related to the semi-crystallinity of the studied copolymer. Investigations on the crystallinity and microstructure of P(VDF-co-HFP) copolymer on gelation kinetics and structure of the gel were therefore conducted. Three new copolymers were used:

iv. Amorphous P(VDF-co-HFP) called Tecnoflon® N535 has a HFP content larger than 20% mol
v. P(VDF-co-HFP) 1 contains the same fraction of HFP than Solef® 21510 but has a different microstructure: compared to Solef® 21510 which is statistical, the comonomer is not homogeneously distributed in the chain but HFP-rich zones exist
vi. P(VDF-co-HFP) 2 has the same polymeric chain structure but has a lower HFP fraction compared to Solef® 21510: the crystalline fraction is higher

The new copolymers were studied in 2-heptanone using a combination of tube-tilting method and WAXS experiments. In the amorphous P(VDF-co-HFP), no gelation was observed even at high concentrations of copolymers. This confirms that gelation of VDF-based copolymers would only occur in semi-crystalline polymers, thus with a HFP content lower than 20wt%. Figure 85 shows the

evolution of the gelation rate t_{gel}^{-1} of P(VDF-co-HFP) – 2-heptanone solutions as a function of concentration at 20°C for the three semi-crystalline copolymers. Below 4wt% of P(VDF-co-HFP) 1 and P(VDF-co-HFP) 2 at 20°C, no gelation occurs over one week (gelation time is considered to be "infinite").

The gelation kinetics in P(VDF-co-HFP) 1 and P(VDF-co-HFP) 2 show very similar trends. It is clear that the gelation rate is highly dependent on the architecture of the copolymer. At higher crystallization tendency (lower fractions of HFP, architecture with HFP blocks) the curves of crystallization rate vs concentration are shifted to higher rates and/or lower gel concentrations compared to the P(VDF-co-HFP) Solef® 21510.

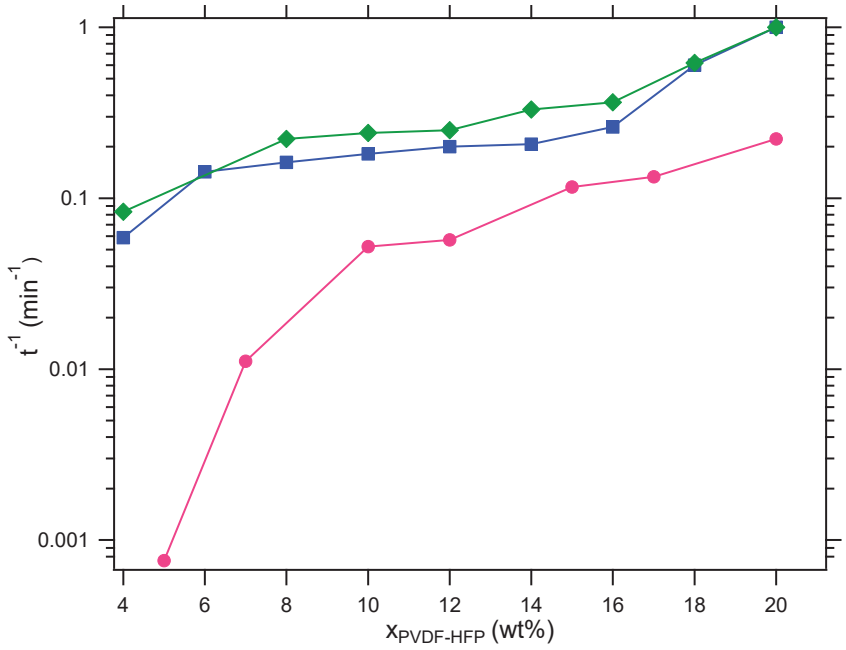


Figure 85 Gelation rate t^{-1} versus concentration for P(VDF-co-HFP) in solution in 2-heptanone measurement at 20°C for three different copolymers: usual P(VDF-co-HFP) Solef® 21510 (pink ●), P(VDF-co-HFP) 1 (blue ■), P(VDF-co-HFP) 2 (green ◆).

Gelation kinetics of the two copolymers P(VDF-co-HFP) 1 and P(VDF-co-HFP) 2 was investigated in MEK at 20°C at three different concentrations (12 and 20wt% of copolymer) and compared with the gelation kinetic of the Solef® 21510 P(VDF-co-HFP). As shown in Figure 86, similar trends as in 2-heptanone are obtained but the rates are about one order of magnitude smaller than in MEK. Indeed, gelation of P(VDF-co-HFP) Solef® 21510 in MEK does not occur below 11wt% (or the gelation time is longer than to 1 month and considered to be "infinite") as was shown in page 82. The change of copolymer with P(VDF-co-HFP) 1 and P(VDF-co-HFP) 2 shifts the gelation point to lower concentrations of copolymer and accelerates the gelation kinetics.

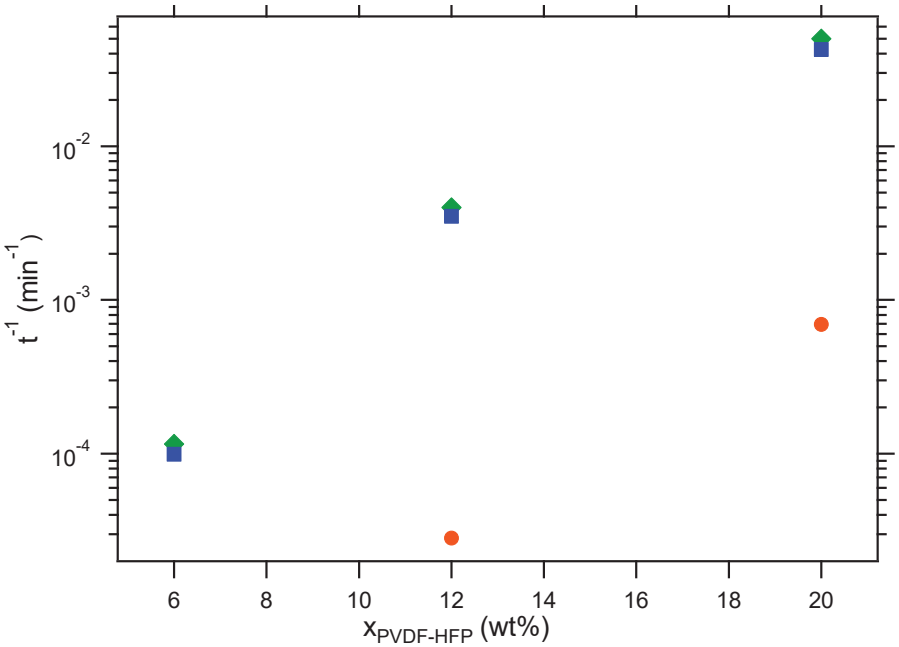


Figure 86 Gelation rate t^{-1} versus concentration for P(VDF-co-HFP) in solution in MEK measurement at 20° C for three different copolymers: usual P(VDF-co-HFP) Solef® 21510 (orange ●), P(VDF-co-HFP) 1 (blue ■), P(VDF-co-HFP) 2 (green ◆).

From this simple test it is clear that the crystalline fraction and the architecture of the copolymer strongly influence the gelation kinetic.

We assumed that the gelation of these two P(VDF-co-HFP) would also be due to the formation of crystalline zones which may act as junction points, forming a network. To check this hypothesis, WAXS measurements were performed on copolymers – 2-heptanone solution and gels at 20wt% of copolymer. The WAXS pattern of an amorphous P(VDF-co-HFP) – 2-heptanone solution is shown in Figure 87-a. Only the amorphous signal is observed, which confirms that no crystalline zones exist in this system, which does not gel. In comparison, the diffractogram measured on a P(VDF-co-HFP) 1 – 2-heptanone system (Figure 87-b) shows peaks at 2θ positions corresponding exactly to the main peaks observed on neat P(VDF-co-HFP) Solef® 21510. The same peaks are observed in gels prepared with P(VDF-co-HFP) 2 (Figure 87-c). These results confirm our hypothesis and crystalline zones exist in the gels.

Therefore, the gelation of P(VDF-co-HFP) only occurs in semi-crystalline copolymer and may result from the formation of crystalline zones, which do not exist in the liquid state. The intensities of the peaks in both cases show that only a small fraction of crystallites exist and these crystalline zones correspond to the α phase (Form II) of neat P(VDF-co-HFP) (V. Tomer 2011). It is difficult to quantify the fractions of crystalline zones in the gels by this method. However from the WAXS patterns in Figure 87, it is qualitatively observed that the fraction of crystallites is higher in gels prepared with the P(VDF-co-HFP) 2, coherent with the fact that P(VDF-co-HFP) is supposed to be highly crystalline in the solid state. In these two gels the fraction of crystalline zones seems to be higher than in the gel of P(VDF-co-HFP) Solef® 21510.

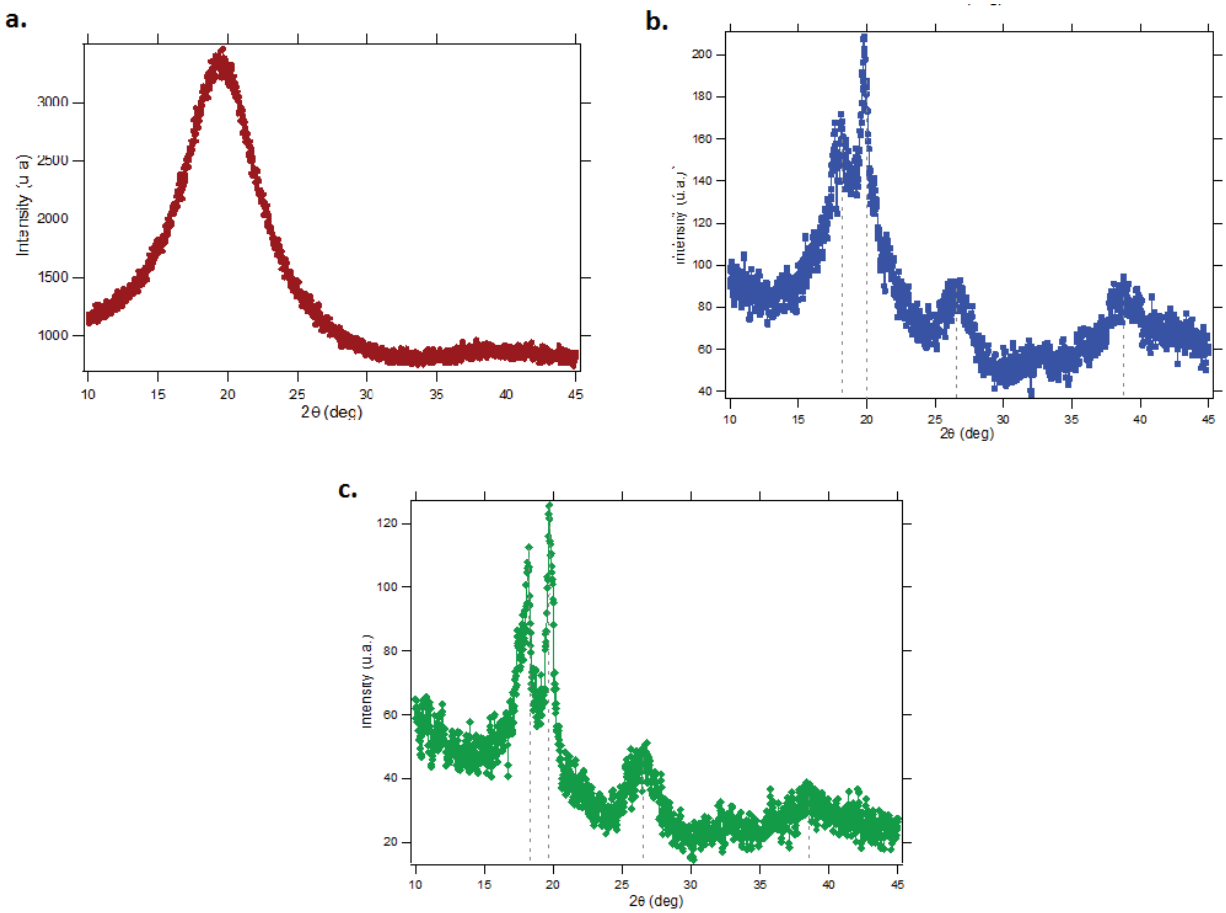


Figure 87 WAXS pattern of P(VDF-co-HFP) – 2-heptanone solution and gels with a composition $X_{P(VDF\text{-}co\text{-}HFP)}$=20wt% in (a) amorphous P(VDF-co-HFP), (b) P(VDF-co-HFP) 1 and (c) P(VDF-co-HFP) 2. Measurement time was fixed at 30 minutes for the solution in amorphous P(VDF-co-HFP) and 6 minutes for the two others copolymer.

3.5. General discussion: gelation mechanism(s) involved in the thermoreversible gelation of P(VDF-co-HFP) copolymers in linear ketone solvents

PVDF and its semi-crystalline copolymers convert to thermoreversible gels at room temperature in various organic solvents such as ketones (γ-butyrolactone, cyclohexanone, cycloheptanone, acetophenone, for example) aromatic diesters (ethyl benzoate) or diesters (glyceryl tributyrate). The gelation of PVDF was studied in the literature in various solvents mostly in dried gels, considering that there is no change in the polymorphic structure during drying (confirmed with FTIR measurement). Depending on the nature of the solvent, the gelation kinetics may change considerably (Tazaki, Wada et al. 1998). Tazaki et al. have shown that gelation of PVDF in aliphatic ketones was faster than in γ-butyrolactone. Conversely no gelation occurs in DMF and DMSO.

Various gelation mechanisms have been proposed, depending on the nature of the solvent, the process used and/or the concentration of polymer: crystallization-induced gelation (Tazaki, Wada et al. 1998), liquid-liquid phase separation followed by solid-liquid phase separation (Cho, Song et al. 1993) or liquid-liquid phase separation via spinodal decomposition depending on the spinodal transition point T_s (Hong and Chou 2000). However, to our knowledge, the thermoreversible gelation of PVDF and VDF-based copolymers was not discussed in linear ketone solvents such as MEK and 2-heptanone.

Several experimental techniques were combined to understand gelation of P(VDF-co-HFP) in these solvents: tube-tilting and linear rheology were used to investigate the gelation kinetics and ^{19}F NMR, DSC, WAXS and SAXS to probe the existence of rigid zones in the gels, assimilated to crystallites.

We found that the gelation of P(VDF-co-HFP) only occurs in semi-crystalline copolymers: even at high concentrations an amorphous P(VDF-co-HFP) does not gel. The gelation of this type of copolymer strongly depends on the fraction of HFP, that is on its degree of crystallinity. The architecture of the copolymer also has a direct impact on the gelation kinetics.

In this work the gelation mechanisms were studied more particularly with P(VDF-co-HFP) Solef® 21510 in MEK, before being generalized to 2-heptanone, i.e. a ketone with a longer backbone chain. The gelation kinetics was found to be highly dependent on the copolymer concentration and the temperature: the increase of the copolymer concentration and decrease of temperature increase the gelation rate, which confirms the findings of numerous studies of the gelation of PVDF (Tazaki, Wada et al. 1998, Kim, Baek et al. 2004). Moreover, as found in the study of Shimizu et al. (Shimizu, Arioka et al. 2011), the melting temperatures were found to increase with the concentration of copolymer in both cases.

^{19}F NMR was used to investigate selectively the segmental dynamics of P(VDF-co-HFP) chains in MEK solutions and gels at different concentrations. In the liquid state no polymer network was observed. Conversely, when the system gels, a rigid fraction appears together with local anisotropy for a fraction of the mobile polymer, indicating the formation of a network. The rigid fraction in the gel is relatively small and seems to increase with the concentration of copolymer. We make the hypothesis that these rigid zones should act as crosslinks between portions of polymer chains in solution to form a three-dimensional network which characterizes the gel state. DSC experiments evidence an endothermic peak that might correspond to the melting of crystalline zones, this thermal event being concomitant with the thermally-induced gel-sol transition (between 40 and 45°C depending on the concentration of copolymer). The fraction of crystallites (referred to the polymer fraction) is qualitatively coherent to the fraction of rigid zones determined by ^{19}F NMR. Therefore, it is possible to assume that the rigid zones detected in the gels by NMR are most probably crystalline zones. To validate this result, WAXS experiments were carried out on these materials. Even though the intensity of the Bragg peaks was generally too low to quantify the fraction of crystalline zones, it was possible to confirm the existence of VDF crystalline zones.

With 2-heptanone, due to the low volatility of this solvent, it was possible to perform rheology and SAXS during the gelation process. Qualitatively similar results were observed with these new gels. According to SAXS experiments, heterogeneities with a typical size similar to that detected in gels in MEK exist in the gel state in 2-heptanone. These heterogeneities are associated to the presence of crystallites as shown in WAXS patterns. As for gels in MEK, the crystalline phase corresponds to the α phase (form II) of PVDF. The presence of crystallites in P(VDF-co-HFP) – 2-heptanone gels was confirmed by DSC: an endothermic peak with a small intensity was detected. The fraction of rigid crystalline zones seems to be larger than the one determined in MEK. Besides the gelation kinetics in 2-heptanone show a similar dependence in P(VDF-co-HFP) concentration and temperature as in MEK but is faster by more than two orders of magnitude. Melting temperatures of gels in 2-heptanone are higher than those determined in MEK and increase with the concentration of copolymer.

All these differences may be explained by the fact that 2-heptanone would be a poorer solvent than MEK for PVDF, with a stronger tendency to phase separate, which would accelerate the gelation, increase the gel melting points and increase the polymer concentration in polymer-rich domains. For example Shimizu et al. (Shimizu, Arioka et al. 2011) have studied the sol-gel transition of PVDF in three different solvents (diethyl carbonate, propylene carbonate, γ-butyrolactone) and shown the dependence of the gel-melting temperature with the polymer concentration and the solvent solubility parameters.

To further check this hypothesis the Flory interaction parameters χ_{Ps} between P(VDF-co-HFP) and MEK and 2-heptanone were estimated using Hildebrand equation (J.H. Hildebrand 1950, J.H. Hildebrand 1962), in terms of solubility parameters:

$$\chi_{Ps} = \frac{\sqrt{V_P V_s}}{RT}\left(\delta_{t,P} - \delta_{t,s}\right)^2 \tag{34}$$

with:

- V_P and V_s, the molar volumes of the copolymer and the solvent respectively
- $\delta_{t,P}$ and $\delta_{t,s}$, the (total) solubility parameters of the copolymer and the solvent respectively

It should be noted that the interaction parameter χ_{Ps} depends on temperature. According to Hansen the δ_t parameter may be split into three components (M. Hansen 2012):

$$\delta_t^2 = \delta_d^2 + \delta_p^2 + \delta_h^2 \tag{35}$$

where δ_d accounts for the dispersive interactions (London forces, non-polar interaction), δ_p for polar interactions (Keesom polarity between permanent dipoles) and δ_h for the hydrogen bonds. Solvents can then be represented in a three dimension space (see Figure 88). Moreover, these three components can be calculated using the group contribution theory and are expressed are:

$$\delta_d = \frac{\sum F_{di}}{V_m} \tag{36}$$

$$\delta_p = \frac{\sqrt{\sum F_{pi}^2}}{V_m} \tag{37}$$

$$\delta_h = \sqrt{\frac{\sum E_{hi}}{V_m}} \tag{38}$$

With:

- E_h the cohesive energy
- F the molar attraction constants
- V_m the molar volume of the polymer or the solvent defined as the ratio between the molar mass of the substance and its density

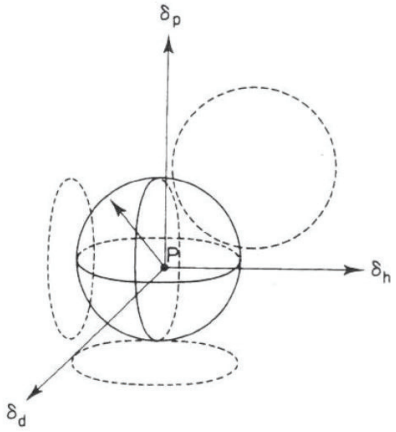


Figure 88 Solubility sphere in the Hansen 3D representation (Utracki 2003)

We only considered here a PVDF polymer, considering that the fraction of HFP is relatively low and therefore negligible (at least below 20wt%). Solubility parameters of PVDF and MEK were taken from Bottino et al. (Bottino, Capannelli et al. 1988) while those of the 2-heptanone were estimated and listed in Table 5 below. It shows that the polarity solubility parameter δ_p of MEK is higher than that of 2-heptanone and closer to that of the PVDF. This may indicate that MEK is a better solvent for PVDF than 2-heptanone. However, as shown in the Hildebrand equation, not only the polarity parameter plays a role in the polymer – solvent interaction but hydrogen bonding and polydispersion energies also contribute to the equation even though their contribution to the total solubility parameter is smaller.

Table 5 Solubility parameters ($MPa^{1/2}$) of PVDF, MEK and 2-heptanone ((a): from Bottino et al ; (b): from Hansen 1970)

	δ_d	δ_p	δ_h	δ_t
PVDF				**23.2 (a)** **19.2 (b)**
MEK	15.55	8.55	4.7	**18.36**
2-heptanone	16.22	5.42	3.76	**17.93**

Molar volumes of the PVDF and the solvents were determined from their molar mass and the density. These values are displayed in the Table 6.

Table 6 Molar masses, densities and molar volumes of PVDF, MEK and 2-heptanone

	M ($g.mol^{-1}$)	d ($g.cm^{-3}$)	V_M ($cm^3.mol^{-1}$)
PVDF	64.01	1.78	35.96
MEK	72.11	0.805	89.58
2-heptanone	114.18	0.802	142

Flory interaction parameters of PVDF in MEK and in 2-heptanone were determined at 20°C and we found $\chi_{P\text{-}MEK} = 0.41$ and $\chi_{P\text{-}heptanone} = 0.51$ - 0.66. Thus these two solvents, though they have close chemical structures, have relatively different polymer – solvent interactions. Even though both are close to 0.5, MEK seems to be a relatively good solvent ($\chi < 0.5$) of PVDF and its behavior should be similar to that of a θ solvent, which may explain the low tendency to gel and thus, which may explain the slow gelation kinetics in this solvent. Conversely, 2-heptanone would be a poor solvent for VDF-based copolymers ($\chi > 0.5$) with a higher tendency to phase-separate: the gelation kinetics might be accelerated and the gel point shifted to lower copolymer concentration in comparison with a better solvent. We have tried to compare our results with the gelation kinetics of PVDF in solvents studied in the literature: acetophenone ($\chi_{P\text{-}acetophenone}$=0.085), ethylene carbonate ($\chi_{P\text{-}ethylene\ carbonate}$=0.510), propylene carbonate ($\chi_{P\text{-}propylene\ carbonate}$=0.358) or γ-butyrolactone ($\chi_{P\ -\ \gamma\text{-}butyrolactone}$=0.193). However relevant comparison was impossible: indeed different grades of PVDF were used in the literature and, as shown in paragraph 3.4 (page 101), the structure and crystallinity of the copolymer strongly influences the gelation kinetics.

Finally, in our case the differences between the gelation kinetics, gel-melting temperatures and fraction of crystallites of P(VDF-co-HFP) in MEK and 2-heptanone are all coherent with a change in solvent quality or equivalently in Flory interaction parameters. In comparison with MEK and other solvents studied in the literature, 2-heptanone is a relatively poorer solvent of the copolymer and changes in the gel point, melting point and crystalline fraction can be explained by the thermodynamics of mixing. Indeed, in 2-heptanone, it seems that heterogeneities observed in SAXS may already exist in the liquid state prior to gelation (Figure 83 and Figure 84). In this case, phase separation would preexist partial crystallization. These results suggest that crystallization would be induced in the polymer-rich domains by thermodynamic phase separation, rather than phase separation being induced by partial crystallization in solution.

In fact, another difference was highlighted in DSC experiments in P(VDF-co-HFP) – 2-heptanone gels in comparison with gels in MEK. Indeed, the endothermic peaks appear at temperatures different from the gel melting temperatures: the endothermic peak was detected around 35°C (as for gels in MEK) while the gel melting temperatures was found to be around 65°C. This confirms that both distinct phenomena (phase separation and crystallization) might be involved in the gelation of P(VDF-co-HFP) in 2-heptanone. This joint mechanism was investigated by Cho et al. (Cho, Song et al. 1993) for PVDF gels in γ-butyrolactone. By combining microscopy and WAXS experiments on dry gels they demonstrated the influence of the concentration of PVDF on the gel structure. At high concentration, only the crystallization is responsible for the formation of a gel while at low concentrations the

solution crystallizes in a two-step process. This two-step gelation results from liquid-liquid phase separation in the early stage of gelation and crystallization in the two-phase gel at the final stage. At low concentration crystallization is not necessary for gelation to occur.

To confirm the existence of a liquid-liquid phase separation, additional experiments would be necessary. For example, crystallization isotherms would allow comparing the crystallization time and gelation time t_{gel}. If the crystallization time is comparable to the gelation time, gelation of the copolymer would be governed by crystallization while if the crystallization time is longer than the gelation time, gelation can take place without crystallization and is governed by liquid-liquid phase separation.

3.6. Conclusions

This chapter has presented the work on the gelation dynamics and the structure of P(VDF-co-HFP) gels using a combination of different experimental approaches: tube-tilting, linear rheology, ^{19}F NMR, DSC, WAXS and SAXS. In this context solutions of P(VDF-co-HFP) in MEK and 2-heptanone have been investigated. From the results we were able to formulate different conclusions:

- Gelation of P(VDF-co-HFP) in MEK and 2-heptanone only occurs with semi-crystalline copolymers. No gelation was highlighted for amorphous P(VDF-co-HFP).
- P(VDF-co-HFP) forms thermoreversible gels in MEK and 2-heptanone with gelation kinetics that strongly depend on both concentration and temperature. Gelation is faster at high concentrations and low temperatures. Moreover Figure 89 shows that the gelation of P(VDF-co-HFP) in 2-heptanone is faster than in MEK.
- SAXS results show that phase separation occurs in both P(VDF-co-HFP)/MEK and P(VDF-co-HFP)/2-heptanone systems. These results show that phase separation occur by a nucleation process of polymer-rich (or solvent-rich) domains in the mixtures. This process may be due to the fact that the PVDF/solvent interaction parameters are not very far from the critical value 0.5. In such conditions, the nucleation rate depends on the distance to the critical value 0.5. Therefore, the difference in gelation kinetics may be attributed to the difference of Flory interaction parameter: 2-heptanone is a relatively poor solvent of the copolymer (Flory interaction parameter > 0.5) while MEK is rather close to theta solvent for PVDF. The nucleation rate of phase-separated domains may thus be faster for 2-heptanone.

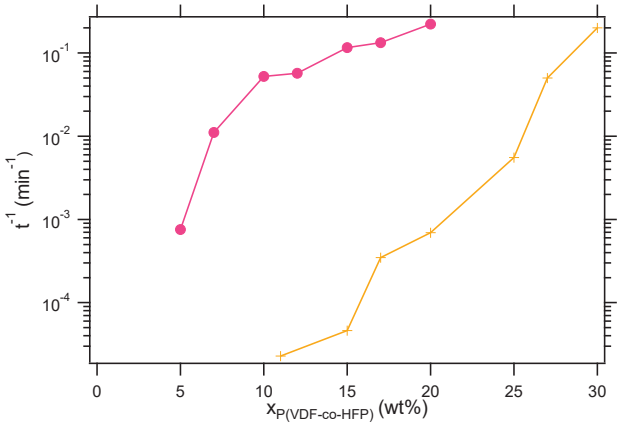


Figure 89 Gelation rate t^{-1} versus concentration for P(VDF-co-HFP) in solution in MEK (orange +) and 2-heptanone (pink ●) measurements at 20°C

- Gel-melting temperatures increase with increasing the concentration of P(VDF-co-HFP). Gel melting temperatures of gels in 2-heptanone were found to be higher than those determined in MEK. Gel-melting temperatures in 2-heptanone were in the range between 61-73°C while in MEK we found a range of 41-44°C. This concords with the theory which explains that the increase of the polymer concentration (Kim, Baek et al. 2004) and poor polymer-solvent interaction (high Flory interaction parameter) (Shimizu, Arioka et al. 2011) cause an increase in the gel-melting temperatures.
- ^{19}F NMR was used in this work to study selectively the segmental dynamics of P(VDF-co-HFP) in the gel state in MEK. It was possible to confirm that rigid zones and a polymer network are formed as the P(VDF-co-HFP) in MEK reaches the gel state, while such rigid regions and elastically active chains are bot present in the liquid state. Thus the fraction of rigid zones in the gel state decreases as the polymer concentration is raised up while thee fraction of cross-linked chains increases with the concentration
- DSC measurements on gels in MEK and 2-heptanone evidence an endothermic peak that might correspond to the melting of crystalline zones. The fraction of crystallites qualitatively corresponds with the fraction of rigid zones determined by NMR indicating that rigid zones might be crystallites and act as crosslink between polymer chains. WAXS patterns on these materials confirm the presence of a tiny fraction of crystallites. **As a consequence gelation of P(VDF-co-HFP) in MEK and 2-heptanone might be caused by phase separation into polymer-rich and solvent-rich domains followed by the formation of a small fraction of crystalline zones in polymer-rich domains**, as schematized in Figure 90.

  As confirms by WAXS patterns, the fraction of crystalline zones is higher in 2-heptanone (around a two-fold increase) than in MEK. This may be due to the difference between the Flory interaction parameters. As 2-heptanone has a higher Flory interaction parameter, it may be farther away from the critical phase separation point, as thus the polymer concentration in the polymer-rich domains may be higher, giving a higher crystalline fraction. In addition, melting temperatures of the crystallites differ from the gel melting temperatures of P(VDF-co-HFP)/2-heptanone. This suggests that liquid-liquid phase separation may be then followed by crystallization (see Figure 90).

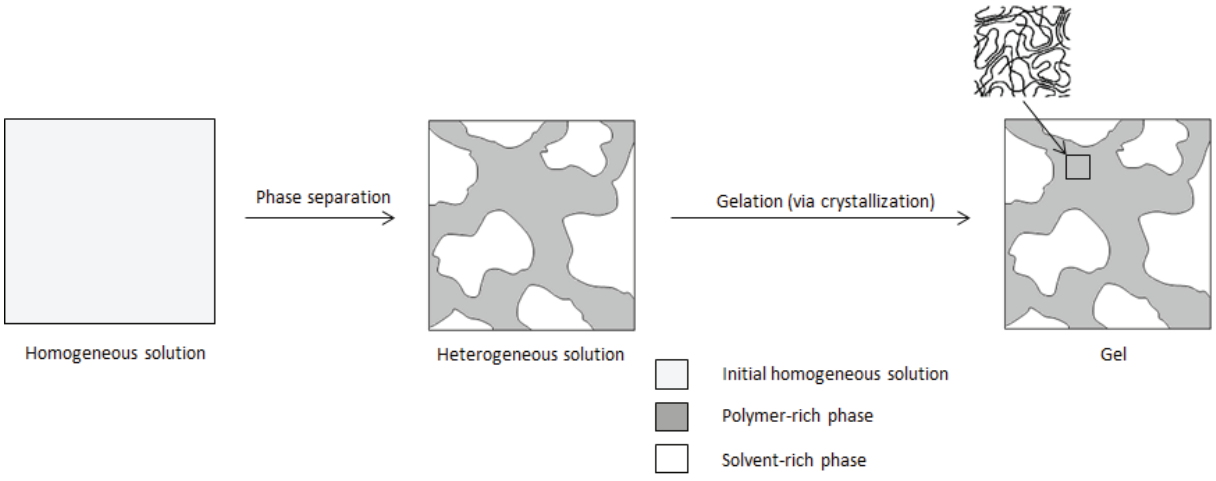


Figure 90 Schematization of gelation of P(VDF-co-HFP) induced by crystallization via the formation of a phase separated medium

Chapter 4: Influence of the presence of fillers on the thermoreversible gelation of P(VDF-co-HFP) in linear ketone solvents: MEK and 2-heptanone

This chapter presents the possible modification of the gelation mechanisms by the incorporation of silica nanoparticles in P(VDF-co-HFP) organogels. Influence of the source of silica used and the solvent is studied by combination of different approaches: USAXS, gelation kinetics and ^{19}F NMR.

4.1. An additional mechanism: polymer – silica interactions 112

4.2. Dispersion state of silica in the gel state: USAXS study 113

4.2.1. Monodisperse silica solutions synthetized in the lab 113

4.2.2. Nissan silica solutions 116

4.2.3. P(VDF-co-HFP) – MEK – silica ternary systems with monodisperse silica synthetized in the lab 118

4.2.4. P(VDF-co-HFP) – MEK – silica ternary systems with Nissan silica 122

4.3. Gelation kinetics 125

4.4. Dynamics of P(VDF-co-HFP) – silica gels in MEK 127

4.5. General discussion: modification of the gelation mechanism with the incorporation of silica nanoparticles 130

4.6. Conclusions 133

4. Influence of the presence of fillers on the thermoreversible gelation of P(VDF-co-HFP) in linear ketone solvents: MEK and 2-heptanone

As reported in Chapter 3, P(VDF-co-HFP) forms thermoreversible gels in linear ketone solvents like MEK and 2-heptanone. By combining different characterization methods, we determined a possible mechanism responsible for the gelation of the copolymer in these solvents: formation of polymer-rich domains in which crystalline zones develop. As the initial objective of the PhD thesis was to develop P(VDF-co-HFP)-based nanocomposite films by solvent route, the impact of the presence of silica nanoparticles on the gelation of the copolymer must now be studied.

In this chapter the gelation of P(VDF-co-HFP) in organic silica solution in MEK and 2-heptanone is described. Three sources of silica were used: (i) silica solution in MEK developed by phase transfer, (ii) silica solution in MEK provided by Nissan and (iii) Nissan silica solution in MEK transferred in 2-heptanone. The influence of the nature of the solvent, the type of silica and the process was investigated by combining different approaches: USAXS, gelation kinetics (by tube-tilting and rheology) and ^{19}F NMR.

4.1. An additional mechanism: polymer – silica interactions

Silica can interact with a polymer via chemical (covalent) or physical (adsorption) interactions. Some general considerations on the interactions between silica and a polymer were presented in Chapter 1 (see page 25). In our case no covalent bond is formed between the silica surface and the polymer during the dispersion step. P(VDF-co-HFP) should interact with silica surface through physical interactions. Adsorption is a dynamic process which has been widely studied (Cohen Stuart, Cosgrove et al. 1985, de Gennes 1987). It comes from Van der Waals, hydrogen, hydrophobic or electrostatic interactions. Macromolecules should adsorb on the solid surface with different conformations in order to optimize the compromise between the interactions with the substrate and the reduction of the degrees of freedom due to the contact with the surface (see Figure 91): segments which are in contact with the surface are called *trains*, *loops* segments have no contact with the surface and connect two trains and finally *tails* are end segments free in solutions (G. J. Fleer 1993).

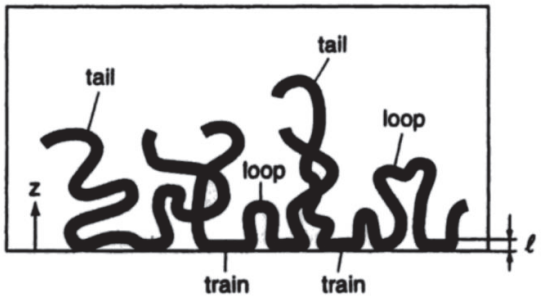


Figure 91 Schematic representation of adsorbed polymer onto solid surfaces

In the case of long polymer chains, adsorption is considered to be irreversible but an adsorbed polymer can be removed by introducing a new polymer which has a better affinity with the surface or a better solvent (Char, Gast et al. 1988, Cooper, Cosgrove et al. 2013). Moreover, polymer adsorption depends on several parameters such as the polymer molecular weight and molecular weight distribution, temperature, chemical modification of surfaces or solvent quality. In aqueous solutions, the pH and the amount of salt can also impact polymer adsorption. The quantity of

adsorbed polymer usually increases with the molecular weight until it reaches a limit from where no dependency can be observed. Moreover, the amount of adsorbed polymer is higher when the quality of the solvent decreases. Finally, the effect of the polymer concentration was widely studied and shows a steep increase of the quantity of adsorbed polymer with polymer concentration. Then a plateau value is reached and does not change with further increase of polymer concentration.

Interactions between silica surface and polymer can be evaluated with numerous analysis methods such as NMR, Photo Correlation Spectroscopy or TGA. From these methods it is possible to determine the quantity of polymer adsorbed per unit area of surface. Therefore, the adsorption isotherms are used to determine the interactions between polymer and a surface. The adsorbed amounts are usually represented as a function of the equilibrium bulk polymer concentration.

4.2. Dispersion state of silica in the gel state: USAXS study

The main objective of this chapter is to study the influence of the presence of silica on the gelation mechanism and we shall first characterize the dispersion state of silica nanoparticles in the solutions and gels. In this context, three different sources of silica were used:

- Silica solution in MEK developed by phase transfer
- Silica solution in MEK provided by Nissan Chemical
- Silica solution in MEK (provided by Nissan Chemical) transferred in 2-heptanone

To normalize the scattered intensities of the materials, the electron densities of all the components have been determined and are reported in Table 7. The density of the silica was taken to be equal to 2.2 g/cm^3.

Table 7 Electron densities of the different gel components

Silica	6.6 x 10^{23} cm^{-3}
PVDF	5.34 x 10^{23} cm^{-3}
H_2O	3.33 x 10^{23} cm^{-3}
MEK	2.683 x 10^{23} cm^{-3}
2-heptanone	2.762 x 10^{23} cm^{-3}

4.2.1. Monodisperse silica solutions synthetized in the lab

USAXS experiments were first carried out on silica solutions before studying the impact of the addition of copolymer on the dispersion state of the nanoparticles. First we observed the silica solutions developed in the laboratory (“phase transfer” process) at different stages: in water, in MEK after phase transfer (treatment with CTAB) and in MEK after phase transfer and grafting with VTMS.

The scattering curve of the initial aqueous silica solution (prepared by sowing process, with ϕ_{SiO2} = 4.6 wt%) is reported in Figure 92. The scattering function is characteristic of diluted, non-interacting particles. It can be described by the form factor of polydisperse spheres with a size distribution P(R) as detailed in section 2.2.5 (page 74). We assumed that the distribution is of log

normal form (green curve) and the parameters of the distribution were fitted (considering a density of 2.2 g.cm^{-3} plus a background of around 3 x 10^{-3} nm^{-2} for silica and a volume fraction of silica of 0.0174 vol%). The log-normal distribution shown in Figure 93 fits quantitatively the experimental curve of the silica solution. It appears that the size distribution of silica nanoparticles in aqueous solution is quite monodisperse with an average radius of 27.6 nm and a width σ = 0.075.

From the log-normal fitting, a nearly perfectly random dispersion of silica is obtained in the case of aqueous silica solution. The increase in intensity below q ≈ 10^{-2} nm^{-1} corresponds to inhomogeneities in the concentration at very large scale. The slight discrepancy between the measured and fitted curves in the range q ≤ 0.07 nm^{-1} may come from a very small overestimation of the contribution of larger particles in the distribution $P(R)$ or from a nearly negligible contribution of a structure factor from excluded volume (as particles cannot interpenetrate).

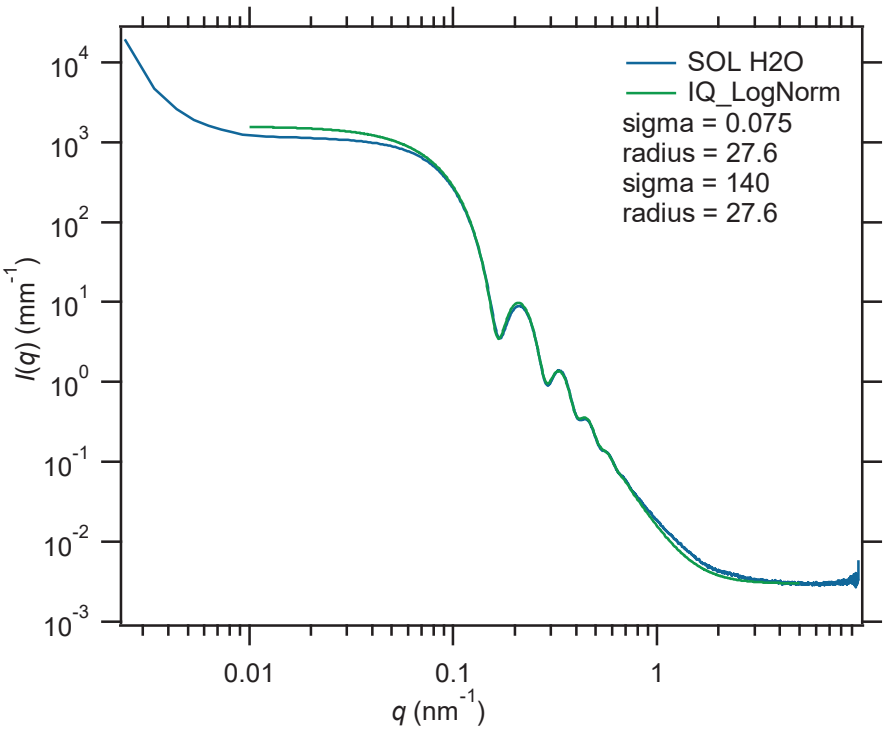
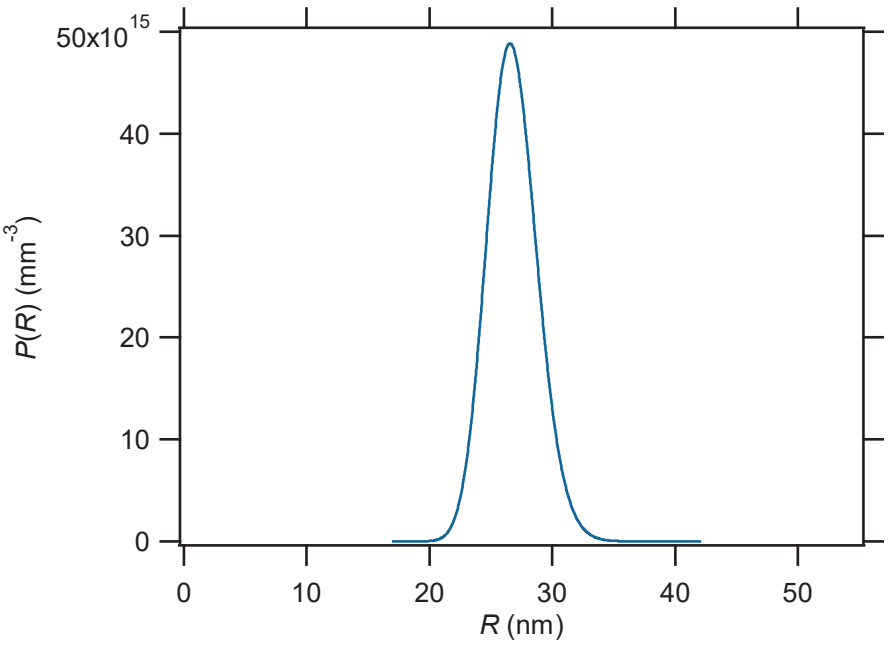


Figure 92 USAXS scattered intensity (normalized with the thickness of the sample) of aqueous silica solution with ϕ_{SiO2}=4.6 wt%. Blue curve is the measured scattering of aqueous silica solution. The green curve is an adjustment with a log-normal size distribution shown in Figure 94.



27

Figure 93 Log-normal distribution of the radius of the silica particles (from aqueous silica solution)

The same experiment was carried out on silica solutions after phase transfer in MEK (red circles) and after the grafting with VTMS organosilane (red line). The scattered intensities of the two solutions, compared with the aqueous silica solution, are shown in Figure 94. The slight difference in absolute intensity compared with the aqueous solution comes from the difference in the factor $\Delta\rho^2$. In both organic solutions, the same size distribution than in water was found. Moreover, the curves in MEK (before and after the VTMS grafting step) overlap perfectly, meaning that the grafting does not induce any difference of dispersion state: silica particles do not aggregate after the VTMS-functionalization step. However, a small difference exists between the aqueous and the organic MEK solutions below $q \approx 0.08$ nm^{-1}. To fit perfectly the scattered intensity of the organic solutions, a very small fraction of small aggregates has to be added. This was modeled by an overall fraction 5.6×10^{-4}vol% of spheres of radius 80 nm, which would mean that around 1.5 vol% of the nanoparticles in solution have a tendency to form small aggregates with a radius of 80 nm, that is, aggregates made of about 2 particles. As a consequence, it is possible to assess that the change of solvent from water to MEK lead to the formation of a very small fraction of small aggregates. Figure 99 also confirms that all silica particles have been effectively transferred to MEK during the phase transfer process, as the absolute intensity is quantitative.

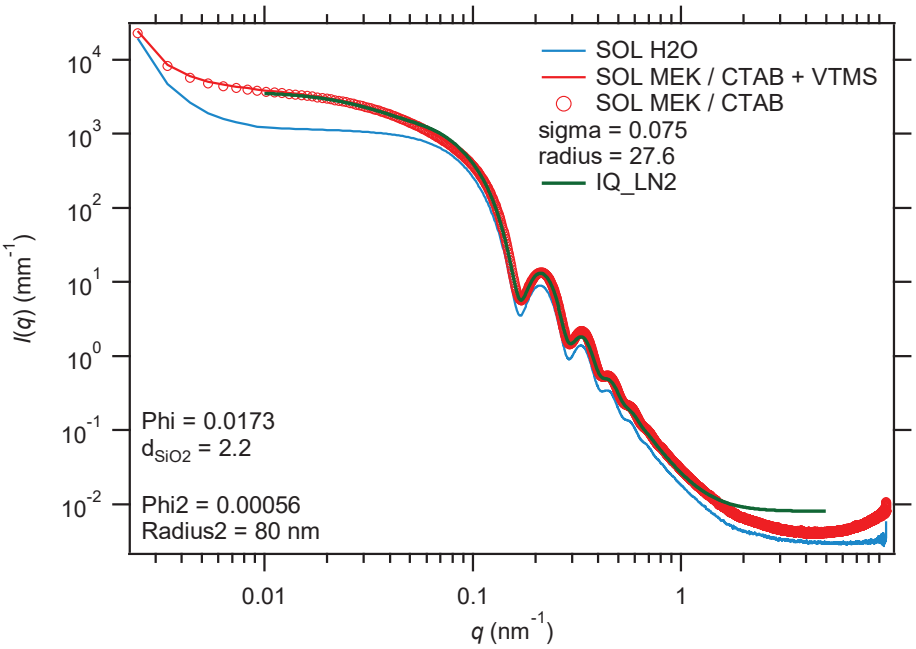


Figure 94 USAXS scattered intensity (normalized with the thickness of the sample) of aqueous silica solution (blue —), silica solution after the phase transfer step (SOL MEK / CTAB, red ○) and silica solution after the phase transfer and VTMS grafting (SOL MEK / CTAB + VTMS, red —) with ϕ_{SiO2}=4.6wt%. The green curve is an adjustment with the same log-normal size distribution as in water plus a small fraction of larger (aggregated) particles.

4.2.2. Nissan silica solutions

Then, the same procedure was applied to Nissan silica solutions in MEK (Nissan MEK) and in 2-heptanone (Nissan 2HPN) diluted to 1.73 vol%. The scattered intensities of the Nissan silica solutions in MEK and in 2-heptanone are plotted in Figure 95. It appears that the Nissan silica solutions are very different from those developed in the laboratory. The curves could be fitted in the range $0.06 < q < 1$ nm^{-1} by a log-normal size distribution. These solutions are quite polydisperse as shown in Figure 96. The size distribution is much broader, with an average radius of 23.33 nm. Qualitatively this corresponds well to the microscopy observations provided by Nissan Chemical (see Figure 37 page 53). Below $q \approx 0.06$ nm^{-1}, there is first a peak, followed by a significant decrease in intensity, compared to the fitted curves for non-interacting particles. This corresponds to a structure factor, related to interactions between particles (see section 2.2.5). An approximate structure factor can be calculated as:

$$S(q) = \frac{I(q)}{I_{ni}(q)} \tag{39}$$

Where $I_{ni}(q)$ is the scattering estimated for non-interacting particles.

This is shown in Figure 97. This function shows a maximum for a value q^*. It is then possible to determine the distance d between silica particles in the organic solutions by taking $d = \frac{2\pi}{q^*}$.

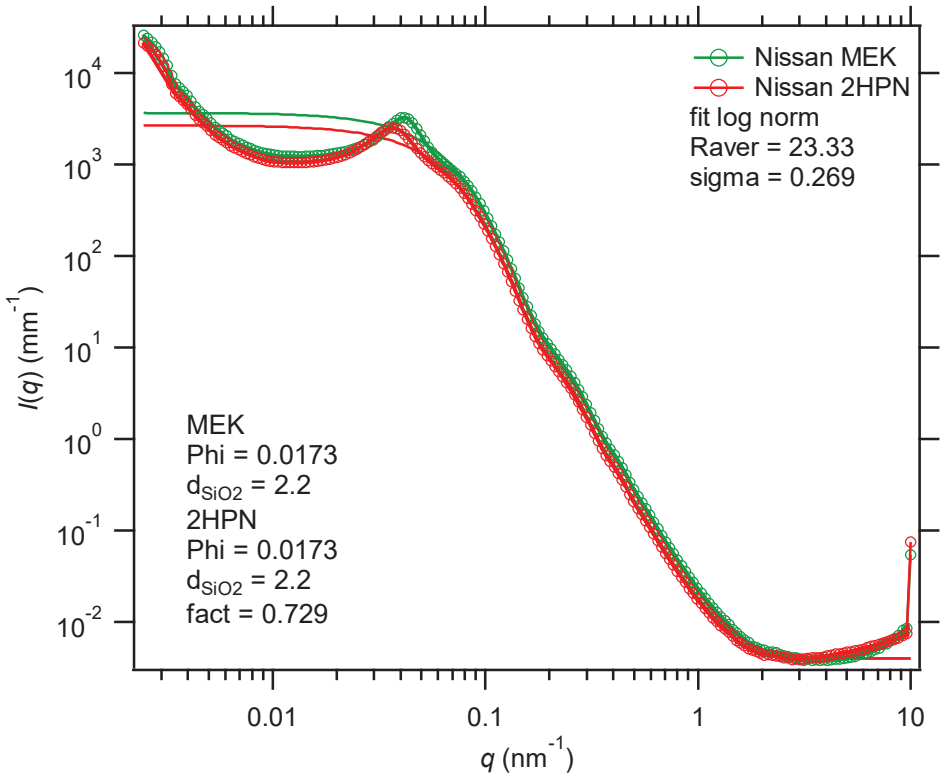


Figure 95 USAXS scattered intensity (normalized with the thickness of the sample) of Nissan silica solution with ϕ_{SiO2}=4.26wt% in MEK (green ○) and in 2-heptanone (red ○). Green curve is an adjustment of the Nissan solution in MEK with a log-normal size distribution of non-interacting particles. Red curve is an adjustment of the Nissan solution in 2-heptanone with a log-normal size distribution of non-interacting particles.

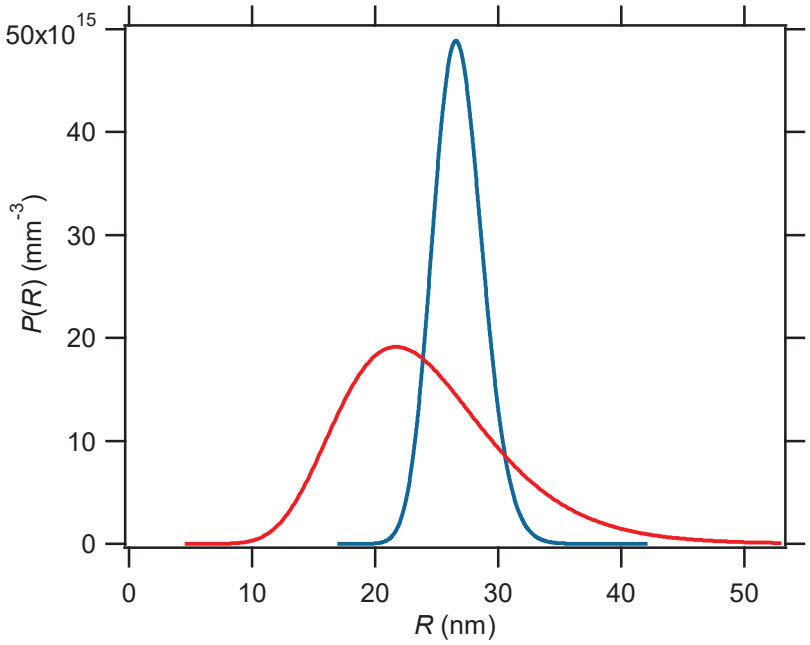


Figure 96 Log-normal distribution of the radius of the silica particles in Nissan solution in MEK (red —), compared with the size distribution of the aqueous silica solution synthetized in the lab (blue —)

In both solvents the peak appears at relatively low q. In MEK we found $q_{MEK} = 0.0427$ nm^{-1} corresponding to a particle-particle distance $d_{MEK} = 147$ nm. When the silica nanoparticles are

transferred in 2-heptanone, the first peak appears at slightly lower q value: q_{2HPN} = 0.0383 nm^{-1} leading to d_{2HPN} = 164nm. The change of solvent induces an increase in the distance between silica particles. These distances between particles are large and are approximately 3 times the diameter of the spheres. Silica particles from Nissan would therefore be organized into some kind of repuslsive colloid where the particles are at a clearly defined distance d_{MEK} or d_{2HPN} from each other, as schematized in Figure 97.

By assuming that particles form a cubic lattice of mesh size *d*, *d* is related to the volume fraction by:

$$\Phi = \frac{4\pi R^3}{3d^3} \quad (40)$$

Taking R = 23.33 nm and ϕ = 0.0173, one finds d = 145 nm which is exactly the measured distance $d = \frac{2\pi}{q^*}$

Thus, the three solutions used during the preparation of the materials show very different characteristics. On the one hand, using the experimental procedure developed in the laboratory, the transfer of silica from water to MEK leads to the formation of a very small fraction (1.5 vol%) of silica aggregates but the solution remains essentially monodisperse (with an average radius of 27.6 nm). On the other hand, silica particles in the Nissan solutions in MEK or in 2-heptanone are polydisperse (R_{av} = 23.33 nm) and might have repulsive interactions. The change of solvent from MEK to 2-heptanone slightly modifies the dispersion state of the silica by slightly increasing the distance between particles.

4.2.3. P(VDF-co-HFP) – MEK – silica ternary systems with monodisperse silica synthetized in the lab

Now that the dispersion state of silica in organic solvents has been characterized, P(VDF-co-HFP) – silica – solvents gels are formulated by adding polymers to the silica solutions (see procedure in Chapter 2 page 61). USAXS measurements were carried out on gels with different concentrations of copolymers at fixed silica concentration ϕ_{SiO2} = 1.6 vol% and on P(VDF-co-HFP) – solvent gels with the same concentration of copolymer.

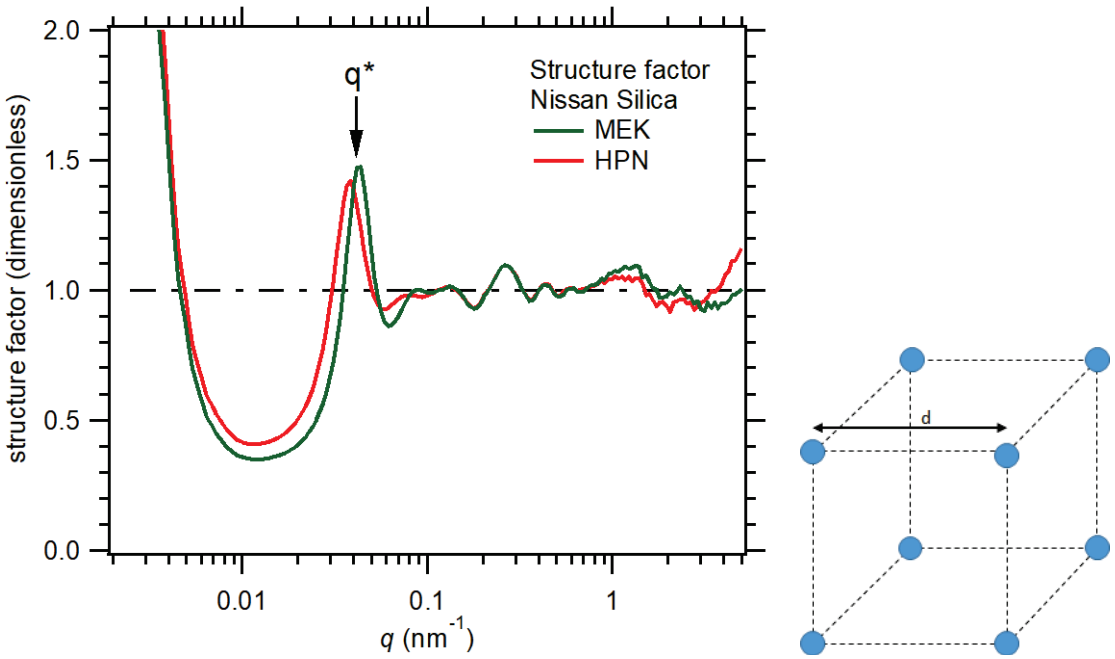


Figure 97 (Right) Structure factor of Nissan silica solution in MEK (green —) and in 2-heptanone (red —). (Left) Possible organization of the silica nanoparticles in the Nissan solution in MEK and in 2-heptanone with *d* the distance between particles

In gels systems, silica particles are embedded in a matrix which itself shows a significant scattering signal (as shown in Figure 98-a). The scattering from the matrix is related to phase separation, as reported in the previous chapter In the presence of silica, the signal is enhanced by a factor about 50. To discriminate the signal from silica dispersion, the signal from the gel matrix has to be subtracted. The total signal (gel + silica particles) is approximately:

$$I_{tot}(q) = I_{gel}(q) + I_{silica}(q) \quad (41)$$

Where $I_{silica}(q)$ is the scattered intensity from silica particles, in which the contrast factor $\Delta\rho^2$ is calculated with the average electron density in the gel.

Therefore

$$I_{silica}(q) = I_{tot}(q) - I_{gel}(q) \quad (42)$$

The normalized, subtracted signal $I_{silica}(q)$ is plotted in Figure 98-b. In ternary gels, the scattered intensity increases at small q values, contrary to the organic silica solution. The position of the maximum q^* = 0.12 nm^{-1} in the Kratky representation $q^2 I_{silica}(q)$ (shown in Figure 98-c) gives a distance between silica particles $d = \frac{2\pi}{q^*} = 52$ nm corresponding to the diameter of silica nanoparticles. For all the concentrations of copolymer (11, 20 and 25 wt%) the position of this peak does not change. This indicates that in these ternary systems silica particles are in contact and are aggregated, contrary to the organic silica solution which is quite well dispersed.

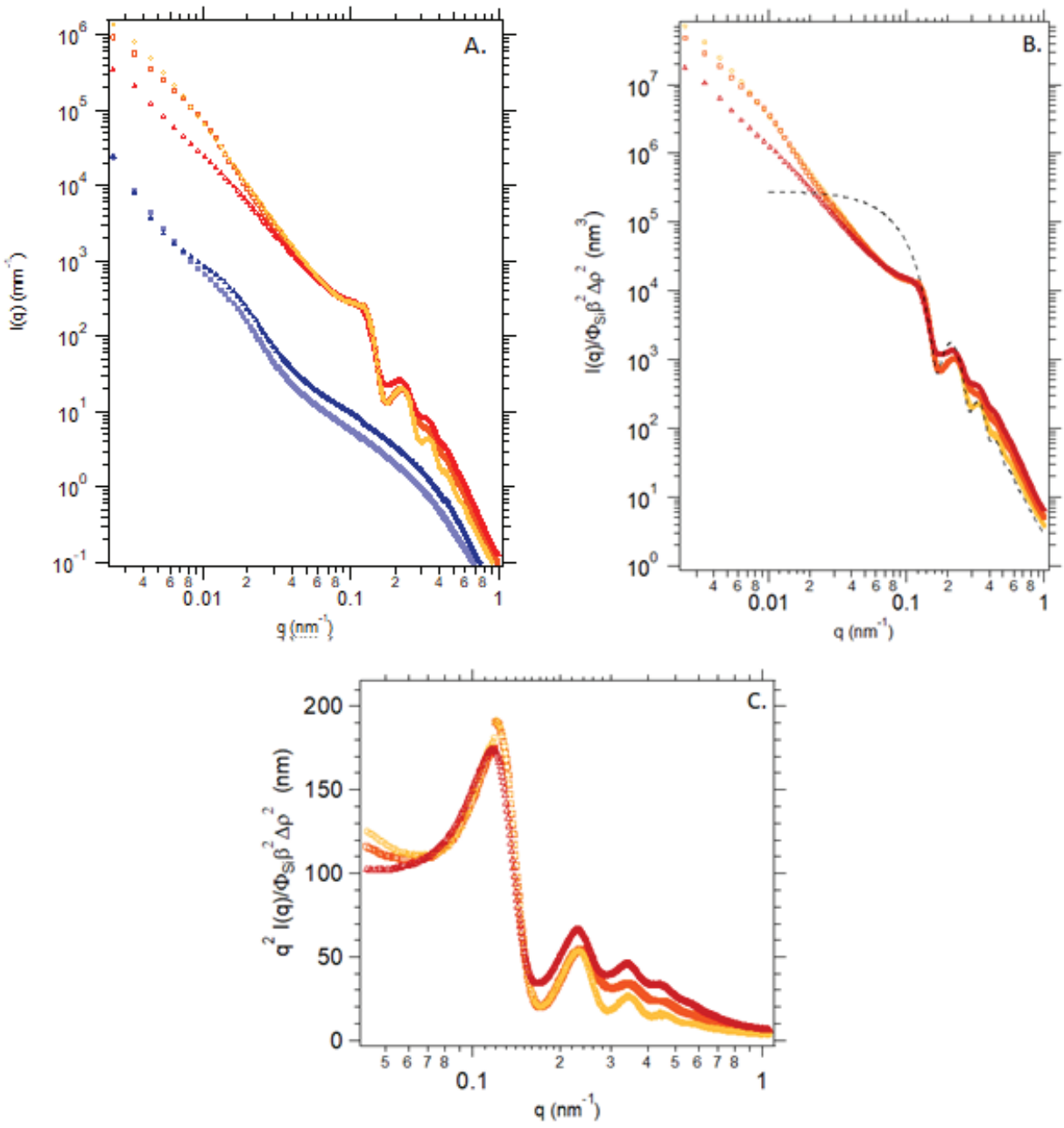


Figure 98 (A) USAXS scattering intensity of P(VDF-co-HFP) – silica – MEK gels (ϕ_{SiO2}=1.6vol%) prepared with the silica solution in MEK by phase transfer with $X_{P(VDF\text{-}co\text{-}HFP)}$=11wt% (yellow ○), $X_{P(VDF\text{-}co\text{-}HFP)}$=20wt% (orange □) and $X_{P(VDF\text{-}co\text{-}HFP)}$=25wt% (red △) (B) Silica scattered intensity of P(VDF-co-HFP) – silica – MEK gels and (C) Kratky representation of the silica scattered intensity of filled physical gels in MEK. In (A) the pure matrix is also shown for comparison: $X_{P(VDF\text{-}co\text{-}HFP)}$=20wt% (light blue ■) and $X_{P(VDF\text{-}co\text{-}HFP)}$=25wt% (blue ▲)

At very small q values (for 0.016 < q <0.002 m^{-1}), the scattering curves show a power law q^{-2}. This may correspond to large scale organization of silica particles in the form of random chains or 2D objects.

We did not attempt to fit the scattering curves quantitatively. The general shape of the curves can be qualitatively explained by the so-called 'sticky hard-sphere' model, in which the structure factor is calculated by using an interaction potential between spheres which incorporates a hard sphere repulsion and a narrow attractive well, as schematized in Figure 99. This potential reflects the

tendency of the particles to stick to each other as they come very close. It contains 3 parameters, the particle diameter, the width of the potential (which should be small compared to the diameter) and the depth of the attractive well. To model scattering curves, we multiplied the scattering curve of non-interacting particles (black curve in Figure 100) with the structure factor calculated with this potential, using a volume fraction ϕ_{SiO2} = 20 vol% and a strongly attractive potential. An example is shown in Figure 99b (green curve in Figure 100). It reproduces qualitatively the general shape of the curve, though it is difficult to adjust more quantitatively. Thus the scattering curves reflect a tendency of the particles to stick together, i.e. to form large domains concentrated in silica, which can be assimilated to agglomerates (Baxter 1968).

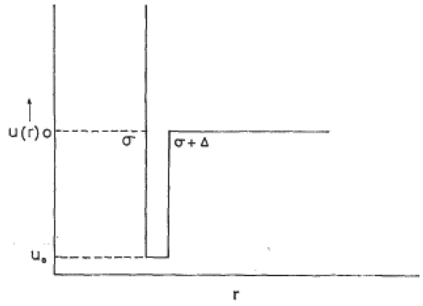


Figure 99 Schematics of the interaction potential in the "sticky hard sphere model" (Menon, Manohar et al. 1991)

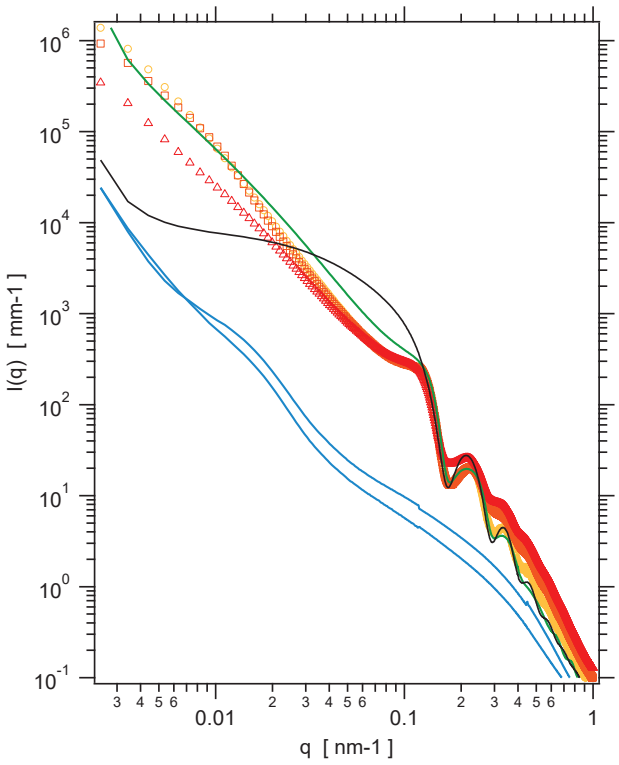


Figure 100 USAXS scattering intensity of P(VDF-co-HFP) – silica – MEK gels (ϕ_{SiO2}=1.6vol%) prepared with the silica solution in MEK by phase transfer with $X_{P(VDF\text{-}co\text{-}HFP)}$=11wt% (yellow ○), $X_{P(VDF\text{-}co\text{-}HFP)}$=20wt% (orange □) and $X_{P(VDF\text{-}co\text{-}HFP)}$=25wt% (red △). The pure matrix is also shown for comparison: $X_{P(VDF\text{-}co\text{-}HFP)}$=20wt% (light blue) and $X_{P(VDF\text{-}co\text{-}HFP)}$=25wt% (blue). Scattering curve of non-interacting particles multiplied with the structure factor calculated with this potential, using a volume fraction ϕSiO2 = 20 vol% and a strongly attractive potential is shown (black curve) to model scattering curves. An example is also represented (green curve).

4.2.4. P(VDF-co-HFP) – MEK – silica ternary systems with Nissan silica

The dispersion state of the nanoparticles in P(VDF-co-HFP) – Nissan silica – MEK solutions and gels has also been investigated for concentrations of copolymer between 11 and 20 wt% with ϕ_{SiO2} = 1.6 vol%. In this case two materials in the liquid state (11 and 20 wt%) and one in the gel state (26 wt%) were studied and their USAXS curves are compared in Figure 101. The curves have the same trend as for the Nissan silica solution in MEK (see Figure 96). Indeed, in the liquid or gel state a structure factor peak is always observed, which would mean that the addition of P(VDF-co-HFP) does not (or only little) disturbs the organization of the silica nanoparticles. However, there is a difference between the liquid state and the gel state. In the liquid state, the position of the peak is independent of the copolymer concentration (see the dashed line) and in both solutions $q \approx 0.04$ nm^{-1}, corresponding to a distance between particles $d \approx 157$ nm. The position of the peak is nearly the same as in the Nissan silica solution in MEK slightly. Therefore, in the liquid state the silica network is very little disturbed by the addition of P(VDF-co-HFP) in the organic solution.

However, when the concentration of copolymer is sufficient to induce a sol-gel transition (here 20 wt%), important changes appear in the scattering curves. A first structural feature appears at $q_1 \approx 0.12$ nm^{-1}, at which the intensity decreases. This may be due to a first structure factor, with a peak corresponding to the distance $d = \frac{2\pi}{q_1} \approx 50$ nm, which corresponds to the particle diameter. Thus, in this case, in the same way as for the solvent-transfer particles, the particles touch each other.

There is then a second peak located at very low values of q, $q \approx 0.02$ nm^{-1} which corresponds to a distance $d \approx 316$ nm. Thus, when the material reaches a gel state, the polymer appears to disturb the silica network by inducing some degree of aggregation and/or large scale organization.

In comparison with the previous ternary gels (prepared with the silica solution in MEK developed by phase transfer), which are in the same solvent, two distinct types of behavior are observed. This could come from different initial dispersion states of silica nanoparticles in the organic solvent but also from different silica – polymer interactions.

The effect of changing the solvent from MEK to 2-heptanone was finally studied. Here all the materials are in the gel state with concentrations of copolymer between 7 wt% and 20 wt% and ternary gels are filled with ϕ_{SiO2} = 1.64 vol% of silica particles from the Nissan solution. Results are shown in Figure 102. In P(VDF-co-HFP) – 2-heptanone gels, as for copolymer – MEK gels, heterogeneities exist and scatter much more than in MEK, as described in the previous chapter. When filled gels are studied, the silica dispersion state seems to be little affected by the presence of copolymer. At 7 wt% and 20 wt% of copolymer, a peak at q = 0.038 nm^{-1} corresponding to a distance d = 164.0 nm is observed, at the same position as in the Nissan silica solution in 2-heptanone. Thus, at these concentrations in 2-heptanone, the addition of copolymer does not change the organization of the network.

It seems that no polymer – silica interactions exist in this solvent. As a result, the polymer network (i.e. phase separation and crystallization) would be organized independently of the silica network during gelation.

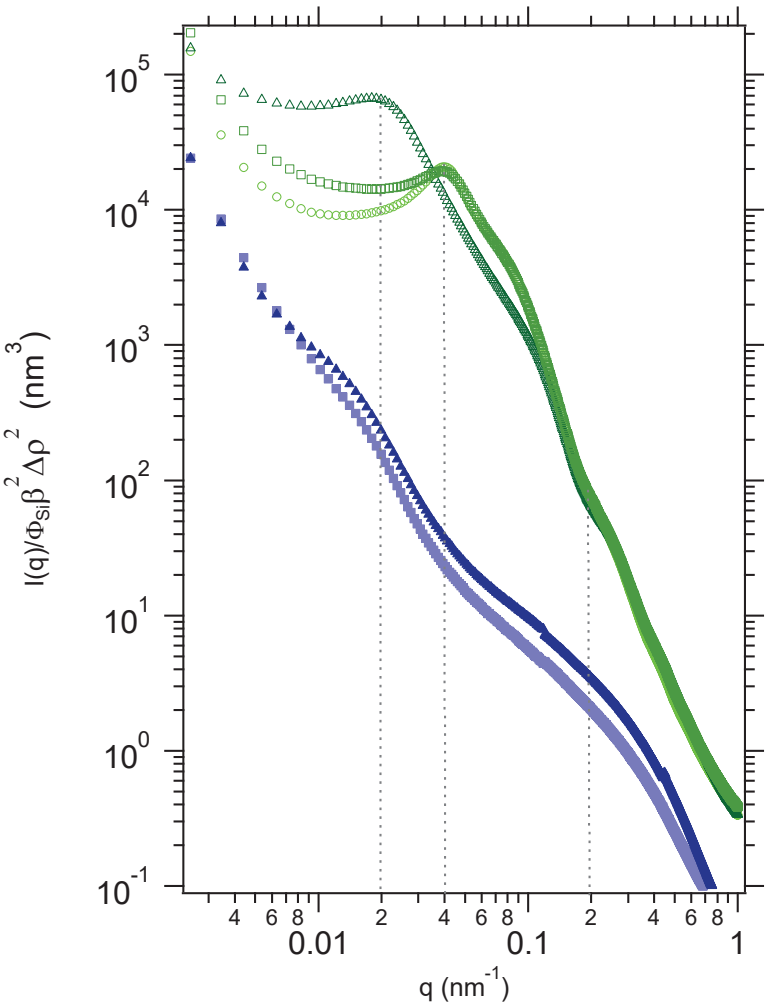


Figure 101 USAXS scattered intensity (normalized with the thickness of the samples) of P(VDF-co-HFP) – Nissan silica – MEK solutions with $X_{P(VDF\text{-}co\text{-}HFP)}$=11wt% (light green ○), $X_{P(VDF\text{-}co\text{-}HFP)}$=20wt% (green □) and gel with $X_{P(VDF\text{-}co\text{-}HFP)}$=25wt% (dark green △). The pure matrix is also shown for comparison: $X_{P(VDF\text{-}co\text{-}HFP)}$=20wt% (light blue ■) and $X_{P(VDF\text{-}co\text{-}HFP)}$=25wt% (blue ▲)

Finally, when comparing the results obtained with the silica nanoparticles from the Nissan solution in both MEK and 2-heptanone, the silica dispersion state or silica network seems to be generally little impacted by the change of solvent or the addition of polymer. In 2-heptanone, all studied systems are in the gel state. Silica does not further aggregate when the polymer is added and the distance between particles is preserved. Conversely, in MEK, the liquid-gel transition induces a strong change in the silica dispersion state, with silica coming in close contact (i.e. forming aggregates) in the gel state. The differences observed by the change of solvent could be attributed to a change in the copolymer – silica interactions which may come from a difference of the solvent quality, MEK being a better solvent for P(VDF-co-HFP) than 2-heptanone (as discussed in the section 3.5 page 104).

To better characterize the influence of silica particles in the gelation mechanisms and gel structure, additional experiments (kinetics by tube-tilting and rheology and ^{19}F NMR) were performed and results are presented in the next sections.

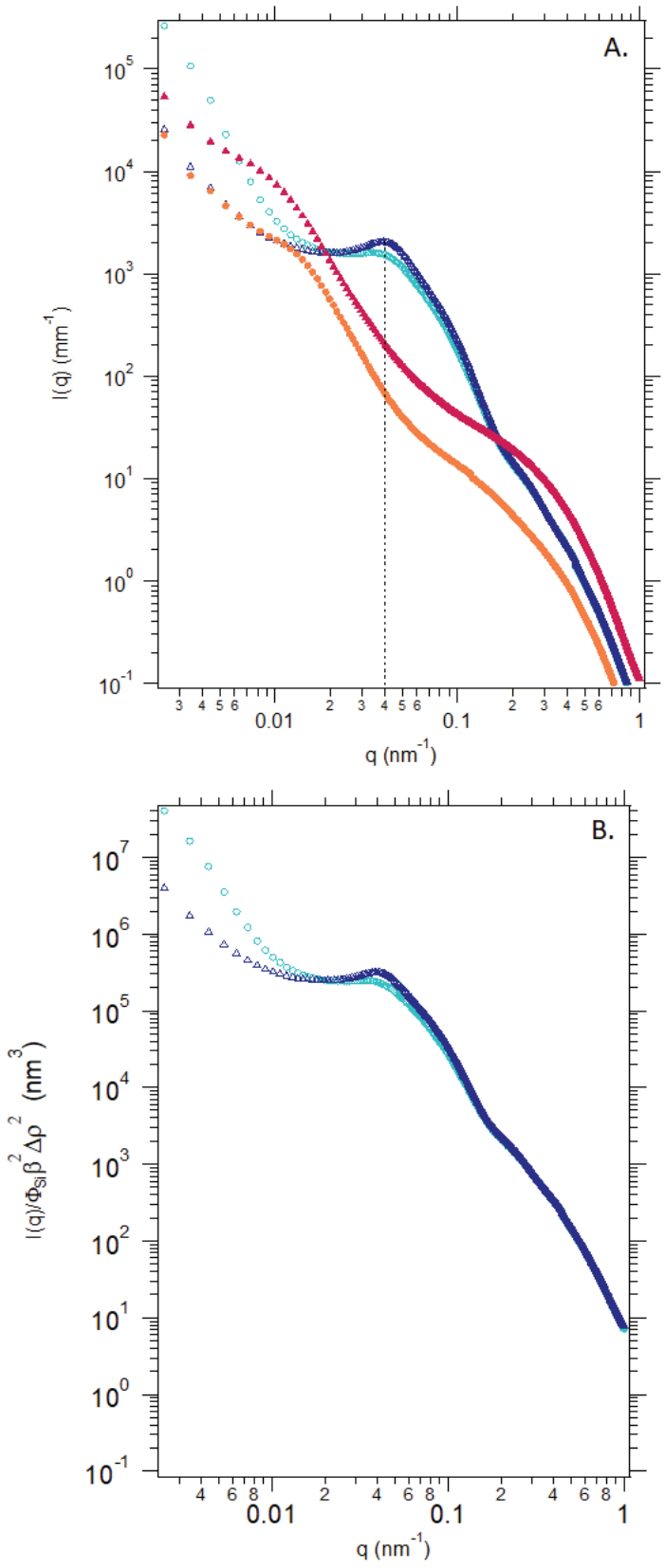


Figure 102 (A) USAXS scattering intensity of P(VDF-co-HFP) – silica Nissan – 2-heptanone gels (ϕ_{SiO2}=1.6vol%) prepared $X_{P(VDF\text{-}co\text{-}HFP)}$=7wt% (light blue ○), $X_{P(VDF\text{-}co\text{-}HFP)}$=25wt% (dark blue △) (B) Silica scattered intensity of P(VDF-co-HFP) – silica Nissan – 2-heptanone gels. In (A) the pure matrix is also shown for comparison: $X_{P(VDF\text{-}co\text{-}HFP)}$=7wt% (orange ■) and $X_{P(VDF\text{-}co\text{-}HFP)}$=25wt% (pink ▲)

4.3. Gelation kinetics

The determination of the gelation time using tube-tilting method and linear rheology was first performed on gels with different fractions of copolymer and silica nanoparticles, in MEK and 2-heptanone.

The tube-tilting method was used on P(VDF-co-HFP) – silica – MEK gels developed by the phase transfer process from the silica solution synthetized in the lab and on P(VDF-co-HFP) – silica – 2-heptanone using the Nissan silica solution in MEK transferred in 2-heptanone. This test was performed at 20°C only and with a fraction of 4.28 wt% of silica nanoparticles within the gel.

The gelation rates of P(VDF-co-HFP) in MEK and 2-heptanone with and without silica nanoparticles are shown in Figure 103. Results are different depending on the considered solvent. In both solvents, the strong dependence on copolymer concentration is retained. In the case of MEK, incorporating silica shifts the critical concentration to lower fractions of copolymer. Below 7wt% of copolymer, in the presence of 4wt% of silica nanoparticles, the gelation does not occur over one month (gelation time is considered to be "infinite") compared to 11wt% in the absence of silica. Gelation rates are about one to two orders of magnitude higher in the presence of silica, depending on the copolymer fraction. Conversely, in the case of gels in 2-heptanone, the presence of nanoparticles does not significantly impact the gelation kinetics.

To complement these tests, we studied the filled gels in linear rheology. These measurements were only carried out for gels in 2-heptanone, because of the high volatility of MEK which makes the rheology measurements impossible on this solvent at the moment.

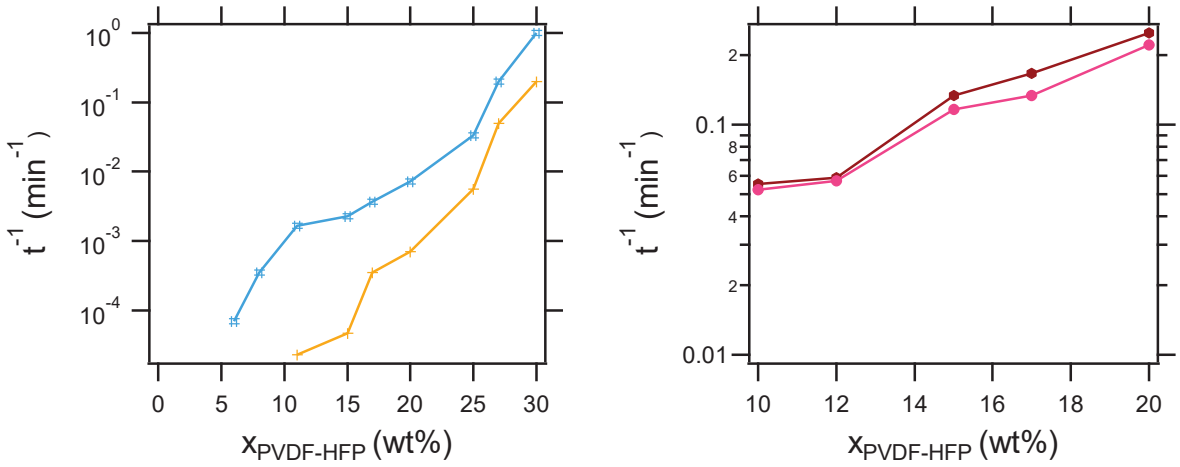


Figure 103 Gelation rate t^{-1} versus concentration for P(VDF-co-HFP) in solution in MEK (left): without silica (orange (orange +) and with silica (ϕ_{SiO2}=4.28 wt%, blue #); in solution in 2-heptanone (right): without silica (pink ●) and with silica (brown ⬟). Measurements were performed at 20°C.

The same experiments than those performed on P(VDF-co-HHFP) – 2-heptanone gels were carried out, namely the evolution of the viscoelastic moduli with time (at 1Hz and a shear strain of 0.1%), followed by frequency-sweep measurements (after 1,5 hours of time-sweep measurement). The gelation time was determined as the crossover between the elastic and viscous moduli. The tests were first carried out on gels with 4.6 wt% of silica. A slight influence on the gelation time was found (see Figure 104) which shows the gelation rate for gels with 7 wt% of copolymer as a function of the

silica content. The gelation rate becomes faster when more silica is added (up to 8.4 wt%). However, the increase is not dramatic, with an increase by less than a factor of two.

The fraction of silica was then fixed at 8.4 wt% (referred to the total mass of the gel) and experiments were conducted for concentrations of polymer between 5wt% and 10wt%. Beyond this concentration the gelation time is too fast to be determined with rheology measurements.

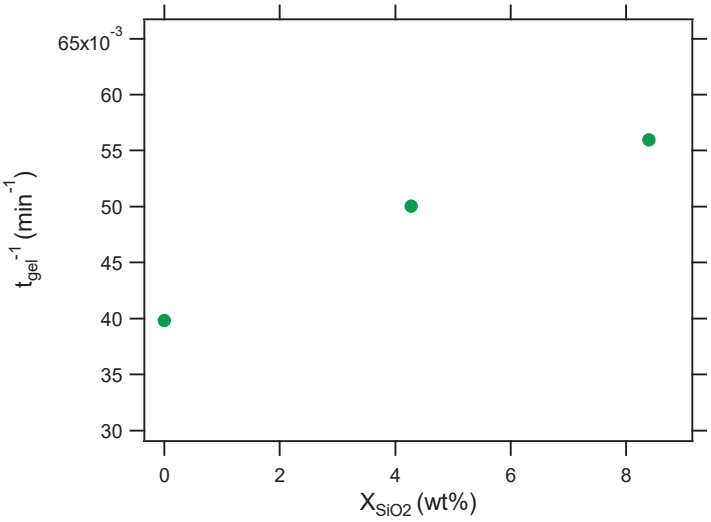


Figure 104 Gelation rate versus concentration of silica nanoparticles for P(VDF-co-HFP) – silica – 2-heptanone gels with $X_{P(VDF\text{-}co\text{-}HFP)}$=7wt% at 25°C, a frequency of 1Hz and a shear strain of 0.1%

The gelation rate of polymer – silica (with 8.4wt% of silica) is plotted as a function of the concentration of P(VDF-co-HFP) in Figure 105. Results are compared with the gelation kinetics of copolymer gels without silica nanoparticles. As for binary gels, the gelation rate increases with the fraction of copolymer. At low concentration of copolymer, the addition of silica in the binary gels increases the gelation kinetics while beyond 8wt% of copolymer, it is found that incorporating silica seems to have no effect (or to slightly decrease) the gelation kinetics in comparison with the binary gels. Note that this result is coherent with Figure 103 (right).

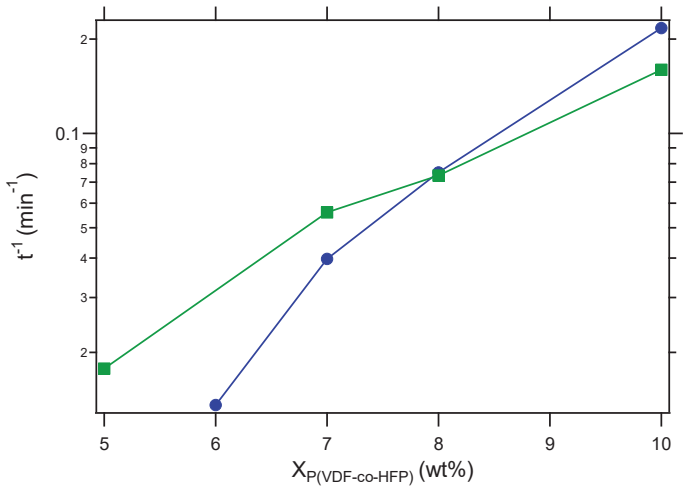


Figure 105 Gelation rate t^{-1} versus concentration for P(VDF-co-HFP) in silica solution in 2-heptanone (ϕ_{SiO2}=8.4 wt%, green ■) compared with P(VDF-co-HFP) in solution in 2-heptanone (blue ●), at 25°C, a frequency of 1Hz and a shear strain of 0.1%

The impact of the presence of silica on the viscoelastic moduli was also investigated. Some results are shown in Figure 106 (after 1,5 hours of time-sweep measurement). In all gels (filled or not with silica) the moduli increase considerably with the copolymer concentration. For example, in the case of unfilled gels, the elastic modulus goes from 240 Pa (at 6wt% of copolymer) to 56000 Pa (for 18wt% of P(VDF-co-HFP). Adding silica nanoparticles in the material does not increase much the values of the elastic modulus in comparison with binary (unfilled) polymer gels at the same copolymer concentration. Modulus measurements in the presence of silica are less reproducible than in binary gels, probably due to some difficulty to obtain reproducible silica dispersions. While the modulus is slightly increased at low concentrations of copolymer, it becomes a little lower than the one of the corresponding binary gel beyond around 8 to 10 wt% copolymer.

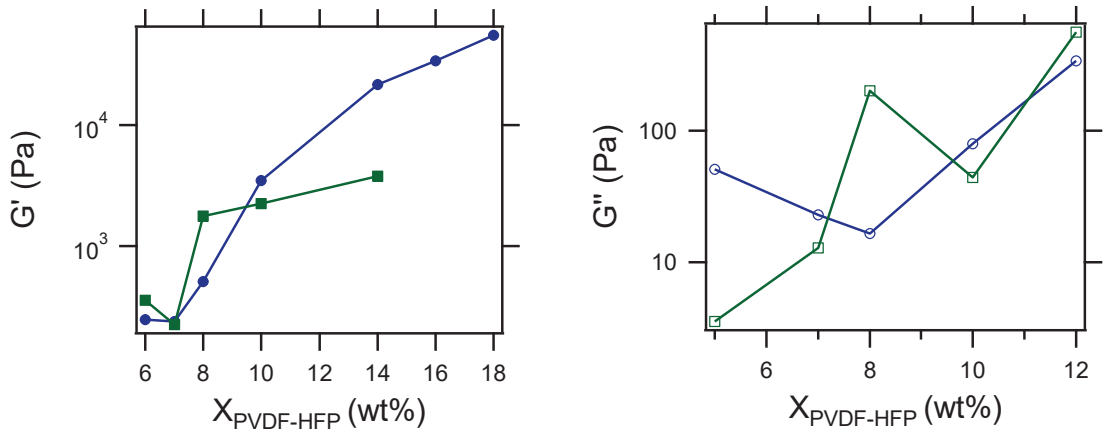


Figure 106 Evolution of the elastic (left) and viscous (right) moduli with the concentration of copolymer for P(VDF-co-HFP) – 2-heptanone gels without (blue ● and ○) and with silica with ϕ_{SiO2} = 8.4wt% (green ■ and □)

4.4. Dynamics of P(VDF-co-HFP) – silica gels in MEK

^{19}F NMR experiments were only performed on P(VDF-co-HFP) – silica – MEK solutions and gels to study the influence of the presence of silica nanoparticles (with ϕ_{SiO2} = 4.26 wt%) on the segmental dynamics of P(VDF-co-HFP) chains. The same DQ measurements (using the 5-pulses and Baum and Pines sequences) than those performed in binary P(VDF-co-HFP) – MEK gels were carried out to investigate the polymer mobility and the network structure.

First, the transverse relaxation curve obtained for a ternary P(VDF-co-HFP) gel in MEK in the presence of 4.26 wt% of silica nanoparticles is displayed in Figure 107, and compared with the binary P(VDF-co-HFP) gel with the same concentration of copolymer. The relaxation becomes a little faster when silica nanoparticles are incorporated in the gel, indicating that the dynamics of the polymer is affected by the presence of silica. In the filled gel, it seems that the fraction of the signal with a short relaxation time is slightly larger. This would indicate that a larger fraction of the polymer, compared to binary gels, has a slower and/or restricted dynamics.

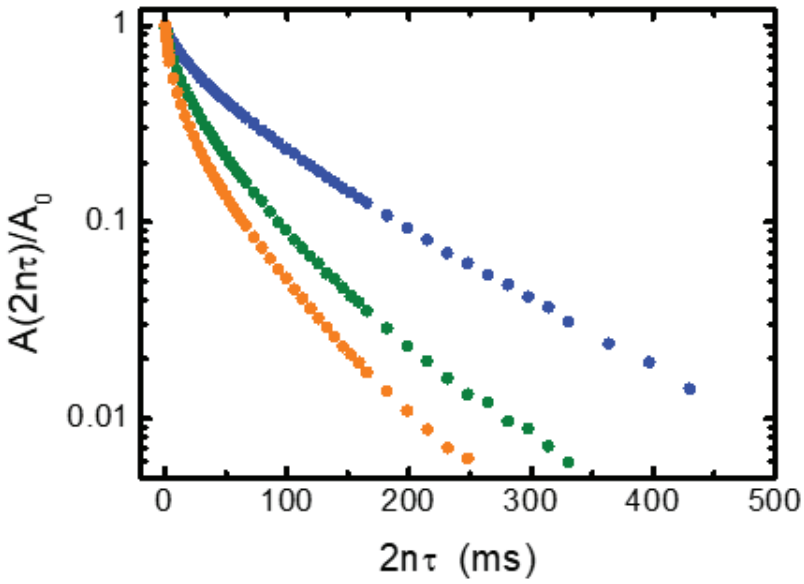


Figure 107 Transverse ^{19}F NMR relaxation obtained with Hahn echo and CPMG sequences for a liquid solution of P(VDF-co-HFP) in MEK with $X_{P(VDF\text{-}co\text{-}HFP)}$=6wt% (blue ●) and for P(VDF-co-HFP) - MEK gels: green ●: $X_{P(VDF\text{-}co\text{-}HFP)}$=20wt%; orange ●: $X_{P(VDF\text{-}co\text{-}HFP)}$=20wt% and ϕ_{SiO2}=4.26wt%

In order to be more precise and to study the impact of silica on the fraction of rigid zones and elastically active chains, ^{19}F DQ NMR measurements were performed on gels filled with silica. First, the five-pulse sequence was used to access the short time scale, i.e. the fraction of rigid or strongly restricted polymer. Figure 108 Shows the amplitude of the ^{19}F DQ coherences as a function of the excitation time t_{DQ}, in the range 2-200 µs, for the ternary P(VDF-co-HFP) – silica – MEK gel with 30 wt% of copolymer, compared with the signal of the unfilled (binary) gel with the same concentration of copolymer. A non-zero signal is observed with a maximum at about t_{DQ} = 12µs. This proves that, as for the corresponding binary gel, a fraction of the polymer is rigid, i.e. immobile over the tens of microsecond time scale. Due to both limited efficiency of the 5-pulse sequence and to dead time effect in the detection, the measured amplitude at the maximum of the DQ signal does not reflect the corresponding rigid polymer fraction in a quantitative way. However, from a semi-quantitative point of view, the amplitude of the maximum increases (by a factor about two) when silica particles are incorporated in the polymer gel, which means that the rigid polymer fraction increases in the presence of silica. In binary gels, the rigid fraction was identified to crystalline zones. In ternary (filled) gels, it may include both crystallites and a fraction of polymer adsorbed on the silica surface. However, it is not possible to discriminate both contributions if the polymer segments are fully immobilized in both cases. To achieve this discrimination, additional independent experiments should be performed.

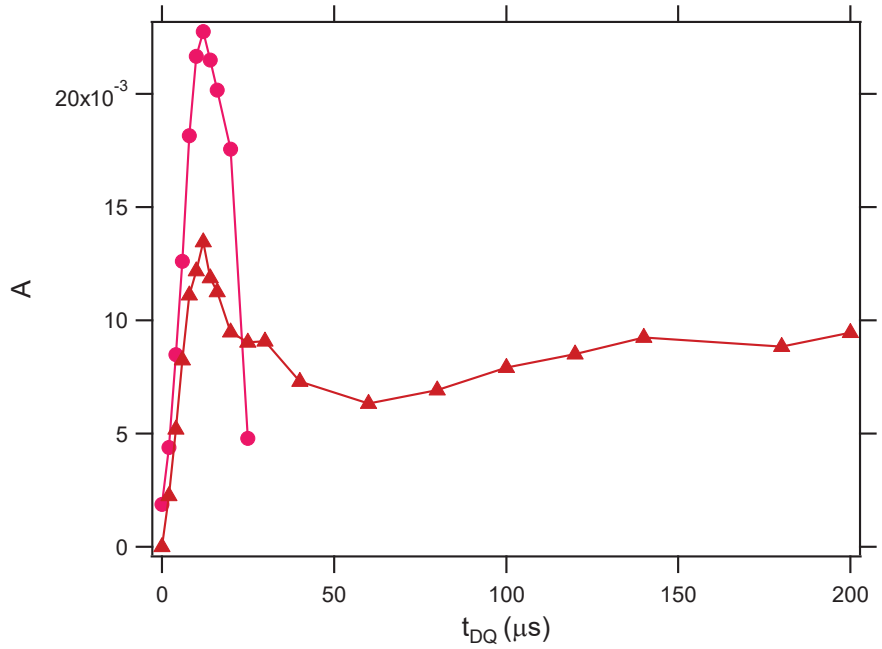


Figure 108 ^{19}F DQ build-up curve obtained after a 5-pulse Baum and Pines sequence as a function of the DQ excitation/reconversion time in the sequence: for P(VDF-co-HFP) – MEK gels with $X_{P(VDF\text{-}co\text{-}HFP)}$=30wt% without silica (brown ▲) and with silica nanoparticles (ϕ_{SiO2}=4.26wt%, pink ●)

Experiments using the Baum and Pines - Saalwächter sequence were performed on ternary gels. Examples for gels containing 20 wt% of copolymer are shown in Figure 109. The DQ build-up curves show a non-zero signal with a maximum at about 1ms, which confirms the existence of a polymer network and elastically active chains. Figure 109 indicates that the DQ signal increases as silica nanoparticles are added (keeping the same copolymer concentration), which means that the fraction of elastically active chains increases. However, the DQ signal intensity remains quite small, which would indicate that a relatively small fraction of polymer chains is still effectively cross-linked, i.e. connected into the elastic network. Due to dead time effect in the detection, and also due to the fact that the shape of the reference signal does not allow discriminating easily the cross-linked and uncrosslinked polymer fractions, it is difficult to quantitatively estimate the fraction of the polymer forming the elastic network. Simply looking at the raw amplitude of the DQ signal, it may be estimated qualitatively that the fraction of elastically active chains increases by a factor of roughly two. Altogether, it is not possible to specify to what extent this increase can be attributed to polymer-silica interactions. To answer this question, it would be necessary to carry out additional measurements such as DSC measurements, to quantify the fraction of crystallites in the gel, or ATG, to determine the sorption isotherms of the P(VDF-co-HFP) copolymer on silica.

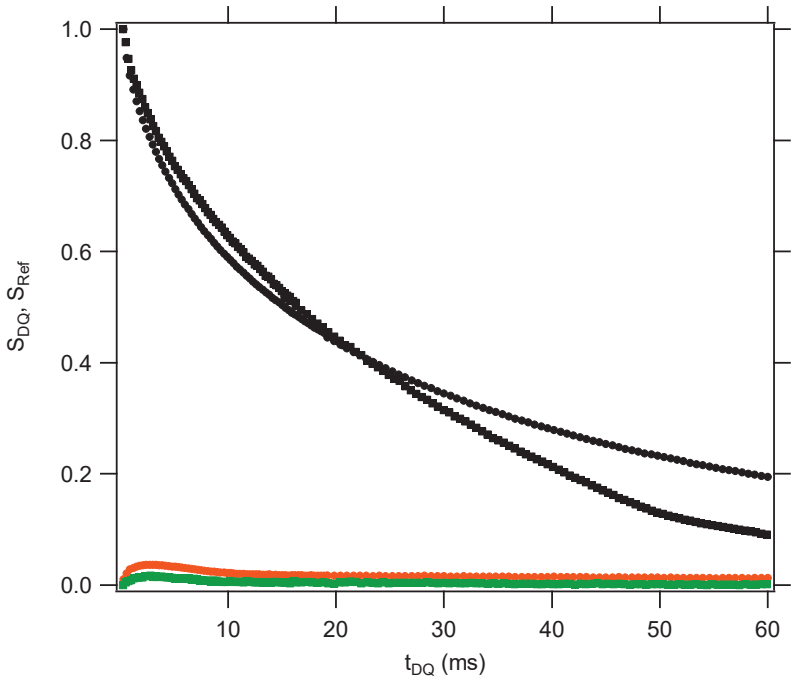


Figure 109 ^{19}F DQ build-up curve obtained after a Baum and Pines sequence (improved by Saalwächter) as a function of the DQ excitation/reconversion time in the sequence of a gel of P(VDF-co-HFP) in MEK with $X_{P(VDF\text{-}co\text{-}HFP)}$=20wt% without silica (green ●, reference signal black ●) and with silica nanoparticles (ϕ_{SiO2}=4.26wt%, orange ●, reference signal black ■)

4.5. General discussion: modification of the gelation mechanism with the incorporation of silica nanoparticles

We have studied on two types of ternary gels P(VDF-co-HFP) – silica – solvent gels, one in MEK with the silica synthetized in the lab and transferred to MEK, and one with the Nissan silica solution transferred to 2-heptanone. We found that the gelation kinetics of these two materials strongly depend on the concentration of copolymer and also depend, though less strongly, on the presence of silica nanoparticles and their concentration. but with a difference in the dispersion of the nanoparticles in the gels. After studying the possible structure of each gel individually it seems interesting to understand where these differences come from. Lastly, from these results, would it be possible to predict the gelation mechanism of systems filled with Nissan silica solution in MEK?

For P(VDF-co-HFP) – silica – MEK (with synthetized silica solution obtained by phase transfer), which are formulated by dissolving a certain amount of copolymer in the silica organic solution we noticed that the presence of silica nanoparticles strongly accelerates the gelation kinetics, from few seconds to several days instead of minutes to months in unfilled (binary) gels. We have determined in Chapter 3 that in MEK, the gelation of P(VDF-co-HFP) can be attributed to phase separation and formation of crystalline zones (likely located in polymer–rich domains), that may act as crosslinks between the polymer chains. While silica in solution in MEK is relatively well dispersed and monodisperse, conversely, when filled (ternary) gels are formulated, silica nanoparticles tend to aggregate.

One first point to discuss is the MEK/water phase diagram. According to the MEK-water phase diagram shown in Figure 110, MEK is partially soluble in water and it solubility depends on temperature. During the phase transfer (detailed in Chapter 2) the quantities of water and MEK are

identical (MEK/water composition 50:50 wt%) and the temperature is around 20°C. Thus, once the organic solution of silica in MEK is obtained, it contains approximately 15 wt% of water (Siegelman and Sorum 1960). This presence of water may be the major difference between the systems prepared in the lab by phase transfer and those prepared from the Nissan silica solution. There is no evidence that the presence of silica disturbs the MEK/water solubility domain in the phase diagram. Conversely, the presence of the copolymer, which is strongly hydrophobic, may shift the miscibility phase boundary and induced some degree of separation between water and a MEK/polymer solution phase. Silica particles might then segregate at interfaces as schematized in Figure 111. Aggregates such as schematized in Figure 111 may indeed be compatible with the scattering data shows in Figure 98 and Figure 100, which correspond to large scale structures or aggregates of dimension 2 (like surfaces, as in Figure 111-b). Note that the electron density contrast between MEK and water should be very small compared to the silica contrast, with $\Delta\rho^2_{MEK-water} = 0.06 \times 10^{20} cm^{-4} \approx 10^{-3}\Delta\rho^2_{MEK-silica}$. Thus water-rich domains would not give measurable scattering.

The presence of water and its impact on the dispersion state of silica in the hybrid nanocomposites will be discussed more in details in the Chapter 6.

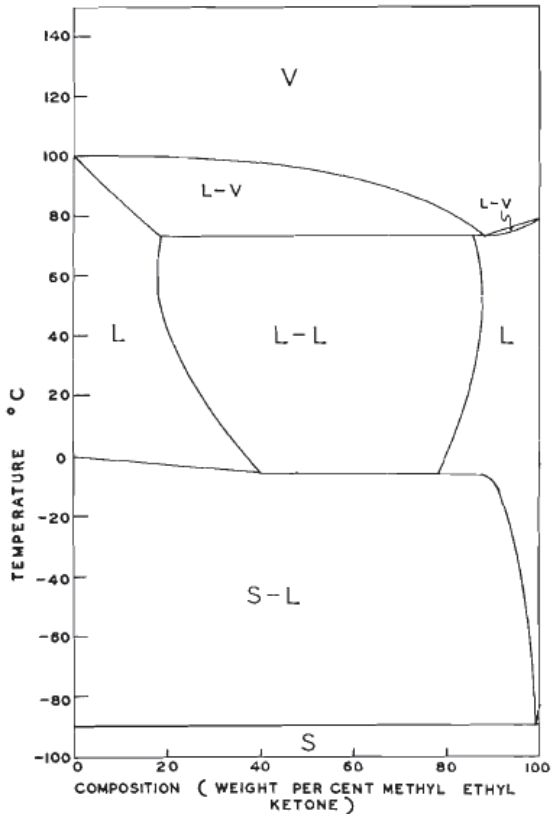


Figure 110 water – MEK/water phase equilibrium diagram (Siegelman and Sorum 1960)

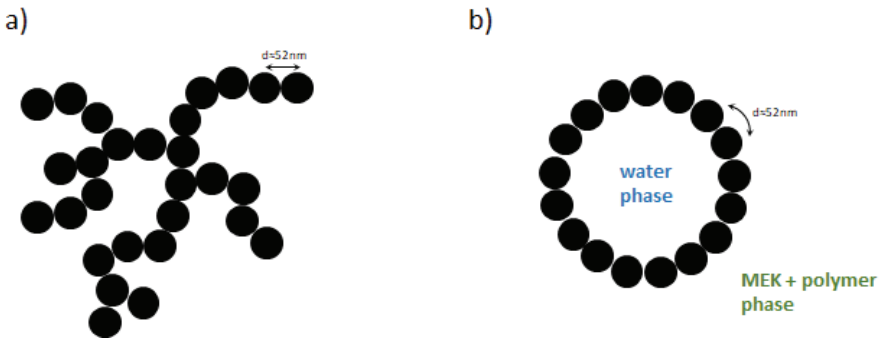


Figure 111 Schematization of the possible structuration of silica nanoparticles in P(VDF-co-HFP) - silica (by phase transfer) - MEK gels with (a) random fractal aggregates or (b) "core-shell" type fractal aggregates

Conversely, with the Nissan silica solution transferred in 2-heptanone, the presence of silica nanoparticles has very little impact on the gelation kinetics. It appears from the USAXS tests that the silica dispersion state is not strongly affected either. In addition, the viscoelastic moduli remain unchanged when adding silica. All these results might be consistent with the fast that none, or very weak, silica – polymer interactions exist. In this case the silica would not impact the gelation of P(VDF-co-HFP) and the same mechanisms than those of binary P(VDF-co-HFP) - 2-heptanone blends, namely phase separation followed by crystallization, as described in Chapter 3, may be considered.

These differences in behavior may alternatively come from differences in the surface chemistry of silica nanoparticles. The surface chemistries of silica nanoparticles prepared and treated in the laboratory for phase transfer and of Nissan silica should not be very different. As a reminder, silica developed by phase transfer are treated with CTAB and VTMS, ie short carbon chains (see their structures in Chapter 2). According to Chen et al. (Chen, Justice et al. 2008) the functionalization of Nissan silica consists in trimethylsilyl (-$SiCH_3$), short chain alkoxysilanes (Si-OCH_3 or Si-CH_2-CH_3) groups (and a small amount of hydroxyl groups), that is to say short carbon chains as well. Therefore, it may be assumed that the polymer – silica interactions would be relatively similar.

For Nissan silica in 2-heptanone, the addition of silica has only small impact on the gelation mechanisms. The differences observed between the two types of filled gels could therefore be explained primarily by the presence of water in the organic solution. Would "core-shell" type silica aggregates appear when gels are formulated (as schematized in Figure 111-b), isolating this fraction of water would effectively increase the concentration of copolymer located in the MEK fraction and no longer in the total fraction of solvent (MEK + water). This might explain the increase in the gelation kinetics and fractions of rigid zones and elastically active chains as detailed in Chapter 3 (see Figure 112).

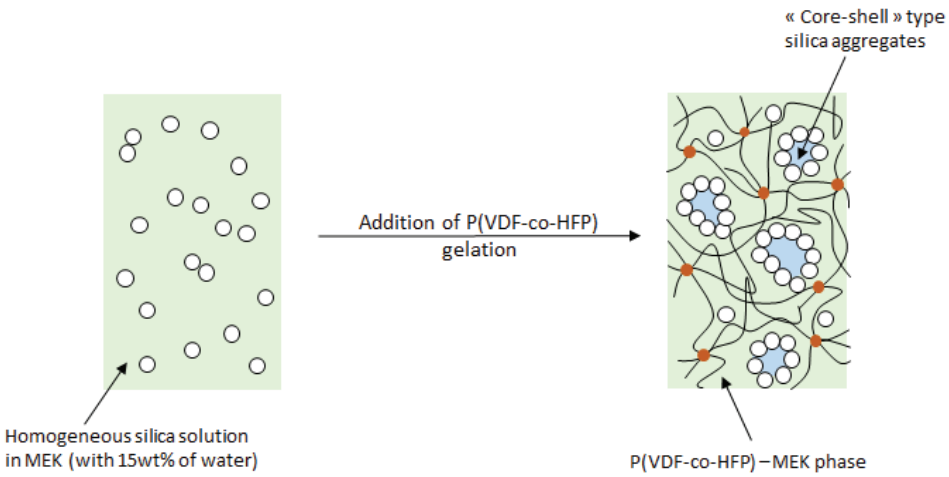


Figure 112 Schematization of the possible gelation mechanism of P(VDF-co-HFP) – silica (developed by phase transfer) – MEK materials. Polymer chains are represented by black lines and crystallites by orange circles.

4.6. Conclusions

This chapter has presented the work on the impact of the incorporation of silica nanoparticles on the gelation dynamics and structure of P(VDF-co-HFP) in MEK and 2-heptanone using a combination of characterization methods: USAXS, kinetics measurements (tube-tilting and rheology) and ^{19}F NMR.

We mainly studied gels prepared from two organic silica solutions: a silica solution obtained in the lab by phase transfer in MEK and a Nissan silica solution in MEK transferred in 2-heptanone. Nissan silica solution in MEK and P(VDF-co-HFP) gels made from this solution were also briefly (with USAXS measurements) studied. In all these cases the silica organic solutions are relatively well dispersed.

From the results we were able to formulate the following conclusions or hypothesis:

- Gelation of P(VDF-co-HFP) in MEK and also in 2-heptanone is thermoreversible and its kinetics depends on both concentrations of silica and copolymer. Gelation is faster when the concentration of copolymer increases (as observed in Chapter 3) and when the fraction of silica increases. The gelation of P(VDF-co-HFP) in MEK is strongly impacted by the addition of silica while it is very weakly impacted in 2-heptanone. However, difference sources of silica and processes (presence of water in the silica solution in MEK developed by phase transfer) are used and might be the primary explanation for this difference.
- Three different dispersion states of silica nanoparticles were found:
    - In gels formulated with silica solution in MEK by phase transfer: the addition of silica particles induces the formation of silica aggregates. As 15wt% of water exists in the material and our copolymer is hydrophobic, silica might segregate at interfaces between water-rich and MEK/polymer-rich domains. Additional experiments, such as microscopy on gels, would be needed to assess definitely this hypothesis.
    - In P(VDF-co-HFP) –Nissan silica – MEK: in the liquid state the addition of polymer does not seem to modify the dispersion of silica nanoparticles in the material significantly. In the gel state silica nanoparticles certainly form aggregates.
    - In P(VDF-co-HFP) – silica Nissan – 2-heptanone: depending on the copolymer concentration in the gels, silica nanoparticles generally remain well dispersed as in the organic silica solution (at 7 and 20wt% of P(VDF-co-HFP))

- The process, and more particularly the presence of water, seems to have a very strong impact on the kinetics and thus on the gelation mechanisms. On the contrary the presence of silica nanoparticles slightly increases the gelation kinetics and maybe weak polymer – silica interactions might be considered.

Chapter 5: Non-linear rheology study of P(VDF-co-HFP) – 2-heptanone thermoreversible gels

As discussed in the previous chapters the gelation of P(VDF-co-HFP) in 2-heptanone is caused by the formation of a heterogeneous solution (phase separation) followed by the formation of crystalline zones that might then be bridged by portions of chains in solution to form a three-dimensional network characteristic of the gel state. The objective of this chapter is to correlate the structure of the P(VDF-co-HFP) gels with their nonlinear rheological behavior. The influence of the copolymer concentration and the presence of silica nanoparticles is studied in this section.

5.1. Non-linear behavior of P(VDF-co-HFP) – 2-heptanone gels 137

5.1.1. Example of LAOS measurements: P(VDF-co-HFP) – 2-heptanone gel with 10wt% of copolymer 137

5.1.2. Effect of the concentration 139

5.2. Effect of the addition of silica nanoparticles on the nonlinear behavior of P(VDF-co-HFP) – 2-heptanone gels 147

5.3. General discussion 152

5.4. Conclusion 156

5. Non-linear rheology study of P(VDF-co-HFP) – 2-heptanone thermoreversible gels

Rheology is an effective method to determine the parameters that characterize the state of the material during gelation: viscoelastic fluid, critical gel and viscoelastic solid. From the measurements presented in the two previous chapters it was possible to determine the gelation times and gel melting temperatures as a function of physico-chemical parameters that modulate the structure of the networks and their mechanical properties: concentration of copolymer, temperature and presence of nanoparticles. LAOS (Large Amplitude Oscillatory Shear) measurements were then conducted to observe the behavior of our gels beyond the linear viscoelastic regime (LVE). Roughly speaking, in the LVE regime, these measurements provide information on the structure of the network, and, in the nonlinear regime, on the strength of the network.

In this chapter, we study the nonlinear rheological properties of the P(VDF-co-HFP) physical gels in 2-heptanone filled or not with silica nanoparticles using LAOS experiments. The impact of the concentration of copolymer and the presence of silica on the non-linear domain is detailed. The silica solution from Nissan (MEK-ST-L) transferred in 2-heptanone was used in all measurements presented here in P(VDF-co-HFP) – 2-heptanone - silica ternary gels. Rheological measurements in MEK could not be performed as MEK is too volatile.

All measurements were performed on each sample with the same sequence schematized in Figure 113. Different kind of sweeps are successively performed on P(VDF-co-HFP) – (silica) – 2-heptanone gels:

1) *Time sweep* (0.1%, 1Hz, 25°C, 5000s) to determine the gelation kinetics of the gels
2) *Frequency sweep* (0.1%, 25°C) to characterize the gel state of the material. The frequency was varied between 0.1 and 10 Hz
3) *Strain sweep* (1Hz, 25°C) with a strain amplitude between 0.01 and 500% (here call upwards ramp) to study the rheological behavior of gels in the nonlinear regime
4) *Time sweep* (1%, 1Hz, 25°C, 5000s) to determine the gelation time at rest directly after the LAOS upward ramp experiment
5) *Strain sweep* (1Hz, 25°C) with a strain amplitude between 500 and 0.01% (here call downwards ramp) to study the reversibility of the behavior in LAOS experiments

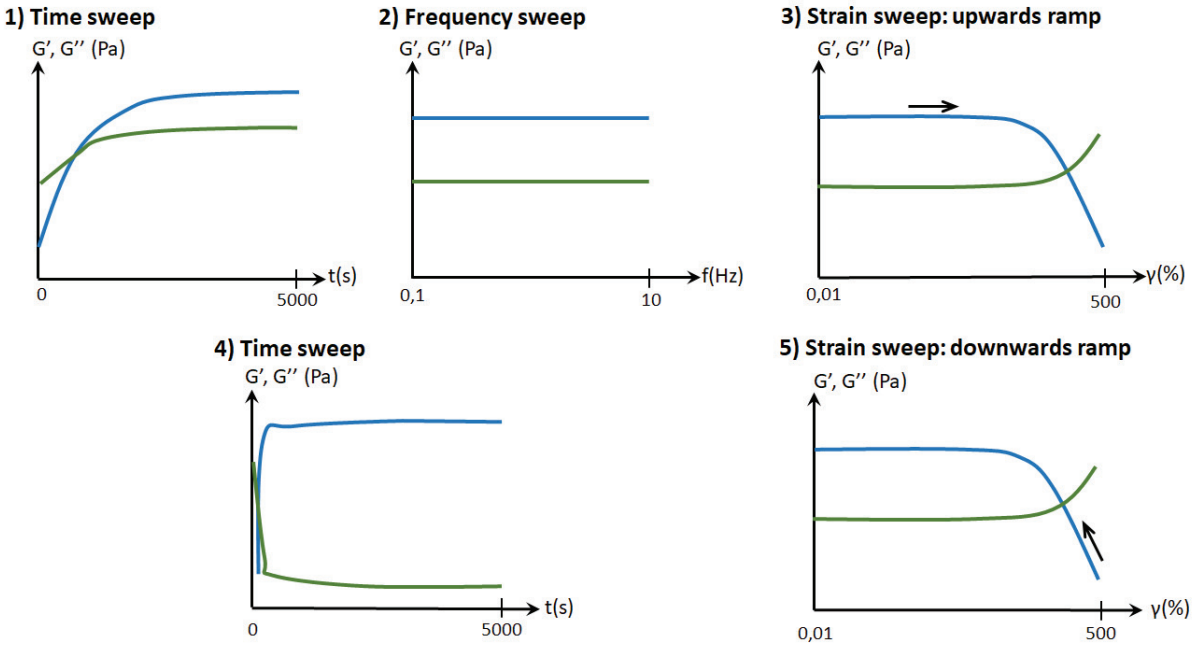


Figure 113 Schematization of the rheology sequence applied on P(VDF-co-HFP) – 2-heptanone filled or not with silica nanoparticles

5.1. Non-linear behavior of P(VDF-co-HFP) – 2-heptanone gels

In the gel state, the independence of the storage and loss moduli on frequency (in the frequency range investigated) was assessed in the previous chapters. As seen in Chapters 3 and 4, the gelation kinetics show a strong dependence on the copolymer concentration and a moderate dependence on the presence of silica nanoparticles. The influences of the temperature and frequency will not be studied here and experiments were all conducted on gels at 1Hz and 25°C over a strain range of 0.01% to 500%. After time sweep and frequency sweep tests to check the gel state of our materials, strain sweep tests allow us to characterize the nonlinear rheological behaviors of the gels.

5.1.1. Example of LAOS measurements: P(VDF-co-HFP) – 2-heptanone gel with 10wt% of copolymer

An example of the evolution of the viscoelastic moduli G', G'' of a P(VDF-co-HFP) – 2-heptanone gel with $X_{P(VDF\text{-}co\text{-}HFP)}$=10wt% as a function of the strain amplitude is shown in Figure 114. At low strain amplitude, the storage modulus remains constant, characteristic of the LVE region and G' is higher than G'' which assesses the solid-like behavior of the material (gel state). Above about γ=4% of strain amplitude the value of the apparent elastic modulus G' increases slightly and then abruptly drops down when the strain increases. Above γ=100%, the loss modulus G'' becomes higher than the storage modulus G' meaning that the system is in the liquid state.

Once the sample is in the liquid state, after shearing at high amplitude a time sweep measurement at fixed frequency and small shear strain was carried out to determine the gelation kinetics at rest after LAOS experiment. As shown in Figure 115, the gelation of a binary P(VDF-co-HFP) – 2-heptanone system is almost instantaneous. It only requires about 1.5 second to reaching a gel state while a gelation time at rest around 500 seconds was determined in Chapter 3. Thus large amplitude shear does not have the same effect as temperature on the gel-sol transition. This result indicates that the state of the material after large amplitude shearing in not the same as the state obtained by thermal

melting. Moreover, the gel recovers values of viscoelastic moduli close to those measured before LAOS experiment.

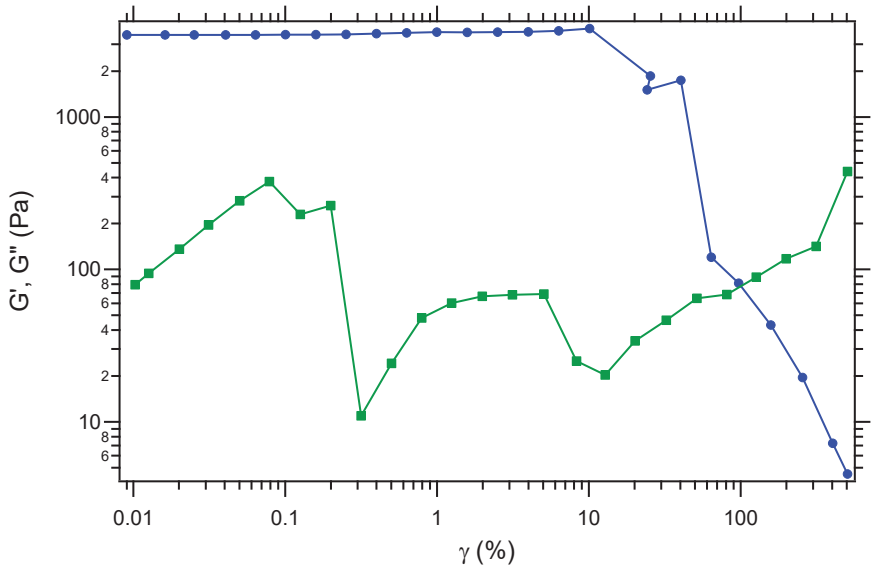


Figure 114 Plot of viscoelastic moduli (G' blue ●, G'' green ■) during oscillatory strain sweeps (from 0.01% to 500%) on a P(VDF-co-HFP) - 2-heptanone gel with $X_{P(VDF\text{-}co\text{-}HFP)}$=10wt%. Experiments were performed at 25°C and a frequency of 1Hz

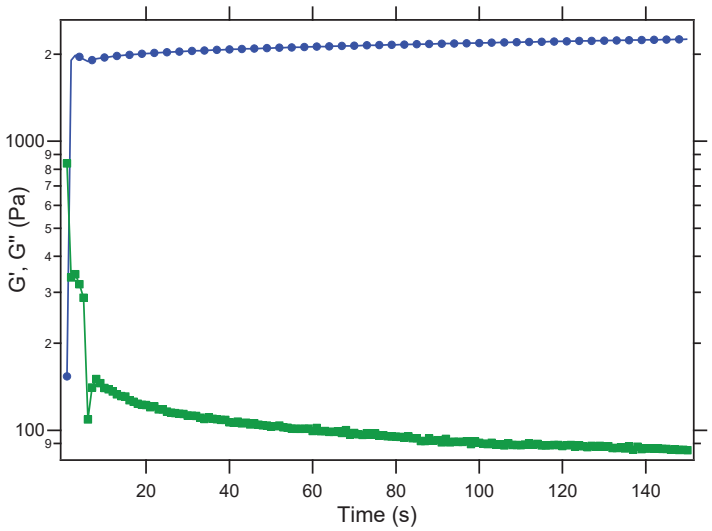


Figure 115 Evolution of the viscoelastic moduli (G' blue ●, G'' green ■) with time after LAOS measurements on a P(VDF-co-HFP) – 2-heptanone solution/gel with 10wt% of copolymer. Experiments were performed at 25°C, a frequency of 1Hz and a shear strain of 1%

Finally, in another series of experiments, to study the reversibility of the experiments, downwards strain sweep tests were performed from 500% to 0.1% after time sweep test. The evolution of the viscoelastic moduli as a function of the shear strain, superimposed with the curve for the upwards strain sweep tests from 0.01% to 500% is shown in Figure 116. A storage modulus close to the one obtained during the upwards strain sweep (0.01% to 500%) is obtained, meaning that we recover a gel with similar properties. However, the downwards curve is monotonous and no strain-hardening phenomenon was detected during the sequence. The gelation (sol-gel transition), as determined by the G' – G'' crossing point, occurs at a shear strain amplitude different from the one determined

during the upwards ramp. Indeed here the sol-gel transition happens at about $\gamma \sim 10\%$ in comparison with $\gamma = 100\%$ determined before.

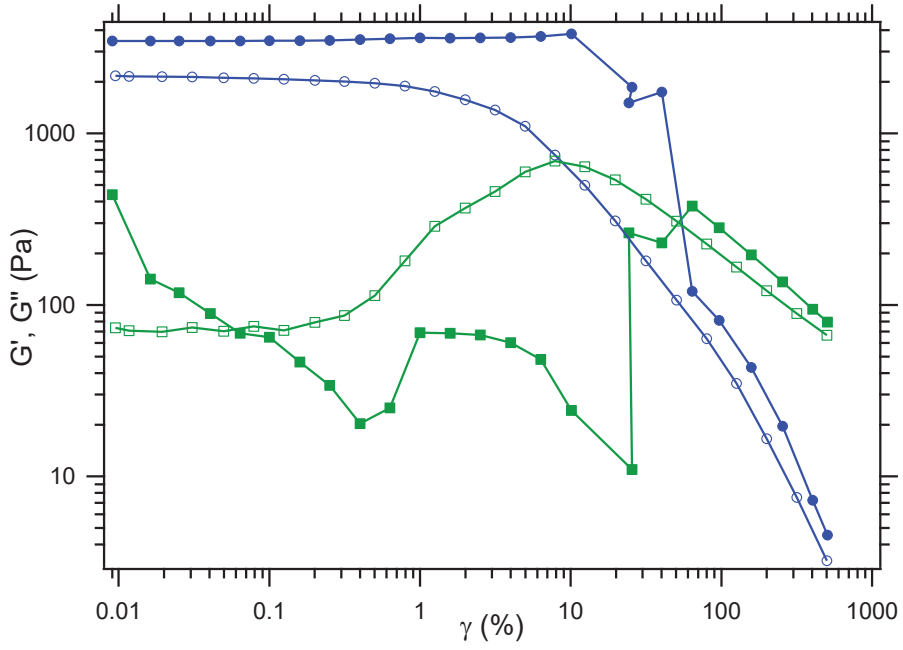


Figure 116 Plot of viscoelastic moduli (from 0.01% to 500%: G' blue ●, G'' green ■ and from 500% to 0.01%: G' blue ○, G'' green □) during oscillatory strain sweeps on a P(VDF-co-HFP) - 2-heptanone gel with $X_{P(VDF\text{-}co\text{-}HFP)}$=10wt%. Experiments were performed at 25°C and a frequency of 1Hz

5.1.2. Effect of the concentration

The same experiments were performed on physical P(VDF-co-HFP) gels with different fractions of copolymer (from 6 wt% to 18 wt%). The general behavior and the repeatability of the LAOS measurements were qualitatively similar to those presented for the gel with 10wt% of copolymer. Once the gels are formed (as characterized through time sweep and frequency sweep measurements as specified above), strain sweeps are performed to characterize the non-linear rheological behavior of our materials.

All curves of the moduli as a function of the strain amplitude on P(VDF-co-HFP) – 2-heptanone gels with concentrations of copolymer between 6 and 10wt% are displayed in Figure 117. In both gels a well-defined plateau, in which both G' and G'' moduli are independent of the strain amplitude, are observed (usually for γ below about 5%). This plateau corresponds to the linear regime. The values of the elastic modulus increase as the concentration increases. During the upward strain sweep tests the elastic modulus increases with the strain amplitude beyond about 5 to 10 % of strain amplitude and it then suddenly decreases and the samples apparently become liquids. The increase of the elastic modulus with the strain amplitude corresponds to a strain-hardening behavior and this phenomenon is not observed during the downwards ramp.

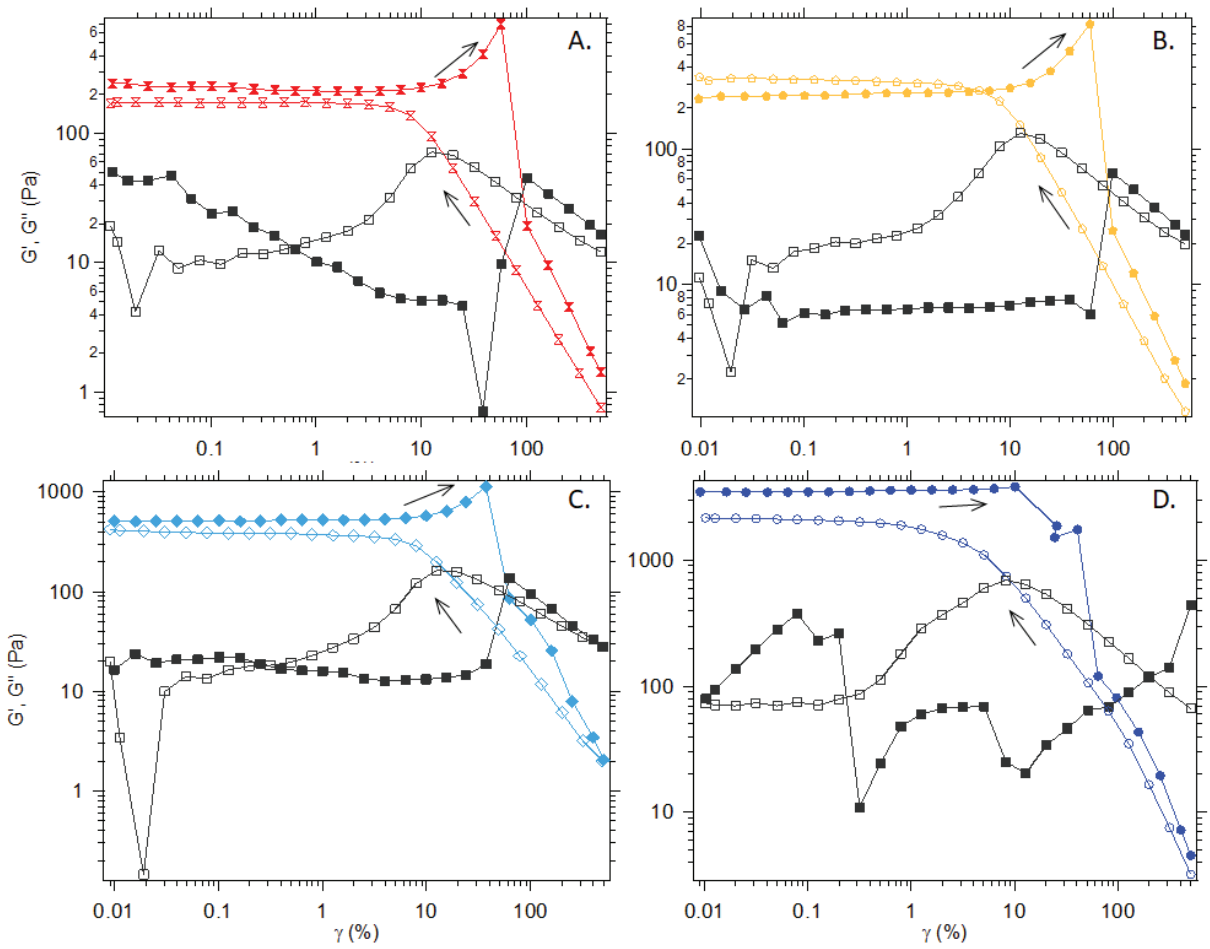


Figure 117 LAOS tests (filled symbols: 0.01% up to 500%; empty symbols: 500% down to 0.01%) on P(VDF-co-HFP) - 2-heptanone gels at different concentrations of copolymer: (A) $X_{P(VDF\text{-}co\text{-}HFP)}$=6wt% (B) $X_{P(VDF\text{-}co\text{-}HFP)}$=7wt% (C) $X_{P(VDF\text{-}co\text{-}HFP)}$=8wt% (D) $X_{P(VDF\text{-}co\text{-}HFP)}$=10wt%. Experiments were performed at 25°C and a frequency of 1Hz

Figure 118 summarizes the measurements of the storage modulus G' as a function of the shear strain for gels having a composition between 6 and 18wt% of copolymer only for the upwards strain sweep test (0.01%-500%). Above 10wt% of copolymer, only the linear regime of the gels could be detected. Indeed, after the LVE region, a strong decrease of the G' modulus was observed (points are not shown in this figure) and it corresponds to the fact that gels are ejected from the geometry at high shear strain. The downwards (return) curves are for both G' and G'' monotonous and do not show discontinuities, indicating that no instability occurs in this case. The point at which the apparent gel-liquid transition occurs may correspond to slippage at the surface of the geometry, and not be related to an intrinsic property of the material. Thus, we shall not discuss further the values (γ_{max}, G_{max}) at which this macroscopic instability occurs, but rather concentrate on the strain hardening phenomenon.

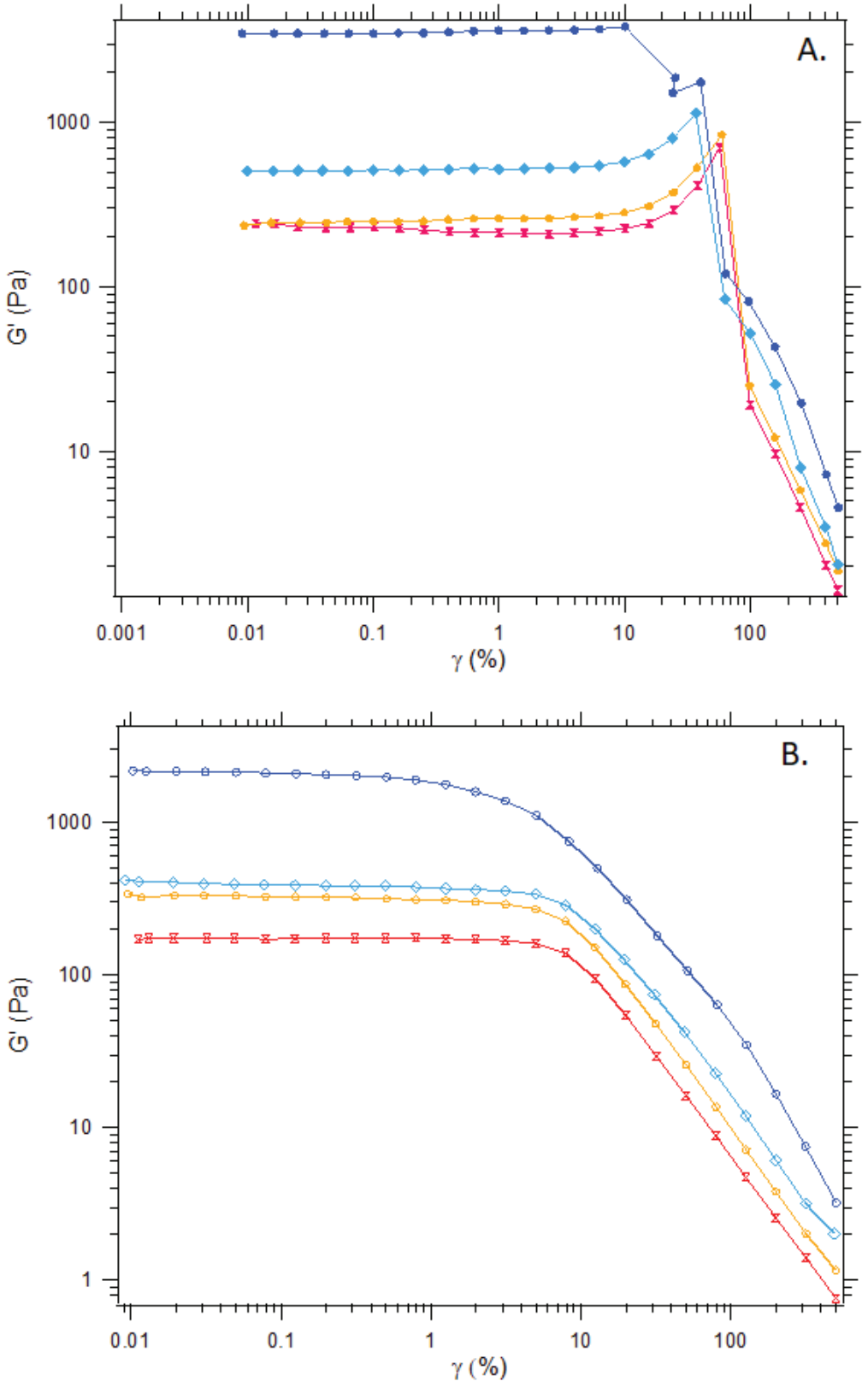


Figure 118 Storage modulus versus shear strain for P(VDF-co-HFP) - 2-heptanone at different compositions: $X_{P(VDF\text{-}co\text{-}HFP)}$=6wt% (red ⧗), $X_{P(VDF\text{-}co\text{-}HFP)}$=7wt% (orange ⬟), $X_{P(VDF\text{-}co\text{-}HFP)}$=8wt% (light blue ◆) and $X_{P(VDF\text{-}co\text{-}HFP)}$=10wt% (blue ●) for (A) upwards ramp (0.01% up to 500%, filled symbols) and (B) downwards ramp (500% down to 0.01%, empty symbols). All measurements were performed at 25°C and a frequency of 1Hz.

The behavior of the materials can be analyzed further by looking at stress-strain (Lissajous) curves. It represents the evolution of the stress as a function of the strain over a cycle with time as a parameter.

Here we describe in details the curves obtained for a P(VDF-co-HFP) – 2-heptanone gel with 7wt% of copolymer, the behavior being qualitatively similar for all the samples. In the linear regime, at low strain, the stress is a sinusoidal wave and stress-strain curves form perfect ellipses. Moreover narrow ellipses are observed which indicates the predominant elastic behavior of the gels, with the loss modulus G'' being about 50 times small than G' at low strain amplitudes (see Figure 119). The slope of the ellipse gives the elastic modulus (Figure 117-b at γ<10%). Beyond about 6% of strain amplitude, the apparent elastic modulus increases which corresponds to a strain-hardening behavior. To analyze further this behavior, it is useful to look at the stress response as a function of time. The Lissajous obtained typically at and beyond 10% strain have a remarkable shape.

First the hysteresis remains extremely weak, meaning that the response remains essentially elastic, with the stress in phase with the strain. In other words, this means that the system responds to the deformation in a quasi-instantaneous way. Then, the stress curves exhibit an extremely pronounced strain-hardening (Papon, Merabia et al. 2012, Mermet-Guyennet, Castro et al. 2015). This behavior will be discussed later in the section "General discussion" (page 152).

Finally, there is an abrupt change in behavior at a critical strain value of order 60%, in which the behavior of the Lissajous curves suddenly change from elastic (with strain-hardening) to a shape closer to a sphere or square, which characterizes the liquid state and more particularly a viscous solution.

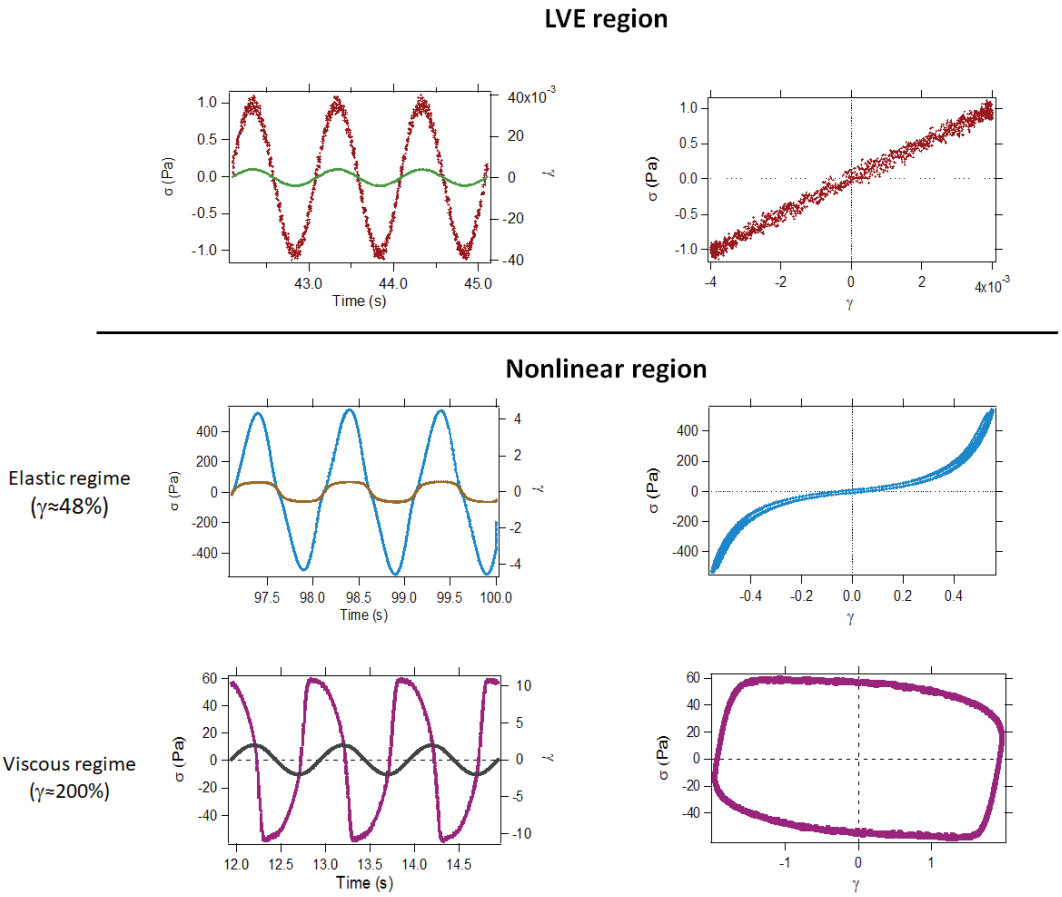


Figure 119 Stress as a function of time and as a function of strain during one cycle in the LVE and nonlinear regions (elastic and viscous states) for a P(VDF-co-HFP) – 2-heptanone gel with $X_{P(VDF\text{-}co\text{-}HFP)}$=7wt%. Experiments were conducted at 25°C and a frequency of 1Hz

Representative Lissajous curves of P(VDF-co-HFP) – 2-heptanone gels with concentrations between 7wt% and 10wt% of copolymer are displayed in Figure 120 for the upwards ramps. At very low γ, narrow ellipses are observed which indicates the high stiffness and predominant elastic behavior of the gels. The area of the ellipses varies little with the strain and therefore the energy dissipated remains the same in the linear domain (all the Lissajous curves in the LVE region are not shown here). The transition to the nonlinear regime is characterized by the deviation of the stress – time curve from its sinusoidal shape as shown in Figure 119. Above 24.5% of strain amplitude, all the ellipses start to distort and show extremely pronounced strain-hardening. This phenomenon is observed in P(VDF-co-HFP) gels at all concentrations. At the highest γ-value (higher than 100%), the shapes of the curves change abruptly to an almost square shape. The gel-sol transition appears to vary little with the concentration of copolymer. Here the samples are in the liquid state and display an abrupt yielding of the gel structure, followed by flow (horizontal part of the loop) and eventually recovery. In this region the area of the square-shape Lissajous plots increases with the strain amplitude. It means that the dissipated energy by the viscous effect increases during high amplitude cycles. Thus the behavior of gels in regimes with high γ is governed by the flow of the material during a cycle.

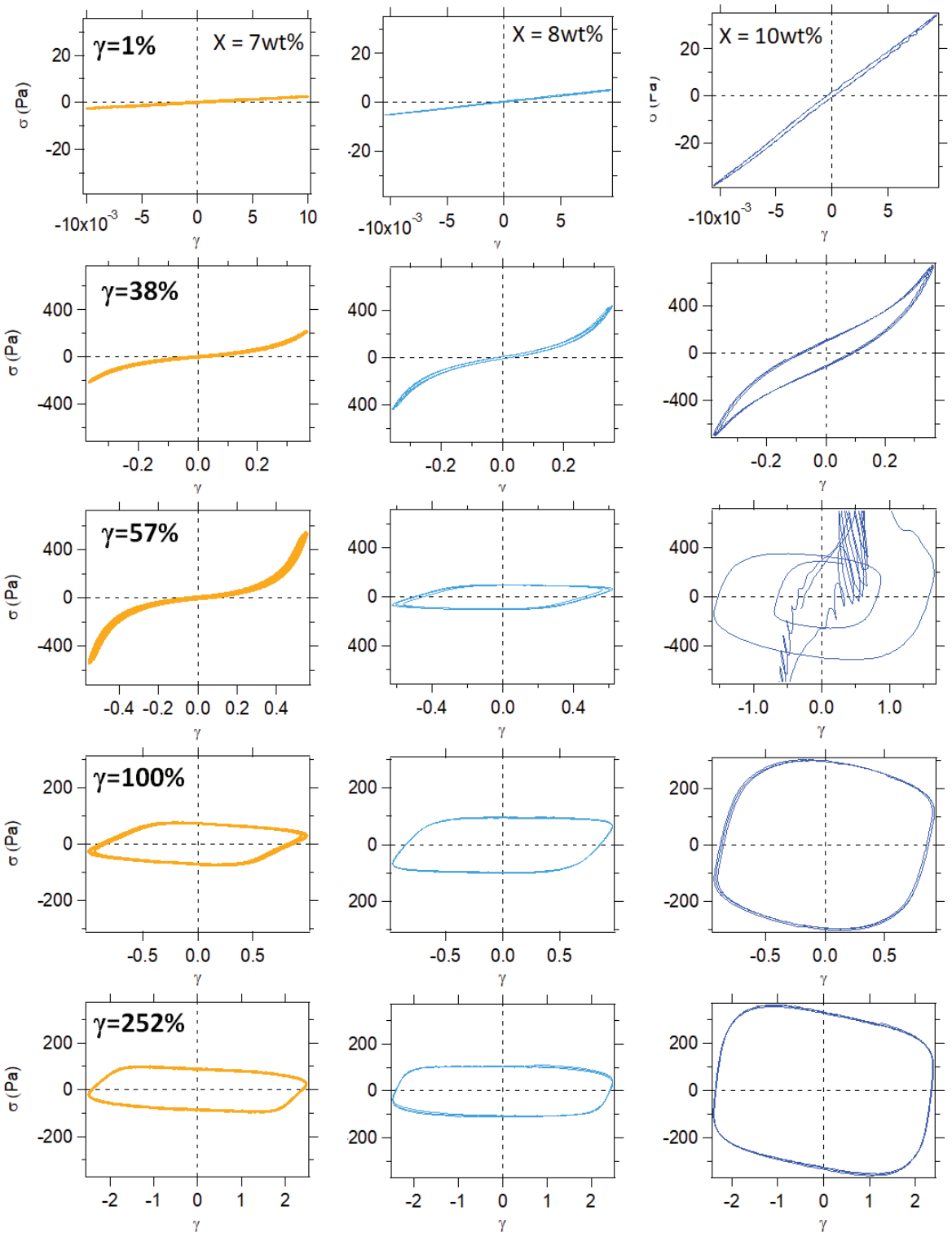


Figure 120 Lissajous curves of the upwards ramp (0.01% up to 500%) for P(VDF-co-HFP) – 2-heptanone gels at three different copolymer concentrations: (a) 7wt%, (b) 8wt% and (c) 10wt% with shear strains of 1%, 38%; 57%, 100% and 252%. Experiments were conducted at 25°C and a frequency of 1Hz

The breakage transition is illustrated in Figure 121, which shows stress and strain as a function of time in the gel with 10wt% of copolymer under a strain amplitude of 57%. Initially, the material is still in the elastic regime (gel state), while at the end of the considered time range, it is in the viscous regime (liquid state). It indicates a gel – liquid transition during a cycle. The transition is preceded by small, fast oscillations, possibly corresponding to stick-sleep.

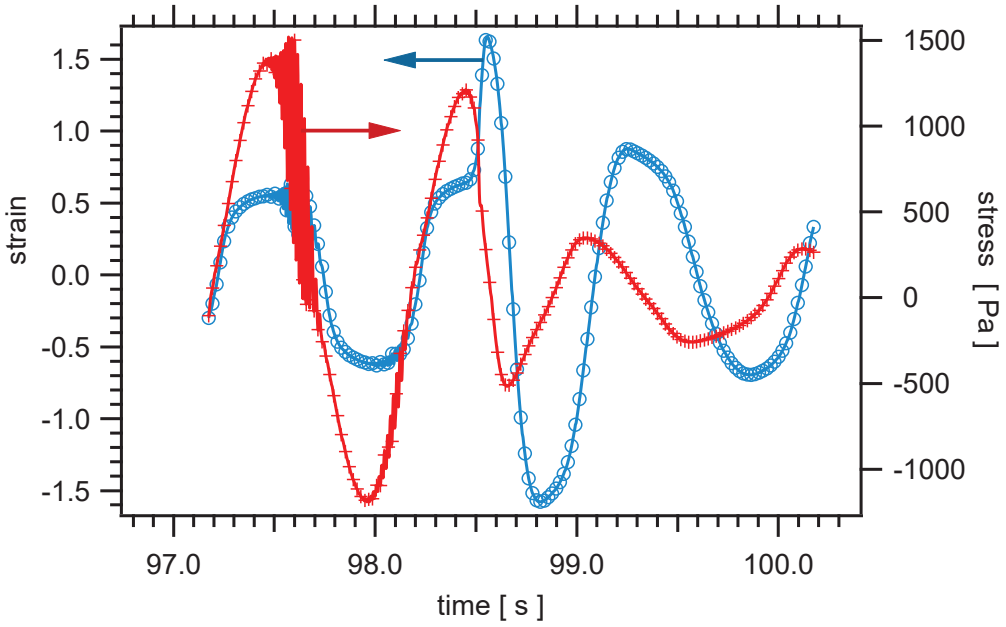


Figure 121 Stress (red +) and strain (blue ○) as a function of time in P(VDF-co-HFP) – 2-heptanone gel with $X_{P(VDF\text{-}co\text{-}HFP)}$=7wt% during three periods, at high strain amplitude. At the beginning of the time window which is shown, the system is elastic, with the stress nearly in phase with the strain and a stress amplitude of order 1.5 kPa (modulus G' of order 2 kPa). Some high frequency stress oscillations then appear, associated to either slippage at the walls of the measuring cell or to internal fracture of the gel. These oscillations are precursor of the overall transition towards the viscous regime, which occurs at about 98.5 s. In the subsequent viscous regime, the stress is nearly in phase with the strain rate (I;e. in quadrature with the strain).

In the same way, Figure 122 shows the representative Lissajous curves of physical gels for the downwards ramp. They all show changes from square-shape curves at large strain amplitude (corresponding to the viscous regime) to narrow ellipses characteristic to the gel state at low strain amplitude. No strain-hardening was detected during this sequence.

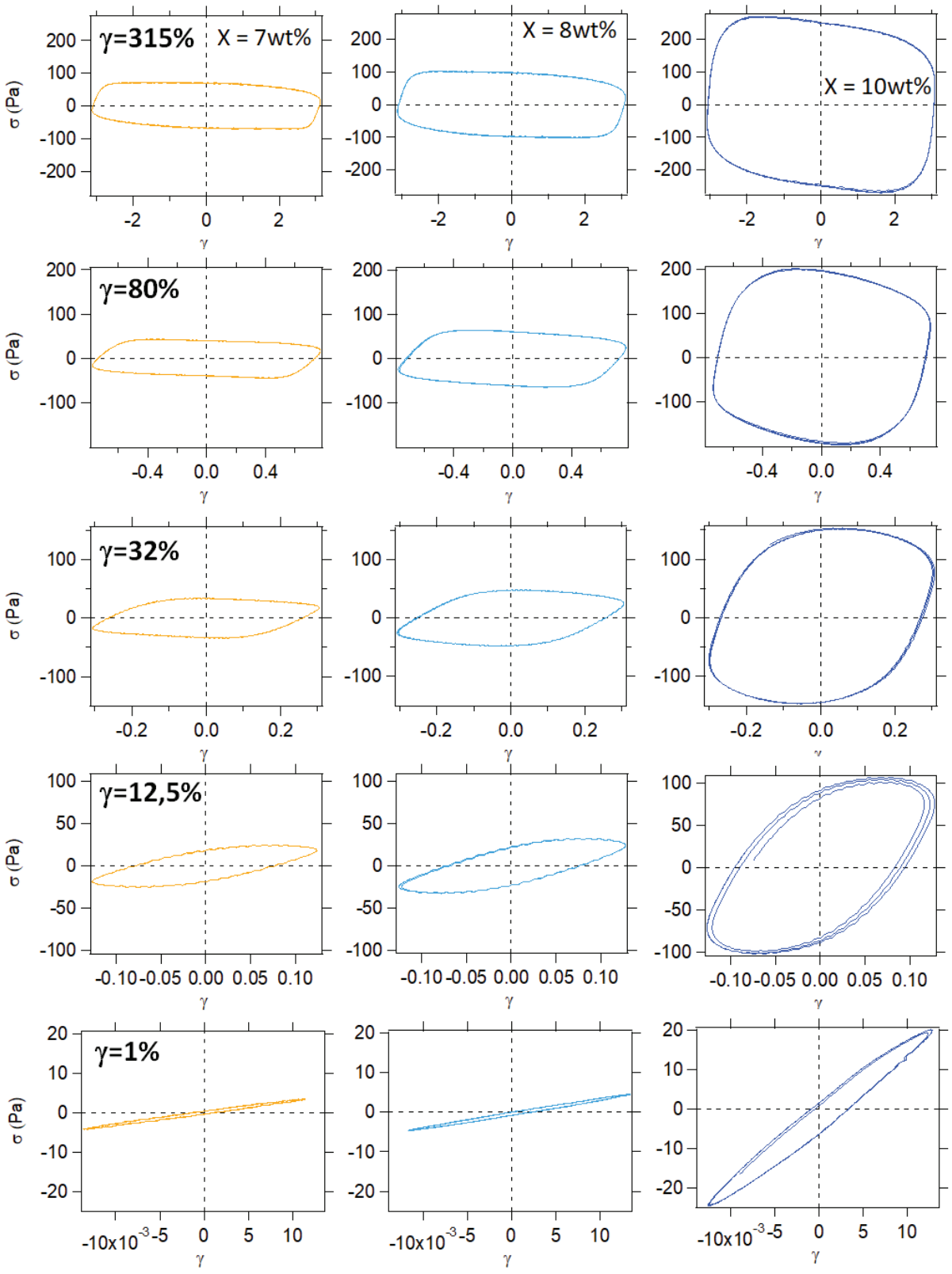


Figure 122 Lissajous curves of the downwards ramp (500% down to 0.01%) for P(VDF-co-HFP) – 2-heptanone gels at three different copolymer concentrations: (a) 7wt%, (b) 8wt% and (c) 10wt% with shear strains of 315%, 80%; 32%, 12.5% and 1%. Experiments were conducted at 25°C and a frequency of 1Hz

5.2. Effect of the addition of silica nanoparticles on the nonlinear behavior of P(VDF-co-HFP) – 2-heptanone gels

The effect of the addition of silica nanoparticles on the nonlinear rheological behavior of P(VDF-co-HFP) – 2-heptanone gels was also investigated. Gels were all formulated with 8 wt% of silica nanoparticles from Nissan silica solution MEK-ST-L transferred in 2-heptanone, as detailed in Chapter 2. The same procedures as for binary gels without silica were applied. Strain sweep tests were performed on gels with different concentrations of P(VDF-co-HFP) at fixed concentrations of silica (8wt%). Qualitatively similar results were obtained for all concentrations of copolymer and are shown in Figure 123. At small strain amplitudes, all systems are in the gel state as G' is higher than G'' with $^{G''}/_{G'}$ of order 10^{-2} to about 5×10^{-2}. In this regime, both moduli are independent of the frequency< This defines the Linear Viscoelastic Regime (LVE). By increasing the concentration of copolymer from 6 to 12wt%, the elastic modulus in the LVE region increases from 225 Pa to 3550 Pa i.e. by more than a decade. In comparison with the binary (unfilled) polymer gels, the initial elastic modulus of the filled gels is similar to (and in some case even lower than) those of the binary polymer gels at the same polymer concentrations. This is surprising and indicates that silica does not reinforce the material.

The behavior under large amplitude shear is then quite different from that of binary, unfilled gels. The LVE regime extends over a much smaller range of strain amplitude. From $\gamma \sim 1\%$ the elastic modulus G' decreases rapidly with the strain amplitude and above $\gamma \sim 10$ - 100% the gel reaches a liquid state (G'' becomes higher than G') with a small dependence on the concentration of copolymer. No strain-hardening (increase of the apparent elastic modulus as the strain amplitude increases) appears. The sol-gel transition during the downwards strain sweep appears between 1 and 10% typically, that is, at smaller strain than in the upwards ramp, and, once again, with no strong dependence on the concentration. Finally, another significant difference can be highlighted: the elastic modulus recovered in the LVE region after the downwards ramp (500% to 0.01%) is sometimes higher than the initial one and more particularly in the gels with 7 wt% and 12 wt% of copolymer. Thus P(VDF-co-HFP) – silica – 2-heptanone gels seem to be weaker than binary gels as they easily dissociate at strain above about 1%. Polymer – solvent interactions or the dispersion state of silica within the polymer matrix should certainly play a role in this difference.

After the upwards ramp of LAOS tests, time sweeps were performed. An example is shown in Figure 124 for a P(VDF-co-HFP) – silica – 2-heptanone gel with $X_{P(VDF\text{-}co\text{-}HFP)}$ = 10wt% and X_{SiO2} = 8wt%. Quasi-instantaneous gelation (less than 1 second) is observed, which strongly differs from thermal gelation time measured in Chapter 4 (a thermal gelation time of 6 minutes was measured in this gel). The formation of ternary gels is even faster than the gelation of binary gels after the strain sweep measurements. Therefore, as for binary polymer gels, the strain sweep does not have the same effect as the temperature on the gel-sol transition. However, contrary to the case of binary gels, viscoelastic moduli keep increasing with time and do not reach a plateau even after 1h20 of measurements. The final elastic modulus is higher than the initial one determined before the LAOS test and still keeps increasing. This indicates that the material continues to evolve over time, unlike a binary polymer gel that reaches a plateau of modulus after a relatively short time (in approximately 500 seconds). This may be related to some degree of rheopexy, in which a material shows hardening (increase of the modulus and/or the yield stress) when it has been previously sheared at increasing

stress amplitudes, i.e. a hardening behavior depending on the previous rheological history. This behavior is sometimes observed in relatively concentrated suspensions of nanoparticles such as carbon blacks.

A further point to notice is that the drop of elastic modulus as the strain amplitude increases (as shown in Figure 123) seems to occur in two successive steps, with a first drop occurring around roughly 1 % and then a second drop with a much steeper slope accruing around roughly 50 to 100%. This might perhaps be related to the successive breaking of the two silica and polymer gel networks.

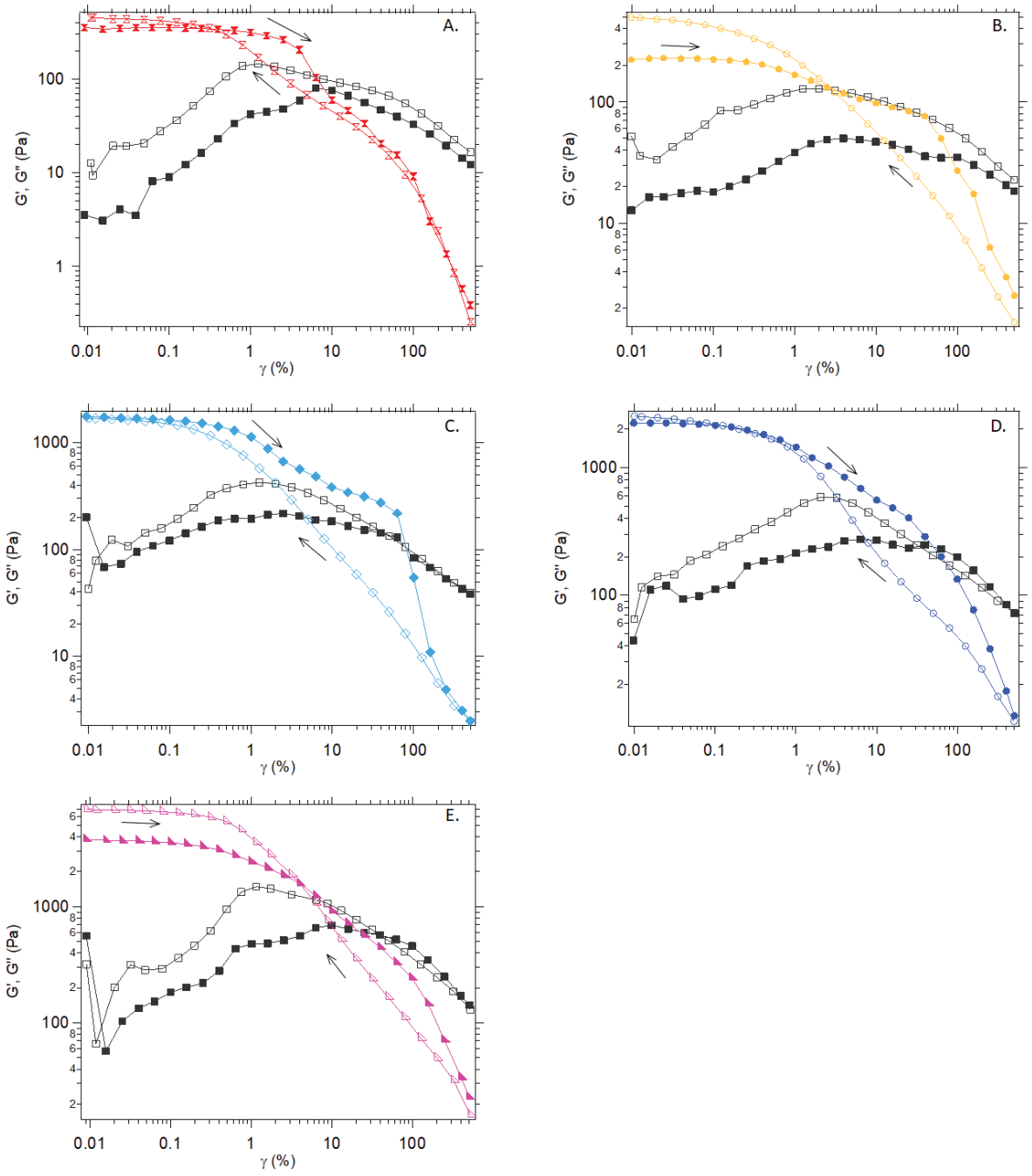


Figure 123 LAOS tests (filled shapes: 0.01% up to 500%; unfilled shapes: 500% down to 0.01%) on P(VDF-co-HFP) – silica – 2-heptanone gels with X_{SiO2}=8wt% and with different concentrations of copolymer: (A) $X_{P(VDF\text{-}co\text{-}HFP)}$=6wt% (B) $X_{P(VDF\text{-}co\text{-}HFP)}$=7wt% (C) $X_{P(VDF\text{-}co\text{-}HFP)}$=8wt% (D) $X_{P(VDF\text{-}co\text{-}HFP)}$=10wt% and (E) $X_{P(VDF\text{-}co\text{-}HFP)}$=12wt%. Experiments were conducted at 25°C and a frequency of 1Hz.

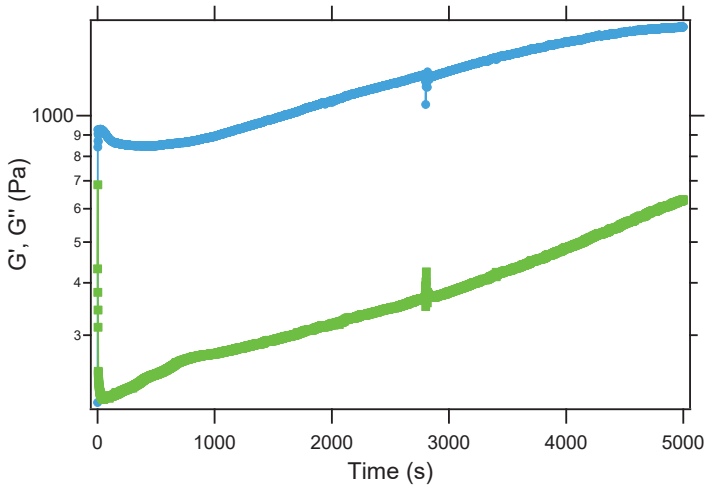


Figure 124 Evolution of the viscoelastic moduli (G' blue ●, G'' green ■) with time after LAOS measurements on a P(VDF-co-HFP) – silica – 2-heptanone solution/gel with 10wt% of copolymer and 8wt% of silica. Experiments were performed at 25° C, a frequency of 1Hz and a shear strain of 1%

Examples of stress – strain Lissajous curves are plotted in Figure 125 for the upwards ramp and Figure 126 for the downwards ramp. These graphs confirm that the behavior of filled (ternary) gels is completely different from that of unfilled (binary) gels, indicating that adding silica induces major changes in the structure and dynamics of the gels. At low γ, narrow ellipses are obtained, which fits well with the gel state of the material. However, the ellipses are wider than in binary polymer gels, meaning that the incorporation of silica nanoparticles induces a larger viscous contribution, with an elastic contribution that remains predominant. In sharp contrast with the case of unfilled (binary) gels, the Lissajous curves distort progressively towards a viscous behavior. They do not show strain-hardening followed by an abrupt transition (break-down) to a viscous regime. When the strain amplitude increases, the curves then distort to a near rhomboidal shape corresponding to a viscous liquid state. The strain at which the ellipses start to distort depends on the concentration of copolymer. Finally, at high strain amplitude, the behavior of the materials is very similar at all concentrations. From the shape of the curves it is possible to verify that samples are all in the liquid state. Very similar Lissajous curves are obtained for the downwards ramp meaning that the materials change from viscous (liquid) state at high strain amplitude to an elastic (gel) state at low strain amplitude, with no strain-hardening.

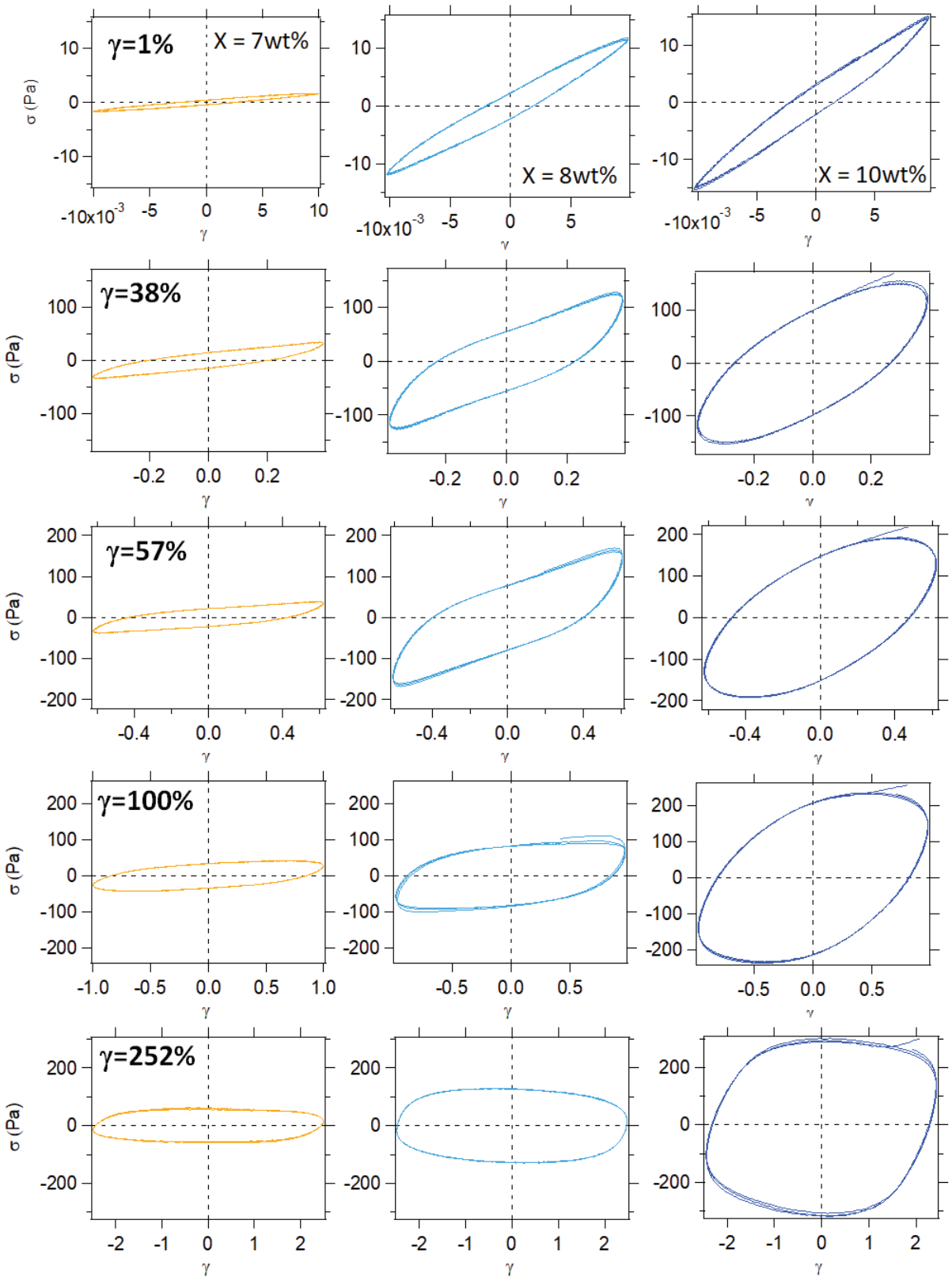


Figure 125 Lissajous curves of the upwards ramp (0.01% up to 500%) for P(VDF-co-HFP) – silica – 2-heptanone gels with X_{SiO2}=8wt% at different copolymer concentrations: (a) 7wt%, (b) 8wt%, (c) 10wt% with shear strains of 1%, 38%; 57%, 100% and 252%. Experiments were performed at 25°C and a frequency of 1Hz.

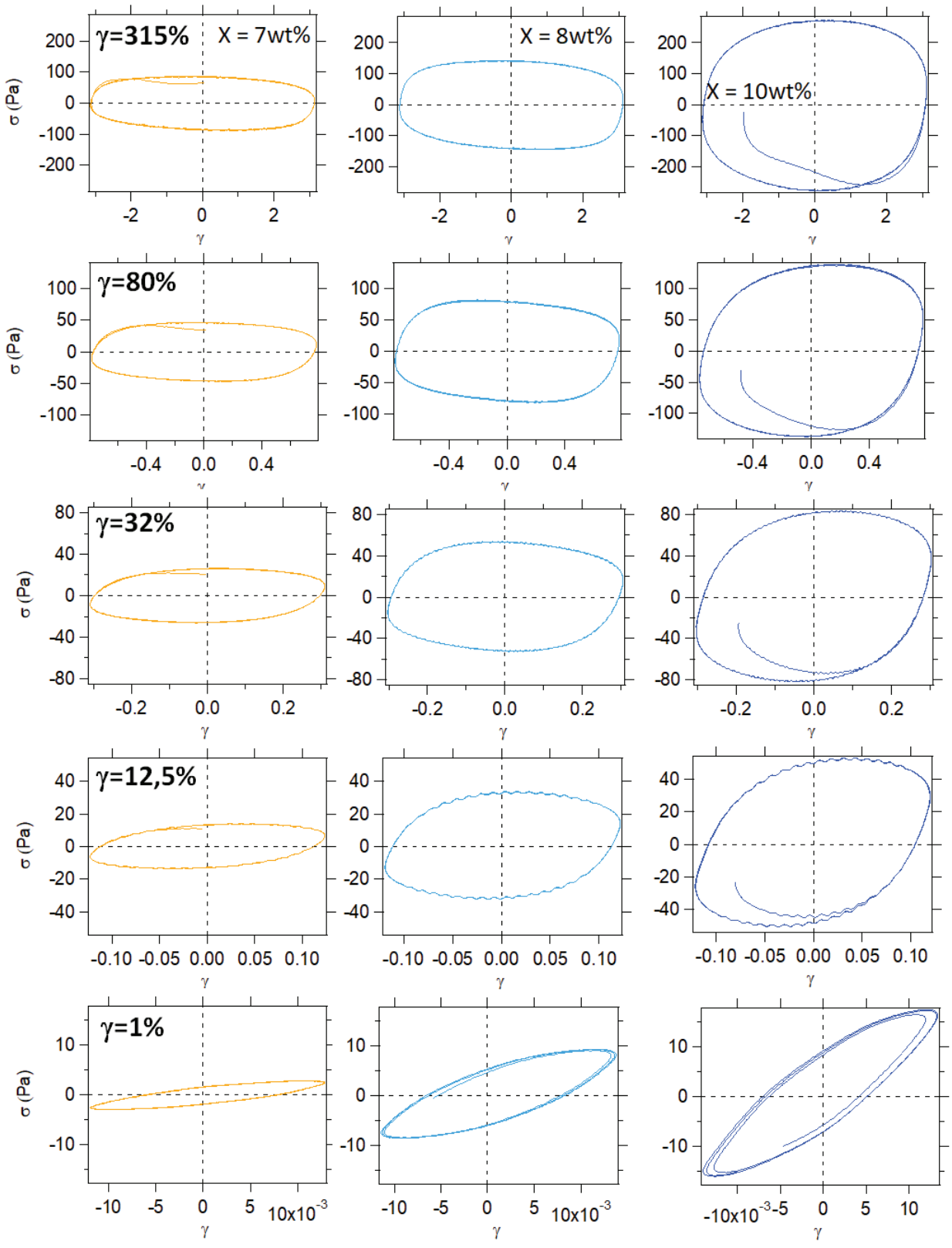


Figure 126 Lissajous curves of the downwards ramp (500% down to 0.01%) for P(VDF-co-HFP) – silica – 2-heptanone gels with X_{SiO2}=8wt% at different copolymer concentrations: (a) 7wt%, (b) 8wt%, (c) 10wt% with shear strains of 315%, 80%, 32%, 12.5% and 1%. Experiments were performed at 25°C and a frequency of 1Hz.

5.3. General discussion: non-linear behavior of P(VDF-co-HFP) gels in 2-heptanone

The rheological behavior of P(VDF-co-HFP) – 2-heptanone physical gels filled or not with silica nanoparticles was measured for various concentrations of copolymer with LAOS experiments. Our results suggest that the concentration of copolymer and the presence of nanoparticles have two different effects on the structure of the gels (and thus on the viscoelasticity of P(VDF-co-HFP) solutions and gels). In the case of binary gels, gels stiffen as they are strained: at approximately 50% of deformation, strain-hardening was observed and it appears that the concentration of copolymer plays a role in the stiffening of the P(VDF-co-HFP) network. In the presence of silica nanoparticles, the behavior is very different. No strain-hardening was observed and the addition of silica into the polymer gels induces strain-softening, similar to Payne's effect in elastomers.

Strain-hardening has been observed in different materials including polymer gels and more particularly biopolymer gels made of DNA (Orakdogen, Erman et al. 2010), gelatin (Groot, Bot et al. 1996) or cellulose for example. However, to our knowledge, we saw very few studies in the literature on the linear rheology study (SAOS) of PVDF gels (Dasgupta, Manna et al. 2008) and none on the nonlinear behavior of such materials. The objective of this chapter is thus to better understand the evolution of the structure of P(VDF-co-HFP) gels with the strain amplitude.

In DNA gels, strain-hardening was attributed to finite extensibility of DNA double-strand chains forming the gel, which have a very long persistence length, i.e. are quite rigid (Orakdogen, Erman et al. 2010). For gels made of flexible chains, finite extensibility would not be observed in the range of deformation which is studied. Let us make this argument more precise.

Let us suppose we have a homogeneous gel (as schematized in Figure 127) made of very flexible chains. The elastic modulus in the linear regime would be expressed as

$$G \sim nRT \sim \left(\frac{\rho\varphi}{\overline{M_c}}\right) RT \tag{43}$$

Where n is the number of moles of elastic chains (twice the number of crosslink points for tetrafunctional crosslinks) per unit volume, ρ the density of P(VDF-co-HFP), φ the volume fraction and $\overline{M_c}$ the average molar mass between crosslinks.

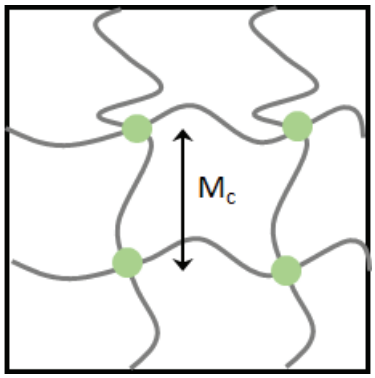


Figure 127 Schematization of a homogeneous, tetrafunctional polymer gel made of very flexible chains

Considering ρ=1.78x10^{3}kg/m^3, φ=6vol%, G=10^{3}Pa at T=313K we found M_c≈278kg/mol, which corresponds roughly to 4500 monomers and to a number of segments $N \equiv 500$.

The force-extension curve of a flexible chain of N Kuhn segments of length α is given by:

$$f = \frac{k_B T}{\alpha} \mathcal{L}^{-1}\left(\frac{R}{N\alpha}\right) \tag{44}$$

Where f is the force exerted on chain ends and R is the end-to-end vector of the chain. $\mathcal{L}^{-1}$(x) is the inverse of the Langevin function $\mathcal{L}(x) = \frac{1}{\tanh x} - \frac{1}{x}$.

In this expression the force f diverges as R reaches the maximum extension R_{max}=Nα (fully stretched chain).

To make a parallel with the behavior of a stretched macroscopic system such as a gel, an equivalent "elongation ratio" λ can be defined as $R / \langle {R_0}^2 \rangle^{1/2}$. Where $\langle {R_0}^2 \rangle \approx N\alpha^2$ is the equilibrium "length" of a chain. Thus the fully stretched state corresponds to an extension ratio of order $N^{1/2}$.

The force as a function of the "extension ratio λ" is plotted in Figure 128. This figure shows that strain-hardening related to finite extensibility would occur at typical (elongation) strain values of order $\approx N^{1/2}$ which is larger than what is observed. Conversely to observe large strain-hardening effect in the range 100%, one should have a value of N of order 2, which means unrealistically short and/or rigid chains in the gel network.

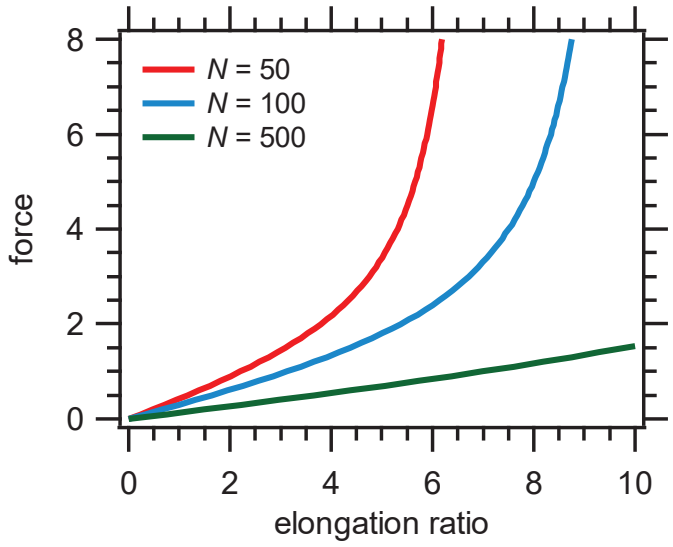


Figure 128 Force as a function of the "extension ratio λ" for different number N of Kuhn segments of length α

Explaining such a high strain-hardening effect is not easy. P(VDF-co-HFP) chains in solvent are certainly not semi-rigid as in the case for double-strand DNA (Orakdogen, Erman et al. 2010).

We may speculate that a picture which would be coherent with other observations (namely SAXS) and considerations about the Flory parameter of the solvent, is a partially segregated, polymer-rich network within a solvent-rich phase as illustrated in Figure 129. The elasticity would then be transmitted only through the solvent-rich domain. In this domain, the density of effective crosslinks (entanglements, crystallites…) could be much higher than the overall average value estimated above. This could lead to much enhanced strain-hardening effect.

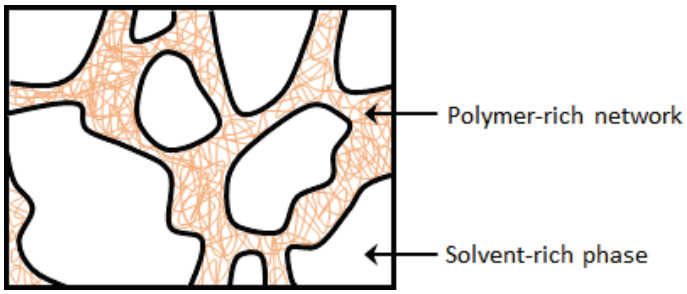


Figure 129 Schematization of the possible structure of P(VDF-co-HFP) – 2-heptanone explaining the strain-hardening

To better understand this phenomenon, we introduced a parameter named *strain-hardening ratio* defined as:

$$strain - hardening\ ratio = \frac{P_1}{P_0}$$

Where P_1 is the slope at the maximum of stress and P_0 the slope at the origin (i.e. the elastic modulus of the gel).

The values of P_1 and P_0 and thus the strain-hardening ratio are thus determined for each value of strain amplitude during the upwards ramp of the LAOS experiment. An example is shown in Figure 130 for a P(VDF-co-HFP) – 2-heptanone gels with 7wt% of copolymer at 40% of strain amplitude.

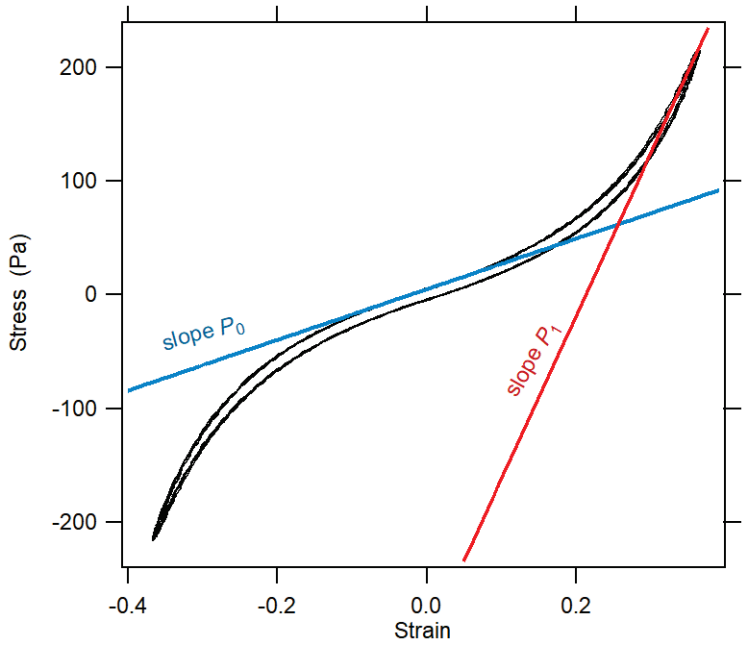


Figure 130 Example of the determination of the P_0 and P_1 parameters used for the calculation of the strain-hardening ratio. Example for a P(VDF-co-HFP) – 2-heptanone gel with $X_{P(VDF\text{-}co\text{-}HFP)}$=7wt% and γ=40%

This ratio was determined for P(VDF-co-HFP) – 2-heptanone gels with concentrations of copolymer between 6 and 10wt%. Its evolution as a function of the strain amplitude during the upwards ramp of the LAOS experiment at different concentrations of copolymer is represented in Figure 131. We show that the strain-hardening ratio depends both on the strain amplitude and the fraction of P(VDF-co-HFP) in the gel. Indeed, when the strain amplitude increases the strain-hardening ratio increases until reaching a maximum value. More precisely between 1 and 10% of strain amplitude, the strain-

hardening ratio is constant and approximately equal to 1, which corresponds to the LVE region. Above 10% of strain amplitude the ratio increases with the increase of the amplitude. We then study the influence of the concentration of copolymer on the value of strain amplitude γ_{max} at which the maximum of the strain-hardening ratio SH_{max} was observed. We noticed that when the fraction of P(VDF-co-HFP) in the gel increases, γ_{max} decreases from 57% (at 6 and 7wt%) to 10% (at 10wt% of P(VDF-co-HFP)). Moreover, the value SR_{max} decreases with the increase of the concentration of copolymer. SR_{max} decreases from 22 for a gel with 6wt% of copolymer to 1.3 at 10wt% of copolymer. We can thus suppose that the strain-hardening phenomenon reduces when the rigidity of the gels increases. When the concentration of copolymer increases the elastic modulus increases (see Figure 118) meaning that the material becomes more resistant to the deformation and therefore gels become more rigid. As a consequence, the strain-hardening phenomenon tends to disappear with the increase of the concentration.

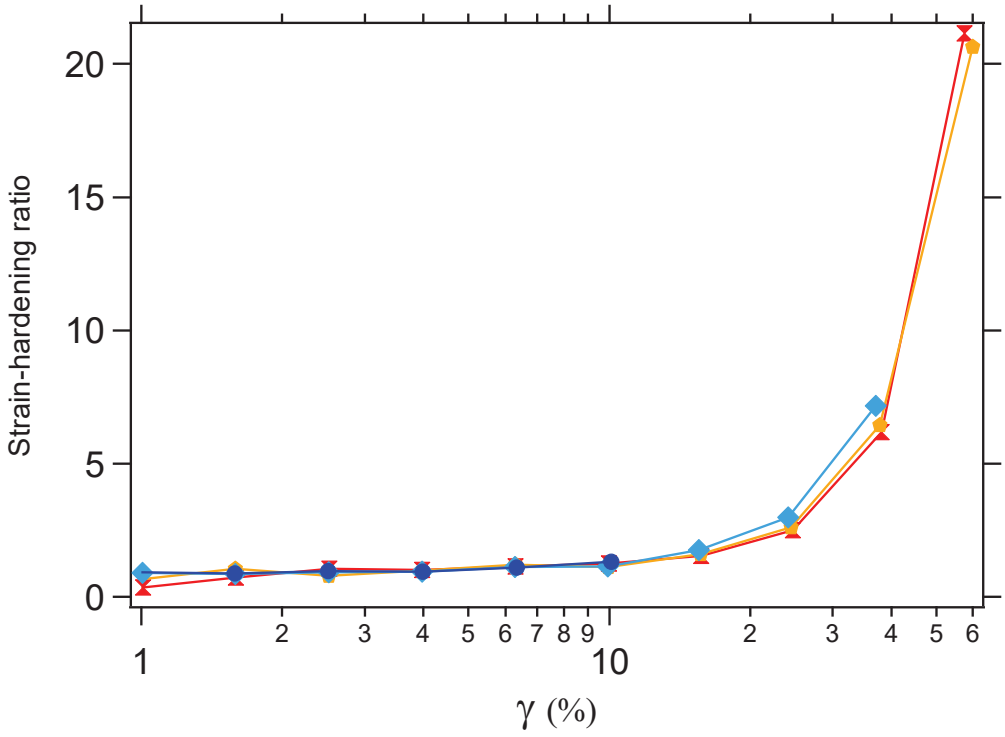


Figure 131 Evolution of the strain-hardening ratio as a function of the strain amplitude for P(VDF-co-HFP) – 2-heptanone gels with different fractions of copolymer: $X_{P(VDF\text{-}co\text{-}HFP)}$=6wt% (red ⧗), $X_{P(VDF\text{-}co\text{-}HFP)}$=7wt% (orange ⬟), $X_{P(VDF\text{-}co\text{-}HFP)}$=8wt% (light blue ◆) and $X_{P(VDF\text{-}co\text{-}HFP)}$=10wt% (blue ●)

The Figure 132 presents a possible mechanism of the restructuration of the gel under an increase of the strain amplitude during the upwards ramp of a LAOS experiment. In the LVE region (for strain amplitude lower than 10%), we assumed in the Chapter 3 that gels may be organized into solvent-rich and polymer-rich regions. In the polymer-rich zones, a polymer network would exist and polymer chains would be cross-linked by physical junction points that are crystallites. When a deformation is applied in a nonlinear transient regime (for 10%<γ<50%), the structure of the material evolves while remaining at the gel state. When the strain amplitude continues to increase the gel softens and shows directly a liquid-like response (for γ>100%). It would suggest that the polymer-rich network breaks inducing a gel-sol transition. Moreover, as shown in Figure 115, when high strain amplitude is removed after the upwards ramps the solution turns back to a gel state quasi immediately and the

initial elastic modulus is fully recovered, suggesting that the same polymer network is reformed. Therefore, we may speculate that when the gel is submitted to oscillations of large amplitude the polymer-rich network (characteristic to the gel state) breaks into a heterogeneous system constituted of smaller polymer-rich zones (liquid state). These polymer-rich zones can connect instantaneously and lead to the formation of the polymer network and thus the gelation of the material. This very fast gelation suggests that the junction points (crystallites) do not break. Thus it is possible to assess that the application of large strain amplitudes on the material will not have the same effect than temperature: the increase of temperature leading to a gel-sol transition due to the breakage of crystalline zones. Finally, the recovery of the initial elastic modulus after the downwards ramp suggests that exactly the same material is formed (same fraction of physical junction point, same polymer-rich network).

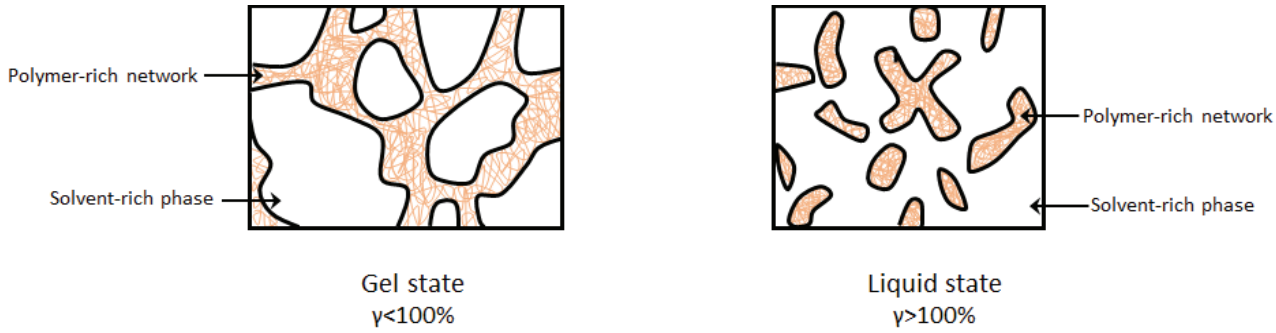


Figure 132 Schematic representation of the restructuration of P(VDF-co-HFP) – 2-heptanone gels during LAOS experiment.

Finally, we show that the incorporation of silica fillers in the gel induces strain-softening and inhibits strain-hardening: the elastic modulus decreases with the strain amplitude. Moreover, the elastic moduli in the linear region are lower than in those of unfilled polymer gels, whereas it is generally considered that the addition of fillers would reinforce the materials. This difference could be explained by the dispersion state of silica within the polymer gel matrix but to date it is difficult to understand why the addition of silica nanoparticles do not lead to an increase of the moduli. Moreover, we noticed that after the upwards ramp of LAOS, the solution gels instantaneously once high strain amplitude are removed, as for unfilled polymer gels. We also shown that during the time sweep measurements after the upwards ramp, the viscoelastic moduli keep increasing with time and a final value of elastic modulus higher than the initial one is recovered. We may suppose that the upwards strain sweep ramp has probably completely broken the silica network (fractal aggregate, repulsive colloid…). Once high strain amplitudes are removed, the gel is reformed instantly (regardless of the presence of silica nanoparticles, as assumed in Chapter 4) but its structure continues to evolve with time. It may be thought that the LAOS experiment leads to the formation of a gel with a different structure and more particularly a restructuration of the silica network which requires longer evolution time.

5.4. Conclusions

In this chapter the nonlinear properties of P(VDF-co-HFP) – 2-heptanone physical gels were studied and more particularly the influence of the concentration of copolymer and the presence of silica nanoparticles. To our knowledge, the complex non-linear rheological properties of a VDF-copolymer in the gel state have not been studied yet. We observed very different types of behavior depending

on the studied systems, binary (P(VDF-co-HFP) – solvent) or ternary (P(VDF-co-HFP) – silica – solvent) gels.

In the case of binary gels, the systems stiffen as they are strained. Strain-hardening (for concentration between 6 and 10wt% of copolymer) is observed and starts to appear around 50% of deformation. It appears that the degree of strain hardening does not depend on the concentration (as shown in Figure 131). This phenomenon may be attributed to the reorganization of the polymer chains which align as the strain amplitude increases. Above a limit strain amplitude $\gamma \approx 100\%$ binary P(VDF-co-HFP) gels exhibit a liquid-like response suggesting that the polymer-rich phase is broken up or slippage occurs at the surfaces. However, when the high strain amplitude is removed, the solution turns back immediately to a gel which suggests that the structure of the material was not completely destroyed by the large amplitude shear. The continuous polymer network containing crystallites may be broken but a heterogeneous solution (polymer-rich domains) still exist which favors subsequent fast gelation as continuity builds again. In order to verify these hypotheses, it would be interesting to combine LAOS measurements with another experiment such as SAXS or NMR. Finally, LAOS experiment from high strain amplitude (500%) to low strain amplitude (0.01%) was performed to study the reversibility of the test and our material. We found a total recovery of the viscoelastic moduli, which suggests that the initial microstructure was essentially recovered.

Ternary gels filled with silica nanoparticles were studied. The addition of nanoparticles does not increase the viscoelastic moduli of the gels, which may be due to the fact that there is no interaction between the nanoparticles and the polymer. As a consequence, an independent silica network could be formed and it could lead to a more fragile material. The addition of silica nanoparticles also inhibits the strain-hardening phenomenon observed in binary gels and leads to strain softening. The gel-sol transition appears at lower strain amplitude ($\gamma \approx 1\%$) than in binary gels. In the same way as in binary gels, once the large amplitude shear has been remove, the filled polymer solution turns back to gel immediately. As for binary gels, maybe the complete structure of the gel may not have been completely destroyed. However, another difference was noticed in the linear domain after the LAOS measurement: more time is necessary to find levels of moduli equivalent to those determined previously in the linear region. This assumes that LAOS may have completely broken a possible nanoparticles network and back in the linear regime a new structure of the silica network that requires longer formation time, leading to a history-dependent, rheopectic-like behavior. Finally, during the downwards LAOS test, higher moduli are recovered. It induces the modification of the microstructure of the gels which become more rigid than initially, which again is coherent with a rheopectic behavior. We show that for binary gel the same microstructure was recovered. As a consequence, it is possible to assume that in the case of filled gels the increase of the moduli would come from the formation of a more rigid silica network and not from the formation of new polymer rigid zones.

Chapter 6: P(VDF-co-HFP) – silica hybrid membranes

This chapter deals with the development of P(VDF-co-HFP) – silica nanocomposite films by solvent route. Combination of structural (SEM and USAXS experiments) and mechanical (tensile tests on films) characterizations was used to study the influence of the surface functionalization, dispersion and concentration of silica nanoparticles on the properties of the final materials.

6.1. Results 160

6.1.1. Influence of the process on the structure of P(VDF-co-HFP) – silica membranes 160

6.1.2. Impact of the dispersion and process on the mechanical properties 166

6.2. General discussion 167

6.2.1. Possible relations between the dispersion state of silica at the gels and in the films 167

6.2.2. Origin of the different mechanical properties 174

6.3. Conclusions 175

6. P(VDF-co-HFP) – silica hybrid membranes

In the previous chapters, attention was focused on the understanding of the gelation mechanisms and gel structure of P(VDF-co-HFP) – MEK or 2-heptanone hybrid thermoreversible organogels filled with silica nanoparticles. It was observed that the gelation kinetics is strongly impacted by the nature of the solvent and the presence of silica. These materials can represent an advantage for the processing of hybrid membranes by solvent casting because of their thermoreversible nature and their stability over time.

In this context the P(VDF-co-HFP) hybrid gels were subsequently used for the development of P(VDF-co-HFP) – silica hybrid membranes by solvent casting. However, the stability and performance of these membranes are related to the processing and formulation of the materials. The experimental protocol to realize materials by solvent casting with a finely controlled microstructure was detailed in chapter 2. In this chapter the influence of the concentration and dispersion state of fillers on the structure and on the electrical and mechanical properties is studied. Three systems of P(VDF-co-HFP) – silica have been investigated with different sources of silica: (i) silica solution in MEK developed by phase transfer, (ii) MEK-ST-L silica solution supplied from Nissan and (iii) Nissan silica solution transferred in 2-heptanone. This allows us to determine the impact of the surface functionalization and the dispersion of nanoparticles on the properties of the final materials.

Structural observations were carried out for characterizing the dispersion of silica in the polymer matrix by SEM or USAXS. Finally, the mechanical performance was evaluated with tensile strength tests.

We demonstrate in this chapter that the process strongly impacts the microstructure of the materials and their final properties. This work opens the path to the generation of functional materials with finely controlled microstructure and enhanced performances by solvent casting or printing.

6.1. Results

As a reminder, P(VDF-co-HFP) – silica films are prepared by dissolving an appropriate amount of copolymer in the silica solution to reach the desired concentration of silica in the film. The solution is stirred at 60°C (in MEK) or 80°C in (2-heptanone) under reflux for 2.5 hours. Once the solutions are prepared the films are cast on a glass substrate and dried in the fume hood at room temperature and then in vacuum oven at 60°C (for MEK) or 80°C (for 2-heptanone). TGA experiments were performed on the final materials to prove that no solvent residues are present in the film.

6.1.1. Influence of the process on the structure of P(VDF-co-HFP) – silica membranes

SEM and USAXS were used to characterize the microstructure of nanocomposites film and more particularly the dispersion state of silica nanoparticles within the polymer matrix.

Table 8 SEM micrographs of P(VDF-co-HFP) films surface of the different systems

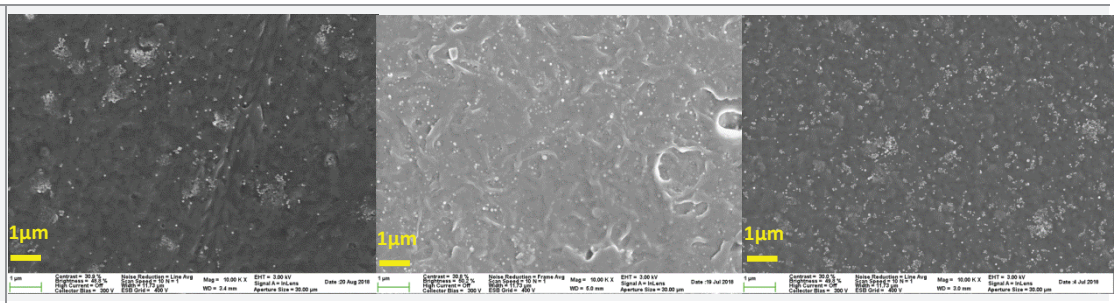
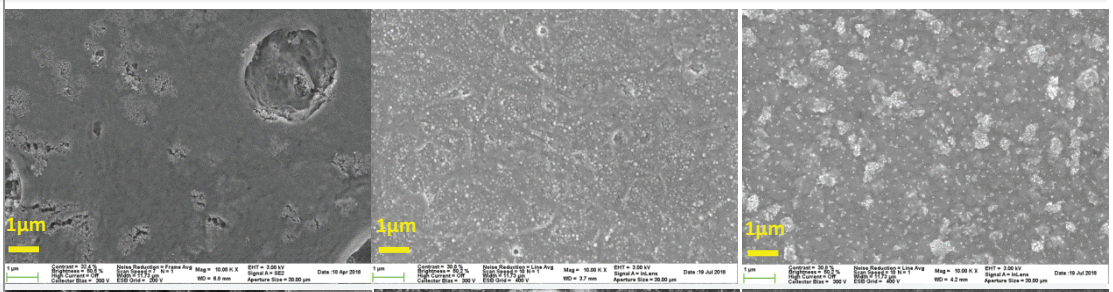
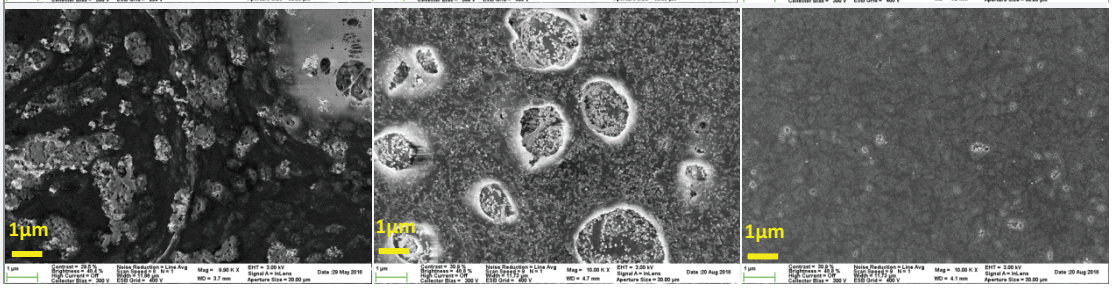
[SILICA]	FROM SILICA IN MEK (BY PHASE TRANSFER)	FROM MEK-ST-L (NISSAN)	FROM SILICA IN 2-HEPTANONE (NISSAN)
5WT.%			
20WT.%			
40WT.%			

Table 8 represents the SEM micrographs of our three systems at various concentrations. The air and glass surfaces of the film were observed for each system at various concentrations from 5wt% to 40wt% of silica nanoparticles. It appears that three different and controlled dispersion states are obtained. It is obvious that the films prepared with the MEK-ST-L solution show the best dispersion of silica nanoparticles up to high concentration of nanoparticles (40wt%). Well-dispersed and well-distributed materials are obtained from this source of silica, even though some surface defects (surface cavities corresponding to bubbles) are observed, which can be eliminated by annealing the films. In the case of films prepared with the solution of silica in 2-heptanone, well-distributed aggregates are present certainly meaning that the solvent exchange from MEK to 2-heptanone destabilizes the dispersion state of the nanoparticles to some extent, as was shown in chapter 4. Finally, an interesting dispersion state of silica was obtained from the solution of silica in MEK developed by phase transfer. Aggregates of silica are also formed in this case and the morphology consists in porous aggregates (cavities). These aggregates differ from the aggregates formed with the silica solution in 2-heptanone. Here the aggregates are real pores surrounded by silica nanoparticles at the interface where the polymer does not apparently penetrate as shown in Figure 133.

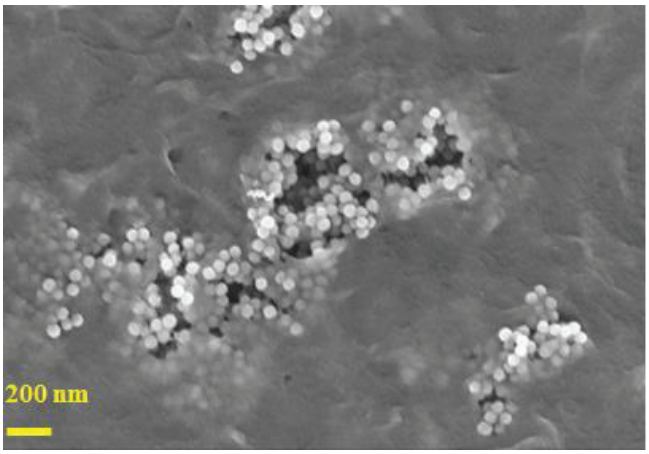


Figure 133 SEM micrograph of P(VDF-co-HFP) - silica film (20wt% of silica, from silica solution in MEK by phase transfer)

In order to better characterize the dispersion state of silica nanoparticles in the nanocomposites, USAXS experiments were also performed on both films at various concentrations of silica.

In films prepared from the silica solution in MEK developed by phase transfer, the scattered intensities for P(VDF-co-HFP) – silica nanocomposites with volume fractions of silica between 8.25 and 25.75 vol% are shown in

Figure 134. We can notice a strong increase of the intensity at low q values, indicating the aggregation of silica nanoparticles in the films, as already observed in SEM micrographs. Note that the scattered intensity curves corresponding to the fraction of silica ϕ_{SiO2}=8.25vol% is slightly lower than the two other curves. In fact, for the preparation of this film another batch of aqueous silica solution (and thus organic silica solution in MEK) was used and the size of the silica particles certainly varies from one batch to another, inducing a difference on the USAXS experimental curves. The scattering curve in the q-range between about 0.005 and 0.055nm^{-1} can be described by a power law $Aq^{-2.4}$, corresponding to the scattering by fractal aggregates (Baeza, Genix et al. 2013, Baeza, Genix et al. 2014). Moreover, the prefactor A decreases when the fraction of silica increases (more especially for ϕ_{SiO2}=16.82vol% and ϕ_{SiO2}=25.75vol%), as described by Baeza et al.. At the beginning of the fractal regime, at q=0.055 nm^{-1}, a distance between particles around 200nm was found. It corresponds to the width of the cavities observed in SEM micrographs. Moreover, at the maximum between the two regimes (slope q^{-4} and $q^{-2.4}$), at q=0.119nm^{-1}, a distance between particles is found to be around 52.36nm which is approximately twice the radius of a silica particles. It indicates and validates that silica nanoparticles are in contact.

In comparison hybrid films prepared with the P(VDF-co-HFP) – silica Nissan – MEK and 2-heptanone were studied with various fractions of silica, scattering spectra are respectively displayed in Figure 135 and Figure 136. In films prepared from silica solution in MEK, the scattered intensity increases slightly at low q in comparison with the previous materials: silica particles do not (or little) aggregates even at high fraction of silica. This confirms the microscopy observations showing well-dispersed systems. In addition, when the concentration of silica nanoparticles in the nanocomposite increases, the distance between silica particles decreases from 94.65nm to 62.65nm approximately. This distance is (much) larger than the average diameter of the silica particles (around 46.3nm) meaning that there is no (or little) contact between the particles. Nanoparticles remain well-dispersed even at high fractions of silica, as shown in SEM micrographs.

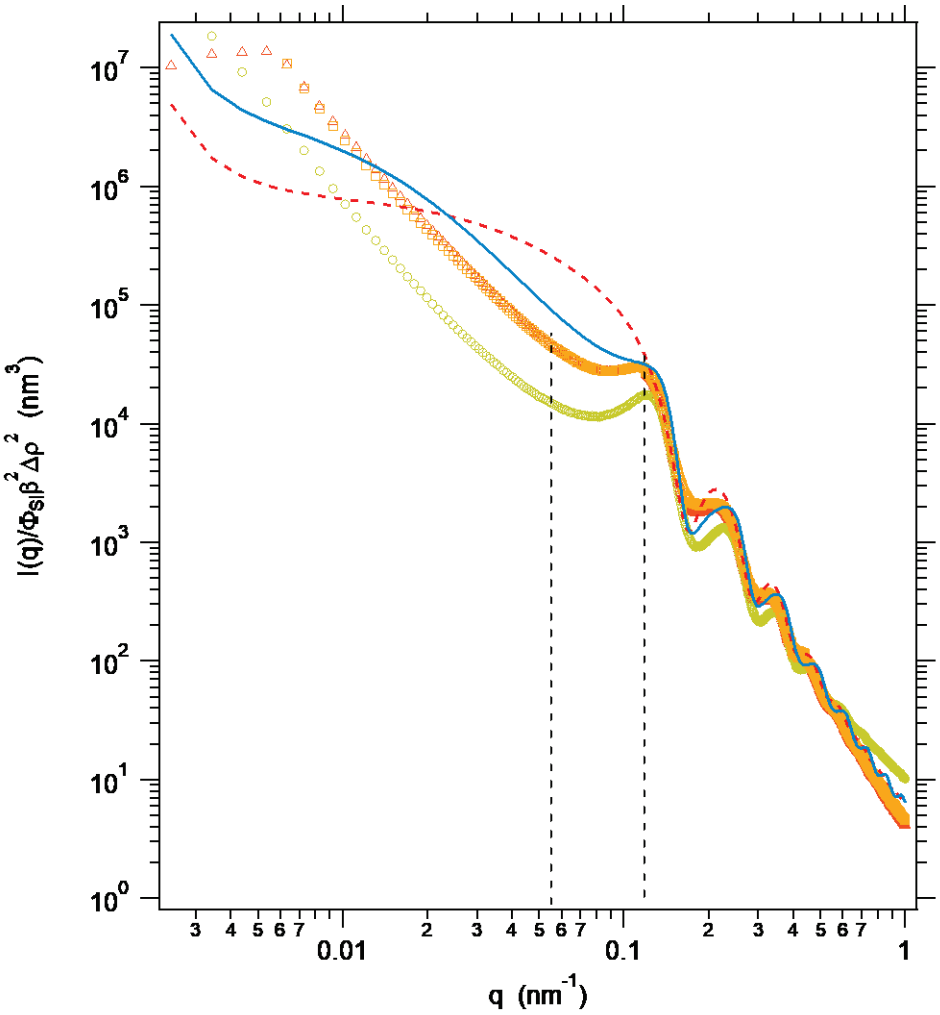


Figure 134 Normalized USAXS scattered intensities of P(VDF-co-HFP) – silica (developed by phase transfer) nanocomposites containing different fractions of silica: 8.25vol% (green ○), 16.82vol% (orange □) and 25.75vol% (red △)

The curves were fitted using hard sphere form factor and the interparticle structure factor was calculated for a hard sphere fluid with a narrow attractive well, using a perturbative solution of the Percus-Yevick closure which is adequate for attractive interparticle potential (Percus and Yevick 1958). The returned value is a dimensionless structure factor, S(q). The strength of the attractive well is described in terms of "stickiness" as defined below (Menon, Manohar et al. 1991).The interaction potential *U* (*r*) is defined as:

$$U(r) = \begin{cases} \infty, r < \sigma_{int} \\ U_0, \sigma_{int} \leq r \leq \sigma_{int} + \Delta \\ 0, r \geq \sigma_{int} + \Delta \end{cases} \quad (45)$$

with Δ, the width of the square well, U_0 the depth of the well (in k_BT units) and σ_{int} the hard sphere diameter $\sigma_{int} = 2R$. The stickiness τ_{int} is defined as:

$$\tau_{int} = \frac{1}{12\epsilon_p}\exp(U_o/k_BT) \quad (46)$$

$$\epsilon_p = \frac{\Delta}{\sigma_{int} + \Delta} \quad (47)$$

with ε_p, the perturbation factor. U_0 is negative for an attractive potential, positive for a repulsive potential. From this definition it is clear that smaller values of τ_{int} will mean stronger attraction.

Finally, films prepared with Nissan silica solution in 2-heptanone were studied with silica fractions ϕ_{SiO2}=4.08 and 8.25vol%. Depending on the concentration of silica, the distribution of silica in the films is different. At low q, the scattering spectra of membranes prepared from the Nissan silica solution in 2-heptanone are higher than those of the films prepared with the Nissan silica solution in MEK. It indicates that silica aggregates exist in the films and have a bigger size. At ϕ_{SiO2}=4.08vol% the nanocomposite is relatively well dispersed even if some aggregates exist (see microscopy in Table 8). By increasing the silica content by a factor 2, a change in slope is observed at q=0.12nm^{-1}, which corresponds to a distance of 52.35nm, ie approximately the size of the silica particles meaning that silica particles are in contact. A low q (q<0.12nm^{-1}), the slope of the scattering spectra is -2.4 validating the existence of fractal-type aggregates (Baeza, Genix et al. 2013).

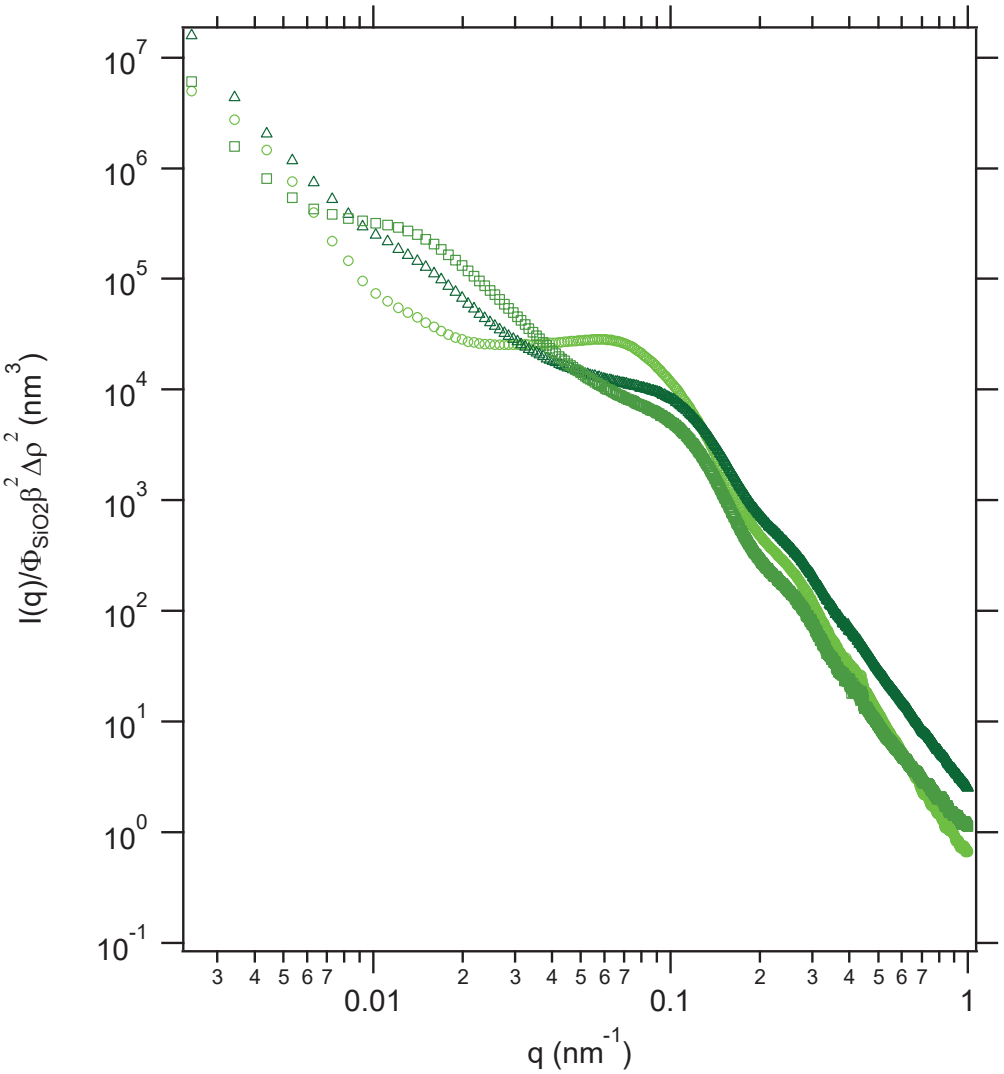


Figure 135 Reduced USAXS scattered intensities of P(VDF-co-HFP) – silica (from Nissan silica solution in MEK) nanocomposites containing different fractions of silica: 12.49vol% (light green ○), 16.82vol% (green □) and 25.75vol% (dark green △).

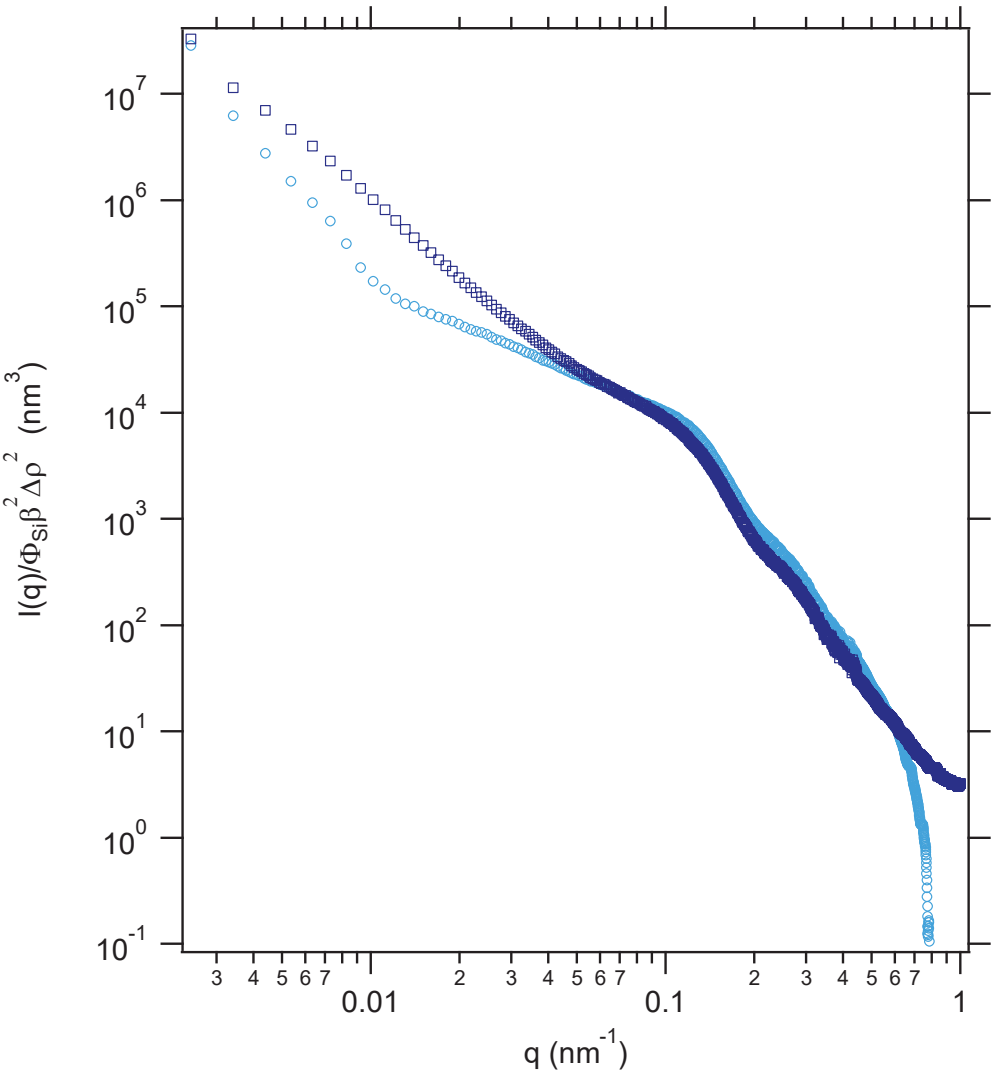


Figure 136 Reduced USAXS scattered intensities of P(VDF-co-HFP) – silica (from Nissan silica solution in 2-heptanone) nanocomposites containing different fractions of silica: 4.08vol% (blue ○), 8.25vol% (dark blue □)

We were able to develop three finely and controlled silica distribution in P(VDF-co-HFP) up to 40wt% of silica. Aggregated and heterogeneous (porous) materials with localized filler particles comprised at the interface of cavities were formed from the silica solution in MEK developed by phase transfer. In addition, other sources of silica were used to develop films. Silica particles solution in MEK supplied by Nissan dispersed in P(VDF-co-HFP) generates well distributed homogeneous films. On the contrary, when this solution is transferred in 2-heptanone, P(VDF-co-HFP) – silica films prepared from this solution present the formation of clusters of silica particles and therefore aggregated homogeneous films. We show here that the dispersion of silica nanoparticles within the polymer matrix strongly depends on the process and on the silica – solvent interactions.

As a consequence, it would be interesting to compare the properties of these different materials as a function of the concentration of silica nanoparticles and more especially the electrical and mechanical performances.

6.1.2. Impact of the dispersion and process on the mechanical properties

The incorporation of inorganic fillers in a polymer is supposed to affect the mechanical properties of the materials. Nanoparticles are usually more rigid than the polymer matrix and as a consequence the addition of nanoparticles should enhance the stiffness of the system. In this context the mechanical properties of P(VDF-co-HFP) – silica nanocomposites as a function of the concentration of silica and the distribution state of silica from both solutions were studied.

Tensile strength tests were carried out to characterize the Young's modulus and the yield stress of the studied samples. It is clear from Figure 137 that the dispersion state of silica and the microstructure of the nanocomposite strongly impact the Young's modulus of the material. Indeed, for porous films, the addition of nanoparticles only slightly reinforces the material while for homogeneous films (from Nissan silica solutions in MEK or in 2-heptanone), the Young's modulus increases a lot with the incorporation of nanoparticles.

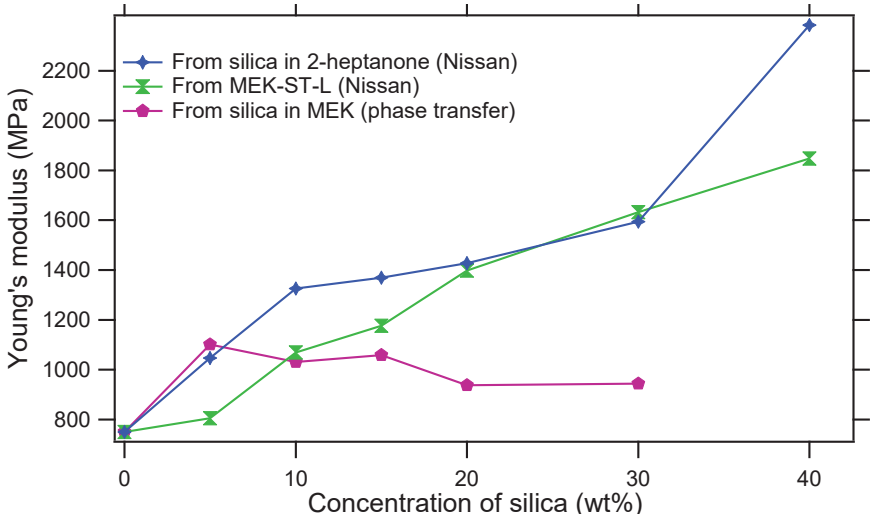


Figure 137 Young's modulus of P(VDF-co-HFP) - silica films as a function of the concentration of silica from (✦) 2-heptanone silica solution (Nissan) (⧗) MEK-ST-L (Nissan) (⬟) silica solution in MEK (by phase transfer)

In addition to Young's modulus measurements, it was possible to determine the yield stress of the different materials as a function of the fraction of filler. Experimental data are displayed in Figure 138 and the same conclusions than for the Young's modulus can be done. The yields stresses of the materials are strongly influenced by the fraction of fillers and of course by their dispersion state and the inhomogeneities (cavities). Indeed, in the case of porous materials, the yield stress slightly increases at 5 wt% and then it decreases by a factor two. This is certainly due to the porous structure of the film and to the fact that interactions between silica particles and the polymer are weak. For aggregated films the yield stress increases up to 10 wt% of silica and it then decreases with the concentration. Finally, in homogeneous and well-dispersed films, the evolution of the yield stress with the concentration is similar to the films made from silica solution in 2-heptanone, but the maximum of yield stress is reached at 20 wt%. This difference between the two systems may be related to the different dispersion states of silica.

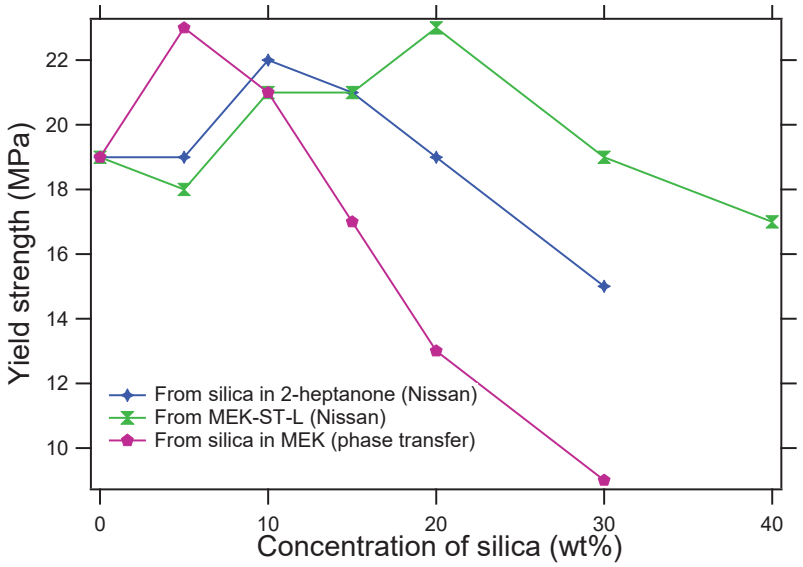


Figure 138 Yield strength of P(VDF-co-HFP) - silica films as a function of the concentration of silica from (✦) 2-heptanone silica solution (Nissan) (⧗) MEK-ST-L (Nissan) (⬟) silica solution in MEK (by phase transfer)

Finally, the elongation at break and the fracture energy of nanocomposites were determined. These measurements are effective tools to characterize the toughness of the materials. Only the image of the rupture profiles will be presented in Figure 139. Materials show different rupture profile depending on the concentration and distribution of fillers. In porous films (from silica solution in MEK prepared by phase transfer, Figure 139-a), samples show ductile profiles up to 40 wt% of silica. In well distributed and homogeneous films (Nissan silica solution in MEK, Figure 139-b) the profiles are ductile at least up to 15 wt% of silica while in aggregated and heterogeneous (Nissan silica solution in 2-heptanone, Figure 139-c), the materials present fragile failure at each concentration of silica.

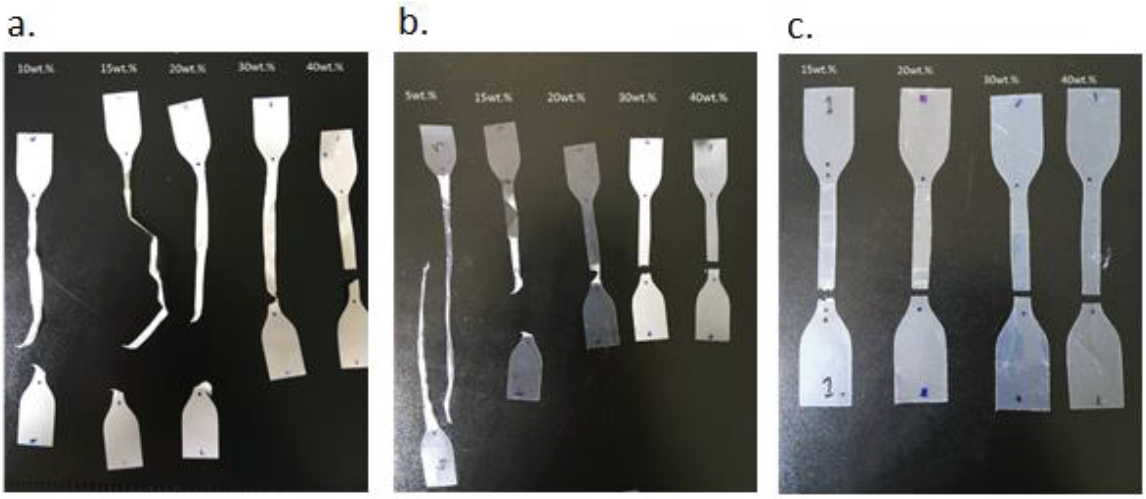


Figure 139 Samples after mechanical tensile test obtained with the three approaches (a) silica in MEK prepared by phase transfer (b) MEK-ST-L (Nissan) and (c) silica in 2-heptanone (Nissan)

6.2. General discussion

6.2.1. Possible relations between the dispersion state of silica at the gels and in the films

We have studied the dispersion of silica nanoparticles in P(VDF-co-HFP) – silica – solvent gels and P(VDF-co-HFP) – silica films by USAXS measurements, in order to possibly relate the dispersion states

of silica in these two materials. For this purpose, we have compared the scattering spectra of gels and films.

We started with materials formulated from the **silica solution in MEK developed in the lab by phase transfer**. We have observed the existence of cavities surrounded by silica nanoparticles in the films. It therefore appears necessary to understand the mechanism of formation of these cavities. From the study of the MEK-water phase diagram by Siegelman et al. (Siegelman and Sorum 1960), we may assume that 15 wt% of water is present in the silica – MEK organic solution. This presence of water may certainly impact the dispersion of the nanoparticles in solution or in the polymer matrices. Three hypotheses may be proposed for the mechanism of formation of porous materials, as schematized in Figure 140:

a) Water nanodroplets surrounded by silica nanoparticles ("micelle" type aggregates) would be formed in solution directly after the phase transfer. Indeed, after the phase transfer step, the silica is still partially hydrophilic since only 18.4% of the silanols are functionalization by CTAB. These aggregates shall then be preserved during the formulation of gels and the realization of films.
b) "Micelle" type aggregates might be formed when the polymer is added to the organic silica solution. It would exclude the fraction of water present in the solution, the polymer being hydrophobic. These aggregates shall then be preserved during the preparation of the films
c) The formation of aggregates would occur during the drying step (solvent evaporation, after the solvent casting of the polymer – silica solution). Indeed, MEK is more volatile than water and will evaporate faster, as a consequence the concentration of MEK decreases during the drying of the material and the composition of the system changes. A phase separation then takes place: silica particles could aggregate around the water-rich phase and the polymer will be excluded from this phase (due to its hydrophobicity). In a second step the water evaporates and cavities are formed.

Hypothesis a) seems to be unlikely for two reasons: first, we estimated that all the silica particles are effectively transferred to MEK, which indicates that, even though they are not fully covered with CTAB, silica particles are hydrophobic enough not to accumulate at the interface with water. Second, USAXS tests on silica solutions in MEK showed homogeneous and well dispersed solutions (see Figure 94 page 116).



Figure 140 Schematization of the possible mechanisms leading to the formation of porous films

Figure 141 compares the scattering spectra of P(VDF-co-HFP) – silica – MEK gels and P(VDF-co-HFP) – silica films. The curves overlap almost perfectly, which indicates that the structures which are formed should be similar. As detailed in Chapter 4, the addition of copolymer to the silica solution leads to the formation of fractal aggregates, with a scattering curve described by a power law $Aq^{-2.4}$ at low q and a center-to-center distance between particles around 52nm, i.e. particles in close contact. Nearly the same features are measured in the films. Thus the same types of objects are present in the gel state and in the films.

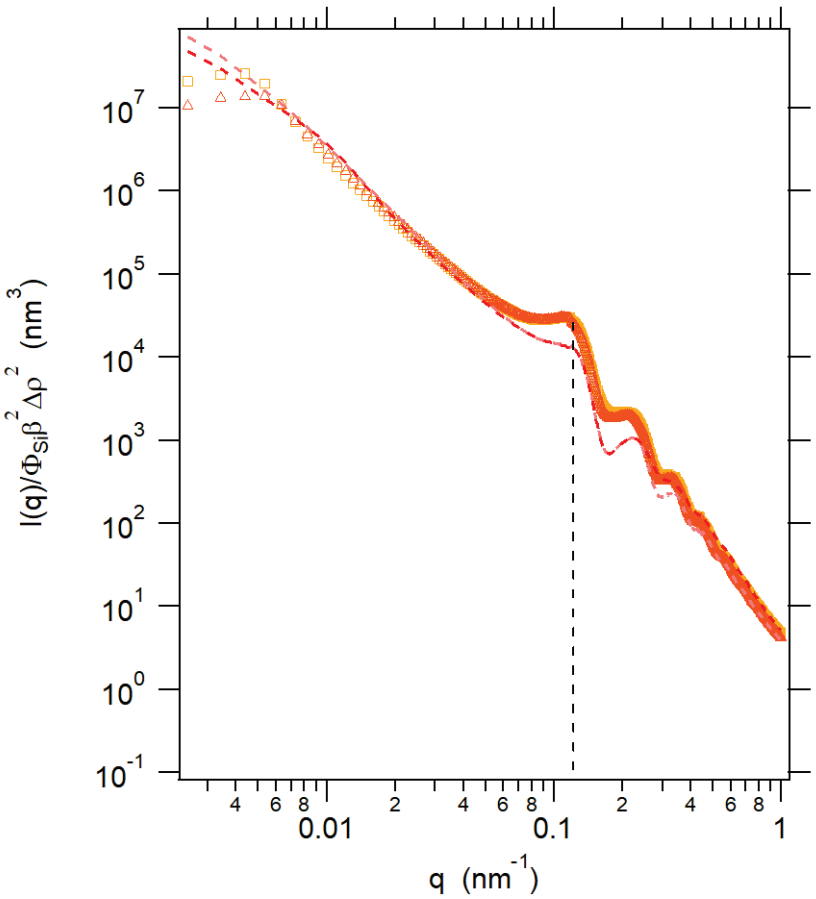


Figure 141 USAXS scattered intensity (normalized with the fraction of silica and $\beta^2\Delta\rho^2$) of P(VDF-co-HFP) – silica – MEK gels (ϕ_{SiO2}=1.6vol% with $X_{P(VDF\text{-}co\text{-}HFP)}$=20wt% in pink – and $X_{P(VDF\text{-}co\text{-}HFP)}$=25wt% in red –) and P(VDF-co-HFP) – silica films (ϕ_{SiO2}=16.82vol% orange □ and ϕ_{SiO2}=25.75vol% brown △) prepared from the silica solution in MEK developed by phase transfer.

From these results it is very likely that the objects observed in the polymer films already exist in the P(VDF-co-HFP) – silica – MEK gels. Electron microscopy performed on films have shown that these aggregates are cavities with silica particles located at the polymer – air interface. This allows us to confirm that micelle-like aggregates probably exist in the gel state. Therefore the mechanism responsible of the formation of porous material may be mechanism (b) as schematized in Figure 142. Therefore, in organic solution in MEK (which contains 15 wt% of water) the silica nanoparticles are relatively well-dispersed, while in ternary systems core-shell aggregates are formed, which correspond to water droplets surrounded by silica wherein the copolymer does not penetrate. Finally, in the films, MEK and water evaporate leading to cavities about 200nm wide surrounded by silica nanoparticles.

We have thus been able, in the case of organic silica solution developed in the laboratory by phase transfer, to relate the dispersion state of silica in the gel state with the one in the films. The porous structure of the hybrid films would be explained by the existence of micelle-like aggregates in the gel state.

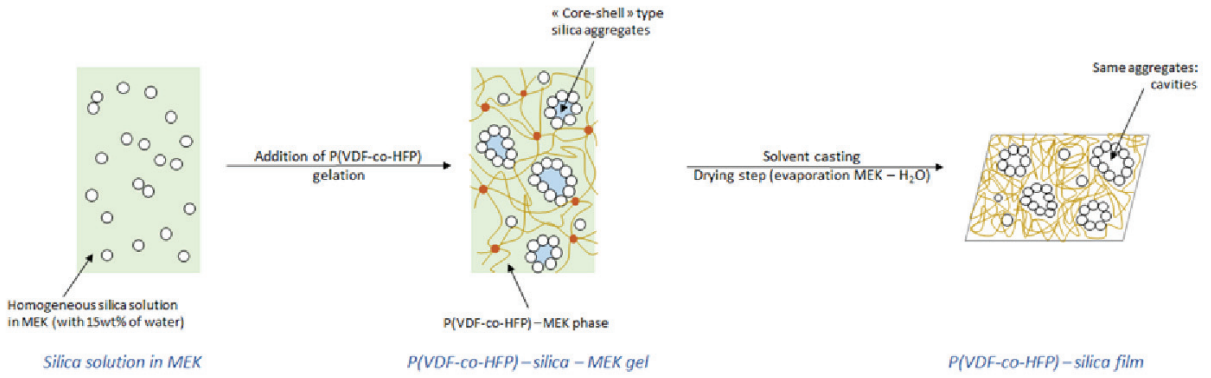


Figure 142 Schematization of the possible mechanism involved in the formation of P(VDF-co-HFP) – silica (developed by phase transfer in MEK) porous films

In a second step we have compared the materials made from the **Nissan silica solution in MEK**. In the organic solution the silica nanoparticles repel each other, with a relatively large average center-to-center distance (see page 119). When ternary systems (solutions or gels) were formulated by adding polymer to the silica solution, we found a difference between the gel state and the liquid state. In gels a possible aggregation of nanoparticles was found. Conversely, in the liquid state, the nanoparticles remained well dispersed. Films are prepared from a P(VDF-co-HFP) – silica – solvent systems in the liquid state, i.e. relatively well dispersed. Figure 143 compares the scattering spectra of a P(VDF-co-HFP) – silica – MEK solution with 1.6vol% of silica and 11wt% of copolymer, and hybrid films with silica fractions between 12.49vol% and 25.75vol%. In hybrid films the center-to-center distance between particles decreases when the concentration of nanoparticles increases. Moreover, this distance in the films decreases compared to a copolymer – silica solution in MEK. This suggests that during the drying of the material the distance between particles decreases but remains larger than the particle diameter, indicating that the nanoparticles do not (or very little) touch each other and do not form aggregates. Therefore, in the case of Nissan silica solution in MEK, the dispersion state of the polymer – silica solution can also be related to the dispersion in the films. A good dispersion state in solution leads to good dispersion of silica nanoparticles in the hybrid films.

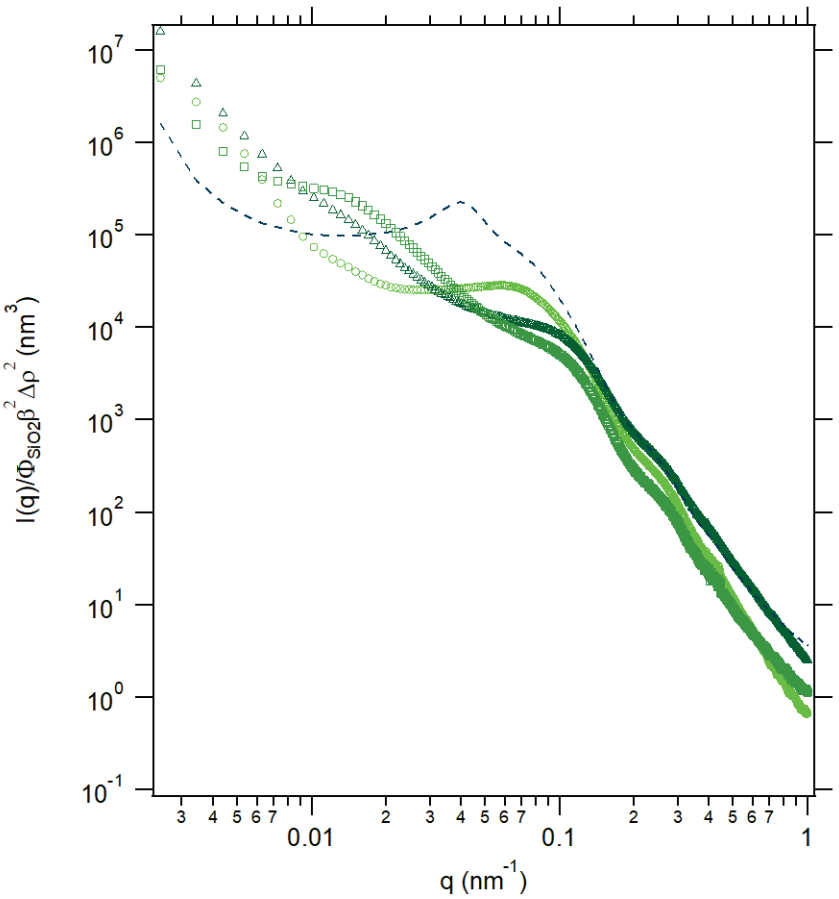


Figure 143 USAXS scattered intensity (normalized with the fraction of silica and $\beta^2\Delta\rho^2$) of P(VDF-co-HFP) – silica – MEK solution (ϕ_{SiO2}=1.6vol% with $X_{P(VDF\text{-}co\text{-}HFP)}$=11wt% in blue –) and P(VDF-co-HFP) – silica films (ϕ_{SiO2}=12.49vol% light green ○, ϕ_{SiO2}=16.82vol% green □ and ϕ_{SiO2}=25.75vol% dark green △) prepared from the Nissan silica solution in MEK.

Finally, the case of materials filled with **Nissan silica solution in 2-heptanone** is more complex. The organic silica solution was prepared by solvent exchange and we noticed that this step does not (or slightly) change the dispersion state of the nanoparticles. Particles still repel each other, with a large average center-to-center distance. Figure 144 summarizes the scattered intensity of ternary gels with ϕ_{SiO2} = 1.6vol% and 7wt%, 11wt% and 20wt% of copolymer, and hybrid films with 4.08 vol% and 8.25 vol% of silica nanoparticles. Scattering curves were less reproducible in this case, showing either relatively well dispersed or more aggregated structures. In films, beyond a certain concentration of copolymer we observed dispersed fractal aggregates by electron microscopy.

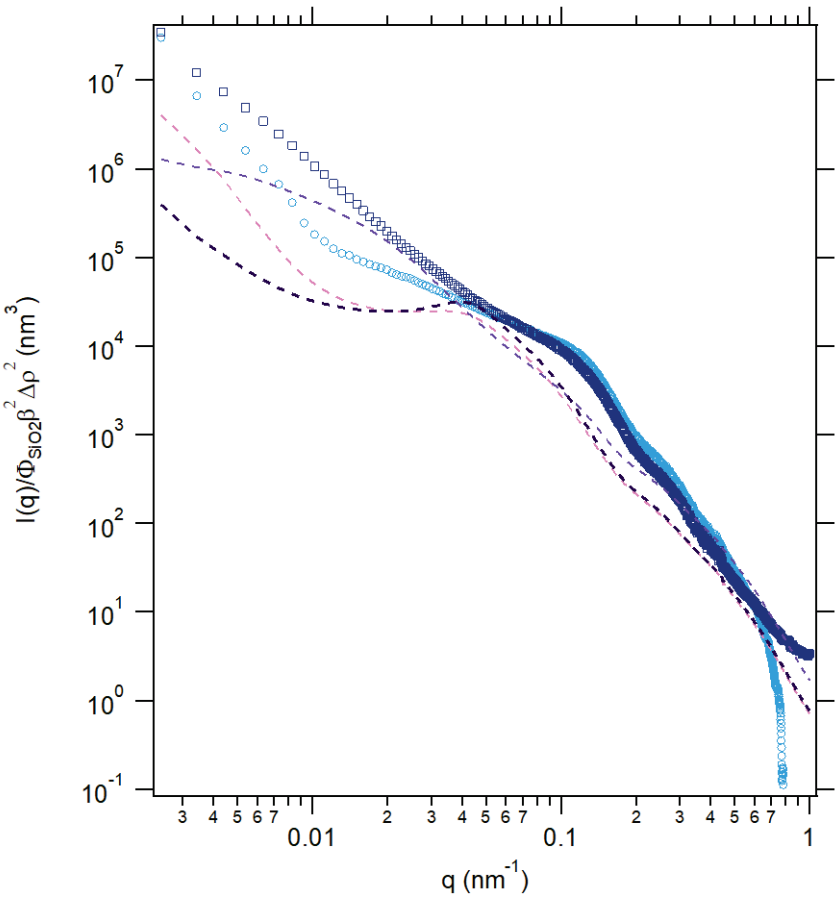


Figure 144 USAXS scattered intensity (normalized with the fraction of silica and $\beta^2\Delta\rho^2$) of P(VDF-co-HFP) – silica – 2-heptanone gels (ϕ_{SiO2}=1.6vol% with $X_{P(VDF\text{-}co\text{-}HFP)}$=7wt% in pink –, $X_{P(VDF\text{-}co\text{-}HFP)}$=11wt% in violet – and $X_{P(VDF\text{-}co\text{-}HFP)}$=20wt% in dark –) and P(VDF-co-HFP) – silica films (ϕ_{SiO2}=4.08vol% blue ○, ϕ_{SiO2}=8.25vol% dark blue □) prepared from the Nissan silica solution in 2-heptanone

Jouault et al. (Jouault, Zhao et al. 2014) have studied the effect of the nature of the solvent on the final dispersion of silica in polymer nanocomposites. Two different theta/good solvents of the studied polymer and nanoparticles were used. In one case the polymer adsorbs on the silica surface and forms a bound layer leading to a good dispersion of silica in the solution and therefore in the dried material. Conversely, in a solvent where the polymer does not adsorb onto the silica surface, large silica aggregates are formed in the solution and thus in the film. Thus the silica dispersion in solution determines the final silica dispersion in the dry nanocomposites and the nature of the solvent plays a critical role. However, aggregation does not always occur in 2-heptanone gels and these aggregates are smaller than in films. As compared with MEK, the nature of the solvent may play a role, but the drying step could perhaps be the main cause of the formation of aggregates. Indeed, as shown in the literature (Sen, Xie et al. 2007, Jouault, Dalmas et al. 2012, Kim, Hyun et al. 2016), the evaporation kinetics of the solvent affects the final dispersion of silica nanoparticles. These authors both show that a fast evaporation of the solvent leads to a good dispersion of silica nanoparticles in the nanocomposites. When copolymer – silica – MEK solutions are cast, the solvent evaporates almost instantly due to its high volatility and a good dispersion of silica nanoparticles is obtained in the material. On the contrary, 2-heptanone is a low volatile solvent. As we used the same drying process as for films made with MEK solutions (drying in fume hood for hours and then in vacuum oven at 80°C for 2hours), the drying of the nanocomposites is much slower in this case, allowing the system to evolve, which can promote the formation of aggregates.

In this case it is difficult to link the dispersion of silica nanoparticles in the gels with the dispersion of silica in the films. It is likely that the process conditions lead to the formation of silica aggregates in the hybrid films and more particularly the solvent evaporation kinetics. This hypothesis should be verified by performing SAXS or SANS tests at different stages of film drying. Also it would be very interesting to dry the cast P(VDF-co-HFP) – silica – 2-heptanone solutions much faster by operating at higher temperature (close to the solvent boiling point), and see if better silica dispersions are obtained. An example would be a fast drying at high temperature like 5 minutes at 120°C.

6.2.2. Origin of the different mechanical properties

Young's moduli were compared with the Guth and Gold and Krieger-Dougherty theoretical models. The Guth and Gold model predicts the Young's modulus of the material as a function of the volume fraction of fillers:

$$E_c(\varphi) = (1 + 2.5\varphi + 14.1\varphi)E_m \tag{48}$$

where E_c and E_m are the Young's moduli of the composite and the polymer matrix respectively and φ is the volume fraction of particles. This equation is valid for rigid particles at relatively low concentration. At higher concentration of fillers, the Krieger-Dougherty model can be used:

$$E_c(\varphi) = E_m\left(1 - \frac{\varphi}{\varphi_m}\right)^{-2.5\varphi_m} \tag{49}$$

Where φ_m is the maximum packing fraction of solid particles, usually around 0.62-0.65 for spheres of uniform diameter.

The Young's moduli of the samples were obtained for the different sources of silica as a function of the concentration of silica nanoparticles and are illustrated in Figure 145.

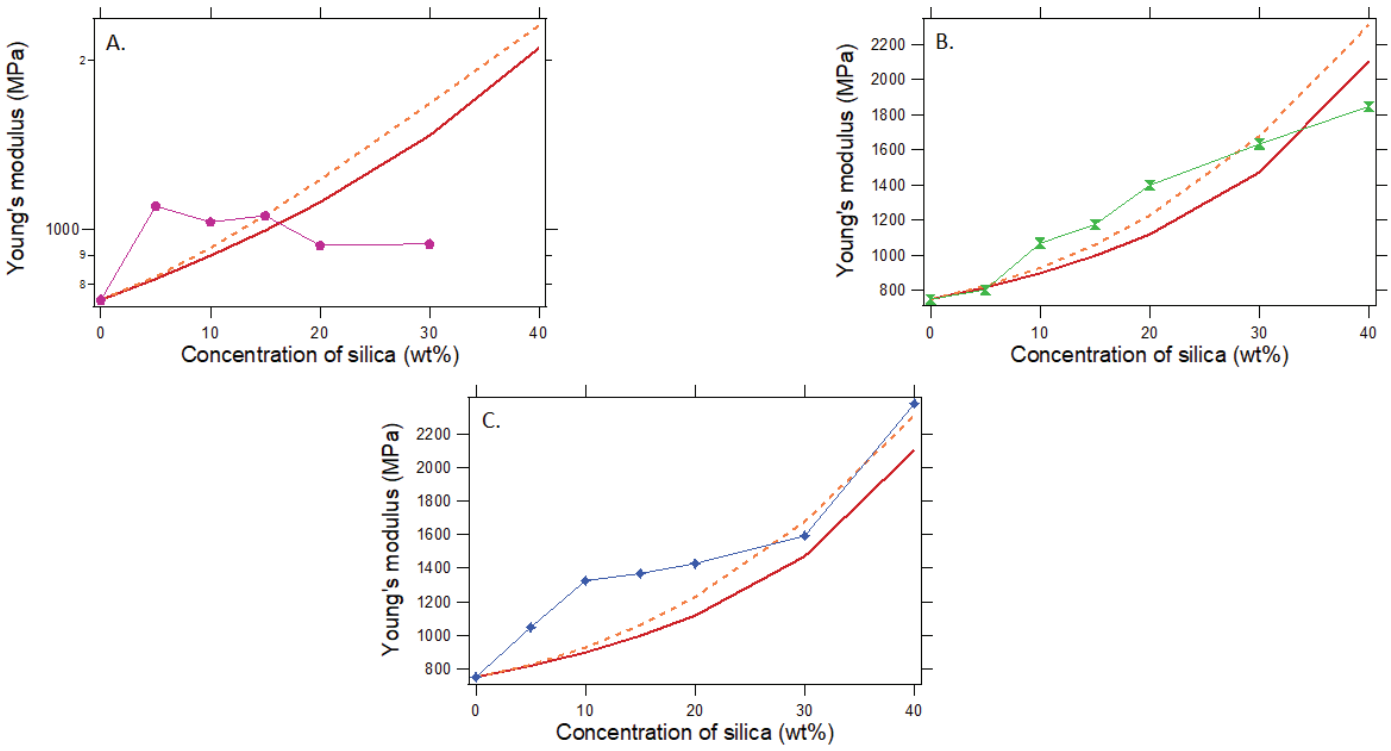


Figure 145 Young's modulus of P(VDF-co-HFP) - silica films as a function of the concentration of silica from (A) silica in MEK prepared by phase transfer (B) MEK-ST-L (Nissan) and (C) silica in 2-heptanone (Nissan). All experimental curves are fitted with K&D model (red —) and G&G model (orange - -)

In materials with defects (Figure 145-a) the Young's modulus increases up to 5wt% of silica and then decreases slightly. This result is not consistent with the models. Combined with the structural information on the films it is possible to observe that the fraction of cavities in the nanocomposites increases with the concentration of fillers and the material becomes more porous. It corresponds to the addition of a soft phase which reduces the stiffness of the materials. The prediction models are not applicable for this system. For example, a film with 40 wt% of silica presents a Young's modulus with more than a two-fold increase (E = 1847 MPa) compared to the pure polymer (E = 750 MPa).

The best dispersion and distribution of silica was reached with the silica solution in MEK from Nissan. The Young's modulus of these films increases quite strongly and in a monotonous way as the silica concentration increases (Figure 145-b). Finally, partially aggregated homogeneous films (from Nissan silica solution in 2-heptanone) were studied. As for the well distributed homogeneous films, the addition of silica nanoparticles strongly increases the modulus of the films. The Young's modulus increases linearly with the amount of silica, from 750 MPa for the pristine matrix to 2500 MPa at 40 wt% of silica (see Figure 145-c).

In these two cases, the increase of the modulus is predicted qualitatively by the Guth and Gold or Krieger & Dougherty models, but the shape of the curve is not well reproduced. Clusters of silica have irregular form compared to spherical nanoparticles; as a consequence, it could lead to a more important increase of the Young's modulus at low concentration. When the concentration increases, the distance between the clusters decreases and the interaction between aggregates may prevail compared to the shape of the aggregates. Further measurements would be needed to assess the modulus variation more quantitatively.

6.3. Conclusions

The objective of this chapter was to present the work on the development of P(VDF-co-HFP) – silica hybrid films by solvent casting. The objective of the work was to develop a strategy to enhance the energy density of thin P(VDF-co-HFP) films. The idea was to add some low dielectric nanoparticles in a high dielectric polymer matrix to enhance the breakdown strength of the polymer and as a consequence its energy density. To do so, silica nanoparticles were added in various amount to P(VDF-co-HFP) up to 40wt% of silica in the final material. Attention has been payed to the optimization of the film preparation and the characterization of the structure and mechanical properties of the materials. Three highly filled model nanocomposites based on P(VDF-co-HFP) with three silica distribution were developed during this work. Homogeneous distribution was obtained for up to 40wt% of silica.

The structure of the materials was first studied. It was performed by SEM and USAXS measurements and it was observed that depending on the sources of silica used three different and finely controlled distributions of silica were obtained:

- **Porous films**: materials were prepared from the silica solution in MEK developed by phase transfer. This leads to white self-supported films of thickness around 50μm up to 40wt%. Electronic microscopy shows the formation of cavities with localized filler particles at the

interface of the cavities. The existence of cavities is certainly due to the presence of water in the silica – polymer – MEK solution (with a 15wt% content) and more especially core-shell aggregates which leads to the existence of cavities in the film.

- **Well-distributed homogeneous films** were obtained from spherical silica particles solution in MEK supplied by Nissan (MEK-ST-L). This leads to mostly transparent films up to 20wt% of silica with homogeneous distribution of silica particles in the polymer matrix
- **Aggregated homogeneous films** were prepared from silica solution in 2-heptanone (prepared by solvent exchange of the Nissan solution in MEK). Slightly milky films up to 40wt% of silica were obtained with well-distributed clusters of silica particles

Then, the effect of the distribution state and microstructure on the properties of the materials was investigated in terms of mechanical characterizations. The mechanical properties were assessed with tensile strength tests.

The incorporation of silica nanoparticles in P(VDF-co-HFP) modifies the mechanical properties of the films: depending on the source of silica used and the concentration of nanoparticles fragile or ductile materials are obtained. Characterizations show that the key factors impacting the performances of the materials are not the same. Mechanical performances are influenced by the **distribution state and the microstructure (heterogeneous air cavities) of the samples**. Samples with large cavities exhibit ductile rupture profile while more homogeneous samples are more fragile.

However, the film fabrication process should be optimized in order to better control the final thickness of the nanocomposites: solvent casting step with a better control of the thickness of the cast solution or drying step. Moreover, as explained in chapter one, the kinetics of the solvent evaporation during the drying step may strongly influence the silica distribution in the final material. Fast drying of the cast solution may prevent the agglomeration of the particles.

General conclusion

The main context of this work is related to the development of advanced functional materials especially for energy storage and conversion applications. Polymer nanocomposites based on VDF copolymers filled with inorganic nanoparticles obtained by solvent casting or printing are attractive systems due to their versatility and combination of properties. Indeed, PVDF and VDF-based copolymer are now widely used due to their high dielectric constant and their piezoelectric and pyroelectric properties. In addition, silica nanoparticles are usually embedded into polymer matrices to reinforce the mechanical properties but also sometimes to improve the electrical performances of materials.

The main objective of this work was to develop P(VDF-co-HFP) – silica nanocomposite materials by solvent route which are related to energy storage applications. More especially the study focused on the impact of the dispersion state and process on the electrical and mechanical properties of the materials.

We found that the addition of nanoparticles to a solution of VDF copolymer impacts the rheological properties and thus, the processing through a casting with sol gel method may not be possible anymore. This is typically the case for VDF-based copolymer (filled or not with nanoparticles) that exhibits thermoreversible physical gelation in ketone solvents. However, while the phenomenology of gelation is of major concern for enabling the processing of those materials, only the structure of dried gels was reported in the literature. Several questions were raised on these polymer gels and guided our work before studying hybrid films. **What are the mechanisms responsible for the gelation of P(VDF-co-HFP) in these solvents?** Indeed, to our knowledge there are no studies in the literature on the gelation of PVDF in linear ketone solvents. Moreover, **what is the influence of experimental conditions (concentration of copolymer, nature of the solvent, temperature, presence of silica and water) on the gelation dynamics and structure? What would be the advantage of the gel state for the processing of nanocomposite materials?**

Thus, this work has been divided into two major parts: gelation of P(VDF-co-HFP) in linear ketone solvents and development of hybrid membranes. Chapter 3 to 5 described the gelation of P(VDF-co-HFP) in MEK and 2-heptanone. A combination of experimental approaches was used to study the dynamics of these gels as well as their behavior in the nonlinear regime. The dynamics and structure of P(VDF-co-HFP) – MEK or P(VDF-co-HFP) – 2-heptanone gels was studied in the Chapter 3, at different concentrations of copolymer and temperatures. The influence of the presence of silica nanoparticles in the materials on the gelation mechanism has been described in Chapter 4. In Chapter 5 we studied the nonlinear rheological properties of P(VDF-co-HFP) – 2-heptanone physical gels (filled or no with silica nanoparticles). The last part of the manuscript dealt with the processing of hybrid films by solvent casting and characterization of their structure and their electrical and mechanical properties.

Solutions of P(VDF-co-HFP) in MEK or 2-heptanone forms thermoreversible gels with gelation kinetics that strongly depend on both nature of the solvent, concentration of copolymer and temperature. The gelation of P(VDF-co-HFP) solutions in such solvents was found to appear only for semicrystalline copolymer and strongly depends on its organization. Combination of characterization methods (DSC, WAXS, ^{19}F NMR) evidences that the **gelation of P(VDF-co-HFP) in linear ketone solvents was attributed to the formation of rigid crystalline zones, which do not exist in the liquid state**. These

crystalline regions would act as junction points between portions of polymer chain to form a three-dimensional network. In both solvents the fraction of polymer involved in the rigid zones and elastically active chains was found to increase with the fraction of copolymer. By increasing the number of carbons of the backbone chain of the solvent (from MEK to 2-heptanone the number of carbons goes from 4 to 7) the fraction of crystallites increases and gelation kinetics increases. It is certainly attributed to the increase of the Flory interaction parameter. However, in 2-heptanone a second phenomenon might be considered, this solvent being a poor solvent of the copolymer: phase separation of the solution into solvent-rich and polymer-rich phases. Nonlinear rheological properties of P(VDF-co-HFP) – 2-heptanone gels was studied at various concentrations of copolymer was studied and **strain-hardening was observed**.

In a second step copolymer – silica gels were formulated from an organic silica solution. To do so we developed a generic approach for the development of silica solution in organic solvent, by using a transfer agent. Since this process has not been yet optimized in 2-heptanone, we used a Nissan commercial solution in MEK transferred into 2-heptanone. Using the same characterization methods as the binary gels, in addition to USAXS experiments we have been able to determine that **the presence of silica nanoparticles in the gels has a very small impact on the gelation mechanism**. It suggests that there is no or few copolymer – silica interactions and therefore the gelation of P(VDF-co-HFP) is independent of the presence the presence of silica nanoparticles. No (or little change) on the gelation mechanism was highlighted. On the contrary we evidenced that the process of formulation of the gels, and more particularly the presence of water, impacts the structure of the gels. This allowed us to obtain very different dispersion states of silica nanoparticles in the polymer matrix: core-shell aggregates of well-dispersed systems. Moreover, in physical gels in 2-heptanone **levels of moduli are decreased and no strain-hardening** was observed in comparison with binary gels. It would suggest very poor copolymer – silica or silica - solvent interactions.

In a last step described in the Chapter 6, P(VDF-co-HFP) – silica hybrid films were developed from P(VDF-co-HFP) – silica solutions in MEK and 2-heptanone. Attention has been paid to the optimization of the film preparation and the characterization of the structure of the materials as well as their electric resistance and mechanical performances, as a function of the dispersion state and concentration of silica, in order to explore the energy storage capability of such materials. Using three different sources of silica organic solutions it was possible to develop materials with three **different and finely controlled distribution of nanoparticles and more particularly porous materials with fillers localized at the air-polymer interface.** The formation **of cavities was attributed to the presence of water of the silica organic solution** in MEK and it was possible to **link the presence of cavities with the existence of core-shell aggregates at the gel state**. We found that the dispersion state and microstructure influences the mechanical properties of the nanocomposites.

This study was the initiation of the development of polymer materials processed by solvent route in LPMA. In this PhD work we rise several hypotheses concerning the gelation dynamics and structure of PVDF and its interaction with different solvents. This research sheds new light on the understanding of the thermoreversible gelation process of VDF copolymer in linear ketone solvent. By combining innovative experimental approaches, and more especially ^{19}F NMR to study selectively the fluorinated copolymer, at the gel state we were able to draw a possible mechanism responsible of the gelation of P(VDF-co-HFP) in these solvents. Although much work remains to be done to confirm these hypotheses, different perspectives have been developed.

Is there a generic gelation mechanism when a polymer is dissolved in a solvent close to a θ solvent (or a bad solvent)? More particularly, can the phase separation mechanism explain the gelation of polymers in solution? Indeed, as shown in the Figure 146, when the Flory interaction parameter between a polymer and a solvent is closer or higher than 0.5 (and thus $1-2\chi<0$), characteristic of a θ solvent or a bad solvent, it is found that a phase separation phenomenon appears and a heterogeneous material is formed (composed of polymer-rich and solvent-rich zones). In MEK, the Flory interaction parameter is close to 0.5, a weakly heterogeneous material is formed. On the contrary, when the number of carbon of the solvent increases, the Flory interaction parameter increases resulting in a faster gelation and a very heterogeneous material. We could therefore extend the gelation mechanism based on phase separation to other polymers and solvents.

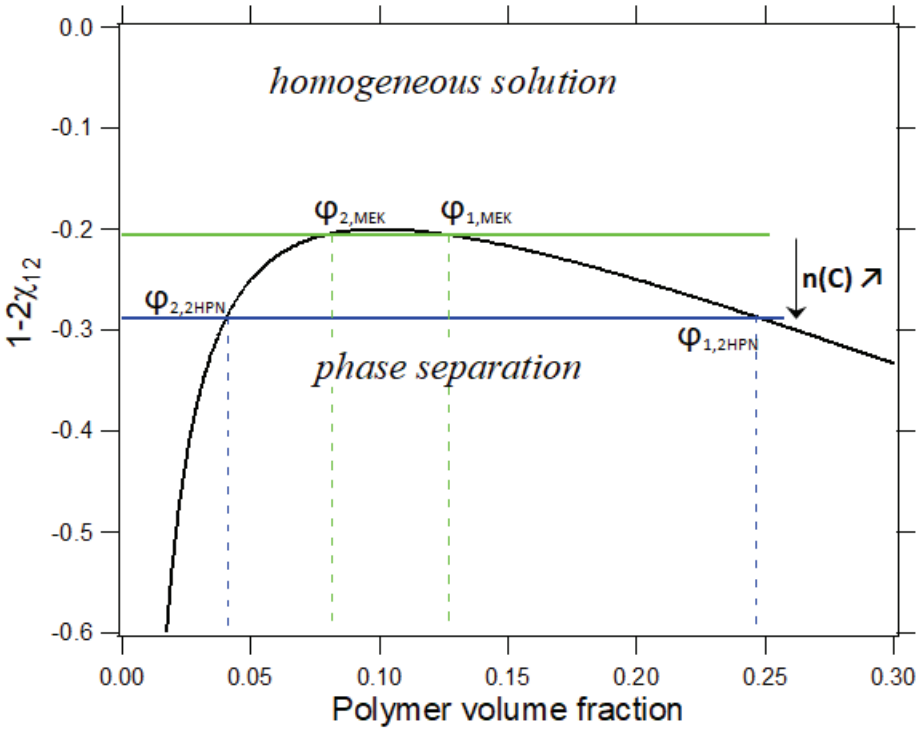


Figure 146 Phase diagram linking the excluded volume (and therefore the Flory interaction parameter) to the polymer fraction in solution for MEK and 2-heptanone. n(C) corresponds to the number of carbon of the backbone chain, here n(C)=4 for MEK and n(C)=7 for 2-heptanone.

This work also provided an important opportunity to use P(VDF-co-HFP) – silica – solvent thermoreversible gels as an advantage for the processing of nanocomposites as silica nanoparticles remains stable in the gel state. Such thermoreversible gels could be used for the processing of materials by solvent casting of by inkjet printing. For these processes, a low volatility solution is needed to avoid drying too fast, resulting in poor dispersion of the fillers in the nanocomposites, but with a gelation kinetics which is not fast enough not to affect the film processing by these two methods. By changing the number of carbon of the solvent backbone chain, it is possible to modify the gelation kinetics but also the volatility of the material. Thus, to continue with linear ketone solvents, an interesting idea would be to work with an intermediary solvent such as 2-pentatone which as a high boiling point around 100°C and a certainly slow gelation kinetics comparable to the gelation of P(VDF-co-HFP) in MEK. As a consequence, this thermoreversible gelation could be extended to other fillers, in order to develop other P(VDF-co-HFP) – fillers nanocomposites, or to other polymers.

We can also wonder what could be the direct applications of P(VDF-co-HFP) – solvent organogels filled or not with fillers. Indeed, to date polymer organogels are useful in many applications such as: drug delivery mediums, cleaning materials for art conservation (Carretti, Dei et al. 2004), personal care products or Li-ion batteries and capacitors (Chatterjee, Liu et al. 2010). However, we did not study the potential applications of the developed gels and it would be interesting to characterize for example the electrical properties of the gels.

Finally, this works also shows the importance of the distribution state of nanoparticles at the liquid state and process on the properties of the final materials. It also opens the path on the development of porous materials by solvent casting and such materials could be used as electrolyte in Li-air batteries (Zhang, Li et al. 2010).

References

Ahmed, S. and Z. Ounaies (2016). Self-Clearing of Metalized Electrodes and its Impact on Electroactive Polymer (EAP) Based Actuators.

Ahmed, T. S., J. M. DeSimone and G. W. Roberts (2007). "Continuous Copolymerization of Vinylidene Fluoride with Hexafluoropropylene in Supercritical Carbon Dioxide: Low Hexafluoropropylene Content Semicrystalline Copolymers." Macromolecules **40**(26): 9322-9331.

Ajroldi, G., M. Pianca, M. Fumagalli and G. Moggi (1989). "Fluoroelastomers-dependence of relaxation phenomena on composition." Polymer **30**(12): 2180-2187.

Albayrak Ari, G. and I. Aydin (2008). "Nanocomposites Prepared by Solution Blending: Microstructure and Mechanical Properties." Journal of Macromolecular Science, Part B **47**(2): 260-267.

Albert, K., B. Evers and E. Bayer (1985). "NMR investigation of the dynamic behavior of alkyl-modified silica." Journal of Magnetic Resonance (1969) **62**(3): 428-436.

Ameduri, B. (2009). "From Vinylidene Fluoride (VDF) to the Applications of VDF-Containing Polymers and Copolymers: Recent Developments and Future Trends." Chemical Reviews **109**(12): 6632-6686.

Améduri, B., B. Boutevin and G. Kostov (2001). "Fluoroelastomers: synthesis, properties and applications." Progress in Polymer Science **26**(1): 105-187.

An, Y., F. J. Solis and H. Jiang (2010). "A thermodynamic model of physical gels." Journal of the Mechanics and Physics of Solids **58**(12): 2083-2099.

Anu Mary, E. and M. P. Saravanakumar (2017). "A review on the classification, characterisation, synthesis of nanoparticles and their application." IOP Conference Series: Materials Science and Engineering **263**(3): 032019.

Apostolo, M., V. Arcella, G. Storti and M. Morbidelli (1999). "Kinetics of the Emulsion Polymerization of Vinylidene Fluoride and Hexafluoropropylene." Macromolecules **32**(4): 989-1003.

Argoud, A. (2011). Control and stabilization of morphologies in reactively compatibilized polyamide 6/high density polyethylene blends, Université Claude Bernard Lyon 1.

Arkles, B. (1977). Tailoring Surfaces with Silanes.

Ash, B. J., L. S. Schadler and R. W. Siegel (2002). "Glass transition behavior of alumina/polymethylmethacrylate nanocomposites." Materials Letters **55**(1): 83-87.

Azzopardi, M. J. and H. Arribart (1994). "In Situ FTIR Study of the Formation of an Organosilane Layer at the Silica/Solution Interface." The Journal of Adhesion **46**(1-4): 103-115.

Bachmann, M. A. and J. B. Lando (1981). "A reexamination of the crystal structure of phase II of poly(vinylidene fluoride)." Macromolecules **14**(1): 40-46.

Baeza, G. P., A.-C. Genix, C. Degrandcourt, J. Gummel, A. Mujtaba, K. Saalwächter, T. Thurn-Albrecht, M. Couty and J. Oberdisse (2014). "Studying Twin Samples Provides Evidence for a Unique Structure-Determining Parameter in Simplifed Industrial Nanocomposites." ACS Macro Letters **3**(5): 448-452.

Baeza, G. P., A.-C. Genix, C. Degrandcourt, L. Petitjean, J. Gummel, M. Couty and J. Oberdisse (2013). "Multiscale Filler Structure in Simplified Industrial Nanocomposite Silica/SBR Systems Studied by SAXS and TEM." Macromolecules **46**: 317-329.

Bagchi, P. (1974). "Theory of stabilization of spherical colloidal particles by nonionic polymers." Journal of Colloid and Interface Science **47**(1): 86-99.

Bagwe, R. P., L. R. Hilliard and W. Tan (2006). "Surface Modification of Silica Nanoparticles to Reduce Aggregation and Nonspecific Binding." Langmuir **22**(9): 4357-4362.

Balsara, N. P., T. J. Rappl and A. A. Lefebvre (2004). "Does conventional nucleation occur during phase separation in polymer blends?" Journal of Polymer Science Part B: Polymer Physics **42**(10): 1793-1809.

Banc, A., A.-C. Genix, M. Chirat, C. Dupas, S. Caillol, M. Sztucki and J. Oberdisse (2014). "Tuning Structure and Rheology of Silica–Latex Nanocomposites with the Molecular Weight of Matrix Chains: A Coupled SAXS–TEM–Simulation Approach." Macromolecules **47**(9): 3219-3230.

Baum, J. and A. Pines (1986). "NMR studies of clustering in solids." Journal of the American Chemical Society **108**(24): 7447-7454.
Baumgärtel, T., C. von Borczyskowski and H. Graaf (2013). "Selective surface modification of lithographic silicon oxide nanostructures by organofunctional silanes." Beilstein Journal of Nanotechnology **4**: 218-226.
Baxter, R. J. (1968). "Percus–Yevick Equation for Hard Spheres with Surface Adhesion." The Journal of Chemical Physics **49**(6): 2770-2774.
Becker, C., B. Kutsch, H. Krug and H. Kaddami (1998). "SAXS and TEM Investigations on Thermoplastic Nanocomposites Containing Functionalized Silica Nanoparticles." Journal of Sol-Gel Science and Technology **13**(1): 499-502.
Belyakova, L. A. and A. M. Varvarin (1999). "Surfaces properties of silica gels modified with hydrophobic groups." Colloids and Surfaces A: Physicochemical and Engineering Aspects **154**(3): 285-294.
Berger, C. E. H., K. O. van der Werf, R. P. H. Kooyman, B. G. de Grooth and J. Greve (1995). "Functional Group Imaging by Adhesion AFM Applied to Lipid Monolayers." Langmuir **11**(11): 4188-4192.
Berghmans, H. (1988). Thermoreversible Gelation of Synthetic Polymers. Integration of Fundamental Polymer Science and Technology—2. P. J. Lemstra and L. A. Kleintjens. Dordrecht, Springer Netherlands**:** 296-305.
Bikiaris, D., V. Karavelidis and G. Karayannidis (2006). "A New Approach to Prepare Poly(ethylene terephthalate)/Silica Nanocomposites with Increased Molecular Weight and Fully Adjustable Branching or Crosslinking by SSP." Macromolecular Rapid Communications **27**(15): 1199-1205.
Bikiaris, D. N., G. Z. Papageorgiou, E. Pavlidou, N. Vouroutzis, P. Palatzoglou and G. P. Karayannidis (2006). "Preparation by melt mixing and characterization of isotactic polypropylene/SiO2 nanocomposites containing untreated and surface-treated nanoparticles." Journal of Applied Polymer Science **100**(4): 2684-2696.
Bluemel, J. (1995). "Reactions of Ethoxysilanes with Silica: A Solid-State NMR Study." Journal of the American Chemical Society **117**(7): 2112-2113.
Blumstein, A. (1965). "Polymerization of adsorbed monolayers. II. Thermal degradation of the inserted polymer." Journal of Polymer Science Part A: General Papers **3**(7): 2665-2672.
Bonardelli, P., G. Moggi and A. Turturro (1986). "Glass transition temperatures of copolymer and terpolymer fluoroelastomers." Polymer **27**(6): 905-909.
Bottino, A., G. Capannelli, S. Munari and A. Turturro (1988). "Solubility parameters of poly(vinylidene fluoride)." Journal of Polymer Science Part B: Polymer Physics **26**(4): 785-794.
Bretz, P. E., R. W. Hertzberg and J. A. Manson (1981). "Mechanisms of fatigue damage and fracture in semi-crystalline polymers." Polymer **22**(9): 1272-1278.
Brunel, D., A. Cauvel, F. Di Renzo, F. Fajula, B. Fubini, B. Onida and E. Garrone (2000). "Preferential grafting of alkoxysilane coupling agents on the hydrophobic portion of the surface of micelle-templated silica." New Journal of Chemistry **24**(10): 807-813.
Burnside, S. D. and E. P. Giannelis (1995). "Synthesis and properties of new poly(dimethylsiloxane) nanocomposites." Chemistry of Materials **7**(9): 1597-1600.
Carraher, C. E. (1984). "Chain Structure and Conformation of Macromolecules (Bovey, Frank A.; Jelinski, Lynn W.)." Journal of Chemical Education **61**(7): A209.
Carretti, E., L. Dei, A. Macherelli and R. G. Weiss (2004). "Rheoreversible Polymeric Organogels: The Art of Science for Art Conservation." Langmuir **20**(20): 8414-8418.
Carrot, G., D. Rutot-Houzé, A. Pottier, P. Degée, J. Hilborn and P. Dubois (2002). "Surface-Initiated Ring-Opening Polymerization: A Versatile Method for Nanoparticle Ordering." Macromolecules **35**(22): 8400-8404.
Caseri, W. (2007). Hybrid materials: synthesis, characterization and applications.

Castagnet, S., J.-L. Gacougnolle and P. Dang (2000). "Correlation between macroscopical viscoelastic behaviour and micromechanisms in strained α polyvinylidene fluoride (PVDF)." Materials Science and Engineering: A **276**(1): 152-159.
Chambon, F., Z. S. Petrovic, W. J. MacKnight and H. H. Winter (1986). "Rheology of model polyurethanes at the gel point." Macromolecules **19**(8): 2146-2149.
Char, K., A. P. Gast and C. W. Frank (1988). "Fluorescence studies of polymer adsorption . 1. Rearrangement and displacement of pyrene-terminated polyethylene glycol on colloidal silica particles." Langmuir **4**(4): 989-998.
Chatterjee, J., T. Liu, B. Wang and J. P. Zheng (2010). "Highly conductive PVA organogel electrolytes for applications of lithium batteries and electrochemical capacitors." Solid State Ionics **181**(11): 531-535.
Chen, C., R. S. Justice, D. W. Schaefer and J. W. Baur (2008). "Highly dispersed nanosilica–epoxy resins with enhanced mechanical properties." Polymer **49**(17): 3805-3815.
Chen, D., T. Sharma and J. X. J. Zhang (2014). "Mesoporous surface control of PVDF thin films for enhanced piezoelectric energy generation." Sensors and Actuators A: Physical **216**: 196-201.
Chen, G., S. Zhou, G. Gu, H. Yang and L. Wu (2005). "Effects of surface properties of colloidal silica particles on redispersibility and properties of acrylic-based polyurethane/silica composites." Journal of Colloid and Interface Science **281**(2): 339-350.
Cho, E. J., H. Holback, K. C. Liu, S. A. Abouelmagd, J. Park and Y. Yeo (2013). "Nanoparticle Characterization: State of the Art, Challenges, and Emerging Technologies." Molecular Pharmaceutics **10**(6): 2093-2110.
Cho, J. W., H. Y. Song and S. Y. Kim (1993). "Thermoreversible gelation of poly(vinylidene fluoride) in γ-butyrolactone solution." Polymer **34**(5): 1024-1027.
Christy, A. A. (2014). "The Nature of Silanol Groups on the Surfaces of Silica, Modified Silica and Some Silica Based Materials." Advanced Materials Research **998-999**: 3-10.
Chu, B., X. Zhou, K. Ren, B. Neese, M. Lin, Q. Wang, F. Bauer and Q. M. Zhang (2006). "A Dielectric Polymer with High Electric Energy Density and Fast Discharge Speed." Science **313**(5785): 334.
Cohen Stuart, M. A., T. Cosgrove and B. Vincent (1985). "Experimental aspects of polymer adsorption at solid/solution interfaces." Advances in Colloid and Interface Science **24**: 143-239.
Cooper, C. L., T. Cosgrove, J. S. van Duijneveldt, M. Murray and S. W. Prescott (2013). "Competition between Polymers for Adsorption on Silica: A Solvent Relaxation NMR and Small-Angle Neutron Scattering Study." Langmuir **29**(41): 12670-12678.
Costa, L. I., G. Storti, M. Morbidelli, L. Ferro, O. Scialdone, G. Filardo and A. Galia (2010). "Copolymerization of VDF and HFP in Supercritical Carbon Dioxide: Experimental Analysis of the Reaction Loci." Macromolecules **43**(23): 9714-9723.
Darbandi, M., R. Thomann and T. Nann (2007). "Hollow Silica Nanospheres: In situ, Semi-In situ, and Two-Step Synthesis." Chemistry of Materials **19**(7): 1700-1703.
Dasgupta, D., S. Manna, A. Garai, A. Dawn, C. Rochas, J. M. Guenet and A. K. Nandi (2008). "Morphology, Structure, Rheology, and Thermodynamics of Piezoelectric Poly(vinylidene fluoride)−Ethylene Carbonate Thermoreversible Gel." Macromolecules **41**(3): 779-787.
de Gennes, P. G. (1987). "Polymers at an interface; a simplified view." Advances in Colloid and Interface Science **27**(3): 189-209.
DeGennes, P. G. (1979). Scaling concept in polymer physics.
Derjaguin, B. and L. Landau (1993). "Theory of the stability of strongly charged lyophobic sols and of the adhesion of strongly charged particles in solutions of electrolytes." Progress in Surface Science **43**(1): 30-59.
Dixon, S., D. R. Rexford and J. S. Rugg (1957). "Vinylidene Fluoride – Hexafluoropropylene Copolymer." Industrial & Engineering Chemistry **49**(10): 1687-1690.
Dohany, J. E. Fluorine‐Containing Polymers, Poly(Vinylidene Fluoride).
Dohi, H. and S. Horiuchi (2007). "Locating a Silane Coupling Agent in Silica-Filled Rubber Composites by EFTEM." Langmuir **23**(24): 12344-12349.

Dong, R., V. Ranjan, M. Buongiorno Nardelli and J. Bernholc (2016). First-principles simulations of PVDF copolymers with high dielectric energy density: PVDF-HFP and PVDF-BTFE.
Dorigato, A., M. Sebastiani, A. Pegoretti and L. Fambri (2012). "Effect of Silica Nanoparticles on the Mechanical Performances of Poly(Lactic Acid)." Journal of Polymers and the Environment **20**(3): 713-725.
E.F. Vansant, P. V. D. V., K.C. Vrancken (1995). Chapter 3 The surface chemistry of silica. Studies in Surface Science and Catalysis. E. F. Vansant, P. Van Der Voort and K. C. Vrancken, Elsevier. **93:** 59-77.
Ebnesajjad, S. (2013). 9 - Introduction to Vinylidene Fluoride Polymers. Introduction to Fluoropolymers. S. Ebnesajjad. Oxford, William Andrew Publishing**:** 133-148.
Ek, S., A. Root, M. Peussa and L. Niinistö (2001). Determination of the Hydroxyl Group Content in Silica by Thermogravimetry and a Comparison with 1H MAS NMR Results.
El Mohajir, B. and N. Heymans (2001). Changes in structural and mechanical behaviour of PVDF with processing and thermomechanical treatments. 1. Change in structure.
Eldridge, J. E. and J. D. Ferry (1954). "Studies of the Cross-linking Process in Gelatin Gels. III. Dependence of Melting Point on Concentration and Molecular Weight." The Journal of Physical Chemistry **58**(11): 992-995.
Epinat, C. (2014). Morphology development and rheological properties of reactively compatibilized polyamide 6 / high density polyethylene blends, Université Claude Bernard Lyon 1.
F. Niepceron, G. G., J.F. Tassin (2008). Matériau composite pour membrane de pile à combustible à base de particules inorganiques organomodifiées et procédé de préparation de ceux-ci. France. **WO2009000779A1**.
Fadeev, A. Y. and Y. V. Kazakevich (2002). "Covalently Attached Monolayers of Oligo(dimethylsiloxane)s on Silica: A Siloxane Chemistry Approach for Surface Modification." Langmuir **18**(7): 2665-2672.
Flory, P. J. (1953). Principles of polymer chemistry.
G. J. Fleer, M. A. C. S., J. M. H. M. Scheutjens, T. Cosgrove and B. Vincent (1993). Polymers at Interfaces.
Gelin, M.-P. and B. Ameduri (2005). "Radical solution copolymerisation of vinylidene fluoride with hexafluoropropene." Journal of Fluorine Chemistry **126**(4): 575-583.
Goerl, U., A. Hunsche, A. Mueller and H. G. Koban (1997). Investigations into the Silica/Silane Reaction System.
Groot, R. D., A. Bot and W. G. M. Agterof (1996). "Molecular theory of strain hardening of a polymer gel: Application to gelatin." The Journal of Chemical Physics **104**(22): 9202-9219.
H.S. Katz, J. V. M. (1987). "Synthetic Silicas." Handbook of fillers for plastics: 36.
Hajji, P., L. David, J. F. Gerard, J. P. Pascault and G. Vigier (1999). "Synthesis, structure, and morphology of polymer–silica hybrid nanocomposites based on hydroxyethyl methacrylate." Journal of Polymer Science Part B: Polymer Physics **37**(22): 3172-3187.
Han, M. G. and S. P. Armes (2003). "Synthesis of Poly(3,4-ethylenedioxythiophene)/Silica Colloidal Nanocomposites." Langmuir **19**(11): 4523-4526.
Hasan, S. (2015). "A review on nanoparticles: their synthesis and types." Research Journal of Recent Sciences **4**: 3.
Hasegawa, R., Y. Takahashi, Y. Chatani and H. Tadokoro (1972). "Crystal Structures of Three Crystalline Forms of Poly(vinylidene fluoride)." Polymer Journal **3**: 600.
He, L., L. F. Allard and E. Ma (1999). "A method to produce two-phase nanocomposites in solid state." Nanostructured Materials **12**(1): 543-546.
Hong, P.-D. and C.-M. Chou (2000). Phase separation and gelation behaviors in poly(vinylidene fluoride)/tetra(ethylene glycol) dimethyl ether solutions.
Hyun, K., M. Wilhelm, C. O. Klein, K. S. Cho, J. G. Nam, K. H. Ahn, S. J. Lee, R. H. Ewoldt and G. H. McKinley (2011). "A review of nonlinear oscillatory shear tests: Analysis and application of large amplitude oscillatory shear (LAOS)." Progress in Polymer Science **36**(12): 1697-1753.
Ibrahim, I., A. A. F. Zikry and M. Sharaf (2010). Preparation of spherical nanoparticles: Stober silica.

Ide, F. and A. Hasegawa (1974). "Studies on polymer blend of nylon 6 and polypropylene or nylon 6 and polystyrene using the reaction of polymer." Journal of Applied Polymer Science **18**(4): 963-974.
Iler, R. K. (1979). "The Chemistry of Silica ".
J.E. Dohany, J. S. H. (1989). "Vinylidene fluoride polymers." Encycl. Polym. Sci. Eng. **4**: 16.
J.H. Hildebrand, R. L. S. (1950). Solubility of nanoelectrolites. N. Y. Reinhold Publ. Corp.
J.H. Hildebrand, R. L. S. (1962). Regular Solutions, Prentice-Hall, Inc.
Jana, S. C. and S. Jain (2001). "Dispersion of nanofillers in high performance polymers using reactive solvents as processing aids." Polymer **42**(16): 6897-6905.
Jeevanandam, J., A. Barhoum, Y. S. Chan, A. Dufresne and M. K. Danquah (2018). "Review on nanoparticles and nanostructured materials: history, sources, toxicity and regulations." Beilstein Journal of Nanotechnology **9**: 1050-1074.
Jouault, N., F. Dalmas, F. Boué and J. Jestin (2012). "Multiscale characterization of filler dispersion and origins of mechanical reinforcement in model nanocomposites." Polymer **53**(3): 761-775.
Jouault, N., P. Vallat, F. Dalmas, S. Said, J. Jestin and F. Boué (2009). "Well-Dispersed Fractal Aggregates as Filler in Polymer−Silica Nanocomposites: Long-Range Effects in Rheology." Macromolecules **42**(6): 2031-2040.
Jouault, N., D. Zhao and S. K. Kumar (2014). "Role of Casting Solvent on Nanoparticle Dispersion in Polymer Nanocomposites." Macromolecules **47**(15): 5246-5255.
Kawanishi, K., M. Komatsu and T. Inoue (1987). "Thermodynamic consideration of the sol-gel transition in polymer solutions." Polymer **28**(6): 980-984.
Kepler, R. G. and R. A. Anderson (1978). "Piezoelectricity and pyroelectricity in polyvinylidene fluoride." Journal of Applied Physics **49**(8): 4490-4494.
Khan, I., K. Saeed and I. Khan (2017). "Nanoparticles: Properties, applications and toxicities." Arabian Journal of Chemistry.
Kim, B. S., S. T. Baek, K. W. Song, I. H. Park, J. O. Lee and N. Nemoto (2004). "Thermoreversible Gelation of Poly(Vinylidene Fluoride) in Propylene Carbonate." Journal of Macromolecular Science, Part B **43**(4): 741-754.
Kim, S., K. Hyun, B. Struth, K. H. Ahn and C. Clasen (2016). "Structural Development of Nanoparticle Dispersion during Drying in Polymer Nanocomposite Films." Macromolecules **49**(23): 9068-9079.
Kim, S. H., S. H. Ahn and T. Hirai (2003). "Crystallization kinetics and nucleation activity of silica nanoparticle-filled poly(ethylene 2,6-naphthalate)." Polymer **44**(19): 5625-5634.
Kobayashi, M., K. Tashiro and H. Tadokoro (1975). "Molecular Vibrations of Three Crystal Forms of Poly(vinylidene fluoride)." Macromolecules **8**(2): 158-171.
Komatsu, M., T. Inoue and K. Miyasaka (1986). "Light‐scattering studies on the sol–gel transition in aqueous solutions of poly(vinyl alcohol)." Journal of Polymer Science Part B: Polymer Physics **24**(2): 303-311.
Łabudzińska, A. and A. Ziabicki (1971). "Effect of composition and gelation conditions on structural changes accompanying the gelation of PAN, PVA and gelatin solutions." Kolloid-Zeitschrift und Zeitschrift für Polymere **243**(1): 21-27.
Lach, R., G.-M. Kim, G. H. Michler, W. Grellmann and K. Albrecht (2006). "Indentation Fracture Mechanics for Toughness Assessment of PMMA/SiO2 Nanocomposites." Macromolecular Materials and Engineering **291**(3): 263-271.
Lefebvre, A. A., J. H. Lee, N. P. Balsara and B. Hammouda (2002). "Critical length and time scales during the initial stages of nucleation in polymer blends." The Journal of Chemical Physics **116**(12): 4777-4781.
Lefebvre, A. A., J. H. Lee, H. S. Jeon, N. P. Balsara and B. Hammouda (1999). "Initial stages of nucleation in phase separating polymer blends." The Journal of Chemical Physics **111**(13): 6082-6099.
Leonardelli, S., L. Facchini, C. Fretigny, P. Tougne and A. P. Legrand (1992). "Silicon-29 NMR study of silica." Journal of the American Chemical Society **114**(16): 6412-6418.
Leyden, D. E. (1996). "Characterization and Chemical Modification of the Silica Surface By E. F. Vansant, P. Van Der Voort, and K. C. Vrancken (University of Antwerp, Belgium). Elsevier: The

Netherlands. 1995. xv + 556. $241.25. ISBN 0-444-81928-2." Journal of the American Chemical Society **118**(12): 3071-3071.
Li, W., Y. Xu, Y. Zhou, W. Ma, S. Wang and Y. Dai (2012). "Silica nanoparticles functionalized via click chemistry and ATRP for enrichment of Pb(II) ion." Nanoscale Research Letters **7**(1): 485.
Liu, Y., M. Tourbin, S. Lachaize and P. Guiraud (2013). "Silica nanoparticles separation from water: Aggregation by cetyltrimethylammonium bromide (CTAB)." Chemosphere **92**(6): 681-687.
Lo, E. S. (1965). Fluorine-containing polymers and perparation thereof. United States, 3M. **3,178,399**.
Logothetis, A. L. (1989). "Chemistry of fluorocarbon elastomers." Progress in Polymer Science **14**(2): 251-296.
Lorthioir, C., M. Khalil, V. Wintgens and C. Amiel (2012). "Segmental Motions of Poly(ethylene glycol) Chains Adsorbed on Laponite Platelets in Clay-Based Hydrogels: A NMR Investigation." Langmuir **28**(20): 7859-7871.
Lovinger, A. J. (1982). "Annealing of poly(vinylidene fluoride) and formation of a fifth phase." Macromolecules **15**(1): 40-44.
Lu, Y.-C., Z. Xu, H. A. Gasteiger, S. Chen, K. Hamad-Schifferli and Y. Shao-Horn (2010). "Platinum−Gold Nanoparticles: A Highly Active Bifunctional Electrocatalyst for Rechargeable Lithium−Air Batteries." Journal of the American Chemical Society **132**(35): 12170-12171.
M. Hansen, C. (2012). Hansen Solubility Parameters: A User's Handbook, Second Edition.
M. Rubinstein, R. H. C. (2003). Polymer Physics.
Ma, W., J. Zhang and X.-L. Wang (2008). Formation of poly(vinylidene fluoride) crystalline phases from tetrahydrofuran/N, N-dimethylformamide mixed solvent.
Maekawa, H., T. Maekawa, K. Kawamura and T. Yokokawa (1991). "Silicon-29 MAS NMR investigation of the sodium oxide-alumina-silica glasses." The Journal of Physical Chemistry **95**(18): 6822-6827.
Maiti, P., P. H. Nam, M. Okamoto, T. Kotaka, N. Hasegawa and A. Usuki (2002). "The effect of crystallization on the structure and morphology of polypropylene/clay nanocomposites." Polymer Engineering & Science **42**(9): 1864-1871.
Mal, S., P. Maiti and A. K. Nandi (1995). "On the Gelation Rates of Thermoreversible Poly(vinylidene fluoride) Gels." Macromolecules **28**(7): 2371-2376.
Mal, S. and A. K. Nandi (1998). "Gelation mechanism of thermoreversible poly(vinylidene fluoride) gels in glyceryl tributyrate1." Polymer **39**(25): 6301-6307.
Mal, S. and A. K. Nandi (1998). "A Thermodynamic Study on the Thermoreversible Poly(vinylidene fluoride) Gels in Acetophenone, Ethyl Benzoate, and Glyceryl Tributyrate." Langmuir **14**(9): 2238-2244.
Martin, J. E. and D. Adolf (2003). The Sol-Gel Transition in Chemical Gels.
Martins, P., A. C. Lopes and S. Lanceros-Mendez (2014). "Electroactive phases of poly(vinylidene fluoride): Determination, processing and applications." Progress in Polymer Science **39**(4): 683-706.
Maus, A., C. Hertlein and K. Saalwächter (2006). "A Robust Proton NMR Method to Investigate Hard/Soft Ratios, Crystallinity, and Component Mobility in Polymers." Macromolecular Chemistry and Physics **207**(13): 1150-1158.
McCarthy, T. F., R. Williams, J. F. Bitay, K. Zero, M. S. Yang and F. Mares (1998). "Surfactant-free emulsion polymerization of chlorotrifluoroethylene with vinylacetate or vinylidene fluoride." Journal of Applied Polymer Science **70**(11): 2211-2225.
Menon, S. V. G., C. Manohar and K. S. Rao (1991). "A new interpretation of the sticky hard sphere model." The Journal of Chemical Physics **95**(12): 9186-9190.
Mermet-Guyennet, M. R. B., J. G. d. Castro, M. Habibi, N. Martzel, M. M. Denn and D. Bonn (2015). "LAOS: The strain softening/strain hardening paradox." Journal of Rheology **59**(1): 21-32.
Mijatovic, J., W. H. Binder and H. Gruber (2000). "Characterization of Surface Modified Silica Nanoparticles by 29Si Solid State NMR Spectroscopy." Microchimica Acta **133**(1): 175-181.
Mittal, K. L. (2009). Silanes and Other Coupling Agents.
Mittal, V. (2012). Characterization techniques for polymer nanocomposites.

Moggi, G., P. Bonardelli and J. C. J. Bart (1982). "Synthesis and properties of some hexafluoropropene-1,1-difluoroethene copolymers." Polymer Bulletin **7**(2): 115-122.
Mora-Barrantes, I., J. L. Valentín, A. Rodríguez, I. Quijada-Garrido and R. Paris (2012). "Poly(styrene)/silica hybrid nanoparticles prepared viaATRP as high-quality fillers in elastomeric composites." Journal of Materials Chemistry **22**(4): 1403-1410.
Morrow, B. A. and A. J. McFarlan (1990). "Chemical reactions at silica surfaces." Journal of Non-Crystalline Solids **120**(1): 61-71.
Mortimer, S., A. J. Ryan and J. L. Stanford (2001). "Rheological Behavior and Gel-Point Determination for a Model Lewis Acid-Initiated Chain Growth Epoxy Resin." Macromolecules **34**(9): 2973-2980.
Mueller, R., H. K. Kammler, K. Wegner and S. E. Pratsinis (2003). "OH Surface Density of SiO2 and TiO2 by Thermogravimetric Analysis." Langmuir **19**(1): 160-165.
Munowitz, M. a. P., A. (1987). "Principles and Applications of Multiple-Quantum NMR." Advances in Chemical Physics **66**: 1-152.
Nasef, M. M., H. Saidi and K. Z. M. Dahlan (2002). "Investigation of electron irradiation induced-changes in poly(vinylidene fluoride) films." Polymer Degradation and Stability **75**(1): 85-92.
Nazari, A. and S. Riahi (2011). "The effects of SiO2 nanoparticles on physical and mechanical properties of high strength compacting concrete." Composites Part B: Engineering **42**(3): 570-578.
Nelson, A., K. S. Jack, T. Cosgrove and D. Kozak (2002). "NMR Solvent Relaxation in Studies of Multicomponent Polymer Adsorption." Langmuir **18**(7): 2750-2755.
Nijenhuis, K. t. (1997). Thermoreversible Networks.
Oberdisse, J. and B. Demé (2002). "Structure of Latex−Silica Nanocomposite Films: A Small-Angle Neutron Scattering Study." Macromolecules **35**(11): 4397-4405.
Ohkura, M., T. Kanaya and K. Kaji (1992). "Gelation rates of poly(vinyl alcohol) solution." Polymer **33**(23): 5044-5048.
Okabe, M., R. Wada, M. Tazaki and T. Homma (2003). "The Flory-Huggins Interaction Parameter and Thermoreversible Gelation of Poly(vinylidene fluoride) in Organic Solvents." Polymer Journal **35**: 798.
Orakdogen, N., B. Erman and O. Okay (2010). "Evidence of Strain Hardening in DNA Gels." Macromolecules **43**(3): 1530-1538.
Osada, Y. and J.-P. Gong (1999). "Soft and Wet Materials: Polymer Gels." Advanced Materials **10**(11): 827-837.
Osada, Y., J. Ping Gong and Y. Tanaka (2004). "Polymer Gels." Journal of Macromolecular Science, Part C **44**(1): 87-112.
Osseo-Asare, K. and F. J. Arriagada (1990). "Preparation of SiO2 nanoparticles in a non-ionic reverse micellar system." Colloids and Surfaces **50**: 321-339.
Papon, A., S. Merabia, L. Guy, F. Lequeux, H. Montes, P. Sotta and D. R. Long (2012). "Unique Nonlinear Behavior of Nano-Filled Elastomers: From the Onset of Strain Softening to Large Amplitude Shear Deformations." Macromolecules **45**(6): 2891-2904.
Park, S.-J. and K.-S. Cho (2003). "Filler–elastomer interactions: influence of silane coupling agent on crosslink density and thermal stability of silica/rubber composites." Journal of Colloid and Interface Science **267**(1): 86-91.
Pathmamanoharan, C., P. Wijkens, D. M. Grove and A. P. Philipse (1996). "Paramagnetic Silica Particles: Synthesis and Grafting of a Silane Coupling Agent Containing Nickel Ions onto Colloidal Silica Particles." Langmuir **12**(18): 4372-4377.
Paul, D. R. (1967). "Reversible gelation of acrylonitrile–vinyl acetate copolymer solutions." Journal of Applied Polymer Science **11**(3): 439-455.
Pauly, C. S., A.-C. Genix, J. G. Alauzun, M. Sztucki, J. Oberdisse and P. Hubert Mutin (2015). "Surface modification of alumina-coated silica nanoparticles in aqueous sols with phosphonic acids and impact on nanoparticle interactions." Physical Chemistry Chemical Physics **17**(29): 19173-19182.
Percus, J. K. and G. J. Yevick (1958). "Analysis of Classical Statistical Mechanics by Means of Collective Coordinates." Physical Review **110**(1): 1-13.

Pham, J. Q., C. A. Mitchell, J. L. Bahr, J. M. Tour, R. Krishanamoorti and P. F. Green (2003). "Glass transition of polymer/single-walled carbon nanotube composite films." Journal of Polymer Science Part B: Polymer Physics **41**(24): 3339-3345.
Price, P. M., J. H. Clark and D. J. Macquarrie (2000). "Modified silicas for clean technology." Journal of the Chemical Society, Dalton Transactions(2): 101-110.
Ramier, J., L. Chazeau, C. Gauthier, L. Guy and M. N. Bouchereau (2005). "Grafting of silica during the processing of silica-filled SBR: Comparison between length and content of the silane." Journal of Polymer Science Part B: Polymer Physics **44**(1): 143-152.
Ranjan, R. and W. J. Brittain (2007). "Combination of Living Radical Polymerization and Click Chemistry for Surface Modification." Macromolecules **40**(17): 6217-6223.
Ravera, F., E. Santini, G. Loglio, M. Ferrari and L. Liggieri (2006). "Effect of Nanoparticles on the Interfacial Properties of Liquid/Liquid and Liquid/Air Surface Layers." The Journal of Physical Chemistry B **110**(39): 19543-19551.
Reculusa, S., C. Poncet-Legrand, A. Perro, E. Duguet, E. Bourgeat-Lami, C. Mingotaud and S. Ravaine (2005). "Hybrid Dissymmetrical Colloidal Particles." Chemistry of Materials **17**(13): 3338-3344.
Reculusa, S., C. Poncet-Legrand, S. Ravaine, C. Mingotaud, E. Duguet and E. Bourgeat-Lami (2002). "Syntheses of Raspberrylike Silica/Polystyrene Materials." Chemistry of Materials **14**(5): 2354-2359.
Rong, M. Z., M. Q. Zhang and W. H. Ruan (2006). "Surface modification of nanoscale fillers for improving properties of polymer nanocomposites: a review." Materials Science and Technology **22**(7): 787-796.
Rong, M. Z., M. Q. Zhang, Y. X. Zheng, H. M. Zeng, R. Walter and K. Friedrich (2000). "Irradiation graft polymerization on nano-inorganic particles: An effective means to design polymer-based nanocomposites." Journal of Materials Science Letters **19**(13): 1159-1161.
Rosenberg, Y., A. Siegmann, M. Narkis and S. Shkolnik (1991). "The sol/gel contribution to the behavior of γ-irradiated poly(vinylidene fluoride)." Journal of Applied Polymer Science **43**(3): 535-541.
Roy, M., J. K. Nelson, R. K. MacCrone and L. S. Schadler (2007). "Candidate mechanisms controlling the electrical characteristics of silica/XLPE nanodielectrics." Journal of Materials Science **42**(11): 3789-3799.
Saalwächter, K. (2007). "Proton multiple-quantum NMR for the study of chain dynamics and structural constraints in polymeric soft materials." Progress in Nuclear Magnetic Resonance Spectroscopy **51**(1): 1-35.
Saalwächter, K. (2017). Multiple-Quantum NMR Studies of Anisotropic Polymer Chain Dynamics. Modern Magnetic Resonance. G. A. Webb. Cham, Springer International Publishing**:** 1-28.
Salimi, A. and A. A. Yousefi (2003). "Analysis Method: FTIR studies of β-phase crystal formation in stretched PVDF films." Polymer Testing **22**(6): 699-704.
Sanchez, J.-Y., F. Alloin and J. Saunier (2005). PVdF-based polymers for lithium batteries**:** 305-333.
Sarwar, M. I., S. Zulfiqar and Z. Ahmad (2008). "Polyamide–silica nanocomposites: mechanical, morphological and thermomechanical investigations." Polymer International **57**(2): 292-296.
Schadler, L. S. (2004). Nanocomposite science and technology.
Schadler, L. S., S. K. Kumar, B. C. Benicewicz, S. L. Lewis and S. E. Harton (2011). "Designed Interfaces in Polymer Nanocomposites: A Fundamental Viewpoint." MRS Bulletin **32**(4): 335-340.
Sen, S., Y. Xie, A. Bansal, H. Yang, K. Cho, L. S. Schadler and S. K. Kumar (2007). "Equivalence between polymer nanocomposites and thin polymer films: Effect of processing conditions and molecular origins of observed behavior." The European Physical Journal Special Topics **141**(1): 161-165.
Shang, X.-y., Z.-k. Zhu, J. Yin and X.-d. Ma (2002). "Compatibility of Soluble Polyimide/Silica Hybrids Induced by a Coupling Agent." Chemistry of Materials **14**(1): 71-77.
Shimizu, H., Y. Arioka, M. Ogawa, R. Wada and M. Okabe (2011). "Sol-gel transitions of poly(vinylidene fluoride) in organic solvents containing LiBF4." Polymer Journal **43**: 540.
Shin, W.-K., J. Cho, A. G. Kannan, Y.-S. Lee and D.-W. Kim (2016). "Cross-linked Composite Gel Polymer Electrolyte using Mesoporous Methacrylate-Functionalized SiO2 Nanoparticles for Lithium-Ion Polymer Batteries." Scientific Reports **6**: 26332.

Shirai, Y. and N. Tsubokawa (1997). "Grafting of polymers onto ultrafine inorganic particle surface: graft polymerization of vinyl monomers initiated by the system consisting of trichloroacetyl groups on the surface and molybdenum hexacarbonyl." Reactive and Functional Polymers **32**(2): 153-160.
Siegelman, I. and C. H. Sorum (1960). "PHASE EQUILIBRIUM RELATIONSHIPS IN THE BINARY SYSTEM METHYL ETHYL KETONE–WATER." Canadian Journal of Chemistry **38**(10): 2015-2023.
Smitham, J. B., R. Evans and D. H. Napper (1975). "Analytical theories of the steric stabilization of colloidal dispersions." Journal of the Chemical Society, Faraday Transactions 1: Physical Chemistry in Condensed Phases **71**(0): 285-297.
Sotta, P., C. Fülber, D. E. Demco, B. Blümich and H. W. Spiess (1996). "Effect of Residual Dipolar Interactions on the NMR Relaxation in Cross-Linked Elastomers." Macromolecules **29**(19): 6222-6230.
Spange, S. (2000). "Silica surface modification by cationic polymerization and carbenium intermediates." Progress in Polymer Science **25**(6): 781-849.
Stöber, W., A. Fink and E. Bohn (1968). "Controlled growth of monodisperse silica spheres in the micron size range." Journal of Colloid and Interface Science **26**(1): 62-69.
Sutra, P., F. Fajula, D. Brunel, P. Lentz, G. Daelen and J. B. Nagy (1999). "29Si and 13C MAS-NMR characterization of surface modification of micelle-templated silicas during the grafting of organic moieties and end-capping." Colloids and Surfaces A: Physicochemical and Engineering Aspects **158**(1): 21-27.
T.A. Ford, W. E. H. (1948). Polyvinylidene Fluoride and process. United State, DuPont Co. . **2,435,537**.
Takei, T., K. Kato, A. Meguro and M. Chikazawa (1999). "Infrared spectra of geminal and novel triple hydroxyl groups on silica surface." Colloids and Surfaces A: Physicochemical and Engineering Aspects **150**(1): 77-84.
Tarascon, J. M., A. S. Gozdz, C. Schmutz, F. Shokoohi and P. C. Warren (1996). "Performance of Bellcore's plastic rechargeable Li-ion batteries." Solid State Ionics **86-88**: 49-54.
Tazaki, M., R. Wada, O. Abe Masaru and T. Homma (1998). "Crystallization and gelation of poly(vinylidene fluoride) in organic solvents." Journal of Applied Polymer Science **65**(8): 1517-1524.
Teng, W.-Y., S.-C. Jeng, C.-W. Kuo, Y.-R. Lin, C.-C. Liao and W.-K. Chin (2008). "Nanoparticles-doped guest-host liquid crystal displays." Optics Letters **33**(15): 1663-1665.
Tessema, A., D. Zhao, J. Moll, S. Xu, R. Yang, C. Li, S. K. Kumar and A. Kidane (2017). "Effect of filler loading, geometry, dispersion and temperature on thermal conductivity of polymer nanocomposites." Polymer Testing **57**: 101-106.
Tokita, M. (1989). "Gelation mechanism and percolation." Food Hydrocolloids **3**(4): 263-274.
Tripp, C. P. and M. L. Hair (1992). "An infrared study of the reaction of octadecyltrichlorosilane with silica." Langmuir **8**(4): 1120-1126.
Tuel, A., H. Hommel, A. P. Legrand, Y. Chevallier and J. C. Morawski (1990). "Solid state NMR studies of precipitated and pyrogenic silicas." Colloids and Surfaces **45**: 413-426.
Tyrode, E., M. W. Rutland and C. D. Bain (2008). "Adsorption of CTAB on Hydrophilic Silica Studied by Linear and Nonlinear Optical Spectroscopy." Journal of the American Chemical Society **130**(51): 17434-17445.
Utracki, L. A. (2003). Polymer blends handbook. Dordrecht, Boston, London, Kluwer Academic Publishers.
V. Tomer, E. M. C. A. R. (2011). "High field properties and energy storage in nanocomposite dielectrics of poly(vinylidene fluoride-hexafluoropropylene)." Journal of Applied Physics **110**: 044107.
Valentin, J. L., M. Lopez-Manchado, P. Posadas, A. Rodriguez, A. Marcos-Fernández and L. Ibarra (2006). Characterization of the reactivity of a silica derived from acid activation of sepiolite with silane by Si-29 and C-13 solid-state NMR.
van Zyl, W. E., M. García, B. A. G. Schrauwen, B. J. Kooi, J. T. M. De Hosson and H. Verweij (2002). "Hybrid Polyamide/Silica Nanocomposites: Synthesis and Mechanical Testing." Macromolecular Materials and Engineering **287**(2): 106-110.

Vassiliou, A. A., G. Z. Papageorgiou, D. S. Achilias and D. N. Bikiaris (2007). "Non-Isothermal Crystallisation Kinetics of In Situ Prepared Poly(ε-caprolactone)/Surface-Treated SiO2 Nanocomposites." Macromolecular Chemistry and Physics **208**(4): 364-376.
Verwey, E. J. W. (1947). "Theory of the Stability of Lyophobic Colloids." The Journal of Physical and Colloid Chemistry **51**(3): 631-636.
Vieyres, A. (2013). Influence of Filler/Polymer interface on reinforcement, strain-induced crystallization and tear resistance in reinforced natural rubber, Université Claude Bernard Lyon 1.
Vilmin, F., I. Bottero, A. Travert, N. Malicki, F. Gaboriaud, A. Trivella and F. Thibault-Starzyk (2014). "Reactivity of Bis[3-(triethoxysilyl)propyl] Tetrasulfide (TESPT) Silane Coupling Agent over Hydrated Silica: Operando IR Spectroscopy and Chemometrics Study." The Journal of Physical Chemistry C **118**(8): 4056-4071.
von Werne, T. and T. E. Patten (1999). "Preparation of Structurally Well-Defined Polymer−Nanoparticle Hybrids with Controlled/Living Radical Polymerizations." Journal of the American Chemical Society **121**(32): 7409-7410.
Walling, C. (1945). "Gel Formation in Addition Polymerization1." Journal of the American Chemical Society **67**(3): 441-447.
Wang, P., S. M. Zakeeruddin and M. Grätzel (2004). "Solidifying liquid electrolytes with fluorine polymer and silica nanoparticles for quasi-solid dye-sensitized solar cells." Journal of Fluorine Chemistry **125**(8): 1241-1245.
Wang, Y. and Y. Xia (2004). "Bottom-Up and Top-Down Approaches to the Synthesis of Monodispersed Spherical Colloids of Low Melting-Point Metals." Nano Letters **4**(10): 2047-2050.
Weinhold, S., M. H. Litt and J. B. Lando (1982). "The crystal structure of the alternating copolymer of hexafluoroisobutylene and vinylidene fluoride." Journal of Polymer Science: Polymer Physics Edition **20**(3): 535-552.
Winter, H. H. and F. Chambon (1986). "Analysis of Linear Viscoelasticity of a Crosslinking Polymer at the Gel Point." Journal of Rheology **30**(2): 367-382.
Wu, T.-M. and M.-S. Chu (2005). "Preparation and characterization of thermoplastic vulcanizate/silica nanocomposites." Journal of Applied Polymer Science **98**(5): 2058-2063.
Wypych, G. (2016). Handbook of Fillers (Fourth Edition). G. Wypych, ChemTec Publishing**:** i.
Xia, W. and Z. Zhang (2018). "PVDF-based dielectric polymers and their applications in electronic materials." IET Nanodielectrics **1**(1): 17-31.
Yan, Z. B., D. H. Brouwer and G. R. Goward (2016). "19F Double Quantum NMR Spectroscopy: A Tool for Probing Dynamics in Proton-Conducting Fluorinated Polymer Materials." Macromolecules **49**(19): 7331-7339.
Yang, X., T. Dai and Y. Lu (2006). "Synthesis of novel sunflower-like silica/polypyrrole nanocomposites via self-assembly polymerization." Polymer **47**(1): 441-447.
Zare, Y. (2016). "Study of nanoparticles aggregation/agglomeration in polymer particulate nanocomposites by mechanical properties." Composites Part A: Applied Science and Manufacturing **84**: 158-164.
Zhang, D., R. Li, T. Huang and A. Yu (2010). "Novel composite polymer electrolyte for lithium air batteries." Journal of Power Sources **195**(4): 1202-1206.
Zhang, J., H. Han, S. Xu, S. Wu, C. Zhou, Y. Yang and X. Zhao (2008). "Phase inversion process to prepare quasi-solid-state electrolyte for the dye-sensitized solar cells." Journal of Applied Polymer Science **109**(2): 1369-1375.
Zhang, L., Y. Wang, Y. Wang, Y. Sui and D. Yu (2000). "Morphology and mechanical properties of clay/styrene-butadiene rubber nanocomposites." Journal of Applied Polymer Science **78**(11): 1873-1878.
Zhao, X. S. and G. Q. Lu (1998). "Modification of MCM-41 by Surface Silylation with Trimethylchlorosilane and Adsorption Study." The Journal of Physical Chemistry B **102**(9): 1556-1561.

Zheng, K., X. Yao, X. Tian, L. Chen, H. He and Y. Li (2006). "Synthesis and Thermal Behavior of Silica‐Graft‐Polypropylene Nanocomposites Studied by Step‐Scan DSC and TGA." Journal of Macromolecular Science, Part B **45**(4): 493-505.
Zhou, Q., S. Wang, X. Fan, R. Advincula and J. Mays (2002). "Living Anionic Surface-Initiated Polymerization (LASIP) of a Polymer on Silica Nanoparticles." Langmuir **18**(8): 3324-3331.
Zhou, X., X. Zhao, Z. Suo, C. Zou, J. Runt, S. Liu, S. Zhang and Q. M. Zhang (2009). "Electrical breakdown and ultrahigh electrical energy density in poly(vinylidene fluoride-hexafluoropropylene) copolymer." Applied Physics Letters **94**(16): 162901.
Zhuravlev, L. T. (2000). "The surface chemistry of amorphous silica. Zhuravlev model." Colloids and Surfaces A: Physicochemical and Engineering Aspects **173**(1): 1-38.
Zou, H., S. Wu and J. Shen (2008). "Polymer/Silica Nanocomposites: Preparation, Characterization, Properties, and Applications." Chemical Reviews **108**(9): 3893-3957.

Illustration table

Figure 1 Schematic structures of homopolymers and copolymers 9
Figure 2 Polymer behavior in solvent in the case of a (A) bad, (B) θ (theta) and (C) good solvent 10
Figure 3 Polymer solutions at various concentrations in a good solvent (a) dilute solution ($\boldsymbol{c} < \boldsymbol{c}*$), (b) semi-dilute where polymer starts to overlap ($\boldsymbol{c} = \boldsymbol{c}*$) and (c) semi-dilute with overlapped polymer chains ($\boldsymbol{c} > \boldsymbol{c}*$). (DeGennes 1979) 11
Figure 4 Correlation length between polymer chains in semi-dilute solution (*c*>*c**) (DeGennes 1979) 12
Figure 5 Schematic representation of blobs in a semi-dilute solution of polymer (DeGennes 1979) .. 12
Figure 6 Vinylidene fluoride structure 13
Figure 7 Polyvinylidene fluoride structure 13
Figure 8 Poly(vinylidene fluoride-co-hexafluoropropylene) structure 15
Figure 9 Radical copolymerization scheme 15
Figure 10 Relation between the Flory-Huggins interaction parameter and temperature for P(VDF-co-HFP) solutions in ten solvents (Okabe, Wada et al. 2003) 16
Figure 11 Main polymorphs of PVDF 18
Figure 12 Variation of the properties (thermoplastic or elastomer) of P(VDF-co-HFP) according to the HFP content 20
Figure 13 Effect of pH in the colloidal silica - water system 23
Figure 14 The surface of silica 24
Figure 15 Surface silanol groups of silica 24
Figure 16 SEM micrographs of (A) unmodified fumed silica (b) polymer-grafted silica particles (Mora-Barrantes, Valentín et al. 2012) 26
Figure 17 Grafting mechanism of a (monoalkoxy)silane on silica surface 27
Figure 18 Silylation mechanism in the gas phase (Brunel, Cauvel et al. 2000) 27
Figure 19 ^{29}Si CP-MAS NMR spectra of (a) unmodified silica (b) silica modified with dichloromethylvynilsilane (c) silica modified with chloromethylvynilsilane (Mijatovic, Binder et al. 2000) 29
Figure 20 Schematic view of different kinds of thermoreversible gels (A) PVC/plasticizer (B) aqueous gelatin (C) attactic PS in CS2 (D) triblock copolymer SBS in tetradecane (E) PO-EO-PO triblock copolymer in water (F) s-PMMA and i-PMMA in toluene (G) dissolved SCLCP (Nijenhuis 1997) 31

Figure 21 Bond percolation responsible of gelation. Infinite chain is dark (M. Rubinstein 2003)..... 32
Figure 22 Molecular mechanism of gelation accompanied by phase separation (a) interpenetrating coils in supercooled solution (b) formation of compact molecular aggregates (c) connection of aggregates and formation of a heterogeneous network (Łabudzińska and Ziabicki 1971)..... 33
Figure 23 Schematic representation of the storage and loss moduli during gelation (formed by a crosslinking reaction) (Mortimer, Ryan et al. 2001)..... 35
Figure 24 SEM micrographs of 7wt% PVDF gels in (a) acetophenone (b) ethyl benzoate and (c) glyceryl tributyrate (Mal and Nandi 1998)..... 36
Figure 25 Difference between distribution and dispersion: (a) good distribution and poor dispersion (b) poor distribution and dispersion (c) poor distribution and good dispersion (d) good dispersion and distribution (Schadler 2004)..... 37
Figure 26 Microscope images of PVC - CaCO3 films with (a,b,c) 40nm and (d,e,f) 220nm CaCO3 particles. Particle contents are (a,d) 3phr (b,e) 5phr (c,f) 10phr (Albayrak Ari and Aydin 2008)..... 39
Figure 27 TEM of 10 wt% silica - P2VP nanocomposites using (a) MEK (b) Pyridine as solvent (Jouault, Zhao et al. 2014)..... 40
Figure 28 TEM image of a polystyrene - silica nanocomposite (Jouault, Vallat et al. 2009)..... 41
Figure 29 (left) TEM and (right) AFM images of natural rubber filled with 60phr carbon nanotubes (Mittal 2012)..... 41
Figure 30 (left) SAXS measurements for nanocomposites filled with 5%v/v of Ludox TM-40 ion PS or PMMA (right) TEM image for 5% v/v Ludox TM-40/PMMA nanocomposite (Jouault, Dalmas et al. 2012)..... 42
Figure 31 TGA thermogram of (a) pure PP and silica-PP nanocomposites with different content of silica (b) silica-PP nanocomposites at different heating rates in nitrogen (Zheng, Yao et al. 2006)..... 43
Figure 32 (a) Correlation between Young's modulus and silica content (b) effect of the coupling agent on the tensile strength at break (▲without coupling agent ■with coupling agent) (c) effect of coupling agent on elongation at break (▲without coupling agent ■with coupling agent) on polyimide - silica nanocomposites (Shang, Zhu et al. 2002)..... 45
Figure 33 (a) Weibull plot of the breakdown probability of PE - silica composites and nanocomposites (b) dielectric permittivity of XLPE composites (c) loss tangent of XLPE composites (Roy, Nelson et al. 2007)..... 46
Figure 34 Poly(vinylidene fluoride-co-hexafluoropropylene) structure..... 50
Figure 35 Chemical structure of (a) 2MeTHF (b) acetone (c) MEK (d) 2-heptanone..... 51
Figure 36 Aqueous silica solution produced by sowing process..... 53
Figure 37 Representation of an example of L-type Nissan silica in organic solution to show qualitatively the size distribution (http://www.nissanchem-usa.com/products/organosilicasol)..... 53
Figure 38 Structure of CTAB surfactant..... 54
Figure 39 Phase transfer in 2MeTHF..... 55
Figure 40 Phase transfer process in MEK..... 56
Figure 41 Solvent relaxation curves of water (top curve, blue ■) and aqueous silica solution containing 4.6wt% of silica (bottom curve, brown +)..... 57
Figure 42 MEK – water phase diagram (Siegelman and Sorum 1960)..... 58
Figure 43 Solvent relaxation curves of aqueous (light blue ■) and organic (blue ■) phases recovered after the phase transfer process..... 59

Figure 44 ^{1}H NMR on (a) (experimental: green ●, fit : black ●)water-rich phase (without silica) and (experimental: blue ■, fit : black ■)aqueous phase of the phase transfer process; (b) (experimental: green ●, fit : black ●)MEK-rich phase (without silica) and (experimental: blue ■, fit : black ■)organic phase of the phase transfer process 59
Figure 45 Surface silica modifiers 60
Figure 46 Preparation of silica solution in 2-heptanone by solvent exchange 61
Figure 47 Formation of P(VDF-co-HFP) - silica films by solvent casting 62
Figure 48 Schematization of Newton and Bingham fluids 63
Figure 49 Stress - strain curves (Lissajous plot) for viscous, elastic and viscoelastic materials 64
Figure 50 Illustration of the strain sweep test (LAOS) at fixed frequency (Hyun, Wilhelm et al. 2011) 65
Figure 51 Strain sweep test at fixed frequency for a 8wt% P(VDF-co-HFP) gel in 2-heptanone 65
Figure 52 Schematic view of the rheometer equipped with a cone-plan geometry, excess of solvent and an enclosure to prevent the evaporation of 2-heptanone 66
Figure 53 Schematic representation of a polymer network 68
Figure 54 Schematics of the transverse relaxation signal of a gel with a rigid fraction of polymer. The signal (FID, red curve) cannot be observed in the dead time, before about 15 ms. The MSE allows observing the signal from t = 0 (blue curve), at the expense of a small decrease of the overall intensity, which can then be renormalized (dashed red curve) 69
Figure 55 MSE sequence (Maus, Hertlein et al. 2006) 69
Figure 56 CPMG sequence 70
Figure 57 Schematic representation of the DQ experiments and schematic representation of the reconversion block (Saalwächter 2007) 72
Figure 58 5-pulses sequence 73
Figure 59 Schematic representation of SAXS measurement 74
Figure 60 X-rays diffraction on crystal planes 77
Figure 61 USAXS measurements at (●) 31m (■) 8m (+) 1m and (-) the total signal for a P(VDF-co-HFP) – silica gel in MEK (11wt%) 78
Figure 62 Emission of a secondary electron 79
Figure 63 Emission of a back-scattered electron 79
Figure 64 (a) Abnormal value and (b) two slope phenomenon in breakdown strength measurements. It is supposed that only the second slope at high field is representative of the intrinsic properties of the material. ..... **Error! Bookmark not defined.**
Figure 65 Alternating voltage and current density for conductivity measurements ..... **Error! Bookmark not defined.**
Figure 66 Specimen for tensile test 80
Figure 67 Gelation rate t^{-1} versus concentration for P(VDF-co-HFP) in solution in MEK measurement for temperatures ranging between -40°C and 20°C 83
Figure 68 Gelation rate t^{-1} versus concentration for P(VDF-co-HFP) in solution in 2-heptanone measurement for temperatures ranging between -40°C and 20°C 84
Figure 69 Evolution of G' (blue ●) and G'' (green ■) during the gelation of a P(VDF-co-HFP) solution in 2-heptanone with 10wt% of copolymer, at 25°C, a frequency of 1Hz and a shear strain of 0.1% 85
Figure 70 Plot of G' (●) and G'' (■) against frequency for P(VDF-co-HFP) - 2-heptanone ($X_{P(VDF\text{-}co\text{-}HFP)=}$10wt%) gel at indicated temperatures 86

Figure 71 Gelation rate t^{-1} versus concentration for P(VDF-co-HFP) in solution in 2-heptanone measurements by linear rheology, at 25°C, a frequency of 1Hz and a shear strain of 0.1% 86
Figure 72 Plot of storage modulus (blue ●) and loss modulus (green ■) with temperature (measured at 1Hz and 0.1% shear strain) for a P(VDF-co-HFP) gel in 2-heptanone with 10wt% of copolymer 87
Figure 73 Evolution of the gel melting temperature $T_{melting}^{gel}$ with P(VDF-co-HFP) concentration for gels in 2-heptanone (measured at 1Hz and 0.1% shear strain) 87
Figure 74 Transverse ^{19}F NMR relaxation obtained with Hahn echo and CPMG sequences for a liquid solution of P(VDF-co-HFP) in MEK with $X_{P(VDF\text{-}co\text{-}HFP)}$=6wt% (blue ●) and for P(VDF-co-HFP) - MEK gels: violet ▲: $X_{P(VDF\text{-}co\text{-}HFP)}$=20wt%; orange ■: $X_{P(VDF\text{-}co\text{-}HFP)}$=30wt% 88
Figure 75 ^{19}F DQ build-up curve obtained after a 5-pulse Baum and Pines sequence as a function of the DQ excitation/reconversion time in the sequence: for gels of P(VDF-co-HFP) in MEK with $X_{P(VDF\text{-}co\text{-}HFP)=}$30wt% (orange ■) and $X_{P(VDF\text{-}co\text{-}HFP)=}$20wt% (purple ▲) and for a solution with $X_{P(VDF\text{-}co\text{-}HFP)=}$6wt% (blue ●). The amplitude of the signal was normalized by the initial transverse relaxation amplitude 90
Figure 76 ^{19}F DQ build-up curve obtained after a Baum and Pines sequence (improved by Saalwächter) as a function of the DQ excitation/reconversion time in the sequence for a gel of P(VDF-co-HFP) in MEK with $X_{P(VDF\text{-}co\text{-}HFP)=}$30wt% (orange ■) the reference signal (black ●). The amplitude of the signal was normalized by the maximum value of the reference signal 91
Figure 77 ^{19}F DQ build-up curves obtained after a Baum and Pines sequence (improved by Saalwächter) as a function of the DQ excitation/reconversion time in the sequence for gels of P(VDF-co-HFP) in MEK with $X_{P(VDF\text{-}co\text{-}HFP)=}$20wt% (purple ▲), $X_{P(VDF\text{-}co\text{-}HFP)=}$30wt% (orange ■) and for a solution with $X_{P(VDF\text{-}co\text{-}HFP)=}$6wt% (blue ●). The amplitude of the signal was normalized by the maximum value of the reference signal..... 91
Figure 78 Plots S_{Ref}-S_{DQ} as a function of the DQ excitation/reconversion time in the sequence for gels of P(VDF-co-HFP) in MEK with (a) $X_{P(VDF\text{-}co\text{-}HFP)=}$20wt% (purple ▲, fitting curve in red) and (b) $X_{P(VDF\text{-}co\text{-}HFP)=}$30t% (orange■, fitting curve in blue) 92
Figure 79 DSC thermograms of P(VDF-co-HFP) - MEK gels with various P(VDF-co-HFP) concentrations. Heating ramp was fixed at 1°C/min and only the first cycle of the DSC measurement was considered. 93
Figure 80 DSC thermograms of P(VDF-co-HFP) – 2-heptanone gels with various P(VDF-co-HFP) concentrations. Heating ramp was fixed at 1°C/min and only the first cycle of the DSC measurement was considered..... 94
Figure 81 DSC thermograms of P(VDF-co-HFP) – 2-heptanone gels with various P(VDF-co-HFP) concentrations. Heating ramp was fixed at 10°C/min and only the first cycle of the DSC measurement was considered..... 95
Figure 82 WAXS pattern of a P(VDF-co-HFP) – MEK gel with a composition $X_{P(VDF\text{-}co\text{-}HFP)=}$20wt% (▲, bottom curve) and a neat P(VDF-co-HFP) film (■, top curve), used as reference. Measurement time was fixed at 75 minutes..... 96
Figure 83 WAXS pattern of P(VDF-co-HFP) – 2-heptanone gels with a composition (a) $X_{P(VDF\text{-}co\text{-}HFP)=}$12wt% (light pink ●, 6minutes measurement time) and (b) $X_{P(VDF\text{-}co\text{-}HFP)=}$20wt% (pink ▲, 30minutes measurement time)..... 97
Figure 84 Normalized SAXS profile for P(VDF-co-HFP) - MEK systems of different composition (light blue ◆) $X_{P(VDF\text{-}co\text{-}HFP)=}$4wt%, (blue ▲) $X_{P(VDF\text{-}co\text{-}HFP)=}$13wt%, (brown ✦) $X_{P(VDF\text{-}co\text{-}HFP)=}$15wt%, (red ●) $X_{P(VDF\text{-}co\text{-}HFP)=}$20wt%, (violet ■) $X_{P(VDF\text{-}co\text{-}HFP)=}$26wt%. The systems with $X_{P(VDF\text{-}co\text{-}HFP)}$=20wt% and 26wt% were in the gel state. Fits of the curves of the gels with Equation 36 are shown. 98

Figure 85 (a): Normalized SAXS profile for P(VDF-co-HFP) – 2-heptanone systems of different composition (brown ⬟) $X_{P(VDF\text{-}co\text{-}HFP)}$=2wt%, (red ●)$X_{P(VDF\text{-}co\text{-}HFP)}$=3wt%, (orange ■) $X_{P(VDF\text{-}co\text{-}HFP)}$=4wt%, (yellow ▲)$X_{P(VDF\text{-}co\text{-}HFP)}$=5wt%, (green ▼)$X_{P(VDF\text{-}co\text{-}HFP)}$=6wt%, (blue ◆)$X_{P(VDF\text{-}co\text{-}HFP)}$=7wt%, (dark blue ✦) $X_{P(VDF\text{-}co\text{-}HFP)}$=15wt%, (black ⧗) $X_{P(VDF\text{-}co\text{-}HFP)}$=20wt%. Only the system with $X_{P(VDF\text{-}co\text{-}HFP)}$=2wt% is at the liquid state. (b): the intensities of the curves shown in (a) measured at q = 0.01 $Å^{-1}$ as a function of $\varphi(1-\varphi)$. 100
Figure 86 Evolution of the scattering intensity during gelation: SAXS measurements on a P(VDF-co-HFP) solution in 2-heptanone with $X_{P(VDF\text{-}co\text{-}HFP)}$=7wt% (blue curve) and comparison with a gel with the same composition previously prepared (green curve). Curves are recorded every 5 min. 101
Figure 87 Gelation rate t^{-1} versus concentration for P(VDF-co-HFP) in solution in 2-heptanone measurement at 20°C for three different copolymers: usual P(VDF-co-HFP) Solef® 21510 (pink ●), P(VDF-co-HFP) 1 (blue ■), P(VDF-co-HFP) 2 (green ◆). 102
Figure 88 Gelation rate t^{-1} versus concentration for P(VDF-co-HFP) in solution in MEK measurement at 20°C for three different copolymers: usual P(VDF-co-HFP) Solef® 21510 (orange ●), P(VDF-co-HFP) 1 (blue ■), P(VDF-co-HFP) 2 (green ◆). 103
Figure 89 WAXS pattern of P(VDF-co-HFP) – 2-heptanone solution and gels with a composition $X_{P(VDF\text{-}co\text{-}HFP)}$=20wt% in (a) amorphous P(VDF-co-HFP), (b) P(VDF-co-HFP) 1 and (c) P(VDF-co-HFP) 2. Measurement time was fixed at 30 minutes for the solution in amorphous P(VDF-co-HFP) and 6 minutes for the two others copolymer. 104
Figure 90 Solubility sphere in the Hansen 3D representation (Utracki 2003) 107
Figure 91 Gelation rate t^{-1} versus concentration for P(VDF-co-HFP) in solution in MEK (orange †) and 2-heptanone (pink ●) measurements at 20°C 109
Figure 92 Schematization of gelation of P(VDF-co-HFP) induced by crystallization via the formation of a phase separated medium 110
Figure 93 Schematic representation of adsorbed polymer onto solid surfaces 112
Figure 94 USAXS scattered intensity (normalized with the thickness of the sample) of aqueous silica solution with ϕ_{SiO2}=4.6 wt%. Blue curve is the measured scattering of aqueous silica solution. The green curve is an adjustment with a log-normal size distribution shown in Figure 96. 114
Figure 95 Log-normal distribution of the radius of the silica particles (from aqueous silica solution) 115
Figure 96 USAXS scattered intensity (normalized with the thickness of the sample) of aqueous silica solution (blue —), silica solution after the phase transfer step (SOL MEK / CTAB, red ○) and silica solution after the phase transfer and VTMS grafting (SOL MEK / CTAB + VTMS, red —) with ϕ_{SiO2}=4.6wt%. The green curve is an adjustment with the same log-normal size distribution as in water plus a small fraction of larger (aggregated) particles. 116
Figure 97 USAXS scattered intensity (normalized with the thickness of the sample) of Nissan silica solution with ϕ_{SiO2}=4.26wt% in MEK (green ○) and in 2-heptanone (red ○). Green curve is an adjustment of the Nissan solution in MEK with a log-normal size distribution of non-interacting particles. Red curve is an adjustment of the Nissan solution in 2-heptanone with a log-normal size distribution of non-interacting particles. 117
Figure 98 Log-normal distribution of the radius of the silica particles in Nissan solution in MEK (red —), compared with the size distribution of the aqueous silica solution synthetized in the lab (blue —) 117

Figure 99 (Right) Structure factor of Nissan silica solution in MEK (green —) and in 2-heptanone (red —). (Left) Possible organization of the silica nanoparticles in the Nissan solution in MEK and in 2-heptanone with *d* the distance between particles 119
Figure 100 (A) USAXS scattering intensity of P(VDF-co-HFP) – silica – MEK gels (ϕ_{SiO2}=1.6vol%) prepared with the silica solution in MEK by phase transfer with $X_{P(VDF\text{-}co\text{-}HFP)}$=11wt% (yellow ○), $X_{P(VDF\text{-}co\text{-}HFP)}$=20wt% (orange □) and $X_{P(VDF\text{-}co\text{-}HFP)}$=25wt% (red △) (B) Silica scattered intensity of P(VDF-co-HFP) – silica – MEK gels and (C) Kratky representation of the silica scattered intensity of filled physical gels in MEK. In (A) the pure matrix is also shown for comparison: $X_{P(VDF\text{-}co\text{-}HFP)}$=20wt% (light blue ■) and $X_{P(VDF\text{-}co\text{-}HFP)}$=25wt% (blue ▲) 120
Figure 101 Schematics of the interaction potential in the "sticky hard sphere model" (Menon, Manohar et al. 1991)..... 121
Figure 102 USAXS scattering intensity of P(VDF-co-HFP) – silica – MEK gels (ϕ_{SiO2}=1.6vol%) prepared with the silica solution in MEK by phase transfer with $X_{P(VDF\text{-}co\text{-}HFP)}$=11wt% (yellow ○), $X_{P(VDF\text{-}co\text{-}HFP)}$=20wt% (orange □) and $X_{P(VDF\text{-}co\text{-}HFP)}$=25wt% (red △). The pure matrix is also shown for comparison: $X_{P(VDF\text{-}co\text{-}HFP)}$=20wt% (light blue) and $X_{P(VDF\text{-}co\text{-}HFP)}$=25wt% (blue). Scattering curve of non-interacting particles multiplied with the structure factor calculated with this potential, using a volume fraction ϕSiO2 = 20 vol% and a strongly attractive potential is shown (black curve) to model scattering curves. An example is also represented (green curve). 121
Figure 103 USAXS scattered intensity (normalized with the thickness of the samples) of P(VDF-co-HFP) – Nissan silica – MEK solutions with $X_{P(VDF\text{-}co\text{-}HFP)}$=11wt% (light green ○), $X_{P(VDF\text{-}co\text{-}HFP)}$=20wt% (green □) and gel with $X_{P(VDF\text{-}co\text{-}HFP)}$=25wt% (dark green △). The pure matrix is also shown for comparison: $X_{P(VDF\text{-}co\text{-}HFP)}$=20wt% (light blue ■) and $X_{P(VDF\text{-}co\text{-}HFP)}$=25wt% (blue ▲) 123
Figure 104 (A) USAXS scattering intensity of P(VDF-co-HFP) – silica Nissan – 2-heptanone gels (ϕ_{SiO2}=1.6vol%) prepared $X_{P(VDF\text{-}co\text{-}HFP)}$=7wt% (light blue ○), $X_{P(VDF\text{-}co\text{-}HFP)}$=25wt% (dark blue △) (B) Silica scattered intensity of P(VDF-co-HFP) – silica Nissan – 2-heptanone gels. In (A) the pure matrix is also shown for comparison: $X_{P(VDF\text{-}co\text{-}HFP)}$=7wt% (orange ■) and $X_{P(VDF\text{-}co\text{-}HFP)}$=25wt% (pink ▲)..... 124
Figure 105 Gelation rate t^{-1} versus concentration for P(VDF-co-HFP) in solution in MEK (left): without silica (orange (orange +) and with silica (ϕ_{SiO2}=4.28 wt%, blue #); in solution in 2-heptanone (right): without silica (pink ●) and with silica (brown ⬟). Measurements were performed at 20°C. 125
Figure 106 Gelation rate versus concentration of silica nanoparticles for P(VDF-co-HFP) – silica – 2-heptanone gels with $X_{P(VDF\text{-}co\text{-}HFP)}$=7wt% at 25°C, a frequency of 1Hz and a shear strain of 0.1% 126
Figure 107 Gelation rate t^{-1} versus concentration for P(VDF-co-HFP) in silica solution in 2-heptanone (ϕ_{SiO2}=8.4 wt%, green ■) compared with P(VDF-co-HFP) in solution in 2-heptanone (blue ●), at 25°C, a frequency of 1Hz and a shear strain of 0.1%..... 126
Figure 108 Evolution of the elastic (left) and viscous (right) moduli with the concentration of copolymer for P(VDF-co-HFP) – 2-heptanone gels without (blue ● and ○) and with silica with ϕ_{SiO2} = 8.4wt% (green ■ and □) 127
Figure 109 Transverse ^{19}F NMR relaxation obtained with Hahn echo and CPMG sequences for a liquid solution of P(VDF-co-HFP) in MEK with $X_{P(VDF\text{-}co\text{-}HFP)}$=6wt% (blue ●) and for P(VDF-co-HFP) - MEK gels: green ●: $X_{P(VDF\text{-}co\text{-}HFP)}$=20wt%; orange ●: $X_{P(VDF\text{-}co\text{-}HFP)}$=20wt% and ϕ_{Si02}=4.26wt% 128
Figure 110 ^{19}F DQ build-up curve obtained after a 5-pulse Baum and Pines sequence as a function of the DQ excitation/reconversion time in the sequence: for P(VDF-co-HFP) – MEK gels with $X_{P(VDF\text{-}co\text{-}HFP)}$=30wt% without silica (orange ■) and with silica nanoparticles (ϕ_{SiO2}=4.26wt%, pink ◆)..... 129

Figure 111 ^{19}F DQ build-up curve obtained after a Baum and Pines sequence (improved by Saalwächter) as a function of the DQ excitation/reconversion time in the sequence of a gel of P(VDF-co-HFP) in MEK with $X_{P(VDF\text{-}co\text{-}HFP)}$=20wt% without silica (green ●, reference signal black ●) and with silica nanoparticles (ϕ_{SiO2}=4.26wt%, orange ●, reference signal black ■)..... 130
Figure 112 water – MEK/water phase equilibrium diagram (Siegelman and Sorum 1960)..... 131
Figure 113 Schematization of the possible structuration of silica nanoparticles in P(VDF-co-HFP) - silica (by phase transfer) - MEK gels with (a) random fractal aggregates or (b) “core-shell” type fractal aggregates 132
Figure 114 Schematization of the possible gelation mechanism of P(VDF-co-HFP) – silica (developed by phase transfer) – MEK materials. Polymer chains are represented by black lines and crystallites by orange circles. 133
Figure 115 Schematization of the rheology sequence applied on P(VDF-co-HFP) – 2-heptanone filled or not with silica nanoparticles 137
Figure 116 Plot of viscoelastic moduli (G' blue ●, G'' green ■) during oscillatory strain sweeps (from 0.01% to 500%) on a P(VDF-co-HFP) - 2-heptanone gel with $X_{P(VDF\text{-}co\text{-}HFP)=}$10wt%. Experiments were performed at 25°C and a frequency of 1Hz..... 138
Figure 117 Evolution of the viscoelastic moduli (G' blue ●, G'' green ■) with time after LAOS measurements on a P(VDF-co-HFP) – 2-heptanone solution/gel with 10wt% of copolymer. Experiments were performed at 25°C, a frequency of 1Hz and a shear strain of 1%..... 138
Figure 118 Plot of viscoelastic moduli (from 0.01% to 500%: G' blue ●, G'' green ■ and from 500% to 0.01%: G' blue ○, G'' green □) during oscillatory strain sweeps on a P(VDF-co-HFP) - 2-heptanone gel with $X_{P(VDF\text{-}co\text{-}HFP)}$=10wt%. Experiments were performed at 25°C and a frequency of 1Hz..... 139
Figure 119 LAOS tests (filled symbols: 0.01% up to 500%; empty symbols: 500% down to 0.01%) on P(VDF-co-HFP) - 2-heptanone gels at different concentrations of copolymer: (A) $X_{P(VDF\text{-}co\text{-}HFP)}$=6wt% (B) $X_{P(VDF\text{-}co\text{-}HFP)}$=7wt% (C) $X_{P(VDF\text{-}co\text{-}HFP)}$=8wt% (D) $X_{P(VDF\text{-}co\text{-}HFP)}$=10wt%. Experiments were performed at 25°C and a frequency of 1Hz 140
Figure 120 Storage modulus versus shear strain for P(VDF-co-HFP) - 2-heptanone at different compositions: $X_{P(VDF\text{-}co\text{-}HFP)}$=6wt% (red ⧗), $X_{P(VDF\text{-}co\text{-}HFP)}$=7wt% (orange ⬟), $X_{P(VDF\text{-}co\text{-}HFP)}$=8wt% (light blue ◆) and $X_{P(VDF\text{-}co\text{-}HFP)}$=10wt% (blue ●) for (A) upwards ramp (0.01% up to 500%, filled symbols) and (B) downwards ramp (500% down to 0.01%, empty symbols). All measurements were performed at 25°C and a frequency of 1Hz. 141
Figure 121 Stress as a function of time and as a function of strain during one cycle in the LVE and nonlinear regions (elastic and viscous states) for a P(VDF-co-HFP) – 2-heptanone gel with $X_{P(VDF\text{-}co\text{-}HFP)}$=7wt%. Experiments were conducted at 25°C and a frequency of 1Hz..... 143
Figure 122 Lissajous curves of the upwards ramp (0.01% up to 500%) for P(VDF-co-HFP) – 2-heptanone gels at three different copolymer concentrations: (a) 7wt%, (b) 8wt% and (c) 10wt% with shear strains of 1%, 38%; 57%, 100% and 252%. Experiments were conducted at 25°C and a frequency of 1Hz 144
Figure 123 Stress (red +) and strain (blue ●) as a function of time in P(VDF-co-HFP) – 2-heptanone gel with $X_{P(VDF\text{-}co\text{-}HFP)}$=7wt% during three periods, at high strain amplitude. At the beginning of the time window which is shown, the system is elastic, with the stress nearly in phase with the strain and a stress amplitude of order 1.5 kPa (modulus G’ of order 2 kPa). Some high frequency stress oscillations then appear, associated to either slippage at the walls of the measuring cell or to internal fracture of the gel. These oscillations are precursor of the overall transition towards the viscous regime, which

occurs at about 98.5 s. In the subsequent viscous regime, the stress is nearly in phase with the strain rate (I;e. in quadrature with the strain). 145
Figure 124 Lissajous curves of the downwards ramp (500% down to 0.01%) for P(VDF-co-HFP) – 2-heptanone gels at three different copolymer concentrations: (a) 7wt%, (b) 8wt% and (c) 10wt% with shear strains of 315%, 80%; 32%, 12.5% and 1%. Experiments were conducted at 25°C and a frequency of 1Hz 146
Figure 125 LAOS tests (filled shapes: 0.01% up to 500%; unfilled shapes: 500% down to 0.01%) on P(VDF-co-HFP) – silica – 2-heptanone gels with X_{SiO2}=8wt% and with different concentrations of copolymer: (A) $X_{P(VDF\text{-}co\text{-}HFP)}$=6wt% (B) $X_{P(VDF\text{-}co\text{-}HFP)}$=7wt% (C) $X_{P(VDF\text{-}co\text{-}HFP)}$=8wt% (D) $X_{P(VDF\text{-}co\text{-}HFP)}$=10wt% and (E) $X_{P(VDF\text{-}co\text{-}HFP)}$=12wt%. Experiments were conducted at 25°C and a frequency of 1Hz. 148
Figure 126 Evolution of the viscoelastic moduli (G' blue ●, G'' green ■) with time after LAOS measurements on a P(VDF-co-HFP) – silica – 2-heptanone solution/gel with 10wt% of copolymer and 8wt% of silica. Experiments were performed at 25°C, a frequency of 1Hz and a shear strain of 1%. 149
Figure 127 Lissajous curves of the upwards ramp (0.01% up to 500%) for P(VDF-co-HFP) – silica – 2-heptanone gels with X_{SiO2}=8wt% at different copolymer concentrations: (a) 7wt%, (b) 8wt%, (c) 10wt% with shear strains of 1%, 38%; 57%, 100% and 252%. Experiments were performed at 25°C and a frequency of 1Hz. 150
Figure 128 Lissajous curves of the downwards ramp (500% down to 0.01%) for P(VDF-co-HFP) – silica – 2-heptanone gels with X_{SiO2}=8wt% at different copolymer concentrations: (a) 7wt%, (b) 8wt%, (c) 10wt% with shear strains of 315%, 80%, 32%, 12.5% and 1%. Experiments were performed at 25°C and a frequency of 1Hz. 151
Figure 129 Schematization of a homogeneous, tetrafunctional polymer gel made of very flexible chains..... 152
Figure 130 Force as a function of the “extension ratio λ” for different number N of Kuhn segments of length α 153
Figure 131 Schematization of the possible structure of P(VDF-co-HFP) – 2-heptanone explaining the strain-hardening..... 154
Figure 132 Example of the determination of the P_0 and P_1 parameters used for the calculation of the strain-hardening ratio. Example for a P(VDF-co-HFP) – 2-heptanone gel with $X_{P(VDF\text{-}co\text{-}HFP)}$=7wt% and γ=40% 154
Figure 133 Evolution of the strain-hardening ratio as a function of the strain amplitude for P(VDF-co-HFP) – 2-heptanone gels with different fractions of copolymer: $X_{P(VDF\text{-}co\text{-}HFP)}$=6wt% (red ⧗), $X_{P(VDF\text{-}co\text{-}HFP)}$=7wt% (orange ⬟), $X_{P(VDF\text{-}co\text{-}HFP)}$=8wt% (light blue ◆) and $X_{P(VDF\text{-}co\text{-}HFP)}$=10wt% (blue ●)..... 155
Figure 134 Schematic representation of the restructuration of P(VDF-co-HFP) – 2-heptanone gels during LAOS experiment. 156
Figure 135 SEM micrograph of P(VDF-co-HFP) - silica film (20wt% of silica, from silica solution in MEK by phase transfer) 162
Figure 136 Normalized USAXS scattered intensities of P(VDF-co-HFP) – silica (developed by phase transfer) nanocomposites containing different fractions of silica: 8.25vol% (yellow ○), 16.82vol% (orange □) and 25.75vol% (red △)..... 163
Figure 137 Reduced USAXS scattered intensities of P(VDF-co-HFP) – silica (from Nissan silica solution in MEK) nanocomposites containing different fractions of silica: 12.49vol% (light green ○), 16.82vol% (green □) and 25.75vol% (dark green △). 164

Figure 138 Reduced USAXS scattered intensities of P(VDF-co-HFP) – silica (from Nissan silica solution in 2-heptanone) nanocomposites containing different fractions of silica: 4.08vol% (blue ○), 8.25vol% (dark blue □) 165
Figure 146 Young's modulus of P(VDF-co-HFP) - silica films as a function of the concentration of silica from (✦) 2-heptanone silica solution (Nissan) (⧗) MEK-ST-L (Nissan) (⬟) silica solution in MEK (by phase transfer) 166
Figure 147 Yield strength of P(VDF-co-HFP) - silica films as a function of the concentration of silica from (✦) 2-heptanone silica solution (Nissan) (⧗) MEK-ST-L (Nissan) (⬟) silica solution in MEK (by phase transfer) 167
Figure 148 Samples after mechanical tensile test obtained with the three approaches (a) silica in MEK prepared by phase transfer (b) MEK-ST-L (Nissan) and (c) silica in 2-heptanone (Nissan)..... 167
Figure 149 Schematization of the possible mechanisms leading to the formation of porous films... 169
Figure 150 USAXS scattered intensity (normalized with the fraction of silica and $\beta^2\Delta\rho^2$) of P(VDF-co-HFP) – silica – MEK gels (ϕ_{SiO2}=1.6vol% with $X_{P(VDF\text{-}co\text{-}HFP)}$=20wt% in pink – and $X_{P(VDF\text{-}co\text{-}HFP)}$=25wt% in red –) and P(VDF-co-HFP) – silica films (ϕ_{SiO2}=16.82vol% orange □ and ϕ_{SiO2}=25.75vol% red △) prepared from the silica solution in MEK developed by phase transfer..... 170
Figure 151 Schematization of the possible mechanism involved in the formation of P(VDF-co-HFP) – silica (developed by phase transfer in MEK) porous films 171
Figure 152 USAXS scattered intensity (normalized with the fraction of silica and $\beta^2\Delta\rho^2$) of P(VDF-co-HFP) – silica – MEK solution (ϕ_{SiO2}=1.6vol% with $X_{P(VDF\text{-}co\text{-}HFP)}$=11wt% in blue –) and P(VDF-co-HFP) – silica films (ϕ_{SiO2}=12.49vol% light green ○, ϕ_{SiO2}=16.82vol% green □ and ϕ_{SiO2}=25.75vol% dark green △) prepared from the Nissan silica solution in MEK. 172
Figure 153 USAXS scattered intensity (normalized with the fraction of silica and $\beta^2\Delta\rho^2$) of P(VDF-co-HFP) – silica – 2-heptanone gels (ϕ_{SiO2}=1.6vol% with $X_{P(VDF\text{-}co\text{-}HFP)}$=7wt% in pink –, $X_{P(VDF\text{-}co\text{-}HFP)}$=11wt% in violet – and $X_{P(VDF\text{-}co\text{-}HFP)}$=20wt% in dark –) and P(VDF-co-HFP) – silica films (ϕ_{SiO2}=4.08vol% blue ○, ϕ_{SiO2}=8.25vol% dark blue □) prepared from the Nissan silica solution in 2-heptanone..... 173
Figure 158 Young's modulus of P(VDF-co-HFP) - silica films as a function of the concentration of silica from (A) silica in MEK prepared by phase transfer (B) MEK-ST-L (Nissan) and (C) silica in 2-heptanone (Nissan). All experimental curves are fitted with K&D model (red —) and G&G model (orange - -).. 175
Figure 159 Phase diagram linking the excluded volume (and therefore the Flory interaction parameter) to the polymer fraction in solution for MEK and 2-heptanone. n(C) corresponds to the number of carbon of the backbone chain, here n(C)=4 for MEK and n(C)=7 for 2-heptanone. 179